National Library
of Canada

Acquisitions and
Bibliographic Services Branch

395 Wellington Street
Ottawa, Ontario
K1A 0N4

Bibliothèque nationale
du Canada

Direction des acquisitions et
des services bibliographiques

395, rue Wellington
Ottawa (Ontario)
K1A 0N4

Your file Votre référence

Our file Notre référence

NOTICE

The quality of this microform is heavily dependent upon the quality of the original thesis submitted for microfilming. Every effort has been made to ensure the highest quality of reproduction possible.

If pages are missing, contact the university which granted the degree.

Some pages may have indistinct print especially if the original pages were typed with a poor typewriter ribbon or if the university sent us an inferior photocopy.

Reproduction in full or in part of this microform is governed by the Canadian Copyright Act, R.S.C. 1970, c. C-30, and subsequent amendments.

AVIS

La qualité de cette microforme dépend grandement de la qualité de la thèse soumise au microfilmage. Nous avons tout fait pour assurer une qualité supérieure de reproduction.

S'il manque des pages, veuillez communiquer avec l'université qui a conféré le grade.

La qualité d'impression de certaines pages peut laisser à désirer, surtout si les pages originales ont été dactylographiées à l'aide d'un ruban usé ou si l'université nous a fait parvenir une photocopie de qualité inférieure.

La reproduction, même partielle, de cette microforme est soumise à la Loi canadienne sur le droit d'auteur, SRC 1970, c. C-30, et ses amendements subséquents.

Canada

Porosity Formation in Sr-Modified Al-Si Alloys

by

Daryoush Emadi

Department of Mining and Metallurgical Engineering
McGill University, Montreal, Canada

A thesis submitted to the Faculty of Graduate Studies and Research
in partial fulfilment of the requirements for the degree of
Doctor of Philosophy

February 1995

ISBN 0-612-05698-8

Canada

Abstract

Modification of the eutectic silicon in Al-Si foundry alloys by adding strontium is accompanied by an increase of porosity in the casting. This effect on porosity is due to an increase in both the pore size and the pore number density. In an attempt to understand the nature of this problem, the effect of strontium on the probable causes for porosity occurrence due to modification has been investigated.

Experimental findings indicate that the addition of strontium to Al-Si alloys increases the volumetric shrinkage due to an increase in solid density, and at the same time reduces the surface tension and increases the viscosity of the liquid. Metallographic observations show that Sr addition slightly decreases the dendrite arm spacing and changes the solid-liquid interface to a more regular shape. Moreover, Sr-modification decreases the eutectic temperature, and therefore, increases the length of the mushy zone while the total solidification time remains constant.

In addition, Sr addition increases the melt inclusion content, but these inclusions do not have a significant effect on pore nucleation. Hydrogen measurement in the liquid shows that Sr-modification has no effect on the rate of melt hydrogen pick-up and does not introduce hydrogen into the melt. Strontium also reduces the hydrogen solubility in the liquid state but has virtually no effect on the solid state solubility.

A solidification model for pore formation has been developed to study the significance of the changes in these parameters on porosity formation. Based on the experimental results and the theoretical analysis, it is concluded that the decrease in the hydrogen solubility in the liquid, the eutectic temperature (or the length of the mushy zone) and the surface tension are the reasons for the observed increase in porosity in modified alloys. Among these parameters, the decrease in the hydrogen solubility in the liquid plays the main role in causing enhanced porosity formation.

Résumé

La modification du silicium eutectique dans les alliages de fonderie Al-Si par l'addition de strontium est accompagnée d'une augmentation de la porosité dans la pièce coulée. Cet effet sur la porosité est dû à une augmentation de la taille et de la densité numérique des pores. Dans une tentative pour comprendre la nature de ce problème, l'effet du strontium sur les causes probables de l'apparition de la porosité associée à la modification, a été examiné.

Les résultats expérimentaux indiquent que l'addition du Sr dans les alliages Al-Si augmente le retrait au refroidissement à cause d'une augmentation de la densité du solide, et en même temps réduit la tension de surface et augmente la viscosité du liquide. Les observations métallographiques montrent que l'addition de Sr diminue un peu l'espace entre les bras dendritiques et change l'interface solide-liquide pour une forme plus régulière. De plus, la modification par le Sr diminue la température eutectique et, par conséquence, augmente la longueur de la zone pâteuse tandis que le temps total de la solidification demeure constant.

L'addition de Sr augmente la teneur en inclusions de la coulée, mais ces inclusions n'ont pas un effet significatif sur la germination des pores. La mesure de l'hydrogène dans le liquide montre que la modification par le Sr n'a pas d'effet sur le taux d'absorption d'hydrogène de la coulée et n'introduit pas d'hydrogène dans la coulée. Le strontium réduit aussi la solubilité de l'hydrogène dans l'état liquide mais n'a pratiquement pas d'effet sur la solubilité dans l'état solide.

Un modèle de solidification pour la formation des pores a été développé pour étudier l'importance de ces paramètres sur la formation de la porosité. En se basant sur les résultats expérimentaux et l'analyse théorique, il a été conclu que la diminution de la solubilité de l'hydrogène dans le liquide, de la température eutectique (ou la longueur de

la zone pâteuse) et de la tension de surface sont les raisons pour l'augmentation observée de la porosité dans les alliages modifiés. Parmi ces paramètres, la diminution de la solubilité de l'hydrogène dans le liquide joue le rôle principal en causant une formation intensifiée de la porosité.

Acknowledgements

I would like to thank my supervisor, Prof. John E. Gruzleski, for his guidance, support, helpful suggestions and constant encouragements throughout this work. His vitality and interest, and insatiable appetite for knowledge, were an encouraging example for me to follow. I would also like to acknowledge the assistance of Prof. J.M. Toguri and Dr. S.W. Ip in the use of the X-Ray equipment and the surface tension measurements at the university of Toronto.

I would like to thank the students and the staff of the Department of Mining and Metallurgical engineering, particularly the members of our group (aluminum group!), who have helped me and encouraged me during my studies at McGill. Special thanks are due to Dr. H. Mulazimoglu and Dr. P.S. Mohanty for their help, friendship and profound discussions. Thanks also go to Dr. Florence Parray for French translation of the abstract and her help in using the Image Analysis System. I am also thankful to Robert Paquette for his help during the castings and Helen Campbell for her help in using the SEM.

I wish to acknowledge the financial support of the Iranian Ministry of Culture and Higher Education as well as the Natural Science and Engineering Research Council of Canada (NSERC). Many thanks to Prof. Parviz Davami and other academic members of Sharif University of Technology (Tehran-Iran) for their encouragement.

Finally, I would like to acknowledge my deep gratitude to my family members, particularly my parents and sisters for their love, guidance and encouragement. The constant support they have given me throughout my studies will always be deeply appreciated. My roommates, and other friends, have been wonderful during the time of this research, and therefore, deserve a special acknowledgement. I thank you all once again for making my four year stay at McGill a memorable one.

Dedicated to my lovely Mother and Father,
you are the best.

Table of Contents

List of Figures

List of Tables

Chapter 1

Modification and Porosity Formation in Al-Si Alloys

1.1 Introduction

Al-Si alloys are currently the most important aluminum based casting alloys because of their excellent castability, mechanical and physical properties. The Al-Si alloy system is a simple eutectic system where the silicon forms as coarse acicular plates which act as internal stress raisers under an applied load. These alloys without any pretreatment are, therefore, characterized by relatively poor mechanical properties, especially low ductility and impact strength. Changing the morphology of the silicon phase from acicular to fibrous form through a process called modification can significantly improve the mechanical properties[1,2,3,4]. The eutectic structure is usually modified by adding sodium or strontium to the melt at levels in the range of 0.01 to 0.02 wt% or by heat treating.

Unfortunately, Na or Sr-modification significantly increases the pore volume fraction and the pore size in the castings. This is important since it can adversely affect the as-cast mechanical properties. Therefore, no significant increase in mechanical properties may be observed in Na or Sr modified castings, even though the microstructure of the modified alloy is more favourable.

Despite various suggestions by different authors to explain this behaviour, the

exact mechanism by which Na and Sr-modification increase the porosity in the casting has not yet been established. The objective of this investigation is, therefore, to obtain a fundamental understanding of the operating mechanism of porosity formation in modified Al-Si alloys. The probable causes for porosity occurrence will be described in this chapter, and the effect of Na and Sr-modification on these parameters will be investigated in the following chapters. Each chapter is written as a "stand-alone" section of the thesis. To facilitate reading, the references for each chapter are given at the end of the chapter.

1.2 Literature Review

1.2.1 Modification

Modification implies the change of the morphology of the eutectic silicon phase. Normally, silicon forms as a coarse plate-like or acicular morphology during solidification of an unmodified casting (Figure 1.1a). In the presence of Sr or Na, the silicon morphology changes to a fine fibrous form as illustrated in Figure 1.1b. The modification of eutectic silicon can be accomplished by:

a) Rapid solidification without any addition (**quench modification**)

b) Heat treatment including solution treating, quenching and aging (**heat treatment modification**)

c) Addition of chemical modifiers such as Na and Sr to the melt (**chemical modification**)

Of these methods, only chemical modification will be the area of concern in the present work.

There have been many theories postulated to explain the mechanism by which modifiers affect the silicon morphology. In early 1960s, Crosley and Mondolfo[5] proposed that in Al-Si alloys, the nucleation of silicon is controlled by aluminum phosphide (AlP).

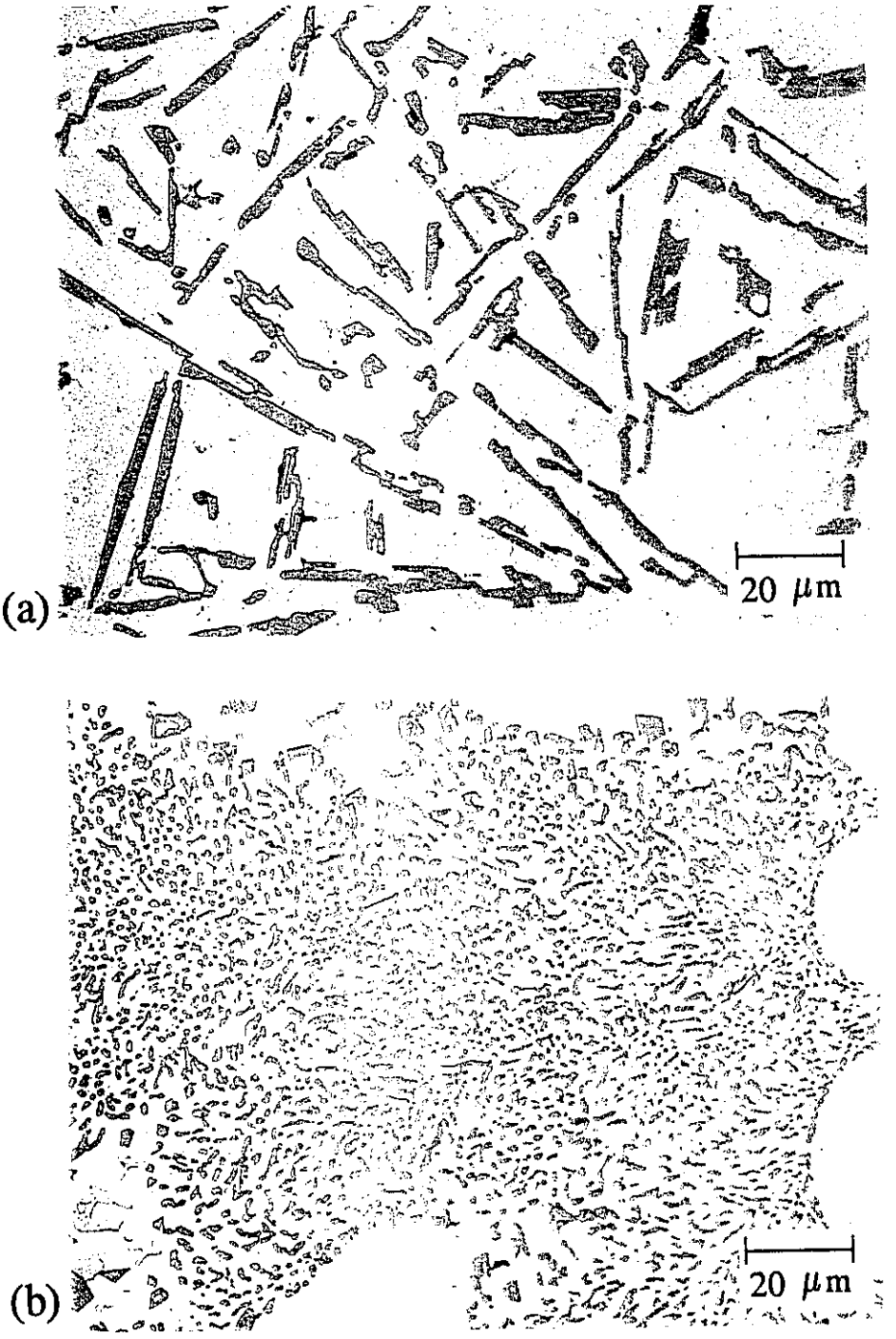

Figure 1.1 : The micrographs of a) unmodified flake structure;
b) Sr-modified fibrous structure in an A356 alloy.

Since AlP has a crystal structure very close to that of silicon, this intermetallic compound acts as an effective nucleus. In commercial Al-Si alloys, the phosphorus content is sufficient to provide an abundance of AlP particles in the melt. This leads to the nucleation of the eutectic silicon at small undercoolings (<2 °C) and the formation of coarse acicular silicon flakes. The modifier neutralizes the phosphorus, thus eliminating the nucleation by AlP, and increasing the undercooling for nucleation of silicon by aluminum which results in fibrous structures. However, this has been shown not to be the case, as the silicon phase is continuous in both the modified and unmodified alloys[6].

Besides the neutralization (or removal of AlP) theory, there have been other postulates to explain the mechanism of modification. The most recently accepted of these is that modifiers retard the growth rate of silicon by a TPRE (twin plane re-entrant edge) poisoning mechanism[2,6,7,8,9]. Lu and Hellawell[8] have shown that modified silicon contains more crystallographic defects known as twins. According to this model, modifiers adsorb onto the re-entrant sites and prevent or retard the subsequent attachment of Si atoms. This results in an increased undercooling of the Si phase, leading to more frequent overgrowth by the Al phase and increased twinning. Therefore, silicon bends and twists during growth and forms a fibrous rather than plate morphology. This phenomenon is supported by the observation that modifiers become concentrated in the silicon not the aluminum phase. Recently, Major and Rutter[9] have done some work which again supports the TPRE growth model for the pure eutectic and a change to non-TPRE growth in the presence of strontium.

Among the modifiers used for chemical modification, only strontium and sodium find significant industrial use. Higher recovery (>90%) and lower rate of loss are the major advantages of strontium over sodium. However, it is reported that the effect of Sr is weaker than that of Na, especially at low freezing rates, and higher Sr concentrations are required than sodium to yield the same effect[2,10,11]. The amount of modifier necessary generally depends on the type of the modifier, the concentration of impurity elements

which poison the modifier and the alloy composition.

Strontium is usually added to the melt in the form of Al-Sr master alloys such as Al-10 wt%Sr or Al-90 wt%Sr alloys. Pure strontium is also occasionally used but it is accompanied by the addition of hydrogen to the melt, and it is more difficult to dissolve than the master alloys due to the formation of a tenacious oxide film[12]. The Al-Sr master alloys have different dissolution characteristics with the optimum treatment temperature ranging from 680 to 750 °C in A356 alloy, and the optimum dissolution time about 5 to 15 min[13,14]. Typically, a strontium level in the range of 0.015-0.02 wt% is required for complete modification, and at higher silicon concentrations, a larger amount of strontium is required. For example, a strontium level of 0.02 wt% is sufficient to modify an alloy with 7 wt% silicon (A356 alloy) whereas 0.04 wt%Sr is necessary when the silicon level is 11 wt%.

Sodium addition is mainly made by two methods: a) surface treatment with flux, or b) use of elemental sodium. Due to the high reactivity of sodium, pure sodium is vacuum packed in small aluminum cans to minimize its oxidation and hydrogenation. Sodium level in the melt is more difficult to control as it vapourizes quickly. Hence, sodium recoveries are poor (<20% of the addition), and typical retained sodium levels are in the range of 0.005-0.01 wt%. Moreover, sodium acts and also fades quickly and sodium treatment is not environmentally friendly, while strontium can be added easily and lasts much longer. In addition, one cannot remelt and recast the sodium modified material due to significant sodium loss on remelting. On the other hand, such a process is possible in the case of strontium, and forms the basis of the use of premodified ingots.

The addition of Na or Sr beyond the values mentioned above (overmodification) may have detrimental effects on microstructure and mechanical properties. Recently, it has been observed that a strontium content more than about 0.015 wt% results in coarsening of the silicon particles (Figure 1.2) [10,15]. It should be noted that this critical

content depends on the cooling rate during solidification. The degree of modification, i.e. the microstructural change of eutectic silicon, has historically been visually determined metallographically. For hypoeutectic Al-Si alloys, Apelian *et al* [16] have developed a rating system to evaluate the different levels of silicon modification. These structures have been divided into six classes with well modified structures identified as class 5.

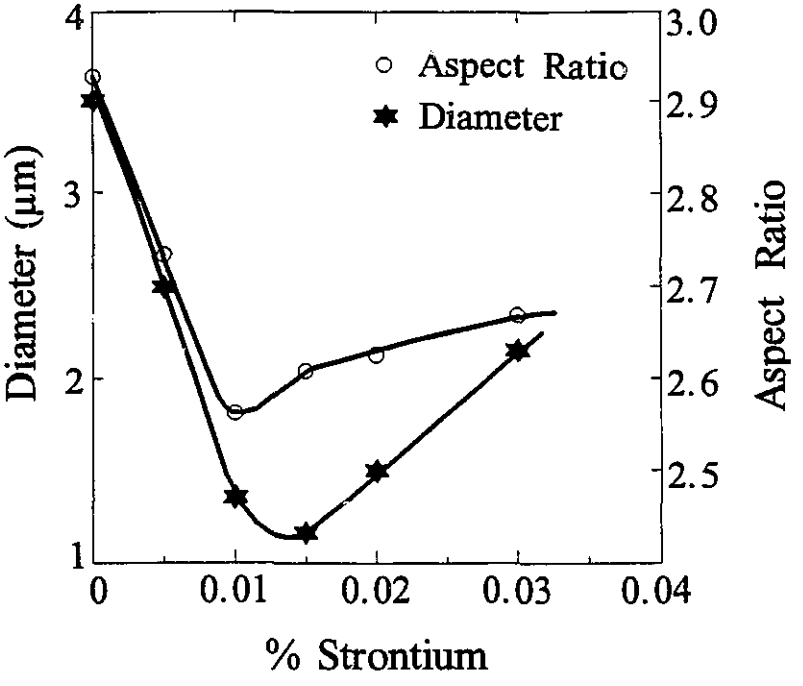

Figure 1.2 : The variation of silicon particle average diameter and aspect ratio with strontium concentration [15].

Thermal analysis technique is also a useful method to evaluate the modification potential of the molten aluminum casting alloy prior to pouring[10,16,17,18]. In thermal analysis, a cooling curve (i.e. plot of temperature vs. time) is obtained as the solidifying sample cools from liquid state to solid state. When an alloy is modified, the cooling curve is affected, and the undercooling (ΔT_N) required to start eutectic freezing is increased,

and the eutectic growth temperature, T_E , is depressed as shown in Figure 1.3. The degree of depression of the eutectic temperature (ΔT_E) is commonly used to evaluate modification. For example, Sr-modification suppresses the eutectic temperature by about 4-10 °C depending on the amount of strontium while the liquidus temperature remains almost constant[17,19,20,21,22,23]. Therefore, the eutectic point in the Al-Si phase diagram shifts to the right as shown in Figure 1.4. Electrical conductivity measurements can also be used to control the degree of modification (or quantity of some alloying elements)[24,25,26]. The electrical resistivity measured by the DC Technique is decreased by modification. More detailed information about different aspects of modification can be found in Refs. 1 and 10.

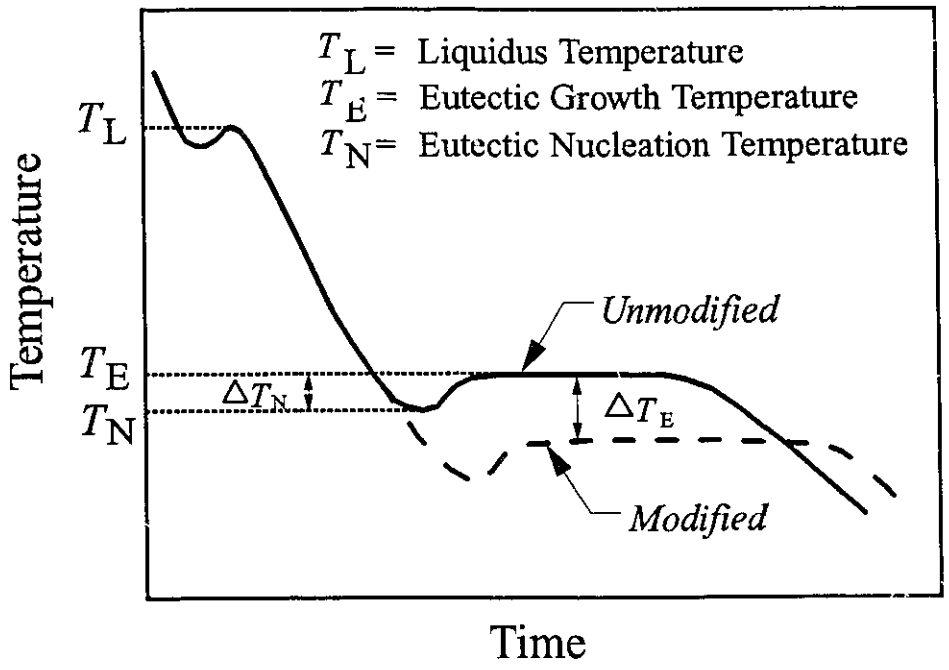

Figure 1.3 : Typical cooling curves for unmodified and modified hypoeutectic Al-Si alloys.

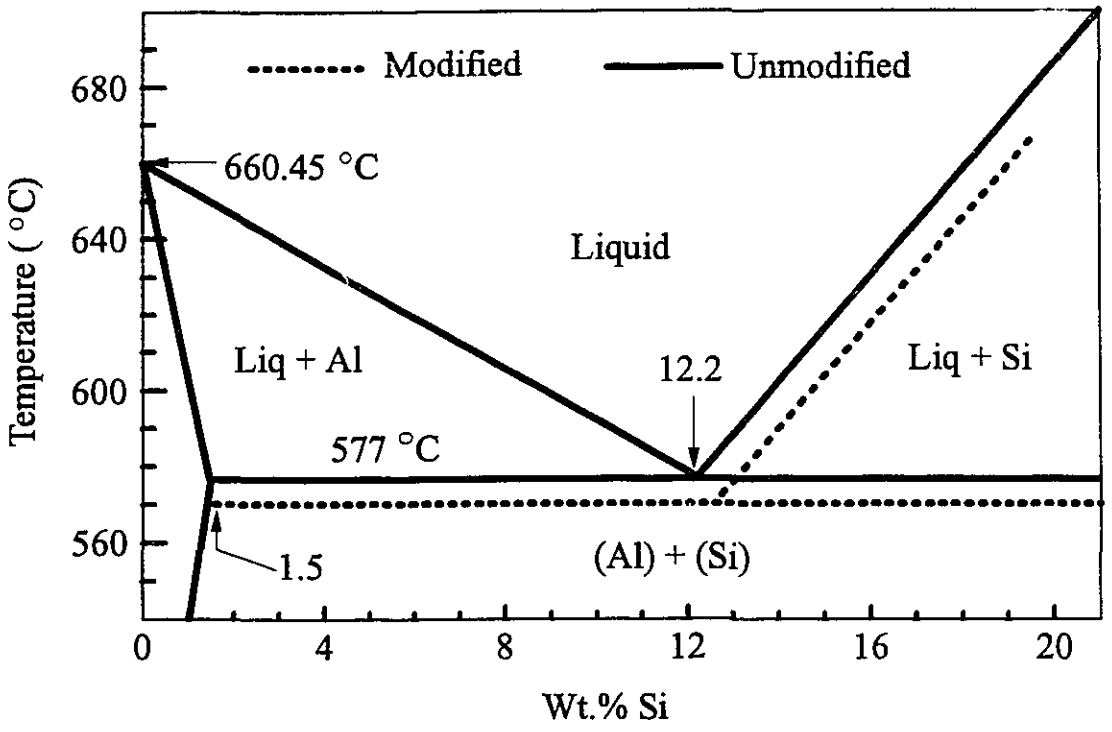

Figure 1.4 : Schematic of binary Al-Si phase diagram illustrating the eutectic shift [10].

Probably the greatest problem associated with modification of Al-Si casting alloys is the fact that modified casting are often more porous than their unmodified counterparts. Sodium and strontium modification significantly increases the pore volume fraction and the pore size in the castings[15,20,27,28,29,30,31,32]. This problem is illustrated in Figures 1.5 and 1.6. This effect may offset any advantages in improved mechanical properties gained by modification, as well as leading to loss of pressure tightness in castings. Before investigating how and why modification enhances porosity in the castings, it is worthwhile here to discuss the fundamentals of pore formation and factors which affect the process.

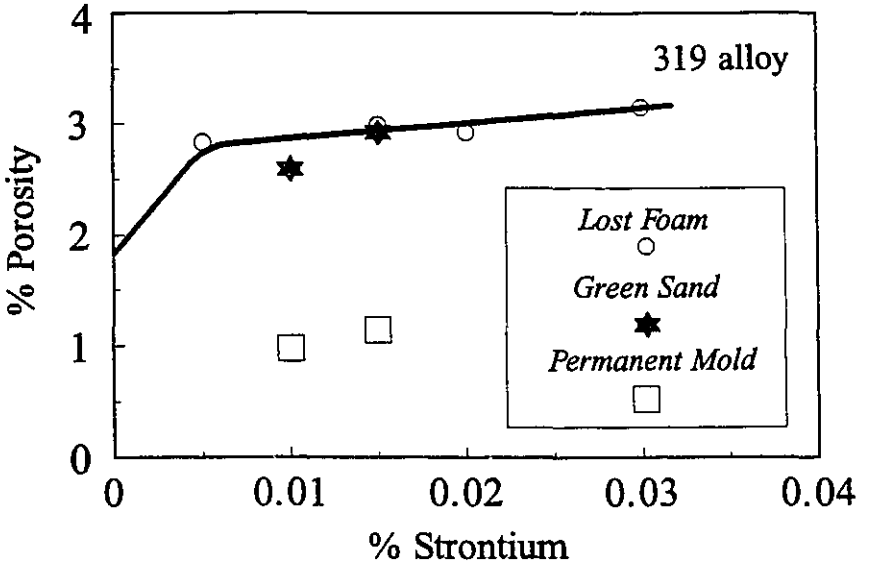

Figure 1.5 : Percent porosity as a function of strontium concentration for different types of castings[15].

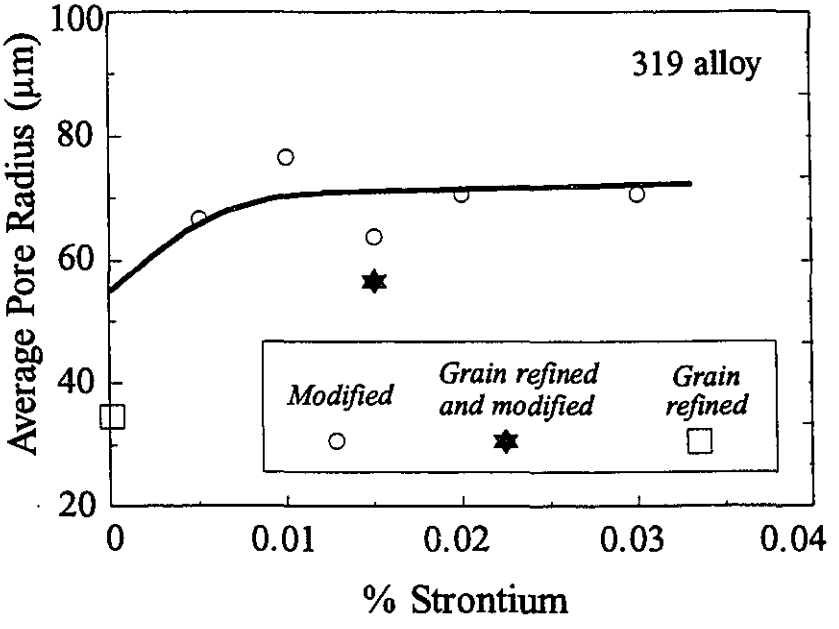

Figure 1.6 : Average pore size as a function of strontium concentration in alloy 319 castings[15].

1.2.2 Porosity

Porosity in aluminum castings is generally considered to be detrimental to the mechanical properties[32,33,34,35]. Porosity occurs in cast aluminum-silicon alloys during solidification due to the negative pressures generated by solidification contraction and the pressure developed by evolution of the dissolved hydrogen from the growing solid into the adjacent liquid. These processes may act either together or separately to produce shrinkage or gas porosity. In order for a pore to be stable and to grow, the internal pressures must be sufficient to overcome all of the external forces which can act to make it collapse. Thus, the following condition must prevail:

$$P_H + P_S \geq P_{atm} + P_M + P_F \qquad (1.1)$$

where P_H is the internal gas (hydrogen) pressure exerted during its evolution at the solid/liquid interface into the liquid , P_S is the shrinkage pressure arising due to thermal and solidification contractions of the metal, P_{atm} is the pressure applied to the surface of the liquid (usually 1 atm), P_M is the metallostatic pressure due to the metal head, and P_F is the fracture pressure associated with the interfacial free energy between the gas bubble and its surrounding liquid. An increase in the terms P_H and P_S , or a decrease in terms P_{atm} , P_M and P_F helps pore formation, and increases the porosity in the casting. The formulation of pore formation during solidification, and the calculation of these pressures will be discussed in detail later in Chapter 8.

1.2.2.1 Factors Affecting Pore Formation

There are several factors which affect directly or indirectly the pore formation in Al-Si alloys, and they are introduced briefly here. The effect of Na and Sr modification

on these parameters will be investigated separately in the next chapters. The factors controlling the formation of porosity in Al-Si alloys can be summarized as follows.

1.2.2.1.1 Cooling Rate

For a given melt hydrogen content, an increase in cooling rate decreases both the total amount of porosity and the average pore size in both modified and unmodified A356 alloy[27,28]. With increased solidification rates, less time is available for hydrogen to diffuse into the interdendritic spaces and so the term P_H in Eq. (1.1) is reduced. In addition, once a pore is nucleated, smaller sized pores will result.

By increasing cooling rate, the dendrite arm spacing (DAS) decreases and interdendritic feeding becomes poor. Therefore, term P_S in Eq. (1.1) becomes larger resulting in more porosity. On the other hand, the higher temperature gradients, present with more rapid solidification, tend to limit the length of the mushy zone which makes feeding easier and porosity formation becomes more difficult. The cooling rate can also affect the effectiveness of chemical modifiers. The higher the solidification rate, the easier it is to modify the microstructure.

1.2.2.1.2 Melt Hydrogen Content (Regassing and Degassing)

Hydrogen is absorbed in liquid aluminum through the following reaction:

$$2\,Al(l) + 3\,H_2O(g) = Al_2O_3(s) + 6\,H \qquad (1.2)$$

This reaction is highly favoured at foundry operating temperatures, but it cannot proceed if the molten bath is protected by an oxide (dross) film on its surface. The rate of melt hydrogen pick-up is influenced by the structure of the oxide film on the surface and the alloying elements present in the melt. It is, however, important to note that

above about 930 °C, the oxide film on the surface of the liquid loses its protective nature through a change in its crystal structure, and water vapour can readily penetrate the film[10]. Fortunately, this temperature is well above normal foundry operating melt temperatures.

An increase in hydrogen content (i.e. term P_H in Eq. (1.1)), for a given cooling rate, increases the amount of porosity in the casting, and this effect becomes greater as the cooling rate decreases[27,28]. There exists a threshold hydrogen content below which porosity does not form. Thomas and Gruzleski[36] have reported that this value is a function of cooling rate and could be above the solid solubility limit of hydrogen. In the case of Al-8%Si alloy, they found that this value is in the range of 0.05 to 0.15 ml/100g Al depending on the cooling rate. The melt hydrogen content can be reduced using vacuum degassing or gas purging. Gas purging is sometimes accompanied by inclusion removal which depends on the type of the gas and how the bubbles are formed [37,38].

1.2.2.1.3 Hydrogen Solubility in Solid and Liquid Aluminum

Hydrogen is the only gas capable of dissolving to a significant extent in molten aluminum. The solubility of hydrogen in aluminum and its alloys in liquid and solid states has been studied by several workers[39,40,41,42,43,44]. The results from their work show that the hydrogen solubility is strongly dependent on the temperature, melt chemical composition and partial pressure of hydrogen in the surrounding atmosphere. The hydrogen solubility exhibits a sharp drop at the transition from liquid to solid metal. A decrease in hydrogen solubility in the solid state results in the rejection of more hydrogen into the liquid during solidification. Therefore, the hydrogen content in the liquid, i.e. term P_H in Eq. (1.1), increases resulting in the formation of pores during solidification.

The actual hydrogen solubility in the liquid is sometimes thought not to be very important since the hydrogen level in the melt almost never reaches the solubility limit[10].

However, this is not true since the hydrogen is rejected into the liquid at the solid/liquid interface, and an enriched hydrogen layer forms at the interface. The concentration in this layer may well reach the solubility limit. Therefore, a decrease in hydrogen solubility in the liquid may cause the concentration in the hydrogen enriched layer to exceed the solubility limit at an earlier stage of solidification resulting in larger pores, and more total porosity.

1.2.2.1.4 Inclusions

Inclusions in the melt offer heterogeneous sites for the nucleation of pores and thus promote pore formation. Several authors have shown the importance of inclusions on porosity formation using the Straube-Pfeiffer (reduced pressure) test[45,46,47]. According to them, the pores in samples with a high inclusion content were larger in size and number and were rounder. Shahani and Fredriksson[48] observed that Al_2O_3-films could be seen at the interface between pores and the aluminum matrix in samples that had been treated under 5 atm hydrogen pressure.

In another study[49], the deliberate addition of oxides skimmed from the melt surface showed their association with the pores. On the other hand, when inclusions were removed by filtration, the porosity level was significantly reduced[29,45,50,51]. There have also been some theoretical analyses on the mechanism of heterogeneous nucleation of pores in metals and alloys[52,53]. Despite these various investigations, the exact mechanism by which inclusions operate to facilitate pore formation is not well understood.

1.2.2.1.5 Grain Refinement

Grain refining has several advantages, including redistribution and reduction of porosity and improving both the resistance to hot tearing and feeding capability. Grain refinement of a casting may alter the amount and the morphology of pores in the casting.

The presence of a grain refiner leads to a uniform redistribution of porosity[10,54,55]. In many cases, there is also an overall reduction in the amount of porosity upon grain refinement in alloys containing small or moderate amounts of gas[15,54,55].

Since the radius of the interdendritic liquid decreases with the addition of Ti (as a grain refiner in Al-Si alloys), the average pore size is lowered. When the alloy is grain refined, the dendritic network is broken down into small equiaxed grains. These fragmented dendrites are transported within the casting and contribute significantly to the mass feeding during solidification.

1.2.2.1.6 Feeding Capability

If the feeding ability is poor, it is expected that eutectic liquid in interdendritic regions becomes isolated from the bulk liquid and the pressure drop due to shrinkage (i.e. term P_S in Eq. (1.1)) results in more porosity with the pores becoming more dispersed. Interdendritic feeding ability is related to the nature of the solid/liquid interface, mode of solidification, freezing range (i.e. the difference between the liquidus and solidus temperatures of the alloy or the length of the mushy zone), dendrite arm spacing (DAS), volumetric shrinkage and viscosity of the interdendritic liquid.

The shorter the freezing range, or the more planar the interface, the shorter the distance that the liquid must flow between the dendrites or between eutectic colonies resulting in less porosity. A lower level of porosity can also be obtained by a decrease in volumetric shrinkage (i.e. less liquid is required to compensate the shrinkage of the liquid) or decrease in the viscosity which makes interdendritic flow easier. The mode of solidification, for example directional solidification or mushy solidification, also plays a significant rule in feeding ability. Directional solidification is a well accepted way to maximize the feeding and hence to minimize porosity [28,30].

1.2.2.1.7 Surface Tension

Considering the thermodynamic theories of gas porosity formation[56,57,58,59], a reduction in surface tension of the liquid can facilitate pore nucleation, and make it possible for pores to form at an earlier stage of solidification and to grow over a longer period of time resulting in larger pores and more porosity. Surface tension is a strong function of temperature and chemical composition.

1.2.2.1.8 Alloying Elements

Only very little work has been done on the effect of different alloying elements on porosity formation. Alloying elements can affect porosity formation by influencing the parameters mentioned above. For example, silicon has been reported to have an influence on DAS[60]. Increasing the silicon content leads to a decrease in the DAS and porosity is dispersed more finely. Strontium and antimony also refine the secondary dendrite arm spacing[61]. Alloying elements may affect the porosity by changing the surface tension. Most of the elements commonly found in aluminum casting alloys such as, Si, Sr, Na or Mg reduce the surface tension of aluminum alloys[62,63,64]. Alloying elements may also affect pore formation by increasing the number of inclusions in the melt or changing the solid/liquid interface or length of mushy zone. As already stated, both Sr and Na increase porosity. The reason for this is not clear and is the main goal of this research.

Besides the above mentioned parameters, there are also many other factors which affect porosity formation, such as: melt superheat, external pressure, casting design and mode of solidification. Since these factors are not believed to be the probable causes of the increase in porosity in modified alloys, they are not discussed in detail here.

1.2.3 Modification and Porosity

It has been demonstrated that both Na and Sr-modification increase pore volume fraction and pore size in castings. As illustrated in Figures 1.5 and 1.6, the addition of 0.03 wt% Sr into 319 alloy, increases the porosity from 2% to 3% and the pore radius from 55 μm to 70 μm. These effects can be so great that no significant increase in mechanical properties may be observed, even though the microstructure of the modified alloy is more favourable[10].

Various suggestions have been put forth by different researchers to explain the enhanced porosity behaviour of modified castings. Denton and Spittle[11] have suggested that modification aggravates the porosity problem by increasing the hydrogen content or the rate of regassing of the melt, and melts containing Sr are more susceptible to hydrogen absorption than those containing sodium. They have suggested that oxidation of Sr during melting causes the structure of the oxide layer on the surface to be changed and to become more pervious to hydrogen. In the case of Na, unlike Sr, a thick oxide is formed on the melt surface, which acts as a barrier to hydrogen dissolution. Contrary to these propositions, there have been reports indicating that no increase in dissolved hydrogen or rate of regassing occurs after strontium addition to the melt[65,66,67], but sodium treatment can cause hydrogen pick-up, if it is accompanied by a violent addition reaction[68]. Some authors have suggested that strontium helps pore formation by increasing both the inclusion content of the melt and the amount of hydrogen absorbed into oxides[28,29].

Argo and Gruzleski[30] have indicated that the increased porosity in modified castings is due to the problems associated with interdendritic feeding. The reduction of the eutectic temperature in modified alloys increases the length of the mushy zone, and, therefore, large pockets of interdendritic liquid may become isolated. Solidification of this liquid may result in the formation of large isolated pores. Others have contended that sodium

improves the feeding capability, and strontium, unlike sodium, has no effect on the shrinkage porosity of castings nor on the feeding ability of the alloy[29].

Several investigators have shown that the modified Al-Si eutectic solidification front possesses a smooth solid/liquid interface unlike its unmodified counterpart[2,11,22,69]. Therefore, a modified eutectic alloy should have less tendency to liquid entrapment and porosity than unmodified alloy. Most commercial castings however are hypoeutectic, and as such exhibit dendritic growth of α-phase prior to eutectic solidification. It has been also suggested that Na and Sr reduce the surface tension and aid in the nucleation of the pores[28,70,71].

Despite this multitude of suggestions, the exact mechanism by which Na and Sr-modification increase the porosity in the casting has not yet been established. The objective of this investigation is, therefore, to obtain a fundamental understanding of the operating mechanism of porosity formation in modified Al-Si alloys. Since Na and Sr-modification have similar effects on porosity, and because of the difficulties in the addition and controlling of Na in the melt, only the effect of Sr will be studied in the present work.

At the present time, it appears that the observed increase in porosity with Sr-modification is due to a change in both nucleation and growth mechanisms of the pore, and may be due not to a single factor, but rather to a complex interaction between the factors described in sections 1.2.2.1.1 to 1.2.2.1.8. In the present thesis, a fundamental and experimental investigation have been carried out to address the effect of Sr-modification on porosity from the view points of the parameters mentioned in sections 1.2.2.1.1 to 1.2.2.1.8.

The experimental investigation begins in a logical progression with the quantitative evaluation of pore volume fraction and size in Sr-modified castings as reported in Chapter

2. The influence of various possible parameters has been studied subsequently on a parameter by parameter basis. Chapter 3 deals with measurements on the changes of surface tension in the presence of Sr by a sessile-drop technique. The influence of Sr-modification on the volumetric shrinkage forms the contents of Chapter 4 while studies on feeding behaviour, inclusion effect and hydrogen solubility form the basis of Chapters 5 to 7, respectively.

As mentioned before, it seems that there are several variables which contribute to the final porosity content in modified castings. To consolidate the effect of various parameters, a mathematical model has been developed which is presented in Chapter 8. The thesis ends with descriptions on the quantitative contribution of the various factors to porosity formation in expressed terms of initial hydrogen content required for pore formation. General conclusions are also given in the last chapter as are various industrial implications of the present study and suggestions for further work.

1.3 References

1. F. Paray; "Heat Treatment and Chemical properties of Aluminum-Silicon Modified Alloys", Ph.D. Thesis, McGill University, Montreal, Canada, 1992

2. G.K. Sigworth; "Theoretical and Practical Aspects of the Modification of Al-Si Alloys", *AFS Trans.*, Vol. 91, 1983, pp.7-15

3. R.C. Harris, S. Lipson and H. Rosental; "Tensile Properties of Al-Si-Mg Alloys and the Effects of Sodium Modification", *AFS Trans.*, Vol. 64, 1956, pp. 470-481

4. Shivkumar, S. Ricci, J.B. Steenhoff, D. Apelian and G. Sigworth; "An Experimental Study to Optimize Heat Treatment of A356 Alloy", *AFS Trans.*, Vol. 97, 1989, pp. 791-810

5. P.B. Crossley and L.F. Mondolfo; "The Modification of Aluminum-Silicon Alloys", *Modern Casting*, Vol. 49, 1966, pp. 53-64

6. R. Elliot; *Eutectic Solidification Processing: Crystalline and Glassy Alloys*, Butterworths and co (publishers) ltd., New York, NY, 1983

7. M. Shamsuzzoha and L.M. Hogan; "The Twinned Growth of Silicon in Chill-modified Al-Si Eutectic", *J. Cryst. Growth*, Vol. 82, 1987, pp. 598-610

8. S. Lu and A. Hellawell; "The Mechanism of Silicon Modification in Aluminum-Silicon Alloys: Impurity Induced Twinning", *Met. Trans. A*, Vol. 18A, Oct. 1987, pp. 1721-33

9. J.F. Major and J.W. Rutter; "Effect of Strontium and phosphorus on Solid/Liquid Interface of Al-Si Eutectic", *Mater. Sci. Technol.*, Vol. 5, July 1989, pp. 645-56

10. J.E. Gruzleski and B.M. Closset; *The Treatment of Liquid Aluminum-Silicon Alloys*, American Foundrymen's Society, Des Olaines, IL, 1990, pp. 57-157

11. J.R. Denton and J.A. Spittle; "Solidification and Susceptibility to Hydrogen Absorption of Al-Si Alloys Containing Strontium", *Mater. Sci. Technol.*, Vol. 1, April 1985, pp. 305-11

12. B. Closset and J.E. Gruzleski; "A Study on the Use of Pure Metallic Strontium in the Modification of Al-Si Alloys", *AFS Trans.*, Vol. 89, 1981, pp. 801-8

13. M.O. Pekguleryuz and J.E. Gruzleski; "Conditions for Strontium Master Alloy Addition to A356 Melts", *AFS Trans.*, Vol. 96, 1988, pp. 55-64

14. G. Chai and L. Backerud; "Factors Affecting Modification of Al-Si Alloys by Adding Sr-Containing Master Alloys", *AFS Trans.*, Vol. 100, 1992, pp. 847-54

15. S. Shivkumar, L. Wang and D. Apelian; "Molten Metal Processing of Advanced Cast Aluminum Alloys", *J. of Metals*, Jan. 1991, pp. 26-32

16. D. Apelian, G.K. Sigworth and K.R. Whaler; "Assessment of Grain Refinement and Modification of Al-Si Foundry Alloys by Thermal Analysis", *AFS Trans.*, Vol. 92, 1984, pp.297-307

17. N. Tenekedjiev and J.E. Gruzleski; "Thermal Analysis of Strontium Treated Hypoeutectic and Eutectic Aluminum-Silicon Casting Alloys", *AFS Trans.*, Vol. 99, 1991, pp. 1-6

18. T.j. Hurley and R.G. Atkinson; "Effects of Modification Practice on Aluminum A356 Alloys", *AFS Trans.*, Vol. 93, 1985, pp. 291-96

19. Q.S. Hamed, R. Elliott and P.S. Cooper; "Solidification Characteristics of Sodium and Strontium Modified Al-Si Casting Alloys", *Light Metals*, 1992, pp. 1391-97

20. R. Fuoco, H. Goldenstein and J.E. Gruzleski; "Evaluation of the Effect of Modification-Induced Eutectic Undercooling on the Microporosity Formation in 356 Aluminum Alloy", *AFS Trans.*, Vol. 102, 1994

21. R.C. Plumb and J.E. Lewis; "The Modification of Aluminum-Silicon Alloys by Sodium", *J. Inst. Met.*, Vol. 86, 1957-58, pp. 393-400

22. M.D. Hanna, S. Lu and A. Hellawell; "Modification in the Aluminum Silicon System", *Met. Trans. A*, Vol. 15A, March 1984, pp.459-69

23. C.B. Kim and R.W. Heine; "Fundamentals of Modification in the Aluminum-Silicon System", *J. Inst. Met.*, Vol. 92, 1963-64, pp. 367-76

24. M.H. Mulazimoglu; *Electrical Conductivity Studies of Cast Al-Si and Al-Si-Mg Alloys*, Ph.D. Thesis, Mcgill University, Montreal, Canada, 1988

25. M.H. Mulazimoglu, R.A.L. Drew and J.E. Gruzleski; "Solution Treatment Study of Cast Al-Si Alloys by Electrical Conductivity", *Can. Metall. Quart.*, Vol. 28, 1989, pp. 251-58

26. B. Closset, K. Pirie and J.E. Gruzleski; "Comparison of Thermal Analysis and Electrical Resistivity in Microstructure Evaluation of Al-Si Foundry Alloys", *AFS Trans.*, Vol. 92, 1984, pp. 123-33

27. D. Emadi and J.E. Gruzleski; "The Effects of Casting and Melt Variables on Porosity in Directionally Solidified Al-Si Alloys", *AFS Trans.*, Vol. 102, 1994

28. Q.T. Fang and D.A. Granger; "Porosity Formation in Modified and Unmodified A356 Alloy Castings", *AFS Trans.*, Vol. 97, 1989, pp. 989-1000

29. H. Iwahori, K. Yonekura, Y. Yamamoto and M. Nakamura; "Occurring Behaviour of Porosity and Feeding Capabilities of Sodium and Strontium Modified Al-Si Alloys", *AFS Trans.*, Vol. 98, 1990, pp. 167-73

30. D. Argo and J.E. Gruzleski; "Porosity in Modified Aluminum Alloy Castings", *AFS Trans.*, Vol. 96, 1988, pp. 65-74

31. X.G. Chen and S. Engler; "Hydrogen and Porosity in Aluminum-Silicon and Aluminum-Magnesium Alloys", *Metall.*, 45 (10), Oct. 1991, pp. 1-17

32. E.N. Pan, H.S. Chiou and G.J. Liao; "Effects of Modification and Solidification Conditions on the Feeding Behaviour of A356 Al Alloy", *AFS Trans.*, Vol. 99, 1991, pp. 605-21

33. *Metals Handbook*, Vol. 15, 9th Edition, ASM, Ohio, OH, 1988, pp.747-60

34. M.K. Surappa, E. Blank and J.C. Jaquet; "Effect of Macro-Porosity on the Strength and Ductility of Cast Al-7Si-0.3Mg Alloy", *Scripta Met.*, Vol. 20, 1986, pp. 1281-86

35. E.N. Pan, C.S. Lin and C.R. Loper; "Effects of Solidification Parameters on the Feeding Efficiency of A356 Aluminum Alloy", *AFS Trans.*, Vol. 98, 1990, pp. 735-46

36. P.M. Thomas and J.E. Gruzleski; "Threshold Hydrogen for Pore Formation During the Solidification of Aluminum Alloys", *Metall. Trans. B*, Vol. 9B, March 1978, pp. 139-41

37. M.J. Lessiter; "Understanding Inclusions in Aluminum Castings", *Modern Casting*, Jan. 1993, pp. 29-31

38. T. Pederson; "Refining Efficiency on Hydrogen, Alkaline Metals and Inclusions in the Hydro Metal Refining System", *Light Metals*, 1991, pp. 1063-67

39. W.R. Opie and N.J. Grant; "Hydrogen Solubility in Aluminum and Some Aluminum Alloys", *Trans. AIME*, Vol. 188, J. Metals, 1950, pp. 1237-41

40. D.E.J. Talbot and P.N. Anyalebechi; "Solubility of Hydrogen in Liquid Aluminum", *Mater. Sci. Technol.*, Vol.4, Jan. 1988, pp. 1-4

41. C.E. Ransley and H. Neufeld; "The Solubility of Hydrogen in Liquid and Solid Aluminum", *J. Inst. Met.*, Vol.74, 1948, pp. 599-620

42. D.E.J. Talbot; "Effects of Hydrogen in Aluminum, Magnesium, Copper and Their Alloys", *Int. Met. Rev.*, Vol. 20, 1975, pp. 166-84

43. R.Y. Lin and M. Hoch; "The Solubility of Hydrogen in Molten Aluminum Alloys", *Metall. Trans. A*, Vol. 20A, 1989, pp. 1785-91

44. P.D. Hess; "An Empirical Equation For Calculating Solubility of Hydrogen in Molten Aluminum Alloys", *Light Metals*, 1974, pp. 591-97

45. G. Laslaz and P. Laty; "Gas Porosity and Metal Cleanliness in Aluminum Casting alloys", *AFS Trans.*, Vol. 99, 1991, pp. 83-90

46. K.J. Brondyke and P.D. Hess; "Interpretation of Vacuum Gas Test Results for Aluminum Alloys", *AIME Trans.*, Vol. 230, Dec. 1964, pp. 1542-46

47. C.E. Eckert; "Inclusions in Aluminum Foundry Alloys", *Modern Casting*, April 1991, pp. 28-30

48. H. Shahani and H. Fredriksson; "On the Mechanism of Precipitation of Pores in Metals", *Scand. J. Metall.*, Vol. 14, 1985, pp. 316-20

49. S.N. Tiwari and J. Beech; "Origin of Gas Bubble in Aluminum", *Met. Sci.*, Aug. 1978, pp. 356-62

50. E.L. Rooy; "Mechanism of Porosity Formation in Aluminum", *Modern Casting*, Sept. 1992, pp.34-36

51. A.M. Samuel and F.H. Samuel; "Porosity Factor in Quality Aluminum Castings", *AFS Trans.*, Vol. 100, 1992, pp. 657-66

52. P.S. Mohanty, F.H. Samuel, J.E. Gruzleski; "Mechanism of Heterogeneous Nucleation of Pores in Metals and Alloys", *Metall. Trans. A*, Vol. 24A, August 1993, pp. 1845-56

53. J. Campbell: *The Solidification of Metals*, ISI Publication No. 110, The Iron and Steel Institute, London, 1967, pp. 18-26

54. W. LaOrchan and J.E. Gruzleski; "Grain Refinement, Modification and Melt Hydrogen-Their Effects on Microporosity, Shrinkage and Impact Properties in A356 Alloy", *AFS Trans.*, Vol. 100, 1992, pp. 415-24

55. G.K. Sigworth; "A Scientific Basis for the Degassing of Aluminum", *AFS Trans.*, Vol. 95, 1987, pp. 73-78

56. D.R. Poirier, K. Yeum and A.L. Maples; "A Thermodynamic Prediction for Microporosity Formation in Aluminum-Rich Al-Cu Alloys", *Metall. Trans. A*, Vol. 18A, Nov. 1987, pp. 1979-87

57. K. Kubo and R.D. Pehlke; "Mathematical Modelling of Porosity Formation in Solidification", *Metall. Trans. B*, Vol. 16B, June 1985, pp. 359-66

58. K. Yeum and D.R. Poirier; "Predicting Microporosity in Aluminum Alloys", *Light Metals*, 1988, pp. 469-76

59. G.K. Sigworth and C. Wang; "Mechanisms of Porosity Formation During Solidification: A Theoretical Analysis", *Metall. Trans. B*, Vol. 24B, 1993, pp. 349-64

60. M. Bamberger, B.Z. Weiss and M.M. Stupel; "Heat Flow and Dendritic Arm Spacing in Chill-Cast Al-Si Alloys", *Mater. Sci. Technol.*, Vol.3, Jan. 1987, pp. 49-56

61. Q.S. Hamed and R. Elliot; "The Dependence of Secondary Dendrite Arm Spacing on Solidification Conditions-II. Al-7Si-0.5Mg Alloys treated with Sr and Sb", *Cast Metals*, Vol. 6, No. 1, 1993, pp. 42-46

62. G. Lang; "The Influence of Alloying Elements on the Surface Tension of Liquid Super Purity Aluminum", *Aluminium*, 50 (11), Nov. 1974, pp. 731-34

63. V.L.Davies and J.M. West; "Influence of Small Additions of Sodium on the Surface Tension of Aluminum and Aluminum-Silicon Alloys", *J. Inst. Met.*, Vol. 92, 1963-1964, pp. 208-10

64. G. Lang; "Casting Properties and Surface Tension of Aluminium and Binary Aluminum Alloys, Part III: Surface Tension", *Aluminium*, 49 (3), March 1973, pp. 231-38

65. F.C. Dimayuga, N. Handiak and J.E. Gruzleski; "The Degassing and Regassing Behaviour of Strontium-Modified A356 Melts", *AFS Trans.*, Vol. 96, 1988, pp. 83-88

66. J.E. Gruzleski, N. Handiak, H. Campbell and B. Closset; "Hydrogen Measurement by Telegas in Strontium Treated A356 Metals", *AFS Trans.*, Vol. 94, 1986, pp. 147-54

67. H. Shahani; "Effect of Hydrogen on the Shrinkage Porosity of Aluminum Copper and Aluminum Silicon Alloys", *Scand. J. Metall.*, No. 14, 1985, pp. 306-12

68. M.H. Mulazimogla, N. Handiak and J.E. Gruzleski; "Some Observations on the Reduced Pressure Test and Hydrogen Concentration of Modified A356 Alloy", *AFS Trans.*, Vol. 97, 1989, pp. 225-33

69. S.C. Flood and J.D. Hunt; "Modification of Al-Si Eutectic Alloys with Na", *Metal Science*, Vol. 15, July 1981, pp. 287-93

70. D. Emadi, J.E. Gruzleski and J.M. Toguri; "The Effect of Na and Sr-Modification on Surface Tension and Volumetric Shrinkage of A356 Alloy and Their Influence on Porosity Formation", *Metall. Trans. B*, Vol. 24B, Dec. 1993, pp. 1-9

71. D. Emadi and J.E. Gruzleski; "The Study of Some Probable Causes of Porosity Formation in Sr and Na-modified Al-Si Alloys", 32nd C.I.M. Conference, Light Metals, Quebec City, Canada, August 1993, pp. 373-82

Chapter 2

Quantitative Evaluation of Porosity in Sr-Modified Al-Si Alloys

2.1 Introduction

As discussed in Chapter 1, Na and Sr-modification significantly increase pore volume fraction and pore size in castings. Studies of porosity formation in modified and unmodified Al-Si alloys have usually been qualitative in nature, but it is essential to define quantitatively the effects of the Na and Sr-modification on porosity. Fang and Granger[1] have studied the effect of Sr-modification on pore volume fraction and pore size in a grain-refined A356 alloy using directional solidification (Figures 2.1 and 2.2).

It is shown in Figures 2.1 and 2.2 that the addition of 0.06 wt% Sr increases both the pore volume fraction and the average pore diameter at different cooling rates (compare curves 2 and 5). However, these results show the combined effects of grain-refinement and modification, and therefore, a separate study on the effect of modification alone on porosity at different hydrogen levels is required. Chen and Engler[2] have also investigated the effect of Sr and Si on porosity at different hydrogen contents in hypoeutectic Al-Si alloys. It is observed from their results that Sr increases the porosity in the casting, and this effect is more significant at higher levels of silicon (by increasing

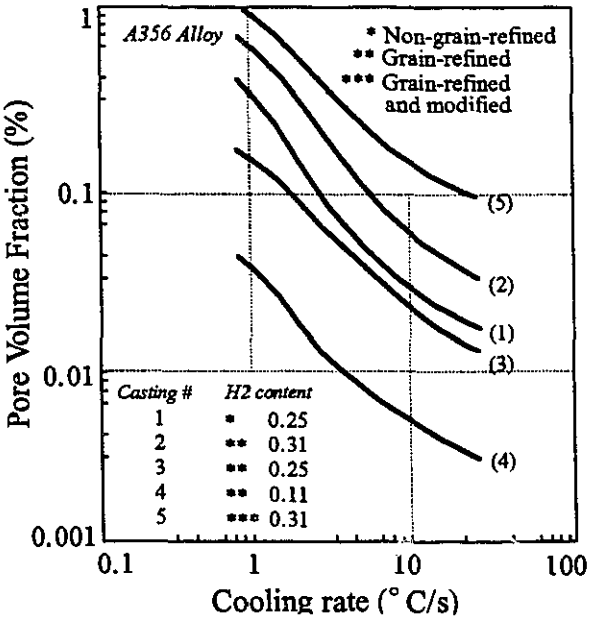

Figure 2.1 : Pore volume fraction as a function of cooling rate for A356 alloy cast under different conditions[1].

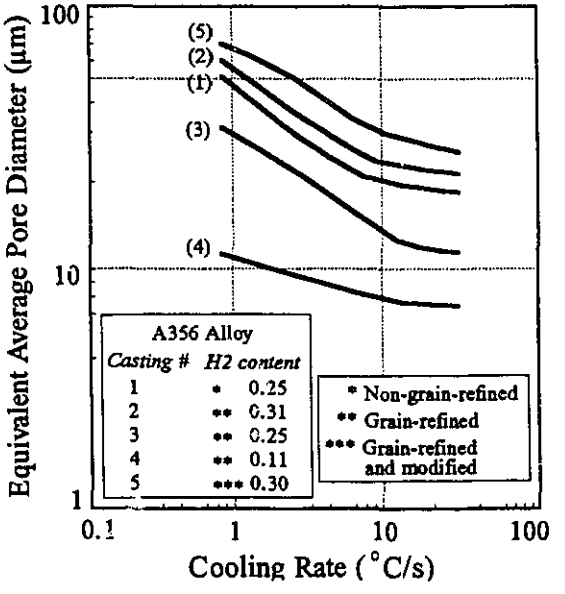

Figure 2.2 : Equivalent average pore diameter as a function of cooling in A356 alloy cast under different conditions[1].

from 7 to 12 wt% Si). However, the effect of strontium at different cooling rates on pore volume fraction and pore size was not studied in their work. Therefore, for a better understanding of the mechanism by which Sr-modification increases the porosity in castings, it is necessary to establish a set of controlled experiments to investigate the effect of Sr on both pore volume fraction and pore size at different hydrogen contents and cooling rates in Al-Si alloys.

2.2 Experimental Procedures

A356 alloy, whose chemical composition is given in Table 2.1, was used in this investigation. In each experiment, a 9-kg melt was prepared in a silicon carbide crucible using an electric resistance furnace. The melt temperature was held constant at about 730 °C for both modified and unmodified melts. To obtain various hydrogen levels, the melt was held under different controlled moist atmospheres for more than two and a half hours to reach equilibrium. Since the same melt was used for both modified and unmodified castings, degassing which may change the inclusion level was not applied. The experiments were carried out at two hydrogen levels of 0.13 and 0.26 ml/100 g Al for both Sr-modified and unmodified alloys.

Hydrogen measurements were performed in-situ using a recirculating gas technique based on the Telegas instrument. In this work, The ALCOA Telegas instrument[3,4] was used with ALSCAN probes[4,5] due to their lower price compared to ALCOA probes. The Telegas instrument operates on the principle of monitoring the hydrogen activity developed in a small quantity of nitrogen continuously recirculated through the molten metal under test until the gaseous hydrogen which diffuses into the nitrogen is in equilibrium with the solute hydrogen in the molten metal. A schematic of the ALSCAN probe is given in Figure 2.3. The hydrogen content (ml/100 g Al at STP) is obtained by

Table 2.1. Chemical Analysis of A356 Alloy

Elements	wt. pct.
Si	7.0 ± 0.15
Mg	0.3 ± 0.01
Fe	0.11 ± 0.002
Cu	0.01± 0.002
Mn	0.01 ± 0.001
Zn	0.02 ± 0.002
Ti	0.10 ± 0.003
Al	balance

measuring the thermal conductivity of the gas mixture with a katharometer. In the present study, three measurements were taken consecutively for a duration of 10 minutes to obtain a reliable measure of the dissolved gas concentration.

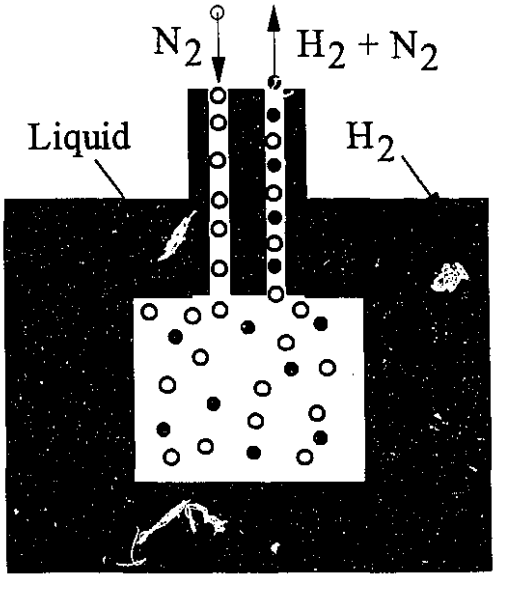

Figure 2.3 : Schematic of the Alcan hydrogen probe.

In addition, Ransley samples[6] were taken and were analyzed by the nitrogen carrier fusion technique (LECO™ sub-fusion method). In this method, a small quantity of the melt was solidified in a specially designed chill mould known as the Ransley mould to trap almost all hydrogen present in the liquid. A cylindrical sample 10 mm diameter by 40 mm length was prepared from this casting. Special care was taken to avoid contamination during preparation of the sample. This method of hydrogen determination comprises the collection and measurement of hydrogen desorbed into an evacuated system from the specially prepared solid sample. The sample is heated to a temperature below the eutectic or solidus, but high enough to allow virtually all of the hydrogen to diffuse out of the sample during the extraction time, which varies from 1-2.5 hrs depending on the heating temperature. A comparison of hydrogen measurements from these two techniques (i.e. Telegas and LECO sub-fusion methods) is shown in Figure 2.4.

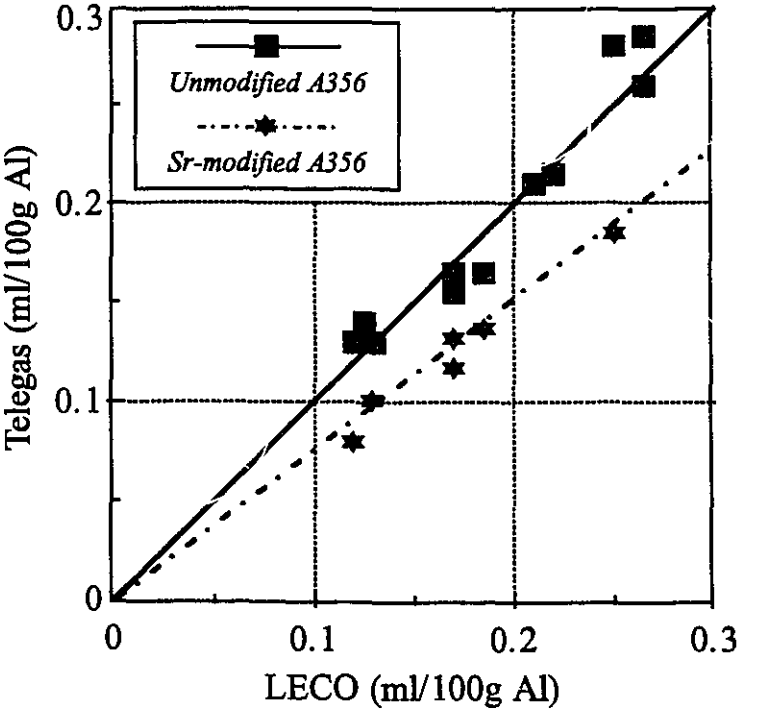

Figure 2.4 : A comparison of the results of hydrogen measurements from Telegas and LECO sub-fusion methods.

It is observed from this figure that the measurements from these two techniques agree well for non-modified alloys, but do not agree when Sr is present, particularly at higher gas levels. The reasons for this are not clear, but may be related to the type of probes used in these experiments (i.e. ALSCAN probe). This idea is supported by the fact that Gruzleski *et al* [7,8] have measured hydrogen in Sr-modified A356 alloy using ALCOA probes and they did not report any problem in the hydrogen measurements. Therefore, the hydrogen analyses obtained by the LECO sub-fusion method were taken as the true values. Samples for chemical analysis were also taken from the melt prior to pouring each casting, and these were analyzed by vacuum emission spectrometry.

To study the effect of cooling rate and to eliminate the feeding problem, castings were unidirectionally solidified using the apparatus shown in Figure 2.5. Moulds were made of BNZ Metalform insulating board, a shock-resistant inorganic refractory material, and machined to the shape and dimensions shown in Figure 2.6. Cooling water was turned onto the base of the casting immediately after pouring, and the copper plate at the bottom of the mould was withdrawn 30 sec after filling the mould (i.e. after establishing a layer of solid) to allow the water jet to impinge directly onto the casting. In order to obtain better unidirectional solidification and eliminate mould moisture, the moulds were coated with an iron oxide wash and preheated up to 500 °C in an electric resistance furnace.

The variation of temperature with time along the castings was monitored from the filling stage to the end of solidification by inserting eight K-type thermocouples along the axis of the mould as shown in Figure 2.6. The cooling rate for each location of thermocouple was calculated from the slope of the temperature-time curves (Figure 2.7) in the mushy zone (i.e. between liquidus and solidus) which yields the average cooling rate ($\Delta T/\Delta t$) between 615 °C and 560 °C (i.e. approximately the liquidus and solidus temperatures of A356 alloy).

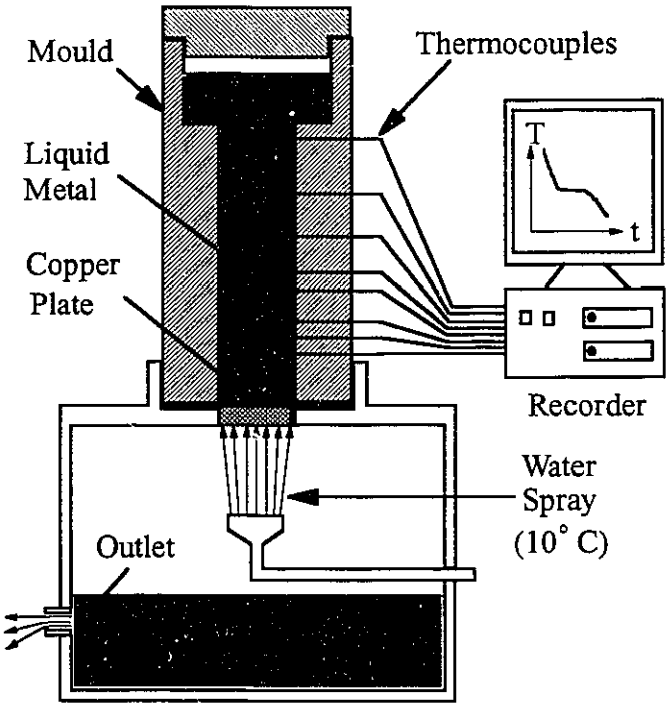

Figure 2.5 : Schematic of the experimental setup.

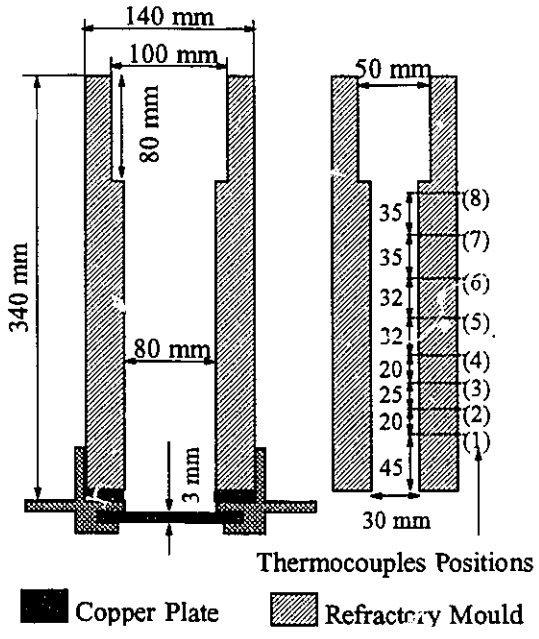

Figure 2.6 : Schematic and dimensions (in mm) of the mould.

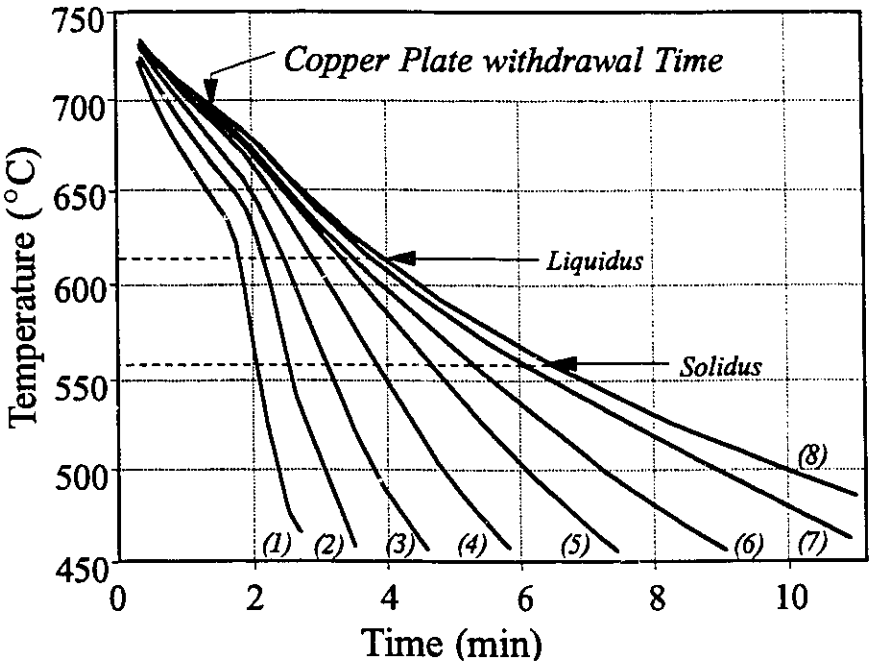

Figure 2.7 : The temperature-time curves from 8 thermocouples along the axis of the mould as shown in Figure 2.6.

After pouring the first casting, the remaining melt was held again for about two and a half hours to stabilize the temperature and the melt hydrogen. At that point, 0.02 wt% strontium was added to the melt by commercial Al-10 wt% Sr master alloy, and the melt was held for thirty minutes to allow dissolution of the strontium. Several hydrogen measurements were made before and after modifier addition in order to determine whether these additions introduced hydrogen into the melt. A minimum of two experiments was carried out for each level of hydrogen for both Sr-modified and unmodified alloys.

After solidification, a 2 cm length from the chilled end and an 8 cm length from the top, which acts as a riser, were discarded because of lack of directional heat

extraction at these locations. The remainder of the casting was cut at the thermocouple positions and machined into nine pieces for various analyses. A layer of about 5 mm was machined from the surface of the samples to remove the surface porosity and to obtain a smooth surface for higher accuracy in density measurements. The density of these samples was measured by weighing them in air and in water. The density of the water itself was measured since a minor amount of Teepol 610, a surface tension reducing agent, was added to the distilled water bath to ensure the wetting of samples.

The amount of porosity (pore volume fraction) in the samples was determined by comparing the density of the samples (ρ_{sam}) to the theoretical density of the porosity-free alloy (ρ_{theo}). The pore volume fraction is therefore equal to (ρ_{theo} - ρ_{sam})/ρ_{theo}. The theoretical densities of the alloys were determined from the bottom portion of degassed specimens cast into a water-cooled copper mould as described in more detail in Chapter 4. The theoretical density of the unmodified and Sr-modified A356 alloy were determined to be 2.675 $\pm$0.002 and 2.678 $\pm$0.002 g/cm^3, respectively.

Image analysis was performed on some of the A356 alloy samples using a LECO 2005 image analysis system. Each sample was evaluated for the area percentage porosity, average pore diameter and pore density (number of pores per square cm). A total area of 2 cm^2 was scanned per sample, and chord sizes less than 14 μm were omitted to eliminate the effect of noise or silicon particles with the same grey level as pores.

2.3 Results and Discussion

The average cooling rate calculated from cooling curves (thermal analysis) as a function of distance from the chill is shown in Figure 2.8. These rates range from about 4.5 °C/sec down to about 0.35 °C/sec which is a typical range of cooling rates found in commercial casting processes from die casting to sand mould casting. Since the castings

were cut at the thermocouple positions, an average of the cooling rates between the two thermocouple positions was considered to be the average cooling rate of that sample. In addition, hydrogen measurements before and after Sr addition showed that strontium does not change the hydrogen level of the melt as reported previously[8,9]. The effect of Sr-modification on hydrogen pick-up will be studied in Chapter 7.

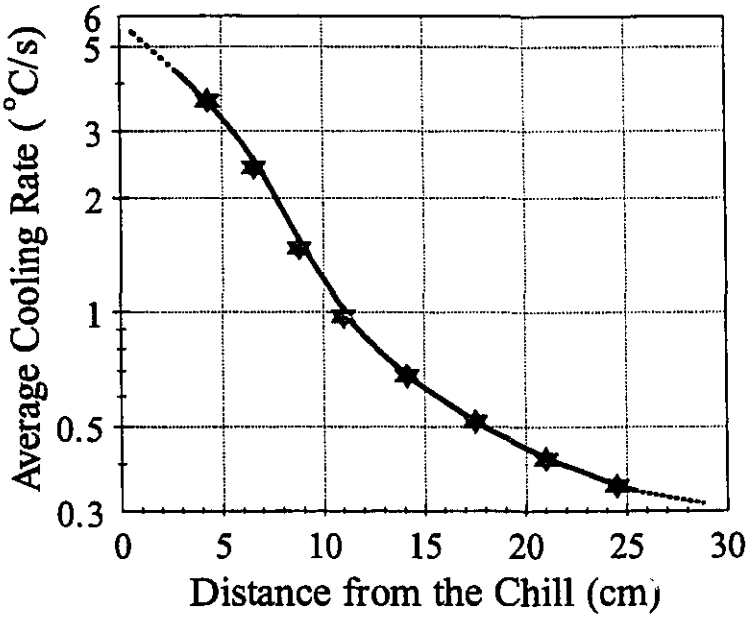

Figure 2.8 : The average cooling rate as a function of the distance from the chill surface in A356 alloy castings.

The average pore volume fractions calculated from density measurements are shown in Figure 2.9 as a function of average cooling rate for unmodified and Sr-modified A356 alloy at two hydrogen levels. It is evident in Figure 2.9 that for both Sr-modified and unmodified alloys, the pore volume fraction decreases as the cooling rate increases for a given hydrogen content, and at a given cooling rate, the pore volume fraction increases with hydrogen content. At lower cooling rates (typically less than 1 °C/sec) the cooling rate dependence of the pore volume fraction increases markedly and the pore

volume fraction becomes much more sensitive to hydrogen level.

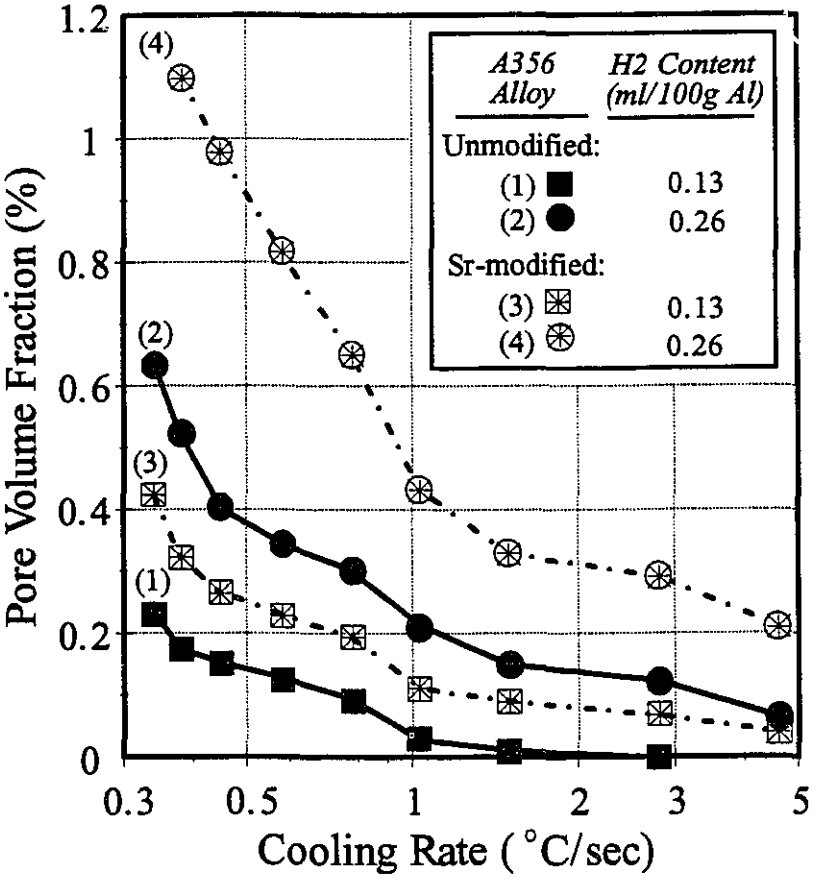

Figure 2.9 : The average pore volume fraction as a function of cooling rate for unmodified and Sr-modified A356 castings.

It is also interesting to note in Figure 2.9 that for the same hydrogen content and cooling rate, strontium modification increases the pore volume fraction significantly. This increase in pore volume fraction due to modification is much higher at lower cooling rates. A comparison of the curves of Sr-modified and unmodified A356 alloys at different hydrogen levels (Figure 2.9) shows that the increase in porosity due to modification is much more at higher hydrogen contents, eg. at 0.26 ml/100g. At low levels of hydrogen,

i.e. below 0.13 ml/100g, the effect of modification on porosity is less significant. It also appears in Figure 2.9 that at high levels of hydrogen, a critical cooling rate of about 1 °C/sec exists below which the difference in pore volume fraction between modified and unmodified alloys becomes more significant. Therefore, to avoid modification induced porosity in A356, the melt hydrogen content should be lowered to at least 0.1 ml/100g alloy by degassing of the melt, and the local cooling rate should be greater than 1.5 °C/sec.

The results in Figure 2.9 are in good agreement with those found by Fang and Granger[1] for similar conditions (Figure 2.1). They have reported that in a non-grain refined A356 alloy containing 0.25 ml/100g hydrogen, the pore volume fraction increases from 0.08% to 0.3% with a change in the cooling rate from 3 °C/sec to 0.8°C/sec. The present results (curve 2 in Fig. 2.10) indicate an increase from 0.1% to 0.3% for the same change in cooling rate. Fang and Granger used generally higher cooling rates (1 to 30 °C/sec) than those used in this work, and Sr addition was carried out at a hydrogen level of 0.31 ml/100g and on grain-refined A356 alloy, whereas no grain refiner was used in the present experiments. A comparison between the results of their work and the present is made in Table 2.2. It is shown that by decreasing the cooling rate, the difference in pore volume fraction between Sr-modified and unmodified alloys decreased in their work, while it increases in the current study.

Table 2.2. Pore volume fraction (P.V.F.) as a function of cooling rate in A356 alloy from the work by Fang and Granger[1] and the present study.

	0.8°C/sec		3°C/sec	
	unmodified	Sr-modified	unmodified	Sr-modified
P.V.F. (Fang *et al*)	0.7 %	1.1 %	0.22 %	0.38 %
P.V.F. (Present study)	0.28 %	0.62 %	0.12 %	0.29 %

The average pore area percent measured by image analysis as a function of average cooling rate is shown in Figure 2.10 for both Sr-modified and unmodified A356 alloy at different hydrogen contents. Observations similar to those made previously on the variation of pore volume fraction with cooling rate or the effect of modification can be made, but the amount of porosity measured by image analysis as pore area percent seems to be less than that calculated from the density (i.e. pore volume fraction), especially at low cooling rates. The reason could be due to this fact that some pores were closed by the soft α-phase matrix during grinding operations, and therefore, the samples should be ground for a sufficient time with a fine grinding paper to open the pores on the surface.

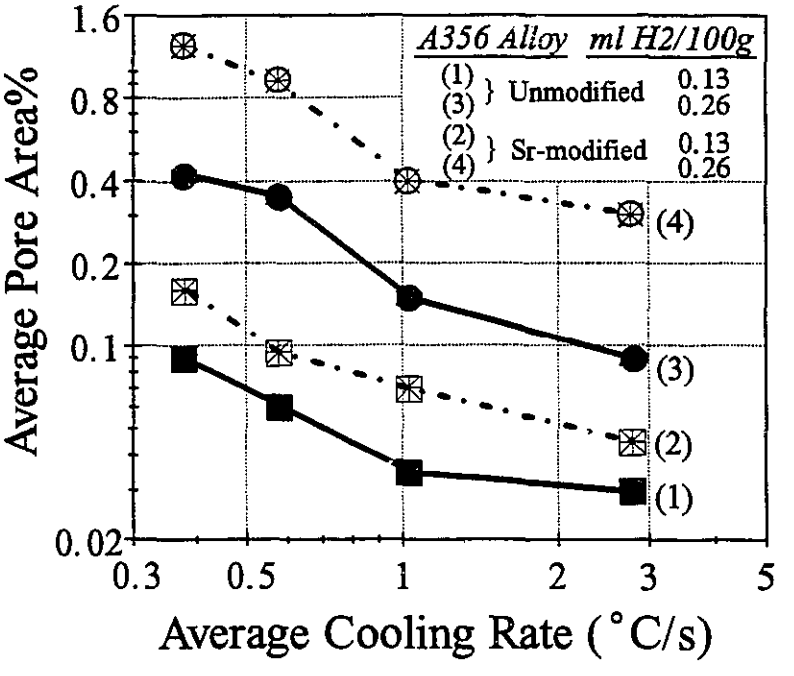

Figure 2.10 : The average pore area percent measured by image analysis as a function of average cooling rate for A356 castings.

To determine whether the increased pore volume fraction observed in Sr-modified alloy is due to the increase in pore size or number of the pores, the pore size was measured as the equivalent average pore diameter, defined as the diameter of a circle with

an area equivalent to the measured average pore area. Variation of this quantity with cooling rate and melt hydrogen content is shown in Figure 2.11 where it is observed that the average pore diameter decreases as the cooling rate increases and as the hydrogen content decreases. This effect is due to the shorter time available for hydrogen diffusion prior to complete solidification. Figure 2.11 also reveals that strontium addition increases the equivalent pore diameter. For example, at a cooling rate of 1 °C/sec and 0.26 ml/100g hydrogen, the equivalent average pore diameter increases from 30 to 50 μm on modification. A comparison of the results in Figure 2.11 with those found by Fang and Granger for non-grain refined A356 alloy containing 0.25 ml/100g hydrogen reveals that their average pore diameter values are higher than those found here over all ranges of cooling rates.

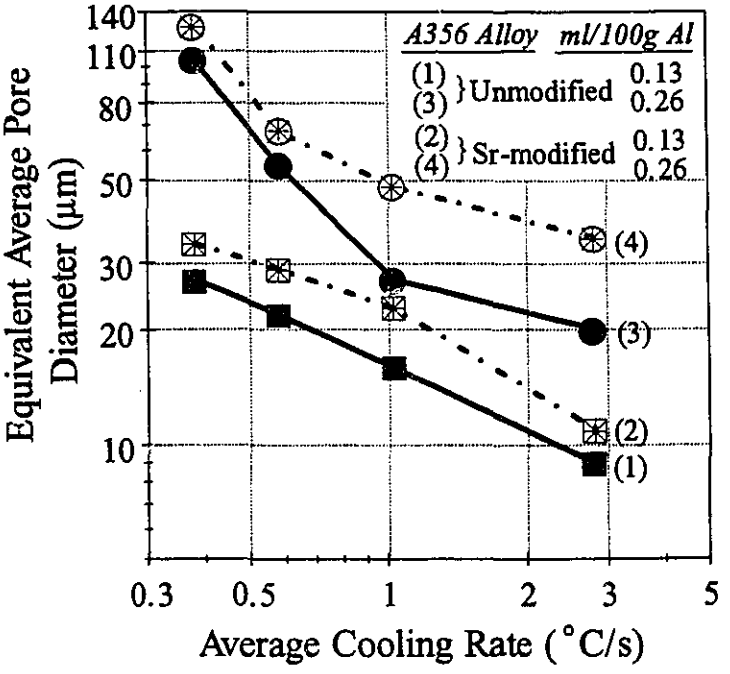

Figure 2.11 : Equivalent average pore diameter as a function of cooling rate for unmodified and Sr-modified A356 castings.

The pore number distributions as a function of size for the samples containing 0.26

ml/100g hydrogen and cooled at a rate of 0.38 °C/sec are shown in Figures 2.12a,b for unmodified and Sr-modified samples, respectively. Figure 2.12a, for unmodified alloy, shows that the maximum pore size is approximately 270 μm. In modified alloys (Figure 2.12b), the pore size range is wider with a maximum pore size of about 390 μm. A comparison of the total pore number density, i.e. the area under the curves in Figures 2.12 does indicate a higher pore number density (about two times) in the strontium-modified alloy. In addition, there seem to be two maxima in the pore size distribution curves (Figures 2.12a,b), with bimodal behaviour more obvious in the case of Sr-modified alloys. Micrographs of the samples from which the data in Figures 2.12a,b were obtained are shown in Figures 2.13a,b where it is evident that larger and rounder pores are present in modified castings. The pores in unmodified alloys are small and irregular while in Sr-modified alloys, most of the pores are round and tend to be isolated. Similar observations have been reported in the literature[1,10,11].

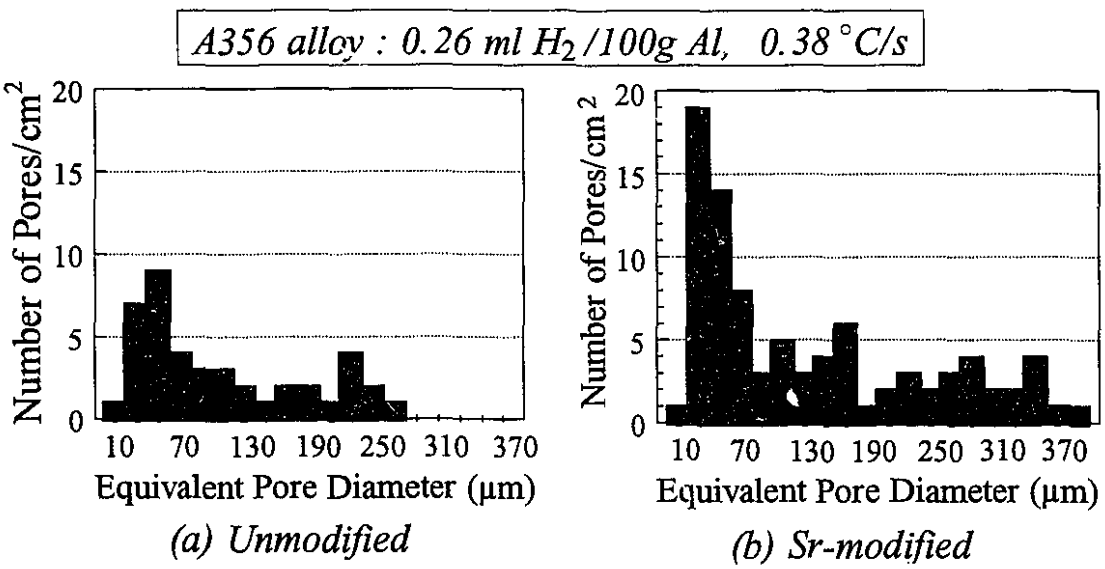

Figure 2.12 : The pore number distributions as a function of size for a) unmodified b) Sr-modified A356 alloy (at 0.38 °C/s and 0.26 ml/100g hydrogen).

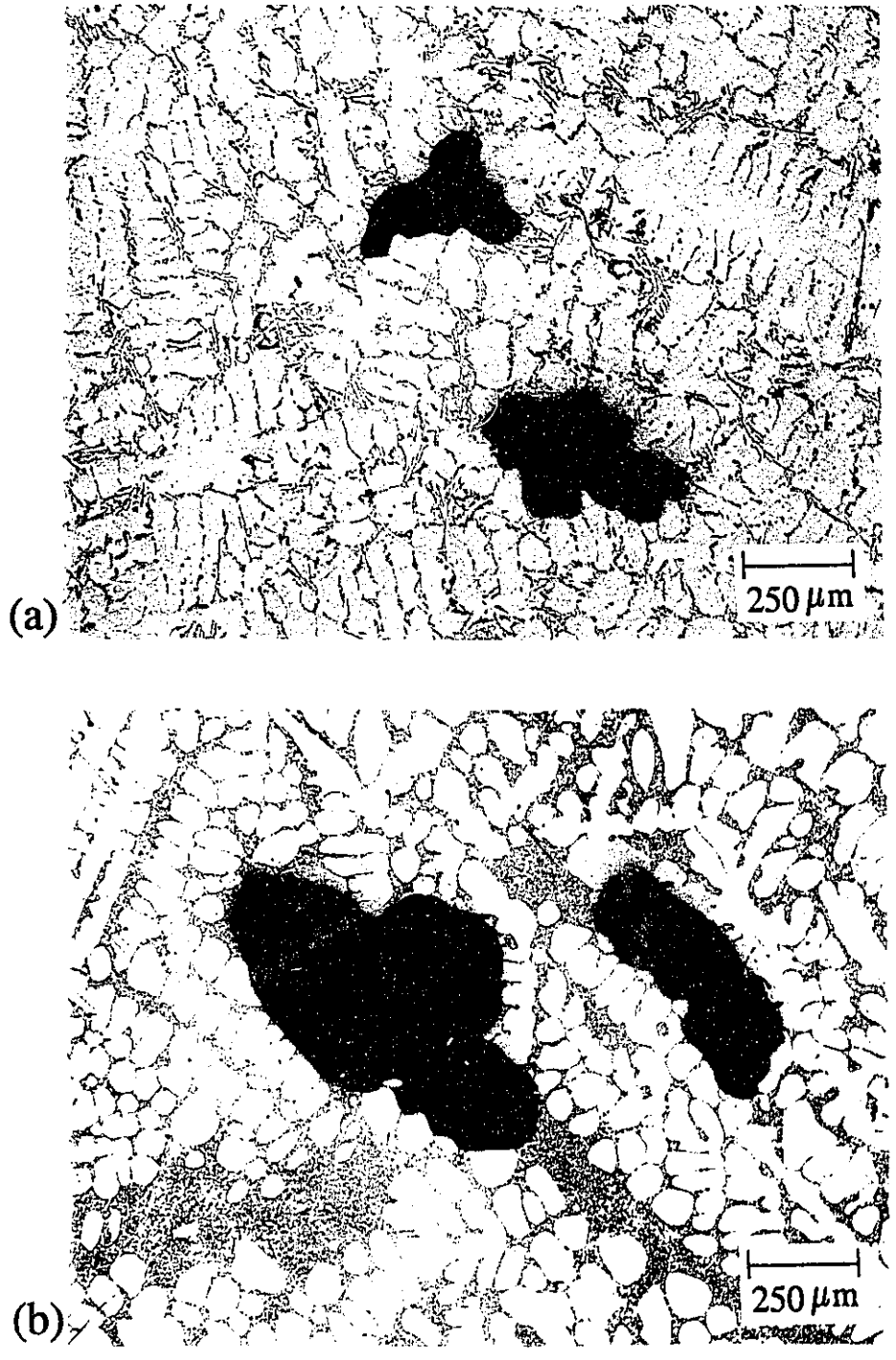

Figure 2.13 : Micrograph of the samples from which the data in Figure 2.12 were obtained a) unmodified b) Sr-modified A356 alloys.

The observations made in these controlled experiments on the quantification of porosity in Sr-modified A356 alloy can be summarized as follows:

1. The addition of strontium in the form of a commercial Al-10 wt%Sr master alloy to A356 alloy does not introduce hydrogen into the melt and hence the hydrogen content of the melt remains unchanged.
2. For a given melt hydrogen content (in both Sr-modified and unmodified A356 alloys), the pore volume fraction and the pore size decrease as the cooling rate increases, and this cooling rate dependence of the pore volume fraction increases markedly at lower cooling rates (typically less than 1 °C/sec).
3. For a given cooling rate (in both Sr-modified and unmodified A356 alloys), the pore volume fraction and the pore size increase with hydrogen content, and this increase becomes larger at lower cooling rates.
4. For the same hydrogen content and cooling rate, strontium modification increases the pore volume fraction, the pore size and the pore number density of A356 alloy significantly. This increase in pore volume fraction due to modification is much higher at lower cooling rates (i.e. below about 1 °C/sec) and at higher hydrogen contents.
5. To avoid modification induced porosity in A356 alloy, the melt hydrogen content should be lowered to at least 0.1 ml/100g by degassing of the melt, and the local cooling rate should be greater than 1.5 °C/sec.

2.4 References

1. Q.T. Fang and D.A. Granger; "Porosity Formation in Modified and Unmodified A356 Alloy Castings", *AFS Trans.*, Vol. 97, 1989, pp. 989-1000

2. X.G. Chen and S. Engler; "Hydrogen and Porosity in Aluminum-Silicon and Aluminum-Magnesium Alloys", *Metall.*, 45 (10), Oct. 1991, pp. 1-17

3. D.A. Anderson, D.A. Granger and R.R. Avery; "The ALCOA Telegas II Instrument", *Light Metals*, 1990, pp. 769-73

4. P.N. Anyalebechi; "Techniques for Determination of the Hydrogen Content in Aluminum and Its Alloys", *Light Metals,* 1991, pp. 1025-45

5. J.P. Martin, F. Tremblay and G. Dube; "Hydral: A New Simple Technique for In-line Analysis of hydrogen in Aluminum Alloys", *Light Metals*, 1989, pp. 903-12

6. C.E. Ransley and D.E.J. Talboy; "The Routine Determination of the Hydrogen Content of Aluminum and Aluminum Alloys by the Hot-Extraction Method", *J. Inst. Met.*, Vol. 84, 1955-1956, pp. 445-53

7. J.E. Gruzleski, N. Handiak, H. Campbell and B. Closset; "Hydrogen Measurement by Telegas in Strontium Treated A356 Metals", *AFS Trans.*, Vol. 94, 1986, pp. 147-54

8. F.C. Dimayuga, N. Handiak and J.E. Gruzleski; "The Degassing and Regassing Behaviour of Strontium-Modified A356 Melts", *AFS Trans.*, Vol. 96, 1988, pp. 83-88

9. M.H. Mulazimogla, N. Handiak and J.E. Gruzleski; "Some Observations on the Reduced Pressure Test and Hydrogen Concentration of Modified A356 Alloy", *AFS Trans.*, Vol. 97, 1989, pp. 225-33

10. E.N. Pan, H.S. Chiou and G.J. Liao; "Effects of Modification and Solidification Conditions on the Feeding Behaviour of A356 Al Alloy", *AFS Trans.*, Vol. 99, 1991, pp. 605-21

11. D. Argo and J.E. Gruzleski; "Porosity in Modified Aluminum Alloy Castings", *AFS Trans.*, Vol. 96, 1988, pp. 65-74

Chapter 3

The Effect of Sr-Modification on Surface Tension of A356 Alloy

3.1 Introduction

Some authors have suggested that the addition of reactive elements, such as strontium and sodium, to the melt reduces the surface tension of the liquid metal and so facilitates the nucleation of pores[1,2,3]. To study whether the observed increase in porosity in modified alloys is due to this factor, it is necessary to determine the surface tension of liquid Al-Si alloys modified with strontium or sodium.

Surface tension is defined thermodynamically as the surface free energy per unit area. When two phases are in contact, for example a condensed and a vapour phase, the surface of separation is in a higher energy state than the condensed phase, because coordination among the atoms at the surface is incomplete. The existence of a tension force acting in the surface leads to a pressure drop across the surface when it is curved as described by the Laplace equation:

$$\Delta P = \gamma \left(\frac{1}{R_1} + \frac{1}{R_2} \right) \qquad (3.1)$$

where γ is the surface tension or interface tension, R_1 and R_2, are the principal radii of

curvature of the surface at a point on the interface, and ΔP is the pressure difference across the interface at the point considered.

The surface tension of a liquid phase can be measured by a number of experimental techniques such as: maximum bubble pressure method, sessile drop method, pendant drop method, capillary rise method, drop pressure method, drop weight method and Wilhelmy plate method[4,5,6,7]. These methods are all based on some form of the Laplace equation. Of these techniques, the first three are the most satisfactory and accurate methods for measuring the surface tension of liquid metals, particularly at high temperatures. In addition, these methods are the simplest to use. In the present work, the sessile-drop technique was chosen and will be explained in some detail.

3.1.1 The Sessile Drop Method

This method is based on the measurement of the dimensions of a liquid drop resting on a horizontal substrate. In the case of an axisymmetric drop, Figure 3.1, equation (3.1) has been modified[5,8] as:

$$\frac{1}{(R'' / b)} + \frac{\sin\phi}{(X/b)} = 2 + \delta \left(\frac{Z}{b}\right) \qquad (3.2)$$

where:

$$\delta = \frac{g b^2 \rho}{\gamma} = \frac{2 b^2}{a^2} \quad (shape\ factor) \qquad , \qquad a^2 = \frac{2\gamma}{\rho g}$$

In this equation, γ is the surface (liquid-vapour) tension, R'' is the radius of curvature at point S (distance PS), b is the radius of curvature at O, ρ is the liquid density, g is the gravitational acceleration and X, Z, ϕ are as shown in the Figure 3.1.

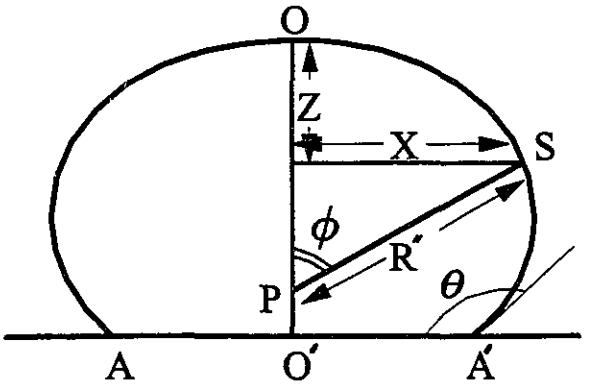

Figure 3.1 : Bashforth and Adams' profile of a sessile drop[5].

Usually, the measurement of X and Z is done at $\phi = 90°$ so that the angle does not have to be measured. Bashforth and Adams[8] prepared tables of δ and X/Z for $\phi = 90°$, and tables of X/b and Z/b for different values of δ and ϕ. From a measurement of X and Z at $\phi = 90°$, δ and b can be determined from these tables, and the surface tension is calculated from:

$$\gamma = \frac{g \rho b^2}{\delta}$$

Other approaches such as the Dorsey equation or the Worthington equation[4,9] have also been developed for calculation of surface tension; however, these calculations are unreliable because they depend on two or three measured values that are difficult to determine with high accuracy.

3.1.2 Evaluation of previous work

The data available for surface tension of aluminum systems are mostly for pure aluminum, and only a few studies have been done on the influence of alloying elements

on the surface tension of aluminum. Davies and West [10] have measured the effects of sodium and silicon on surface tension of pure Al and binary Al-Si alloys at different temperatures using the maximum bubble pressure method. Their results are shown in Figures 3.2 and 3.3.

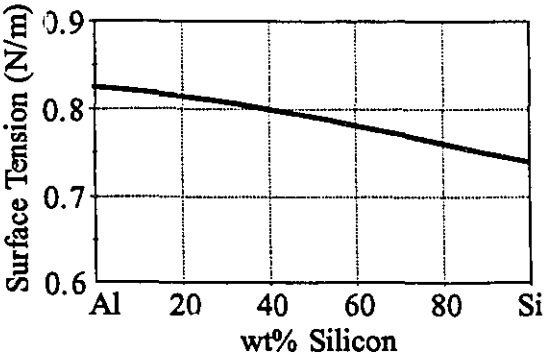

Figure 3.2 : Surface tension as a function of silicon concentration[10].

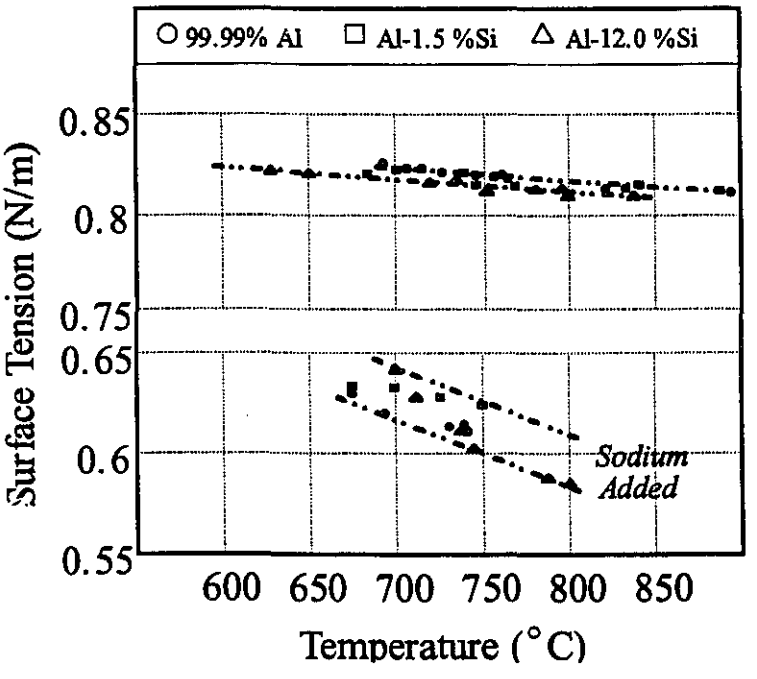

Figure 3.3 : The effect of Na on surface tension of pure Al and binary Al-Si alloys[10].

It is seen in Figure 3.2 that silicon addition has a small effect on the surface tension of liquid aluminum, i.e., the surface tension of pure aluminum changes from 0.825 N/m to 820 N/m by adding 12 wt% Si (i.e., eutectic composition). The results in Figure 3.3 show that Na-modification decreases the surface tension of binary Al-Si alloys in the range of 0.60-0.65 N/m depending on the silicon content and temperature. However, the exact amount of Na added was not reported.

Lang[11,12] has measured the influence of additional alloying elements such as Si, Sr, Mg, and Fe, on the surface tension of pure aluminum at 700 °C using the maximum bubble pressure method. According to his investigations, 0.01 wt% Na reduces the surface tension of pure aluminum by about 0.230 N/m and the dependence for Sr, Si, Mg and Fe has been expressed as:

$\gamma_{AlSr} = 0.862 - 0.03784 \ln(46.09 \text{ wt.\% Sr} + 1)$ (N/m) for up to 0.4 wt.% Sr

$\gamma_{AlSi} = 0.851 - 0.00217 \text{ wt.\% Si}$ (N/m) for up to 18 wt.% Si

$\gamma_{AlMg} = 0.851 - 0.0419 \text{ wt.\% Mg}$ (N/m) for up to 1.5 wt.% Mg

$\gamma_{AlFe} = 0.851 + 0.00062 \text{ wt.\% Fe}$ (N/m) for up to 2 wt.% Fe

The higher value of surface tension for pure aluminum in the case of Al-Sr (i.e., 0.862 N/m) compared to the others (i.e., 0.851 N/m) is due to the different ratio of the impurities in the pure aluminum used for those experiments.

Other data[4,9,13,14] on surface tension of binary and ternary aluminum alloys show a good agreement with the results mentioned above. The surface tension of binary alloys can also be predicted using a thermodynamic model given by Poirier and Speiser[15]. According to them, the surface tension of the hypoeutectic Al-Si alloys along the liquidus can be calculated as [16]:

$$\gamma = 0.864 - \frac{24.781\,C_L + 2.7856\,C_L^{\,2} - 0.11532\,C_L^{\,3}}{1000} \qquad (N/m) \qquad (3.5)$$

where the surface tension, γ, is in N/m and the liquid composition (along liquidus), C_L, is in wt% Si.

Despite the data available on the effect of Sr and Na on the surface tension of pure aluminium, no work has been published on the effect of strontium on the surface tension of Al-Si alloys. Since A356 alloy has been used as the base alloy in this research, this chapter deals with the surface tension measurement of liquid A356 alloy in the presence of sodium and strontium.

3.2 Experimental Procedure

3.2.1 Materials

Materials investigated in the present study were prepared by adding pure sodium and Al-10 wt% Sr master alloy to an A356 base alloy. In order to obtain a homogeneous material, the alloys were cast in a cylindrical graphite mould with an inner diameter of 10 mm, and the samples were machined to the desired size. The chemical analysis of A356 has been summarized in Table 2.1 (in Chapter two).

Surface tension evaluation was done on four series of specimens. A total of 6 series of samples with different compositions was used, and at least six experiments were carried out on each sample, as follows:

- A356, as received
- Al-10 wt% Sr (Sr master alloy)
- Na modified A356 with sodium level: a) 0.009 wt% b) 0.015 wt%

- Sr modified A356 with strontium level: a) 0.025 wt% b) 0.04 wt%

3.2.2 Apparatus

The schematic of the apparatus used in these experiments is shown in Figures 3.4 and 3.5. Since this equipment (Fig. 3.4) was originally designed for measurement of the surface tension of slags, a new set-up was used for the present work, as shown in Figure 3.5. Since oxygen is highly reactive with aluminum alloys and since the oxides have a significant effect on surface tension[14,6,17] , the surface of all specimens was ground and cleaned with HF solution and washed with methyl alcohol. In addition, the experiments were done under ultra high purity argon after outgassing the system by a vacuum of 10^{-2}-10^{-3} mm Hg. The argon was further purified by bubbling it through liquid sodium held at 150 °C and the remaining oxygen in the system was reduced by a titanium getter placed inside the graphite cell (Fig. 3.5).

The polishing procedure of the alumina substrates used in these experiments consisted of grinding the samples using 240 and 600 grit diamond grinding discs followed by polishing using 15 μm diamond paste on nylon polishing cloth. The furnace temperature was controlled by placing a thermocouple at the bottom of the reaction tube, and the real melt temperature was measured separately by inserting another thermocouple (K-type) inside the reaction tube in direct contact with the graphite tube (Fig. 3.5).

After the sample was melted and the temperature was stabilized at 685 $\pm$1 °C, the melt was forced through the hole in the bottom of the graphite tube (crucible) by means of a graphite plunger, and the droplets were formed on the alumina substrate (Fig. 3.5). Photographs of these drops were taken by X-Ray radiography, first at 685 °C (in the liquid state), and then after solidification at about 450°C (in the solid state). The X-Ray fluoroscopy system, which was part of the overall set-up, made it possible to view the sample inside the furnace and to take photographs. The high resolution X-Ray films

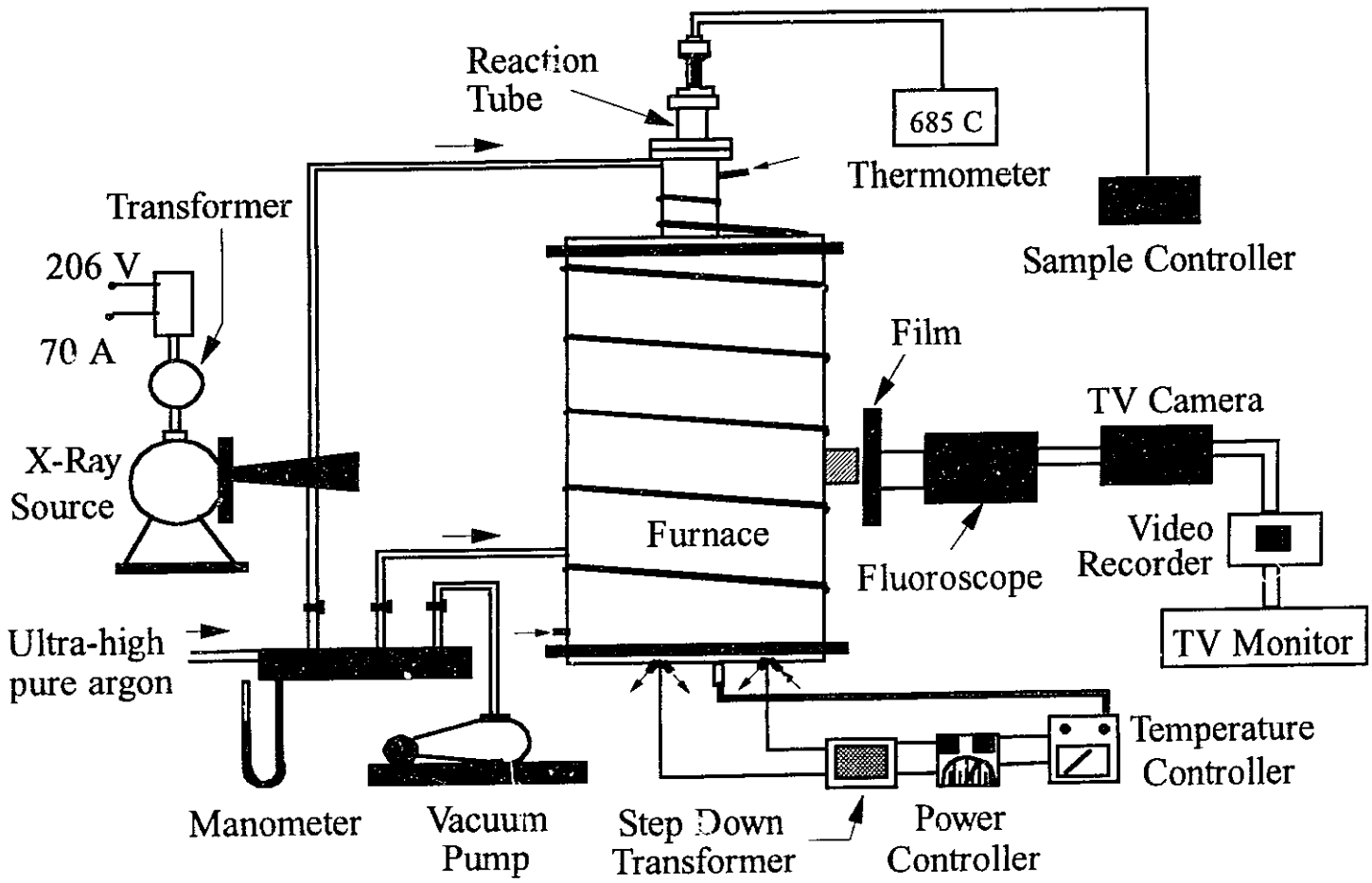

Figure 3.4 : High temperature x-ray radiographic apparatus surface tension measurements.

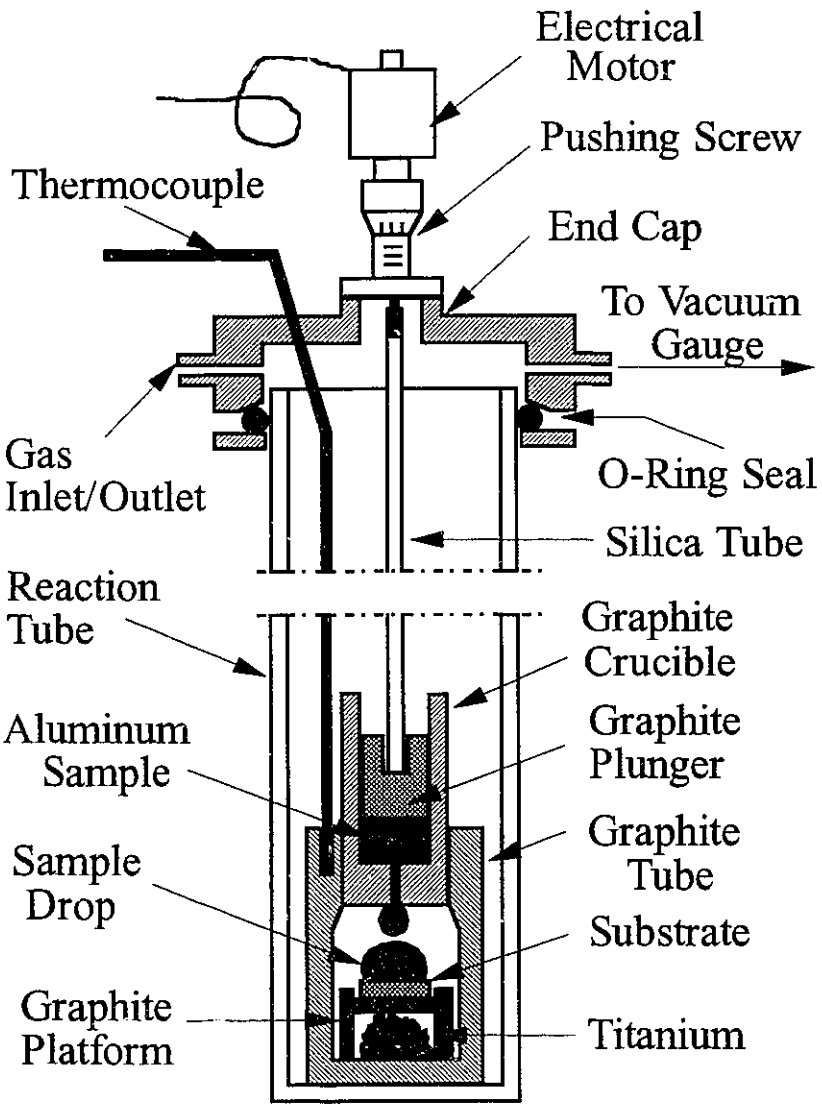

Figure 3.5 : Apparatus used for sessile-drop method.

were developed and the image was digitized using an image-analyzer system. The magnification of the images was calculated by comparing to a reference sample. A typical X-Ray photograph of a liquid droplet is shown in Figure 3.6.

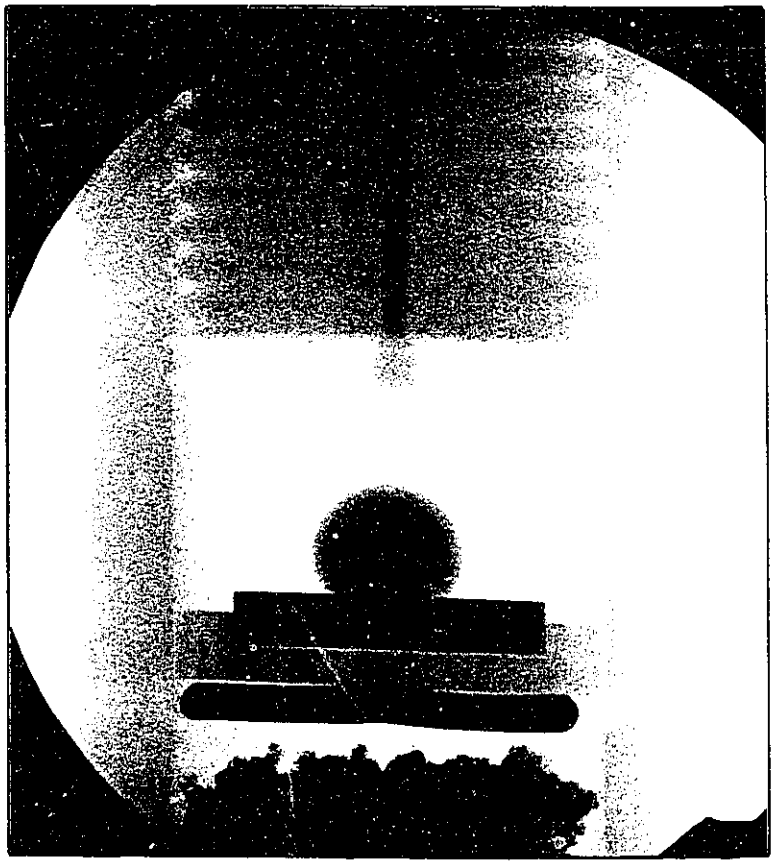

Figure 3.6 : Photograph of a Sr treated drop on an alumina substrate inside the furnace at 685 °C.

The digitized image was scanned by a computer program to obtain the drop-profile coordinates based on the maximum grey-level variation. A computer program developed by Rotenberg *et al* [18] was used to calculate surface tension by numerically solving Laplace's equation and obtaining the theoretical Laplace curve that best fit the observed experimental drop profile (see also Ref. 19).

3.3 Results And Discussion

After solidification, some droplets were used for chemical analysis while others were examined metallographically to determine the efficiency of the modification treatment and to estimate the retained modifier concentration. Typical droplet microstructures are shown in Figure 3.7. On average, it was estimated from the chemical analysis and microstructure that the retained sodium level was 0.004-0.006 wt% while strontium was 0.008-0.012 wt%. These concentrations which are typical of industrial modifier levels are lower than the target values mentioned earlier due to Na and Sr loss during remelting and holding the samples at high temperature which is accelerated by the small droplet size.

To calculate the surface tension of the liquid, modified or unmodified A356 alloy at 685 °C, it is necessary to know the density of the liquid at that temperature. The density of liquid A356 alloy has been measured in this research (see chapter 4), and is estimated to be 2.45 g/cm^3 at 685 °C for both unmodified and Sr-modified A356 alloy. This value is similar to that used in Ref. [20]. The liquid density of Na-modified A356 is assumed to be the same as Sr-modified alloy.

It is well known that surface tension measurements are highly sensitive to oxides present on the liquid surface. In the case of strontium or sodium treated melts, these may arise not only from reaction between the liquid metal and oxygen present in the atmosphere, but also from reactions between the elements present in the alloy (for example, modifiers) and alumina which may release oxygen into the melt. Such melt phase reactions are thermodynamically possible and in some cases may play a significant role in determining contact angle and surface tension. However, the sodium or strontium concentration (activity) is low (about 50-100 ppm) in the present experiments, and the driving force for such reactions is not large. In addition, the liquid droplets were photographed within a very short period of time (about 20 sec after contact with the substrate), and in some experiments a sequence of photographs was taken at times up to

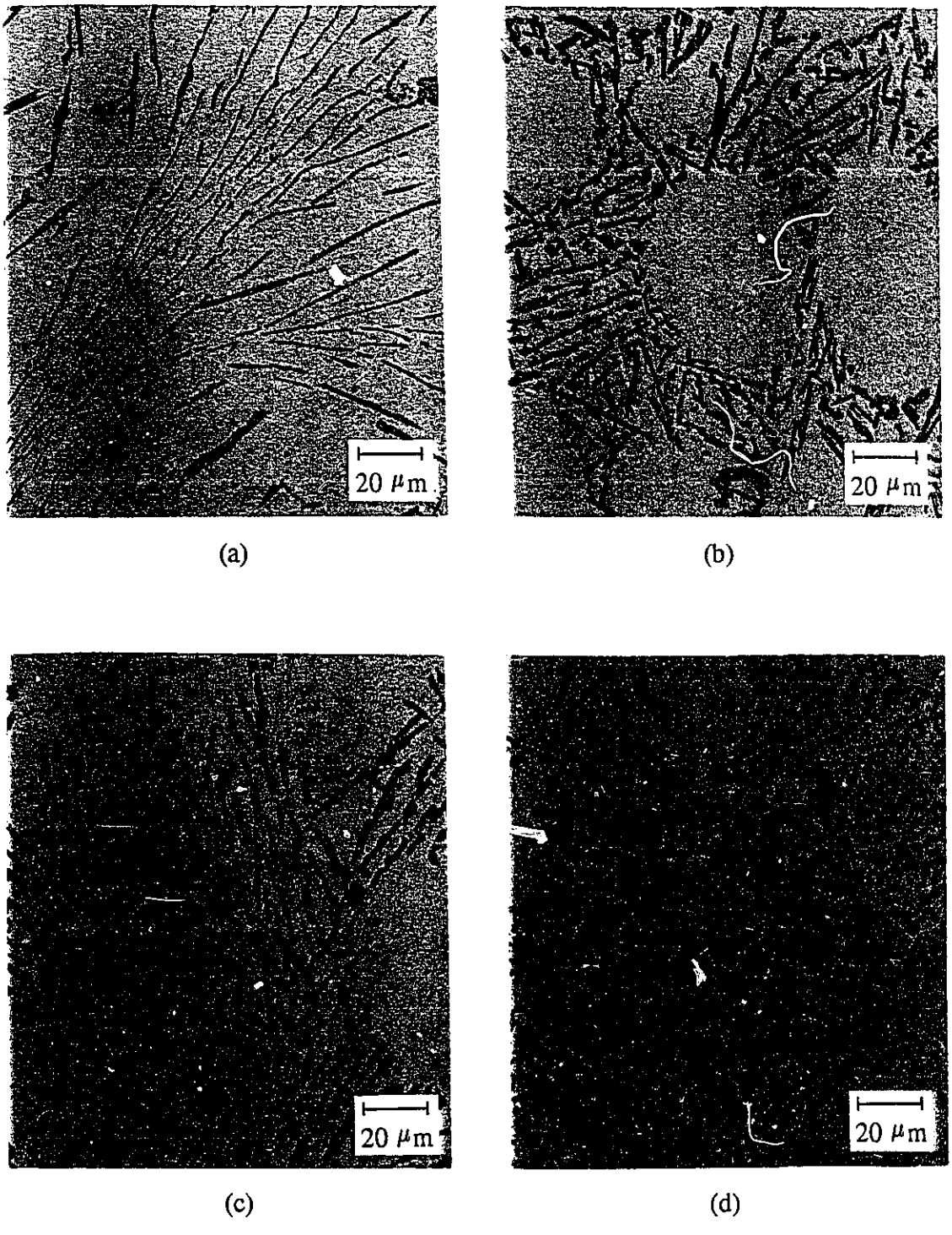

Figure 3.7 : Microstructure of the solidified droplets a) Al-10 wt%Sr b) A356 c) Na-modified A356 d) Sr-modified A356.

two minutes after contact. No change in droplet shape or contact angle was observed indicating that such reactions, if they do occur, do not have a significant effect within a few minutes of contact time.

For each sample, 6 to 7 surface tension values were obtained. Most of these fell into a narrow range, but often 1 or 2 points were far out of this range. Careful examination of these droplets showed asymmetry or a noticeable oxide coat which was presumed to arise from oxides entrained during the initial sample preparation or from a leak in the system at the O-ring seal. Consequently these points were omitted from further consideration. The average values of surface tension calculated from the remaining points are given in Table 3.1 along with the standard deviation of these values.

Table 3.1. Results of surface tension measurements

Sample	γ (N/m)	Contact Angle (θ)*
A356	0.790 $\pm$ 0.025	135 $\pm$ 4
Sr-Modified A356	0.640 $\pm$ 0.030	142 $\pm$ 5
Na-Modified A356	0.715 $\pm$ 0.030	141 $\pm$ 5
Al-10 wt% Sr	0.685 $\pm$ 0.035	136 $\pm$ 6

* Contact angle measured from liquid droplets.

It is observed that sodium (~ 0.005 wt%Na) reduces the surface tension of A356 alloy by about 10% and strontium (~ 0.01 wt%Sr) by about 19%. In addition, 0.01 wt% strontium reduces the surface tension of A356 alloy more than does 10 wt%Sr in pure

aluminum (Table 3.1), perhaps due to the effects of the alloying elements in the A356 alloy. These results are not in particularly good agreement with those found by other workers and described in section 3.1.2. For example, Davies and West[10] showed that the surface tension of unmodified and Na-modified binary Al-7 wt% Si alloy at 685 °C are in the range of 0.82-.825 N/m and 0.62-0.64 N/m, respectively (the Na content is not reported). The difference between the present results and those found by Davies could be due to: a) the effect of other alloying elements present in A356 compared to binary Al-7 wt% Si alloy, b) the difference in Na content, c) the difference in density value used in the calculations, or d) the presence of oxygen in the system.

As mentioned in section 3.1.2, Lang[11,12] has also measured the influence of additional alloying elements on the surface tension of super-purity aluminium at 700 °C. According to his investigations, 0.01 wt% Na reduces the surface tension of pure Al by about 0.230 N/m and the surface tension of Al-7.3%Si-0.4%Mg (which is similar to the A356 composition) calculated from his equations is about 0.820 N/m. In addition, 0.01 wt%Sr reduces the surface tension of super purity aluminium by about 2% and 0.01 wt% Na by about 26%. The calculated value of the surface tension of A356 alloy is in reasonable correspondence with that measured in the present work, but a significant difference is observed for the Sr and Na treated alloy. This difference may be due to the effect of alloying elements, the different oxidation rate of Sr and Na-modified alloys or the different density value used in the calculations.

In addition, the surface tension of A356 alloy was calculated from the shape of the solidified droplets. Although the solidified droplets are not axisymmetric and the results are considerably scattered, they show a reduction of about 18% $\pm$ 6% in surface tension compared with those calculated from liquid droplets. This reduction is less for the Sr and Na-modified A356 alloy. Therefore, the surface tension calculated from the solidified droplet shape does not correspond to that calculated from the liquid droplet, and the method proposed by Yavari[21] for determination of surface tension of a liquid metal at its

melting temperature from the shape of solidified droplets with contact angle greater than 90° is not reliable, at least for these alloys.

The contact angle (θ in Fig. 3.1) between the liquid phase and alumina (Al_2O_3) substrate is given in Table 3.1. It is observed that Na and Sr increase the contact angle, or on the other hand, decrease the wettability. It can be also concluded from the present observations that the contact angle (θ) decreases approximately 1 to 8 degrees on solidification.

Having established the effect of Na and Sr on surface tension, it is necessary to determine whether these changes can account for the significant observed increase of porosity associated with modification which will be discussed in the last chapter (i.e. Chapter 9). As a conclusion to the present chapter, the following major points can be drawn:

1. The addition of about 0.01 wt% strontium to A356 alloy decreases the surface tension of the liquid from 0.79 N/m to 0.64 N/m (by about 19%) at 685°C.
2. The addition of about 0.005 wt% sodium to A356 alloy decreases the surface tension of the liquid from 0.79 N/m to 0.715 N/m (by about 10%) at 685°C.
3. Surface tension calculated from the shape of solidified A356 droplets is less than that determined from the shape of liquid droplets, and thus the measurement of the surface tension of liquid metals from solidified droplets is not reliable.

3.4 References

1. Q.T. Fang and D.A. Granger; "Porosity Formation in Modified and Unmodified A356 Alloy Castings", *AFS Trans.*, Vol.97, 1989, pp. 989-1000

2. D. Argo and J.E. Gruzleski; "Porosity in Modified Aluminum Alloy Castings", *AFS Trans.*, Vol. 96, 1988, pp. 65-74

3. H. Shahani; "Effect of Hydrogen on the Shrinkage Porosity of Aluminum Copper and Aluminum Silicon Alloys", *Scand. J. Metall.*, No. 14, 1985, pp. 306-12

4. T. Iida and R.I.L. Guthrie; *The Physical Properties of Liquid Metals*, Oxford University Press, New York, NY, 1988, pp. 109-20

5. J.F. Padday; *Surface and Colloid Science*, Vol. 1, E. Matijevic, ed., Wiley Interscience, New York, NY, 1969, pp. 39-157

6. D.W.G. White; "The Surface Tension of Liquid Metals and Alloys", *Metall. Rev.*, Vol. 13, 1968, pp. 73-96

7. D.W.G. White, "Theory and Experiment in Methods for the Precision Measurement of Surface Tension", *ASM Trans.*, Vol. 55, 1962, pp. 757-89

8. D.W.G. White; *A Supplement to the Tables of Bashforth and Adams,* Queen's Printer, Ottawa, Canada, 1967, pp. 1-11

9. L.E. Murr; *Interfacial Phenomena in Metals and Alloys*, Addison-Wesley Publishing Co., Reading, Massachusetts, 1975, pp. 87-115

10. V.L. Davies and J.M. West; "Influence of Small Additions of Sodium on the Surface Tension of Aluminum and Aluminum-Silicon Alloys", *J. Inst. Met.*, Vol. 92, 1963-1964, pp. 208-10

11. G. Lang; "Casting Properties and Surface Tension of Aluminum and Binary Aluminum Alloys, Part III: Surface Tension ", *Aluminum*, Vol. 49 (3), 1973, 231-38

12. G. Lang; "The Influence of Alloying Elements on the Surface Tension of Liquid Super Purity Aluminum", *Aluminum*, Vol. 50 (11), 1974, 731-34

13. J. Goicoechea, E. Louis and A. Pamies; "Surface Tension of Binary and Ternary Aluminum Alloys of the Systems Al-Si-Mg and Al-Zn-Mg", *J. Mater. Sci.*, No. 27, 1992, pp. 5247-52

14. C. Garcia-Cordovilla, E. Louis and A. Pamies; "The Surface Tension of Liquid Pure Aluminum and Aluminum-Magnesium Alloy", *J. Mater. Sci.*, No. 21, 1986, pp. 2787-92

15. D.R. Poirier and R. Speiser; "Surface Tension of Aluminum Rich Al-Cu Liquid Alloys", *Metall. Trans. A*, Vol. 18A, June 1987, pp. 1156-60

16. K. Yeum and D.R. Poirier; "Predicting Microporosity in Aluminum Alloys", *Light Metals*, 1988, pp. 469-76

17. A. Pamies, C.G. Cordovilla and E. Louis; "The Measurement of Surface Tension of Liquid Aluminum by Means of the Maximum Bubble Pressure Method: The effect of Surface Oxidation", *Scripta Metallurgica*, Vol. 18, 1984, pp. 869-72

18. Y. Rotenberg; *The Determination of the Shape of Non-axisymmetric Drops and the Calculation of Surface Tension, Contact Angle, Surface Area and Volume of Axisymmetric Drops*, Ph.D. Thesis, University of Toronto, Toronto, 1983

19. L. Liggieri and A. Passerone; "An Automatic technique for Measuring the Surface Tension of Liquid Metals", *High Temp. Technol.*, May 1989, pp. 82-86

20. D. Emadi, J.E. Gruzleski and J.M. Toguri; "The Effect of Na and Sr Modification on Surface Tension and Volumetric Shrinkage of A356 alloy and Their Influence on Porosity Formation", *Metall. Trans. B*, Vol. 24B, Dec. 1993, pp. 1055-63

21. A. Yavari; "A New Method for Determination of Surface Tensions of Liquid Metals and Alloys", *Z. Metallkd.*, Vol. 79(9), 1988, pp. 591-94

Chapter 4

The Effect of Sr-Modification on the Volumetric Shrinkage of A356 Alloy

4.1 Introduction

After the casting of a superheated melt, there are three quite different contractions to be dealt with during cooling to room temperature, as illustrated in Figure 4.1. As the temperature reduces, the first contraction to be experienced occurs in the liquid state. This is the normal thermal contraction of the liquid in which the volume of the liquid metal reduces almost exactly linearly with falling temperature. In metal casting, the shrinkage of the liquid metal is usually not troublesome, and the liquid required to compensate for this small volume reduction is provided without difficulty.

The contraction on solidification occurs at the freezing point because of the greater density of the solid compared to that of the liquid. This contraction causes the movement of either liquid or solid for compensation of solidification contraction, and failure of the feeding process results in shrinkage porosity. The final stages of shrinkage take place in the solid state, and can cause a reduction in the size of the casting and may also lead to more localized problems such as hot tearing or cracking [1].

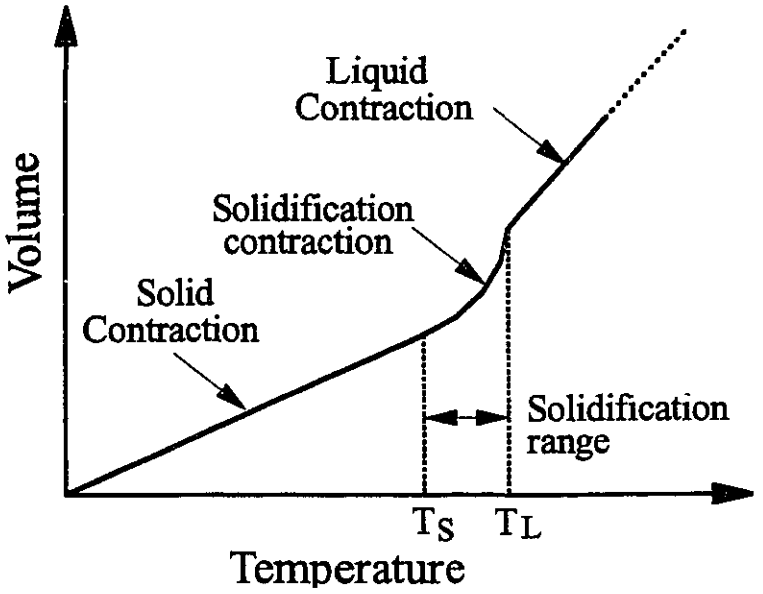

Fig. 4.1 : The volume contractions of the liquid aluminum during cooling to room temperature[1].

The volume change resulting from the solidification contraction is a function of composition, and is in the range of about 3 to 8 percent for Al alloys[2,3]. This contraction causes a pressure drop in the remaining liquid which results in fluid flow between dendrites. If the feeding ability is poor, it is expected that interdendritic liquid becomes isolated from the bulk liquid and the pressure drop due to shrinkage results in dispersed porosity. The effect of this pressure drop on porosity formation has been discussed and formulated in Chapter 8. This parameter has so far been largely ignored in the search for an explanation for the increased porosity on modification. It is therefore of interest to determine if there is a change in volumetric shrinkage by addition of Sr or Na to the melt, and to examine whether this change has a significant effect on porosity formation.

The volumetric shrinkage, β , is defined as:

$$\beta = \frac{\rho_S - \rho_L}{\rho_S} \qquad (4.1)$$

where ρ_L is the liquid density, and ρ_S is the theoretical solid density. In the case of Al-Si alloys, solidification contraction occurs in two stages, first the contraction due to formation of primary alpha-aluminum dendrites in the range of liquidus to eutectic temperature (alpha contraction), and secondly the contraction due to solidification of the eutectic liquid between the dendrites (eutectic contraction). These contractions are defined as β_α and β_E, respectively.

The density of the solid or liquid can be measured by a number of experimental techniques[4,5]. Some work has also been done to predict the densities of the solid and liquid as functions of temperature and composition for the Al-Si and Al-Cu systems[6,7]. Edwards *et al* [2] have measured the solid and liquid densities of Al-7.8 %Si alloy as a function of temperature as plotted in Figure 4.2. They have also measured the liquid density of Al-Si alloys as a function of silicon content at different temperatures (Figure 4.3). Despite these few works on the effect of alloying elements on the volumetric shrinkage of aluminum alloys, no study has been done on the effect of Sr or Na on the volumetric shrinkage of Al-Si alloys. In the present work, two experimental approaches, i.e. sessile-drop method[4] and direct Archimedean method[4] were employed for measuring the volumetric shrinkage of Al-Si alloys in the presence of strontium.

4.2 Sessile-drop Method:

In this approach, the solidification shrinkage of the alloys was determined by comparing the cross-sectional area of the droplets (as seen on the X-ray images) in the liquid state to the area of the droplets after solidification. The sessile-drop method has

been explained in more detail in Chapter 3.

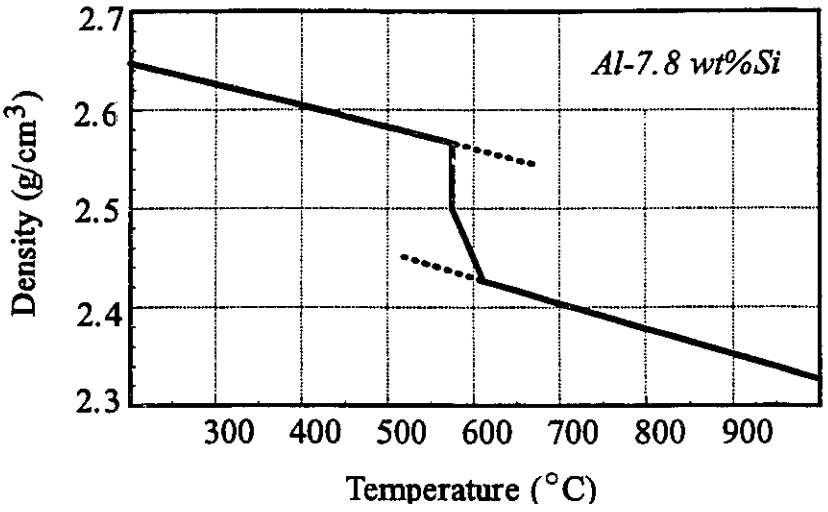

Figure 4.2 : The solid and liquid densities of Al-7.8 %Si as a function of temperature[2].

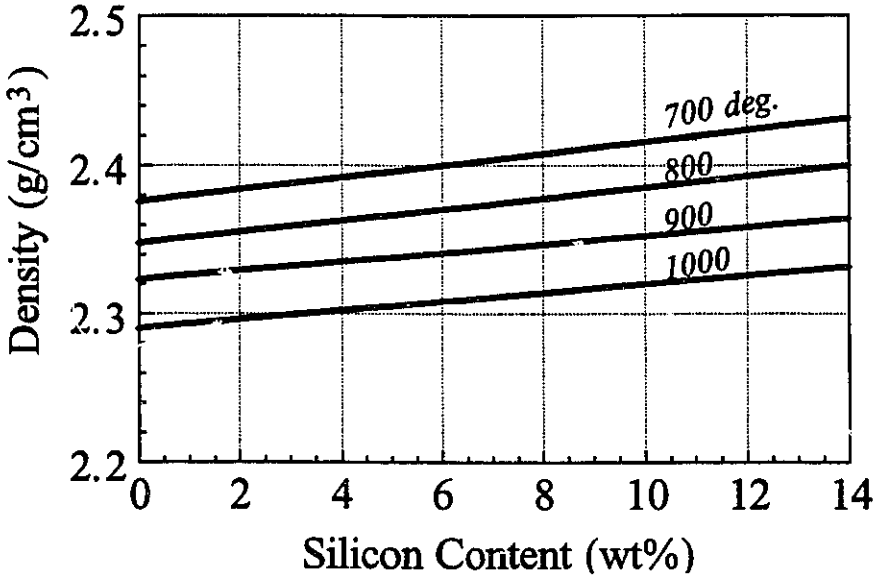

Figure 4.3 : The liquid density as a function of silicon content and temperature[2].

4.2.1 Experimental Procedures

The experimental procedure, materials used, and the experimental setup are the same as those employed for the surface tension measurements described in Chapter 3. The photographs of the drops were taken by X-Ray radiography, first at 685°C (in the liquid state), and then after solidification at about 450°C (in the solid state). The volumetric shrinkage of these alloys was determined by comparing the cross sectional area of the droplets as seen on the X-Ray images in the liquid state to the area of the droplets in the solid state. Subsequent destructive examination of the solidified droplet revealed no internal porosity; hence, it is realistic to consider the volume change of the droplets as volumetric shrinkage.

4.2.2 Results and Discussion

To provide uniform contraction of the droplets and to prevent local shrinkage, the samples should be solidified at low cooling rate. The cooling rate (dT/dt) was estimated from the secondary dendrite arm spacing (DAS) according to[8]:

$$\log \frac{dT}{dt} = - \frac{\log DAS - 2.37}{0.4} \quad °C/\min \tag{4.2}$$

The average measured DAS was 60 μm and hence the cooling rate calculated from equation (4.2) was about 0.5 °C/s. This rate is low, and is typical of sand mould casting.

Considering the cross sectional area of the droplets as the volume of the droplets, the volumetric shrinkage was calculated from Eq. (4.1) as: $\beta = (V_L - V_S)/V_L$. The measured volumetric shrinkage is given in Table 4.1. It is observed that the addition of, either 0.01 wt%Sr or 0.005 wt%Na increases the volumetric shrinkage of A356 alloy by

about 12%. The volumetric shrinkage of Al-7.8 %Si (which is similar to the A356 composition) calculated from the data in Figure 4.2 is not in good correspondence with that measured in the present work for unmodified A356 alloy. The volumetric shrinkage calculated from Figure 4.2 for the range of 685°C/s to 450°C/s is 7.2%, which is about 26% higher than that measured in the present work for A356 alloy.

Table 4.1 : Results of volumetric shrinkage measurements

Sample	Volumetric Shrinkage (%)
A356	5.7 ±0.3
Sr-Modified A356	6.4 ±1
Na-Modified A356	6.4 ±0.5
Al-10 wt%Sr	-*
Pure Al[20]	-

* It was difficult to calculate the volume of the solidified samples due to local shrinkage at the top of the droplet.

The calculated volumetric shrinkage in the present work is, in fact, the sum of the following contractions:

a) liquid contraction from 685 °C to the liquidus temperature (about 613 °C).

b) solidification contraction due to the formation of the primary alpha-aluminum dendrites from the liquidus to the eutectic temperature (alpha contraction, β_α).

c) contraction of the interdendritic liquid from the liquidus to eutectic temperature (about 577°C).

d) contraction of solid alpha-aluminum dendrites from liquidus to eutectic temperature.
e) solidification contraction of the interdendritic eutectic liquid at the eutectic temperature (eutectic contraction, β_E).
f) solid contraction from the eutectic temperature to about 450°C .

Since the contractions from stage (b) to (e) are playing the main role on porosity formation during solidification (especially in the case of directional solidification), it is necessary to calculate the contraction due to these stages by subtracting the contractions due to stages (a) and (f) from the total measured volumetric shrinkage.

The variation of the liquid and solid densities of most metals with temperature has been found to be well represented by a linear equation as[9]:

$$\rho = \rho_0 + (T - T_0)(d\rho / dT) \qquad (4.3)$$

where ρ is the density of the solid or the liquid in g/cm^3, T is the temperature in °K, and ρ_0 , T_0 and $d\rho/dT$ are constants. As shown in Figure 4.2, the decrease of the liquid temperature from 685°C to 613°C (stage a), and the decrease of the solid temperature from 577°C to 450°C (stage f) increase the liquid and solid densities by about 0.8% and 1%, respectively. These changes are negligible compared to the increase in the density due to solidification (i.e. decrease of the temperature from 613°C to 577°C) which is about 5.6%. It is therefore a good assumption that the measured volumetric shrinkage is the solidification contraction, i.e. the contractions of stages (b) to (e).

It is also interesting to note that the solubility of strontium in solid aluminum is almost zero[10] which results in the rejection of Sr into the interdendritic liquid during solidification, and enrichment in the eutectic liquid. Therefore, the observed increase in volumetric shrinkage due to Sr-modification by about 12% is related to the change in

eutectic contraction (i.e. stage e), and in fact, Sr-modification increases β_E by about 12% while β_α remains almost constant.

4.3 Archimedean Method:

In this approach, the volumetric shrinkage was calculated from the solid and liquid densities according to Eq. (4.1). The density of the liquid was measured using the direct Archimedean method, and the density of the solid was measured on directionally solidified samples solidified at high cooling rate and low level of hydrogen.

4.3.1 Liquid Density Measurement

The direct Archimedean method uses a solid sinker of known weight (in vacuum or, more generally, air) suspended by a wire attached to the arm of a balance. When the sinker is immersed in the liquid metal specimen, as shown in Figure 4.4, a new weight (or an apparent loss of weight) is observed. The difference, Δw, in the two weights, i.e. the apparent loss of weight of the immersed sinker, originates mainly from the buoyant force exerted by the liquid metal. The density of the liquid metal, ρ_L, is given by [4] :

$$\rho_L = \frac{\Delta w + s}{g\,(V + v)} \quad , \quad \textit{in which} \quad s = 2\,\pi\, r\, \gamma \cos\theta \qquad (4.4)$$

where g is gravitational acceleration, V is the volume of the sinker, v is the volume of the immersed suspension wire, s is the surface tension correction, i.e. the force acting against the suspension wire of radius r in the liquid for which the surface tension is γ and the contact angle between the wire and the liquid is θ.

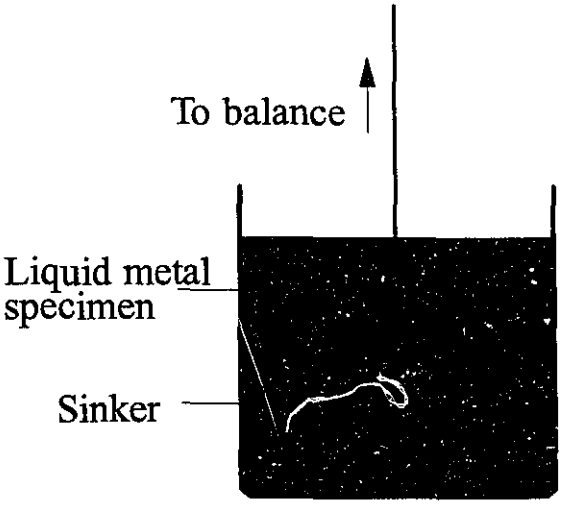

Figure 4.4 : The direct Archimedean method.

In order to obtain accurate data, the volumes of the sinker and the immersed suspension wire must be corrected for thermal expansion to operating temperature, since their volumes are, in general, determined experimentally at room temperature.

4.3.1.1 Experimental Procedure

A356 alloy, of chemical composition given in Table 2.1, was used in this investigation. In each experiment, a 500-g melt of A356 alloy was prepared in a fire-clay crucible using a small electric resistance furnace. The melt was held at about 730°C for about one hour to stabilize the temperature. A closed-end cylindrical (test tube shape) alumina sinker with a diameter of 2.2 cm and length of 5.5 cm was suspended by an alumina rod with a diameter of 0.085 cm attached to a balance. The schematic of the setup used in these experiments is shown in Figure 4.5.

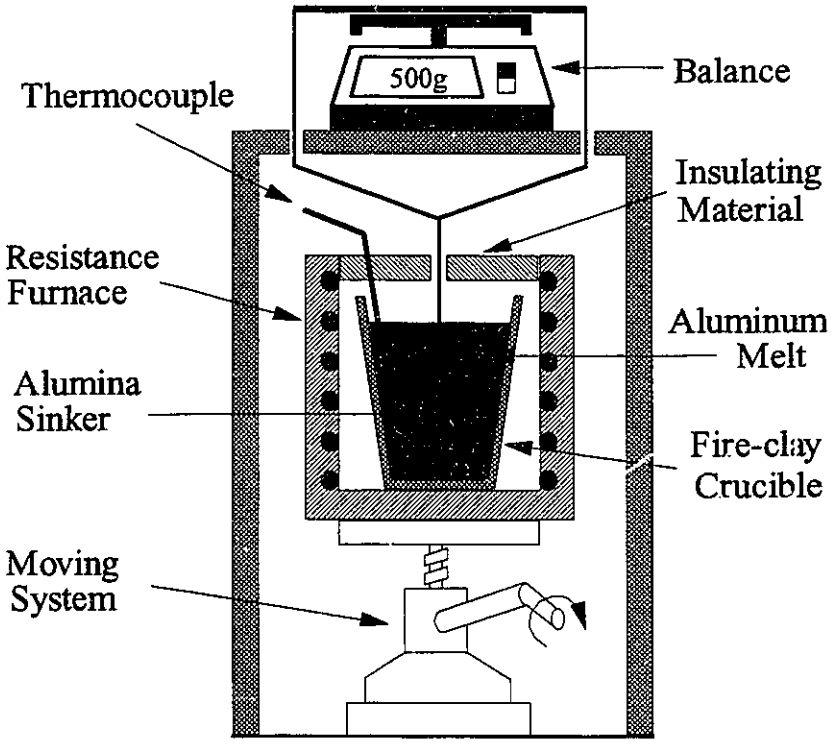

Figure 4.5 : The setup used for density measurement of the liquid.

The density of the alumina sinker was increased to about 3.70 g/cm^3 by filling it with lead and refractory cement, and its volume was measured to be 15 $\pm$ 0.2 cm^3. An alumina sinker was used in these experiments since alumina does not react with liquid aluminum. After the dross layer was removed from the surface of the melt, the balance was set to zero, and the sinker was immersed into the liquid aluminum to about 1 cm below the surface (i.e., 1 cm of the alumina rod was within the liquid). Weight measurements were carried out after 20 minutes to allow the sinker to reach the melt temperature, and to allow the temperature to stabilize. At this point, the balance showed a negative value due to the weight loss, Δw.

Measurements were taken on both unmodified and modified alloys. Modification of the alloy was done by adding 0.03 wt. pct. strontium to the melt in the form of commercial Al-10 wt% Sr master alloy. The melt was held for 20 minutes to allow dissolution of the strontium, and at that point, the reading was taken while the sinker was still in the melt. Another reading was taken for the modified melt by withdrawing the sinker and allowing it to re-enter the melt. Both readings for modified alloy were in good agreement.

4.3.1.2 Results and Discussion

The density of the liquid A356 alloy at 730°C calculated from Eq. (4.4) is given in Table 4.3 using the values in Table 4.2. It is observed that the difference in density between the liquid of the Sr-modified and unmodified A356 is not significant, and is within the range of errors of the measurements. Therefore, Sr-modification does not change the density of the liquid A356 alloy, and the difference in volumetric shrinkage found in the sessile-drop measurements must be due to a change in the density of the solid. In addition, the liquid density measured in this work is larger than that obtained from Figure 4.3 for Al-7 wt%Si at 730°C which is about 2.41 g/cm^3. However, the difference is in the range of errors of the measurements, and may be due to the other alloying elements present in A356 alloy.

Table 4.2 : Constants Used in Calculation

g (cm/s^2)	V (cm^3)	v (cm^3)	r (cm)		γ (dyne/cm)	θ* (°)
981	15 ±0.2	5.67x10^{-3}	0.0425	Modified:	790	135
				Unmodified:	640	142

* From Table 3.2

Table 4.3 : Results of Liquid Density Measurements

Alloy	Δw (g)	ρ_L (g /cm^3)
Unmodified A356	36.95 ± 0.8	2.45 ± 0.08
Sr-modified A356	37.05 ± 0.9	2.46 ± 0.09

4.3.2 Solid Density Measurement

This thesis deals with the calculation of volumetric shrinkage and pore volume fraction of Al-Si castings with different levels of silicon. Therefore, it is necessary to determine the theoretical density of solid Al-Si alloys as a function of silicon content.

4.3.2.1. Experimental Procedure

Five Al-Si alloys with different silicon levels of 4.8 wt%, 5.7 wt%, 7 wt%, 8.1 wt% and 12 wt% were prepared by adding pure silicon and commercial purity aluminum to an A356 alloy as the base metal (Table 2.1). The alloys were prepared in a large quantity to be also used in other experiments. To determine the true density of the Al-Si alloys in the solid state, samples should be free of porosity or other defects. In this experiment, the alloy was melted in an induction furnace and the melt was degassed for about 30 minutes using pure argon. The melt was then cast into a water-cooled copper mould with an insulating material at the top as shown in Figure 4.6. Both unmodified and modified (0.02 wt% Sr) alloy samples were prepared in this way.

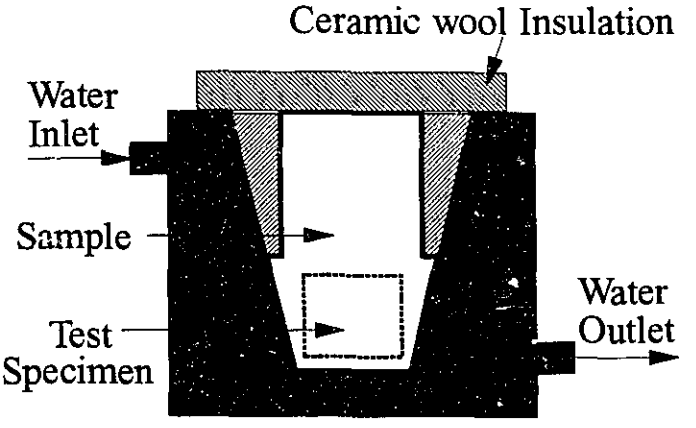

Figure 4.6 : The setup used for density measurement of the solid.

Density measurement was carried out on the bottom portion of these directionally solidified specimens, which, due to the relatively rapid solidification rate, would be expected to have a density very close to the theoretical. The density of the cylindrical test specimens with a diameter of 25 mm and a length of 35 mm was determined according to Archimedes principle by weighing them in air and in water. The density of the water itself was measured, since a minor amount of Teepol 610, a surface tension reducing agent, was added to the distilled water bath to ensure wetting of the samples.

4.3.2.2. Results and Discussion

The measured solid density as a function of silicon content for both unmodified and Sr-modified Al-Si alloys is given in Table 4.4, and is shown in Figure 4.7. A standard deviation of $\pm$ 0.002 applies to all of these measurements. It is observed that

silicon decreases the density of solid Al-Si alloys, and Sr-modification increases the solid density. The addition of 0.02 wt%Sr to A356 alloy increases the density of the solid from 2.675 g/cm^3 to 2.678 g/cm^3 , an increase of about 0.11%.

Table 4.4 : Results of Solid Density Measurements

Alloy	Solid Density, ρ_s	
	Unmodified	Sr-modified
Al-4.8 %Si	2.685	2.687
Al-5.7% Si	2.680	2.682
Al-7.0% Si	2.675	2.678
Al-8.1% Si	2.669	2.671
Al-12% Si	2.654	2.656

These results are not in very good agreement with those found by other workers. For example, Engler and Chen[5] have measured the density of Al-Si alloys having a chemical composition similar to the present alloys. According to their work, strontium decreases the density of solid Al-7%Si alloy, but increases the densities of Al-10 wt%Si and Al-12 wt%Si alloys. However, their density values for unmodified alloys are higher than those measured here.

Sigworth *et al*[11] have also calculated the solid density of A356 alloy from pore volume in samples using quantitative metallographic analysis. They found the same value of density for Sr-modified alloy (i.e. 2.6775 g/cm^3), and a lower value for unmodified alloy (i.e. 2.6672 g/cm^3). The difference may be due to the fact that the pore volume fraction measured by metallographic analysis is inaccurate.

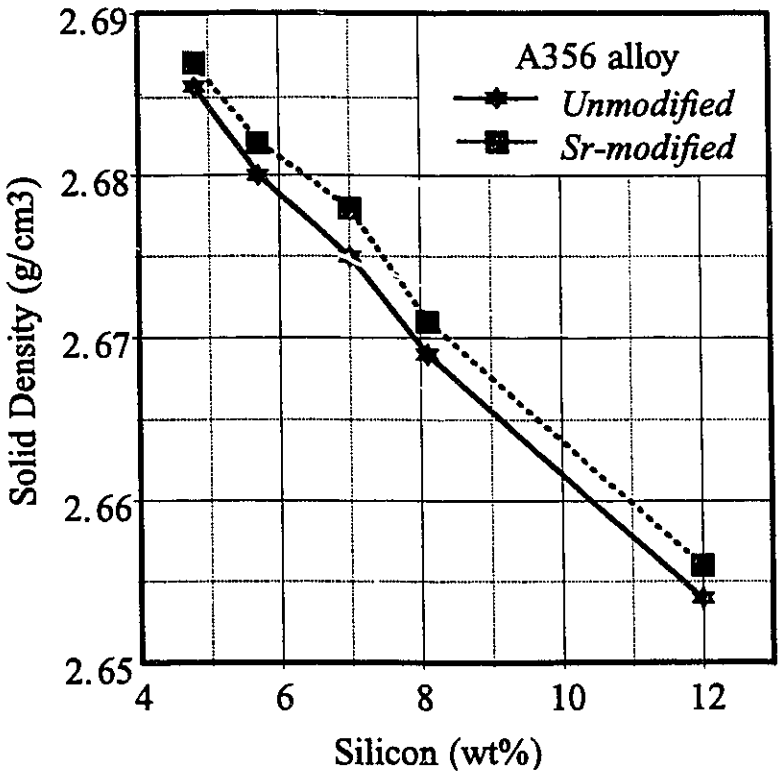

Fig. 4.7. The results of solid density as a function of silicon content.

It is also interesting to note that the solid density of aluminum is larger than the solid densities of silicon or strontium[2,12], and therefore, the Sr-modification is expected to lower the solid density of solid Al-Si alloys. However, it is observed in the present work that the solid densities of Sr-modified Al-Si alloys are larger than unmodified alloys. The reason for this is not clear at present.

The volumetric shrinkage of A356 alloy can be calculated using Eq. (4.1) and the values of solid and liquid density in Tables 4.3 and 4.4. Considering the standard deviation of solid and liquid densities, the volumetric shrinkage of unmodified A356 alloy

is about 8.41 (±1.95) %. Using the same value of liquid density as unmodified alloy, the volumetric shrinkage of Sr-modified A356 alloy is about 8.5 (±1.95) %.

These results are not in good agreement with those measured by the sessile drop method, and the differences are significant. The reason is that the volumetric shrinkage calculated from Archimedean measurements is for the range of 730°C to room temperature, while in the case of sessile drop measurements, it is for the range of 685°C to 450°C. To compare the results of these two methods, it is necessary to calculate the solid and liquid densities of A356 alloy at 450°C and 685°C, respectively. Assuming the solid and liquid densities of A356 alloy to be a linear function of the temperature with the same slope as that shown in Figure 4.2 for Al-7.8 wt%Si, the solid and liquid densities can be calculated at 685°C and 450°C, respectively. The calculated densities and volumetric shrinkage are given in Table 4.5.

Table 4.5 : Calculated solid and liquid densities at 450°C and 685°C from the Archimedean measurements.

	Solid Density at 450°C	Liquid Density at 685°C		Volumetric Shrinkage (%)
Unmodified A356	2.590 ±0.002	2.435 ±0.08	→	5.9 ±0.2
Sr-modified A356	2.593 ±0.002		→	6.1 ±0.2

By comparing Tables 4.1 and 4.5 it can be seen that the volumetric shrinkage of unmodified and Sr-modified A356 alloy from the sessile drop and the Archimedean measurements are, in fact, in good agreement , and the differences are within the range of error. This small difference may be due to the fact that the solidified droplets are not

axisymmetric, and the cross-sectional area of the droplets does not represent the true volume of the droplets. In addition, the results of volumetric shrinkage in Table 4.5 show an increase of about 3.5% in volumetric shrinkage due to Sr-modification.

The errors in the volumetric shrinkage measurements in both approaches are relatively large, and the increase in volumetric shrinkage by about 3.5% (in Archimedean method) to 12% (in sessile-drop method) lies within the range of error. Nevertheless, the present results are an indication of an effect of Sr-modification on volumetric shrinkage, and it is significant that two different approaches both lead to the conclusion that strontium increases the solid density thereby increasing the volumetric shrinkage.

Having established the effect of Sr on volumetric shrinkage, it is necessary to determine whether these changes can account for the significant observed increase of porosity associated with modification. This will be discussed in the Chapter 9. As a conclusion to the present chapter, the following major points can be drawn:

1. The addition of about 0.01 wt% strontium and about 0.005 wt% sodium to A356 alloy increases the volumetric shrinkage of A356 alloy.

2. The addition of 0.02 wt% Sr does not change the density of the liquid A356 alloy, and the increase in volumetric shrinkage by Sr addition must be due to the increase in the solid density.

3. The observed increase in volumetric shrinkage seems to be due to the increase in eutectic contraction (β_E), while β_α remains constant.

4.4 References

1. J. Campbell; *Casting*, Butterworth-Heinemann, Oxford, 1991, pp. 219-31

2. J.D. Edwards; "Thermal Properties of Aluminum-Silicon Alloys"; *Chemical and Metallurgical Eng.*, Vol. 28, No. 4, 1923, pp. 165-69

3. A.M. Korolkov; *Casting Properties of Metals and Alloys*, Consultants Bureau Enterprises Inc., New York, NY, 1963, pp. 90-100

4. T. Iida and R.I.L. Guthrie; *The Physical properties of Liquid Metals*, Oxford University Press, New York, NY, 1988, pp. 47-67

5. X.G. Chen and S. Engler; "Hydrogen and Porosity in Aluminum-Silicon and Aluminum-Magnesium Alloys; Part I: Aluminum-Silicon Alloys", *Metall.*, Vol.45, No. 10, Oct. 1991, pp. 995-1000

6. S. Ganesan and D.R. Poirier; "Densities of Aluminum-Rich Aluminum-Copper Alloys During Solidification", *Metall. Trans. A*, Vol. 18A, April 1987, pp. 721-23

7. K. Yeum and D.R. Poirier; "Predicting Microporosity in Aluminum Alloys", *Light Metals*, 1988, pp. 469-76

8. G. Gustafsson, T. Thorvaldsson and G.L. Dunlop; "Development of Microstructure in a cast Al-7Si-0.3Mg-0.2Fe Alloy", *The Metallurgy of Light Alloys*, Institute of Metallurgists, London, March 1983, pp. 288-94

9. E.A. Brandes and G.B. Brook; *Smithells Metals Reference Book*, 7th Ed., Butterworth-Heinemann Ltd, Oxford, 1992, Chapter 14, pp. 1-16

10. B. Closset, H. Dugas, M. Pekguleryuz and J.E. Gruzleski; "The Aluminum-Strontium Phase Diagram", *Metall. Trans. A*, Vol. 17A, July 1986, pp. 1250-53

11. G.K. Sigworth, C. Wang, H. Huang and J.T. Berry; "Porosity Formation in Long Freezing Range Alloys", AFS Trans., Vol. 102, 1994

12. *CBC Handbook of Chemistry and Physics*, 60th Edition, CRC Press Inc., Boca Raton, Florida, 1981

Chapter 5

The Effect of Sr-Modification on Feeding Capability of A356 Alloy

5.1 Introduction

As solidification progress, liquid metal flows through a mushy zone in order to compensate for the volume contraction at the solid/liquid interface. In this case, the dendritic network imposes resistance to liquid flow. If the feeding ability is poor, the interdendritic liquid becomes isolated from the bulk liquid and the pressure drop results in evolution of dissolved hydrogen in the melt and dispersed porosity. This pressure drop is known as shrinkage pressure and has been formulated for the case of directional solidification in Chapter 8.

In an attempt to explain the increase in porosity observed in Sr and Na-treated Al-Si alloys, the effect of Na and Sr on feeding capability should be considered. Sr and Na may influence the interdendritic feeding capability through the following parameters:

1. dendrite arm spacing (DAS)
2. interdendritic liquid viscosity
3. length of the mushy zone
4. shape of the solid/liquid interface

An increase in DAS, a decrease in liquid viscosity, a smoother solid/liquid interface and/or a shorter length of the mushy zone decrease the porosity by improving the feeding capability. On the other hand, a porosity increase may be due to an increase in the time available for hydrogen diffusion and pore growth due to an increase in the freezing range caused by a depression of the eutectic solidification temperature. In this chapter, the effect of Na and Sr-modification on these parameters will be investigated, and the significance of any changes in these factors on porosity will be discussed.

5.2 Dendrite Arm Spacing(DAS)

In most cast aluminum alloys, solidification begins with the development of a dendritic network of primary (α) aluminum. The smaller the secondary dendrite spacing, the more difficult is interdendritic liquid flow resulting in more porosity in the casting. The secondary dendrite arm spacing (DAS) is determined by alloy composition, cooling rate, local solidification time and temperature gradient. Among primary alloying elements, silicon has been reported to have an influence on DAS, i.e. an increase in silicon content leads to a decrease in the DAS[1,2]. Strontium and antimony have the same effect as silicon, i.e. the addition of Sr or Sb refines the DAS, and decreases the rate of coarsening[2]. Therefore, strontium and sodium may increase porosity in the casting by decreasing the DAS.

The secondary dendrite arm spacing is a function of solidification time, and this relationship has been described for unmodified, Sr and Sb-modified Al-7Si-0.5Mg alloy by the following equations[2]:

$$DAS = (10.27 \pm 0.55)\, t_f^{0.3\pm0.01} \qquad : Unmodified \tag{5.1}$$

$$DAS = (9.35 \pm 0.50)\, t_f^{0.3\pm0.01} \qquad : Sr\text{-}modified \tag{5.2}$$

$$DAS = (8.44 \pm 0.45)\, t_f^{0.3\pm0.01} \qquad :Sb\text{-}modified \tag{5.3}$$

Where the total solidification time (i.e., time from beginning to end of solidification), t_f, is in seconds and secondary dendrite arm spacing, DAS, is in μm.

Using the data from the directional solidification experiments described in Chapter 2, the solidification time, i.e., the required time for cooling from 615 °C to 577 °C, can be calculated from the cooling curve (Figure 2.7) at a distance of 21 cm from the chill, i.e. thermocouple No.7 in Figure 2.6. This value is about 108 seconds at a cooling rate of 0.4 °C/s. The DAS for unmodified and Sr-modified alloys calculated from Eqs. (5.1) and (5.2) are found to be 42 $\pm$4 μm and 38 $\pm$4 μm, respectively. The difference in DAS between modified and unmodified alloys is within the range of standard deviation of DAS measurements, and therefore, may not be of significant importance. These values of DAS are much lower than the 66 μm value calculated from Eq. (2) in Chapter 4 for a cooling rate of 0.4 °C/s. Measuring the DAS of the directionally solidified A356 castings (in Chapter 2) at a distance of 21 cm from the chill (i.e. thermocouple No. 7 in Figure 2.6) with cooling rate of about 0.4 °C/s by metallography gives an average value of about 60 $\pm$8.3 μm and 54.5 $\pm$6.6 μm for unmodified and Sr-modified A356 alloys, respectively. The micrographs of the dendrite structure of these samples, i.e. directionally solidified unmodified and Sr-modified A356 castings with a cooling rate of about 0.4 °C/s are shown in Figure 5.1.

It is seen that DAS is decreased by modification, and this decrease in DAS is within the range of standard deviations. In addition, the measured values of DAS are larger than those calculated from Eqs.(5.1) and (5.2) for both unmodified and Sr-modified alloys while the result for unmodified alloy is in reasonable agreement with that calculated from Eq. 2 in Chapter 4. Table 5.1 gives a comparison of these values. The results of these measurements and the calculations from Eqs. (5.1) and (5.2) are an indication of a decrease in secondary dendrite arm spacing (DAS) by about 9% due to Sr-modification.

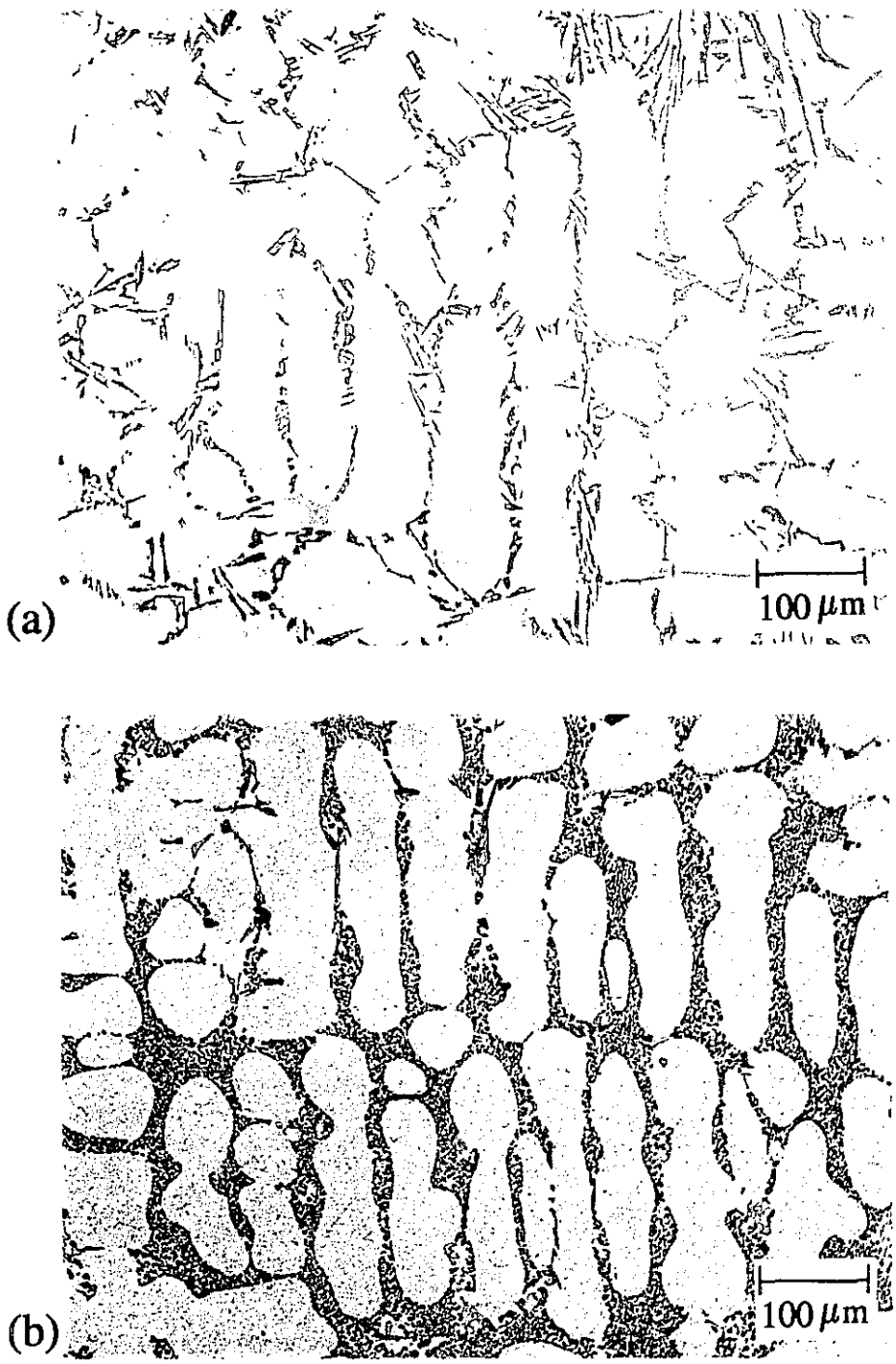

Figure 5.1 : Micrographs of directionally solidified a) unmodified and b) Sr-modified A356 castings at a cooling rate of about 0.4 °C/s.

Table 5.1 : Secondary dendrite arm spacing (DAS) at cooling rate of 0.4 °C/s.

Obtained from:	DAS (μm)		%decrease in DAS
	Unmodified	Sr-modified	
Eqs. 1 and 2	42 ±4	38 ±4	9%
Measured in this work	60 ±8.3	54.5 ±6.6	9%
Eq. 2 in Chapter 4	66		

5.3 Viscosity

Strontium and sodium may increase the porosity in the casting by increasing the viscosity of the liquid. The higher the viscosity of the liquid, the more difficult is the flow of interdendritic liquid between dendrites to compensate for shrinkage.

When a incompressible liquid is subjected to a uniform shear stress, a velocity gradient is set up perpendicular to the direction of the applied stress as a result of the resistance of the fluid to the applied motion. This resistance is known as a viscous force. Thus, when adjacent parts of a liquid move at different velocities, viscous forces act so as to cause the slower-moving regions to move more rapidly, and the faster-moving ones to move more slowly. The definition of the coefficient of viscosity, or simply 'viscosity' is based on the following mathematical expression by Sir Issac Newton:

$$\tau = \mu \frac{dv}{dz} \qquad (5.4)$$

where μ is the dynamic viscosity, and τ is the force exerted by the fluid per unit area of

a plane parallel to the x direction of motion when the velocity v is increasing with distance z measured normal to the plane, at the rate dv/dz. This equation is known as Newton's law of viscosity. If a liquid obeys this equation, i.e. the shearing force τ is proportional to the velocity gradient dv/dz, it is known as a Newtonian liquid. All liquid metals are believed to be Newtonian.

Numerous experimental measurements of liquid metal viscosities have been made over the last hundred years or more[3,4,5,6,7,8]. In spite of this, accurate and reliable data are still not in abundance. Fairly large discrepancies exist between experimental viscosities obtained for some liquid metals, particularly iron, aluminium, and zinc. The reason for these discrepancies is attributed to the high reactivity of metallic liquids and the technical difficulty of taking precise measurements at elevated temperatures. It is very difficult to state definitely the accuracy of viscosity measurements for liquid metals. Errors of ± 1 to ± 20 percent would seem to be a fair estimate, with the exception of a few metals[3].

The viscosity of liquid metals is sensitive to the composition, temperature and pressure. There are relatively few data available on the effect of temperature and composition on viscosity, especially for liquid aluminum alloys. Jones *et al* [5] have measured the viscosity of liquid Al-Si alloys as a function of silicon content and temperature as shown in Figures 5.2 and 5.3.

As shown in Figure 5.2, the eutectic alloy with 11.7 wt%Si has the lowest viscosity among the binary Al-Si alloys. It is also observed from Figure 5.3 that viscosity increases by decreasing the temperature, and there is a sharp increase in viscosity near the liquidus. This behaviour is due to variations occurring in the structure of the liquid in the precrystallization period.

The results in Figures 5.2 and 5.3 are in a good agreement with those measured

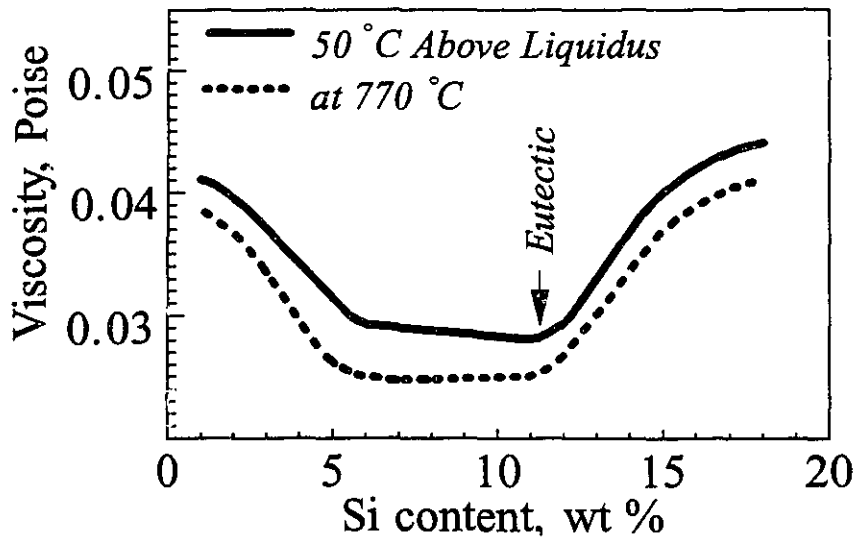

Figure 5.2 : Viscosity of Al-Si alloys as a function of silicon content[5].

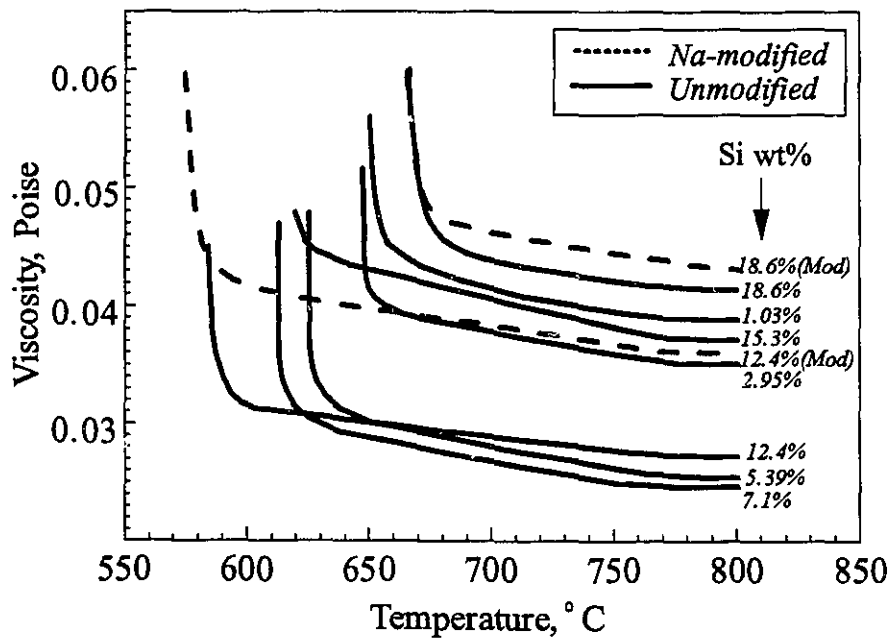

Figure 5.3: Viscosity-Temperature curves for Al-Si alloys[5].

by Korolkov[4], but a significant difference is observed with those determined by Ajersch *et al* [5]. According to Ajersch's work, the viscosity of liquid A356 alloy at 700°C is about 0.065 poise, while the viscosity of Al-7.1%Si alloy with a chemical composition similar to A356 alloy at 700 C obtained from Figure 5.3 is about 0.028 poise. The difference between these two results could be due to experimental errors or the effect of other alloying elements present in A356 alloy.

The only data available on the effect of modifiers on viscosity is for sodium as shown in Figure 5.3. Sodium (of the order of 0.05%) increases the viscosity of liquid Al-Si alloys, and this increase is about 31% for Al-12.4 %Si alloy, and about 6% for Al-18.6 %Si alloy. The reason for the stronger effect of Na on the viscosity of Al-12.4%Si compared to Al-18.6%Si is not clear, and may be due to differences in the amount of Na in these two melts. In this study, it is assumed that Sr has the same effect as Na on viscosity, and both Na and Sr increase the viscosity of A356 alloy by about 31%. The effect of a 31% increase in viscosity on porosity will be demonstrated in Chapter 9.

5.4 Length of the Mushy Zone

As mentioned in Chapter 1, Na and Sr-modification suppress the eutectic temperature by about 6-10 °C without changing the liquidus temperature. Some authors have suggested that the reduction of eutectic temperature in modified alloys increases the freezing range and the length of the mushy zone, and, therefore, interdendritic feeding becomes more difficult resulting in large pockets of isolated interdendritic liquid and more porosity[9,10]. According to their work, Sr-modification redistributes microshrinkage causing it to be widely dispersed and to form large isolated pores rather than the fine interconnected pores found in unmodified castings (Figure 5.4). As a result, Sr-modified castings are more prone to microshrinkage and less prone to macroshrinkage piping than unmodified castings.

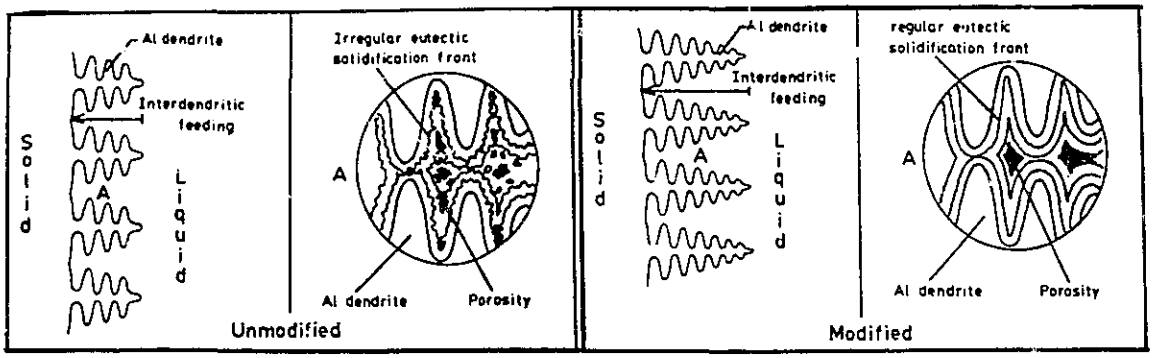

(a) (b)

Figure 5.4 : Two stage solidification process showing microshrinkage formation in a) an unmodified casting with a short interdendritic feeding distance and irregular eutectic solidification front; b) a modified casting with a long interdendritic feeding distance and a regular eutectic solidification front[10].

On the other hand, Iwahori *et al*[11] have contended that sodium improves the feeding capability of Al-Si alloys, while Sr has no effect on the increase in the feeding capability, or the decrease in the shrinkage porosity of the castings. As a result, Na-modified alloys can produce sound castings free from shrinkage porosity, even if risers smaller than those of unmodified alloys are used. The reason for the different behaviour of Na and Sr has not been clearly explained.

There is some evidence on the influence of the freezing range on porosity. Wittenberger and Rhines[12] have observed an increase in microporosity in binary Al-Si alloys due to widening of the freezing range (obtained by decreasing the silicon content). Coble and Flemings[13] have directly correlated the tendency to microporosity formation with the length of the mushy zone. They have concluded that the pressure drop due to solidification shrinkage is proportional to the square of the freezing range. Further

evidence that the suppression of the eutectic temperature may have a significant effect on porosity lies in the observation that no increase in porosity has been observed in Sb-modified alloys[14,15],and antimony results in no depression of the eutectic temperature[15].

Nyoco *et al*[15] have also studied the effect of the length of the mushy zone on porosity and concluded that the change in the length of the mushy zone due to modification-induced eutectic undercooling is not responsible for the increased porosity in modified alloys and the effect of other variables should also be considered.

The effect of the length of the mushy zone on porosity was studied as part of the present thesis research to examine whether the increased porosity in modified alloys is due to the increase in the length of the mushy zone. The length of the mushy zone can be increased in the unmodified condition by decreasing the melt silicon content in order to obtain the same freezing range as in modified alloys. Studying the porosity in this unmodified alloy with longer freezing range should show the importance of the increase in the length of the mushy zone (due to modification) on porosity.

5.4.1 Experimental Procedure

A356 alloy with the chemical composition given in Table 2.1 (in Chapter two) was used as the base metal. Using thermal analysis, the average liquidus and solidus temperatures of A356 alloy were determined to be about 614 °C and 575 °C, respectively. Modifying A356 alloy with strontium in the range of 0.02-0.025 wt%, the eutectic temperature decreased about 4 to 7 °C. Therefore, Sr-modification was considered to decrease the eutectic temperature by a maximum of about 7 °C as shown in Figure 5.5. At the same time, Sr-modification increases the freezing range (i.e. the difference between liquidus and solidus temperatures) of A356 alloy from 39 °C to about 46 °C .

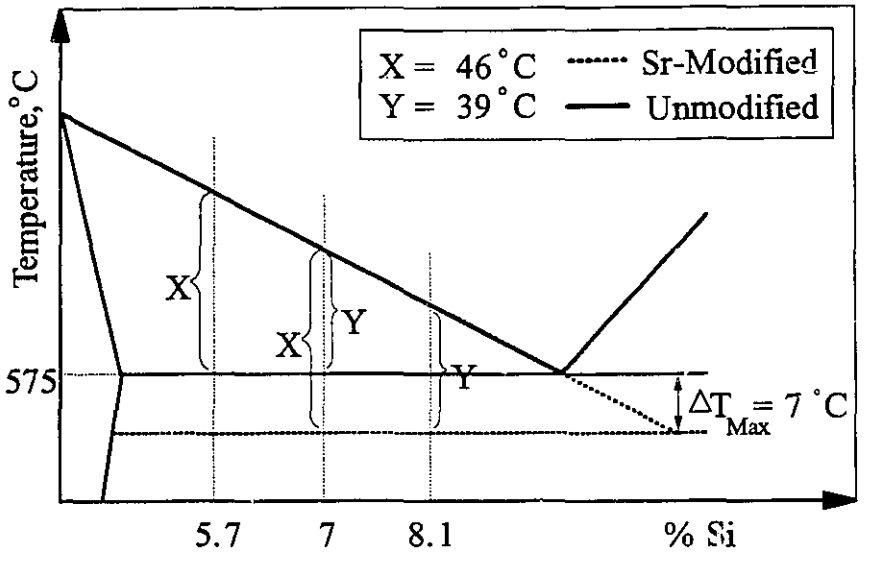

Figure 5.5 : Suppression of the eutectic temperature due to modification.

Two freezing ranges of 39 °C and 46 °C were considered for this investigation. In order to obtain these freezing ranges, three Al-Si alloys with silicon levels of 5.7 wt%, 7 wt% and 8.1 wt% were selected (Figure 5.5). As shown in Figure 5.5, the freezing range of Sr-modified Al-7 wt%Si and Sr-modified Al-8.1 wt%Si alloys are almost equal to the freezing range of unmodified Al-5.7 wt%Si and Al-7 wt%Si alloys, respectively. Therefore, the porosity in Sr-modified Al-8.1 wt%Si and Sr-modified Al-7 wt%Si should be compared to unmodified Al-7 wt%Si and unmodified Al-5.7 wt%Si, respectively to examine the significance of the increase of about 7 °C in freezing range on porosity.

The Al-5.7 wt%Si and Al-8.1 wt%Si alloys were prepared by adding pure silicon and commercial purity aluminum to a base A356 alloy with 7 wt%Si, and modification was carried out by adding 0.02 wt%Sr to the melt by a commercial Al-10 wt%Sr master alloy. The experimental procedure and setup are the same as those employed in Chapter 2 for quantitative evaluation of porosity in Sr-modified Al-Si alloys (section 2.2). The

theoretical densities of the alloys used for calculating the pore volume fraction were derived from Figure 4.7 and are summarized in Table 5.2.

Table 5.2 : Theoretical densities of Al-Si alloys used for calculating the pore volume fraction.

Alloy	Solid Density, ρ_s , g/cm^3	
	Unmodified	Sr-modified
Al-5.7%Si	2.681	2.683
Al-7.0% Si	2.675	2.678
Al-8.1% Si	2.671	2.673
Al-12% Si	2.654	2.656

5.4.2 Results and Discussion

The average pore volume fractions calculated from density measurements for alloys with silicon contents of 5.7%, 8.1% and 7% are shown in Figures 5.6 to 5.8 as a function of average cooling rate for both Sr-modified and unmodified conditions, and different hydrogen levels. The same conclusions as reached in Chapter 2 can be derived from Figures 5.6 to 5.8, i.e. in both Sr-modified and unmodified alloys, the pore volume fraction decreases as the cooling rate increases for a given hydrogen content, and at a given cooling rate the pore volume fraction increases with hydrogen content. In addition, for the same hydrogen content and cooling rate, strontium modification increases the pore volume fraction significantly. This increase in pore volume fraction due to modification is much higher at lower cooling rates (i.e. < 1°C/sec) and at higher hydrogen contents.

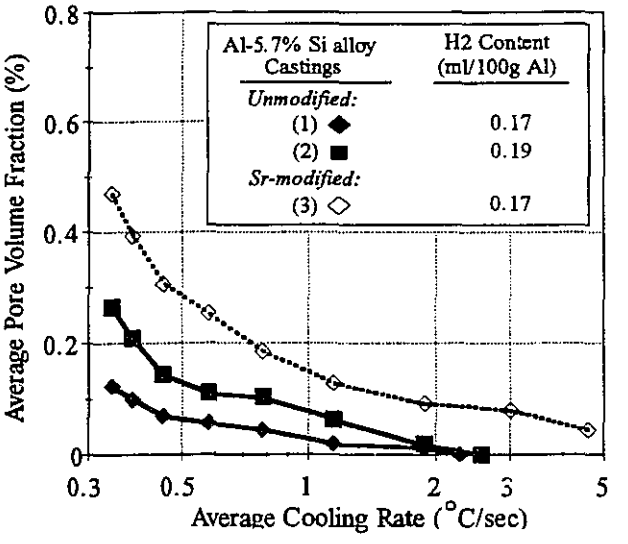

Figure 5.6 : Average pore volume fraction as a function of average cooling rate for directionally solidified Al-5.7%Si alloy.

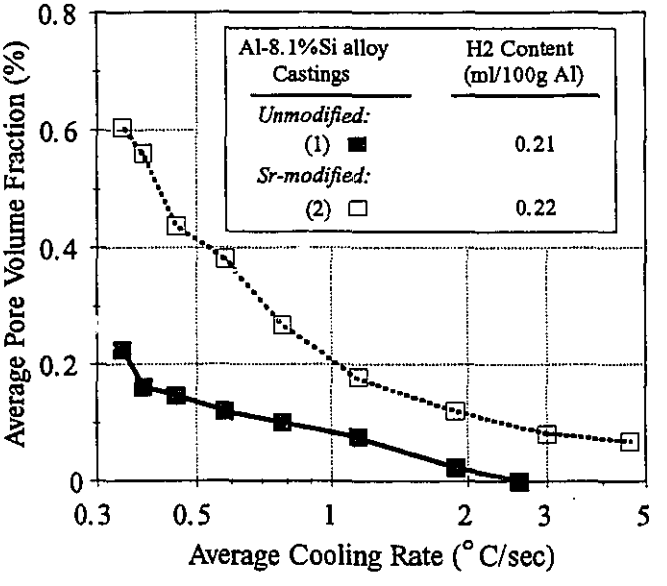

Figure 5.7 : Average pore volume fraction as a function of average cooling rate for directionally solidified Al-8.1%Si alloy.

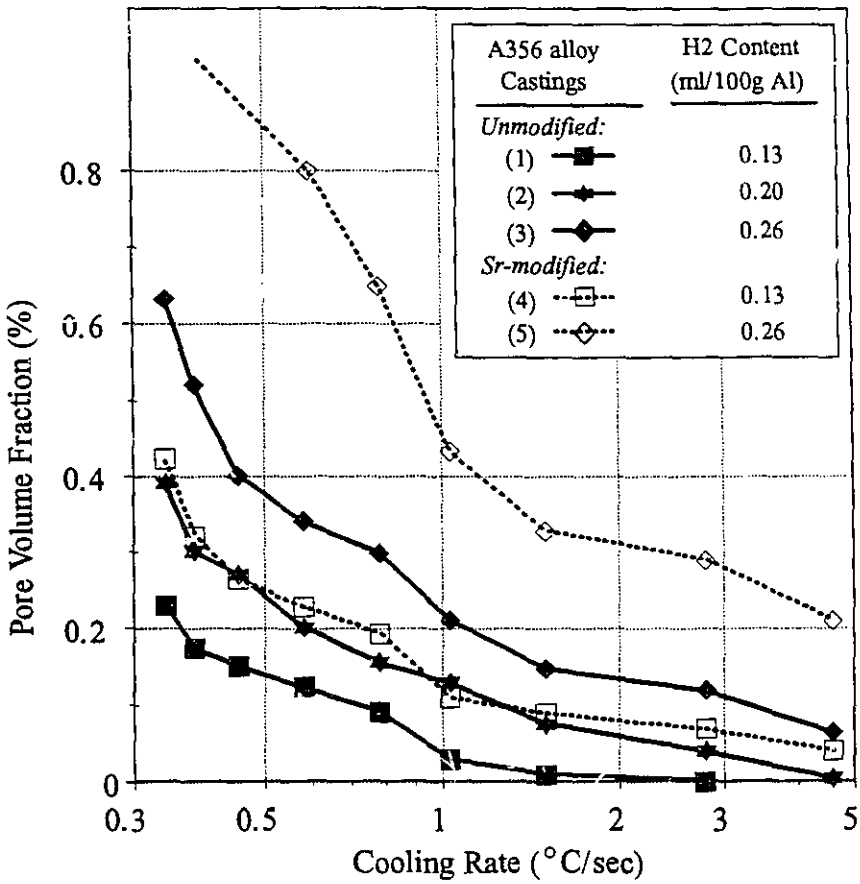

Figure 5.8 : Average pore volume fraction as a function of average cooling rate for directionally solidified Al-7%Si alloy.

To determine the effect on porosity of the increase in the freezing range obtained by decreasing the melt silicon content, the curves for unmodified alloys with a hydrogen content of about 0.2 ml/100g in Figures 5.6 to 5.8 have been replotted in Figure 5.9. It is seen that the pore volume fraction in A356 alloy is higher than in 5.7 wt%Si or 8.1 wt%Si alloys over all ranges of cooling rates, and the porosity level in Al-5.7 wt%Si alloy is virtually the same as in Al-8.1 wt%Si alloy. There is, therefore, an indication of a maximum in the curve of porosity level versus silicon content at about 7 %Si over the

range from 5.7 to 8.1 wt%Si. Thus, A356 alloy, with 7 wt%Si, may well be the Al-Si alloy most prone to porosity formation among all Al-Si alloys with the silicon range from 5.7 wt% to 8.1 wt%.

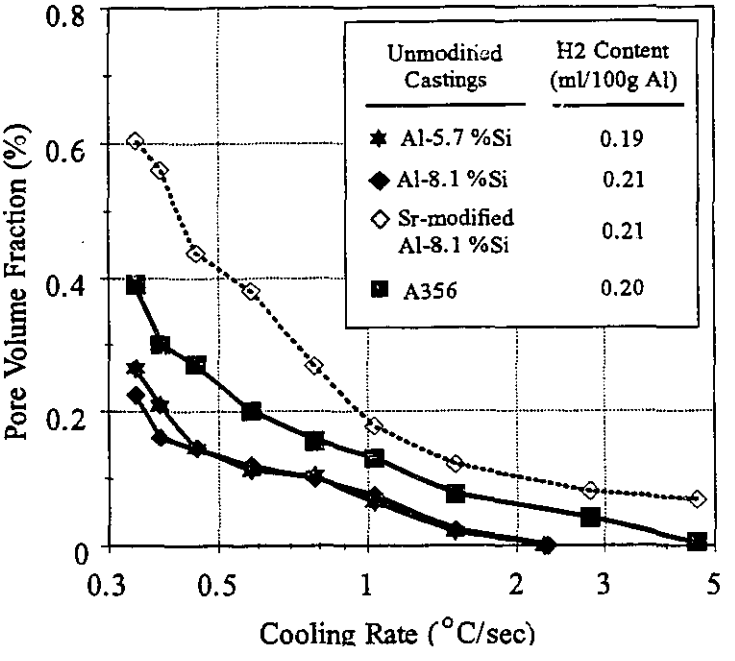

Figure 5.9 : Average pore volume fraction as a function of average cooling rate for Al-Si alloys with different silicon contents.

The maximum in porosity at 7% Si (Figure 5.9) makes it difficult to examine the significance of the effect of the increase in the freezing range on porosity. The reason for this maximum porosity at 7% Si is not clear. However, this behaviour most lead us to the conclusion that the increase in silicon content not only decreases the freezing range, resulting in less porosity, but also affects other factors which somehow increase porosity. These factors may be the surface tension and hydrogen solubility in the liquid, both of which are decreased by increasing the silicon content.

When the Al-8.1% Si alloy is modified with strontium, the freezing range increases to the same level as unmodified Al-7%Si alloy. As shown in Figure 5.9, the increase in porosity due to modification in Al-8.1% Si alloy is much higher than that due to the increase in freezing range obtained by decreasing the silicon content. Therefore, the observed increase in porosity due to modification cannot be attributed only to the increase of freezing range due to eutectic undercooling, and the effect of other parameters should also be considered.

Fuoco *et al* [15] have also shown that the freezing range has only a small effect on porosity compared to modification, and the widening of the freezing range due to modification induced eutectic undercooling alone cannot account for the higher propensity to microporosity formation in Na and Sr-modified melts (Figure 5.10). Different freezing ranges in Figure 5.10 were obtained by changing the melt silicon content. In addition, it is observed from their work that porosity in Al-Si alloys increases linearly by decreasing the silicon content, and no maximum in porosity has been reported at 7%Si (Figure 5.10).

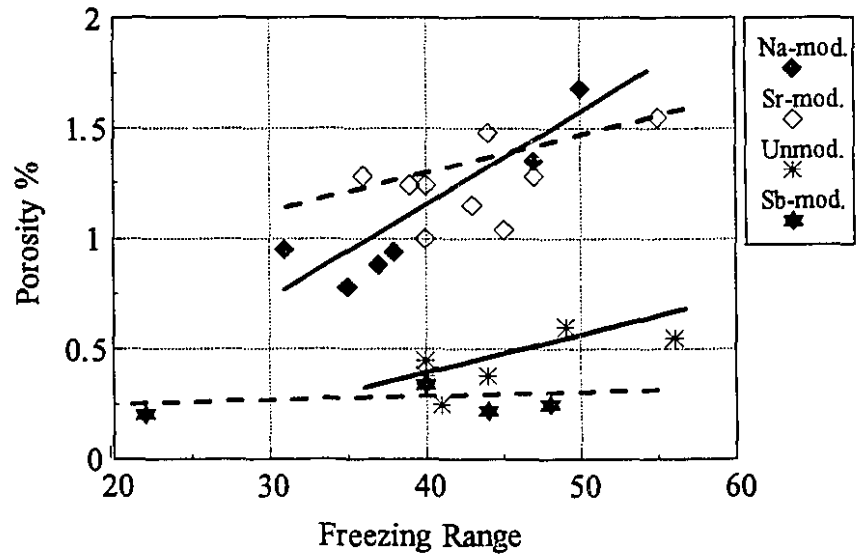

Figure 5.10 : Variation of microporosity content with the freezing range for alloys with various melt treatments[15].

Chen and Engler[16] have also observed that porosity in AlSi7Mg alloy is the highest among the hypoeutectic Al-Si alloys. However, their results on modification are not in good agreement with those found in this study. According to their work, modification has a small effect on porosity in Al-7%Si alloy especially at lower hydrogen contents, and the effect of modification on porosity becomes more significant at higher silicon contents. It can also be observed from their results that an increase in silicon by about 1-2% has a similar effect on porosity as does modification. This observation is not in good agreement with the present work where it has been shown that the effect of modification on porosity is greater than the effect of the change in silicon content.

For a better understanding of the role of silicon content on porosity, the porosity in Al-12 wt%Si alloy was also studied as a function of cooling rate. This alloy was prepared by adding pure silicon to the base A356 alloy. The average pore volume fraction calculated from density measurements for Al-12%Si alloy is shown in Figure 5.11 as a function of average cooling rate for both Sr-modified and unmodified conditions.

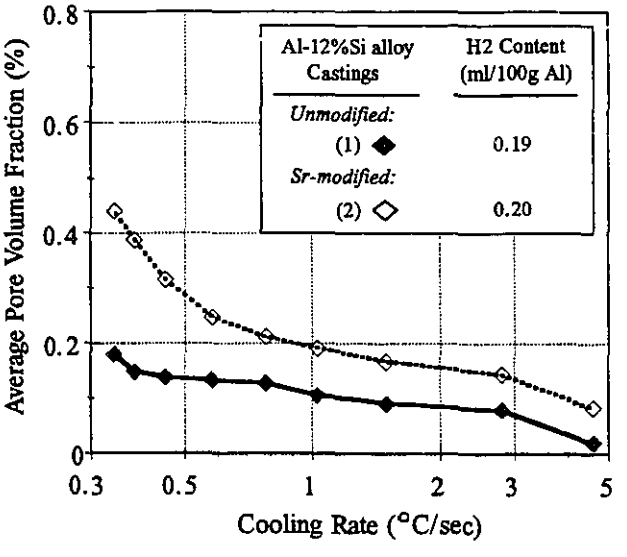

Figure 5.11 : Average pore volume fraction as a function of average cooling rate for directionally solidified Al-12%Si alloy.

As shown in Figure 5.11, Sr-modification significantly increases the porosity. A comparison of Figures 5.9 and 5.11 shows that porosity in Al-12%Si alloy is almost at the same level as in Al-6%Si and Al-8.1%Si alloys. This is again an indication of the small effect of the silicon content, or freezing range, on porosity. In addition, Al-12%Si alloy solidifies with an almost zero mushy zone length, and any increase in freezing range does not have a significant effect on the feeding capability in this alloy.

It is important to realize that an increase in the silicon content can affect the porosity not only by decreasing the freezing range, but also by changing other parameters such as surface tension, hydrogen solubility, viscosity and inclusion content. The change in these parameters may have an effect on porosity corresponding or opposite to that of the freezing range. Consequently, the effect of freezing range on porosity may be magnified or offset by a change of these parameters. Furthur discussion of the effect of the increase in the freezing range will be given in Chapter 9.

It is also possible that the observed increase in porosity in modified alloys is caused by an increase in the time available for hydrogen diffusion and pore growth due to the increase in the freezing range (resulted from depressing the eutectic solidification temperature). This factor will be studied in the following section.

5.5 Solidification Time

If the observed increase in porosity in modified alloys is due to an increase in solidification time, more time is available for hydrogen diffusion and pores can grow over a longer period of time resulting in more porosity. There have been many investigations on the effect of Na or Sr-modification on the cooling curves of Al-Si alloys, and in most

of these, the emphasis has been on the extent of eutectic temperature depression due to modification[9,15,17,18,19,20,21,22,23]. However, at present we are interested in the effect of modifiers on the total solidification time, and especially on the length of the eutectic plateau, as shown in Figure 5.12. The longer the solidification time or the length of the eutectic plateau, the longer time is available for the diffusion of hydrogen and the growth of pores. In Figure 5.12, t_E is the time corresponding to the beginning of the eutectic plateau, t_S is the time at the end of the plateau, and t_F is the time at the end of the eutectic reactions.

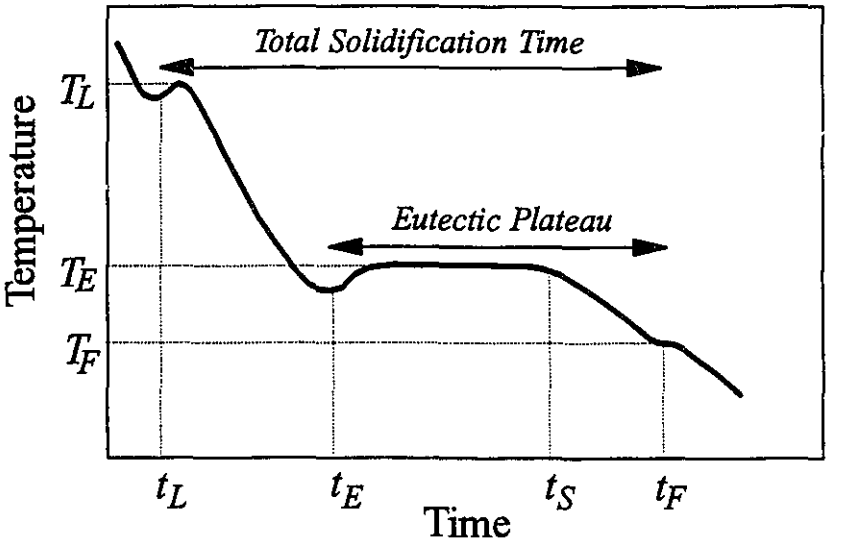

Figure 5.12 : Typical cooling curve of an hypoeutectic Al-Si alloy.

Tenekedjiev and Gruzleski[17] have studied the effect of Sr-modification (at three strontium levels of 0.002%, 0.017% and 0.051%) on the time interval t_E-t_S (in Figure 5.12) in different Al-Si alloys. It is observed from their work on hypoeutectic alloys (i.e. in A355.2, A356.2, A357.1 and A380.2 alloys) and eutectic A413 alloy that there is first

an increase and then a decrease in the time t_E-t_S by strontium addition.

It should be noted that it is very difficult and sometimes impossible to determine the time t_S especially in modified hypoeutectic alloys, and, in actual fact, it is t_F which plays the main role in the diffusion of hydrogen and growth of the pores, since this is the time at which the last interdendritic liquid solidifies.

Flood and Hunt[21] and Meyer[24] have also studied the effect of Na- and Sr-modification on the cooling curve of Al-Si alloys, and have shown that modification depresses the eutectic temperature without changing the shape of the cooling curve or the length of the eutectic plateau. On the other hand, other investigators have shown that Sr and Na-modification decrease both the time t_E-t_S and time t_E-t_F , and therefore, the total solidification time decreases by modification[9,19,20,22,25]. As a result of these apparent contradictions, thermal analysis was conducted to determine the effect of Sr-modification on solidification time.

5.5.1 Experimental Procedure

A356 alloy with the chemical composition given in Table 2.1 (in Chapter 2) was used, and the alloy was modified by adding 0.02 wt%Sr to the melt by a commercial Al-10 wt%Sr master alloy. For thermal analysis, the alloy was melted in an induction furnace and then poured into a fire-clay crucible wrapped with insulating material. Two K-type thermocouples were inserted into the center of the crucible and a continuous record was kept of the temperature vs time. To be able to withdraw the thermocouples from the solidified samples, thermocouples were covered with 304 stainless steel tubes sealed at one end. The experiments were carried out at different cooling rates by preheating the fire-clay crucibles to different temperatures.

5.5.2 Results and Discussion

The cooling curves of unmodified and Sr-modified A356 alloys are shown in Figures 5.13 and 5.14, respectively. For better comparison of the cooling curves of unmodified and Sr-modified A356 alloy, the cooling rates were calculated for each cooling curve as equal to $(T_L-T_F)/(t_F-t_L)$ in Figure 5.12. These cooling rates are plotted as a function of total solidification time (i.e., t_F-t_L) in Figure 5.15.

As shown in Figures 5.13 to 5.15, Sr-modification does not change the total solidification time or the eutectic plateau length, and therefore, has no effect on the time available for the diffusion of hydrogen and the growth of the pores, and the effect of other parameters should be studied to explain the observed increase in porosity in modified alloys.

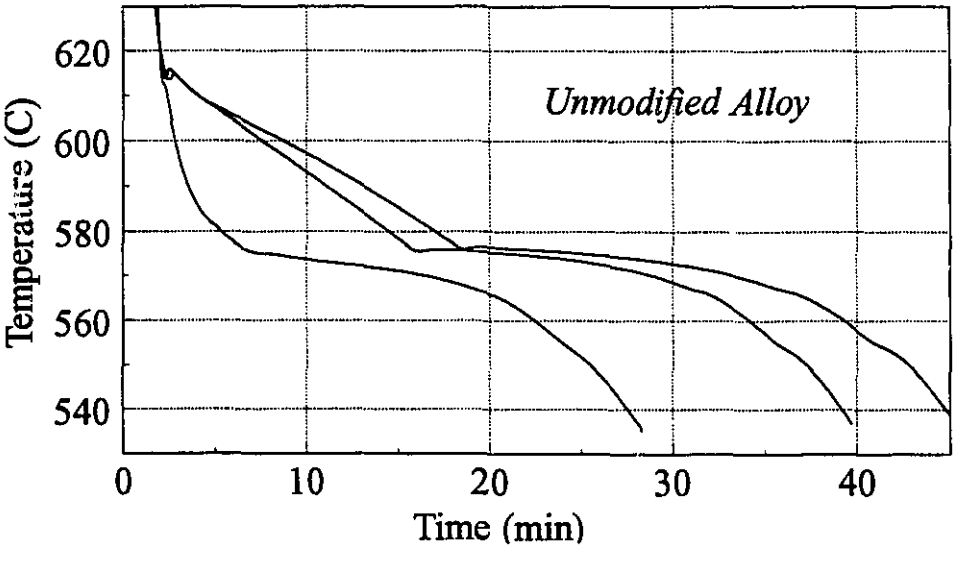

Figure 5.13 : Cooling curves of unmodified A356 alloy at different cooling rates.

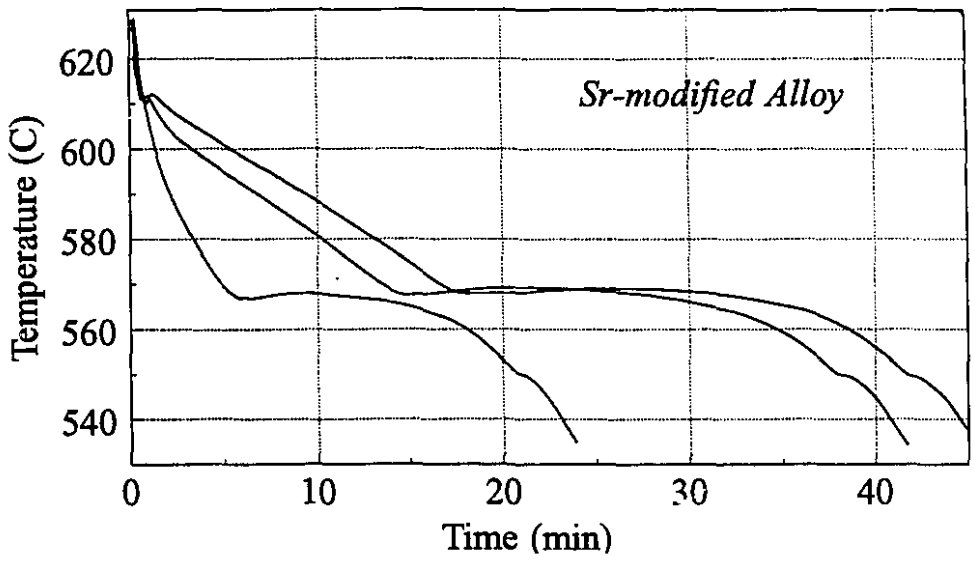

Figure 5.14 : Cooling curves of Sr-modified A356 alloy at different cooling rates.

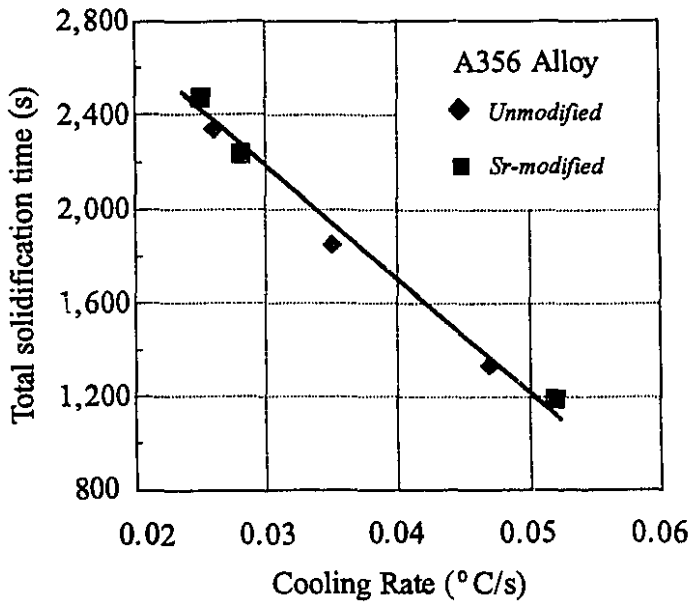

Figure 5.15 : Cooling rate of unmodified and Sr-modified A356 alloy as a function of total solidification time.

5.6 Solid/Liquid Interface Morphology

Another factor related to interdendritic feeding ability is the nature of the solidification front, and modification may increase porosity by changing the shape of the solid/liquid interface. Several investigators, in studying modified and unmodified Al-Si eutectic alloys, have shown that the modified eutectic possesses a smooth solid/liquid interface[20,21,22,26,27,28], although it may be slightly scalloped in nature[9,29]. The changes in shape of the solid/liquid interface of Al-Si eutectic alloy reproduced from the works of Flood and Hunt[21], Denton and Spittle[29] and Glenister and Elliott[26] are shown in Figures 5.16 to 5.18, respectively.

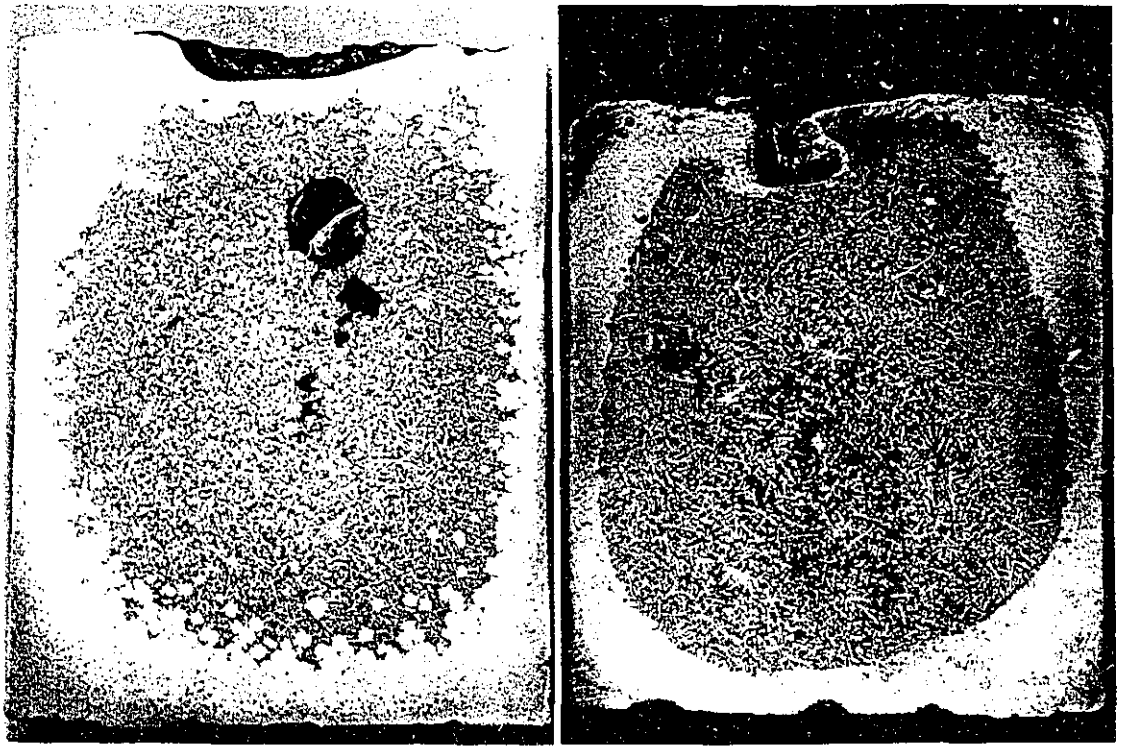

(a) (b)

Figure 5.16 : Quenched structures of solid/liquid interface of Al-Si eutectic alloy in two conditions: a) unmodified alloy b) Na-modified alloy[21].

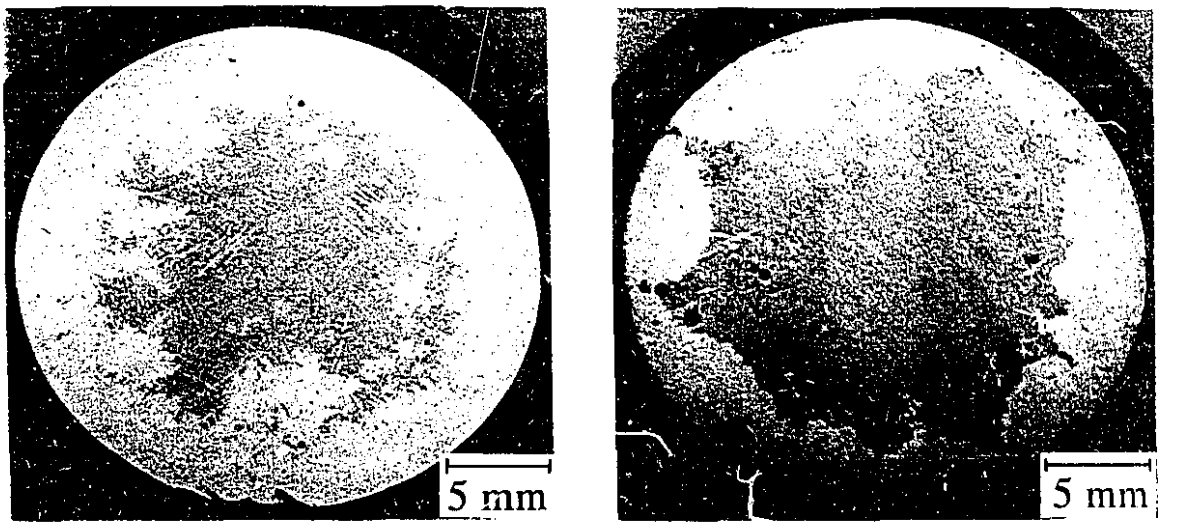

(a) (b)

Figure 5.17 : Structure of solid / liquid interface of a) unmodified LM6 alloy quenched after holding for 3.5 min at 555 °C, and b) Sr-modified LM6 alloy quenched after holding for 2.5 min at 555 °C[29].

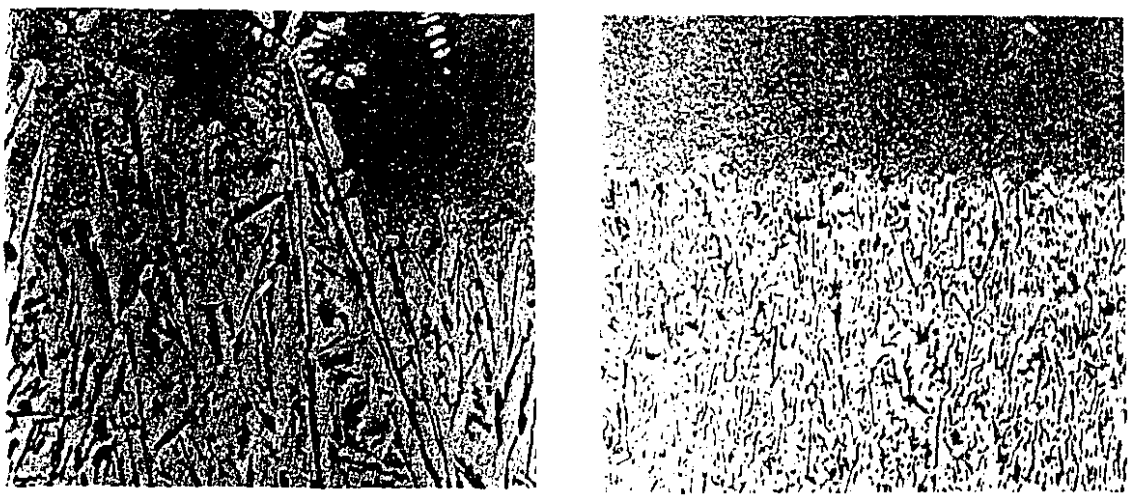

(a) (b)

Figure 5.18 : Quench solid/liquid interfaces of a) unmodified , and b) Sr-modified Al-12.7%Si alloys solidified at interface growth velocity of 10μm/s[26].

It is evident in these figures that growth occurs in a different manner in modified and unmodified alloys. In unmodified alloys, nucleation of the silicon takes place on the Al dendrites ahead of the main eutectic front resulting in an irregular interface, whereas, in the presence of modifiers, growth occurs with a smooth eutectic front. In an unmodified alloy, liquid must flow a long distance between the eutectic colonies, and logically these alloys should have more microporosity.

However, it was demonstrated in Figure 5.11 for a directionally solidified eutectic alloy that porosity in the modified alloy is higher than in unmodified alloys. Since most of the studies on solid/liquid interface shape have been on eutectic Al-Si alloys while most porosity measurements are on hypoeutectic alloys, a short investigation on interface shape in hypoeutectic alloys was done.

5.6.1 Experimental Procedure

Unmodified and Sr-modified (0.02 wt% Sr) A356 alloys were cast at 730 °C into one end closed thin graphite tubes, 150 mm in height, 20 mm in diameter and 1.5 mm thickness. Two graphite crucibles (for unmodified and Sr-modified samples) were held together in the middle of a resistance furnace and the furnace was insulated at the top and the bottom with Kaowool. After a period of time to stabilize the temperature inside the furnace and to allow the upper part of the samples to be melted, the graphite crucibles were moved down very slowly by about 2 cm to obtain a directional solidification. Then, the crucibles were quickly quenched, and metallography was carried out on the cross section of the quenched samples. The schematic of the setup used in this experiment is shown in Figure 5.19.

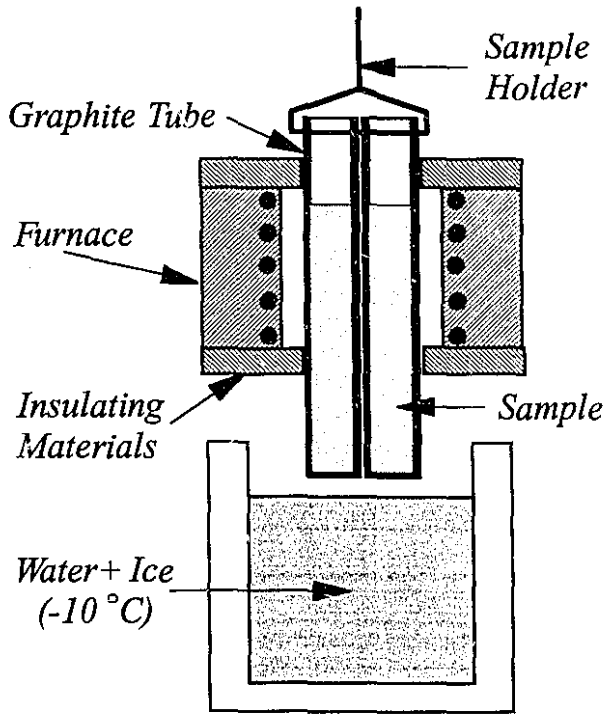

Figure 5.19 : Schematic of the setup used to quench the partially melted samples.

5.6.2 Results and Discussion

Figure 5.20 shows the microstructure of the solid/liquid interface of the quenched unmodified and Sr-modified A356 samples. As shown in Figure 5.20, the solid/liquid interface of unmodified and Sr-modified A356 alloys are similar. However, the liquid interface of unmodified alloy seems to be more irregular compared to modified alloy. For this reason, an unmodified alloy may even have more tendency to liquid entrapment and to microporosity formation. However, it was observed in Chapter 2 and section 5.4 in the present chapter that unmodified alloys have less porosity compared to modified alloys, and therefore, the change in the shape of the solid/liquid interface due to modification is not responsible for the observed increase in porosity in modified alloys.

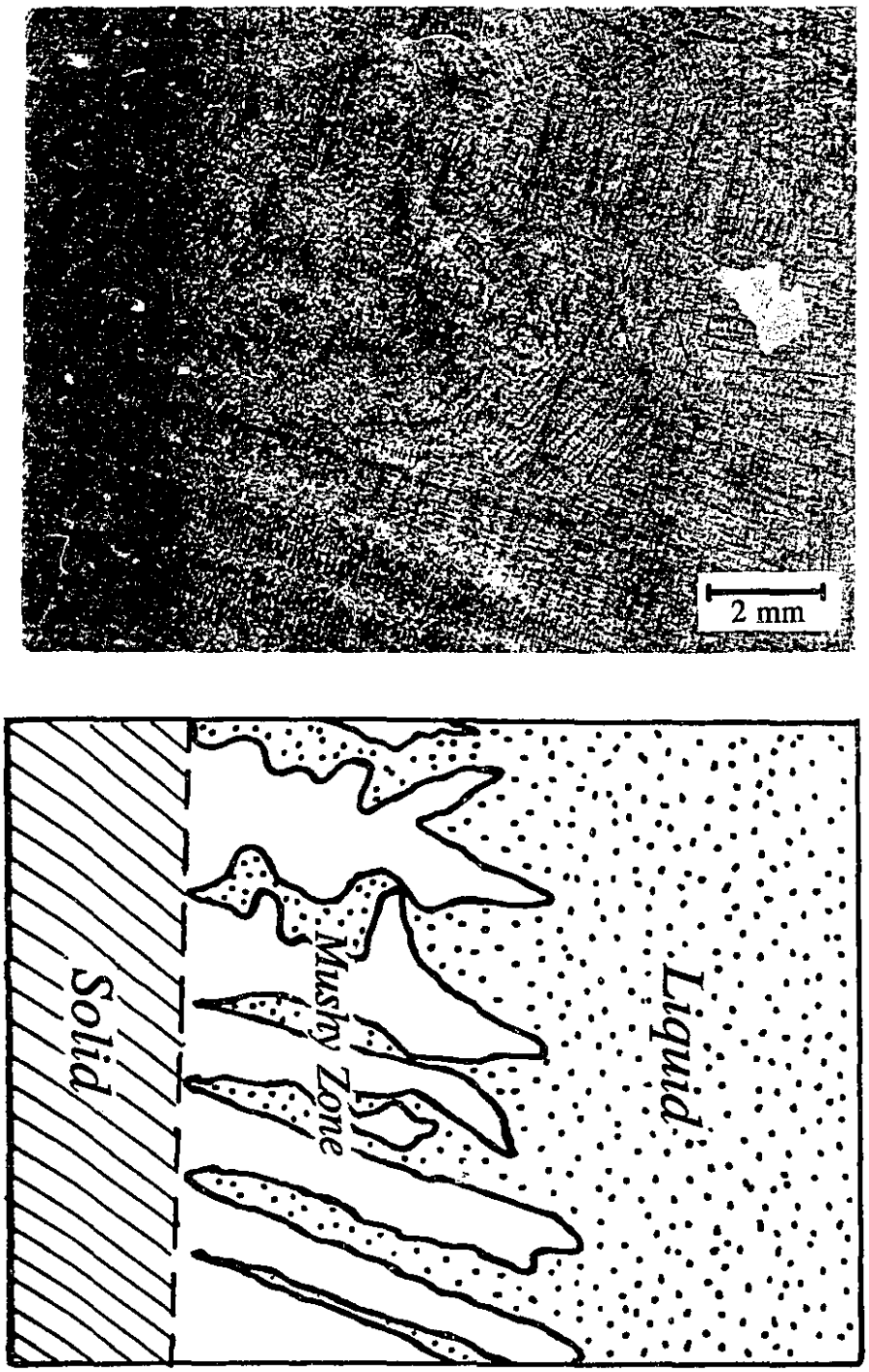

Figure 5.20a : Microstructure of the quenched solid/liquid interfaces of an unmodified A356 alloys.

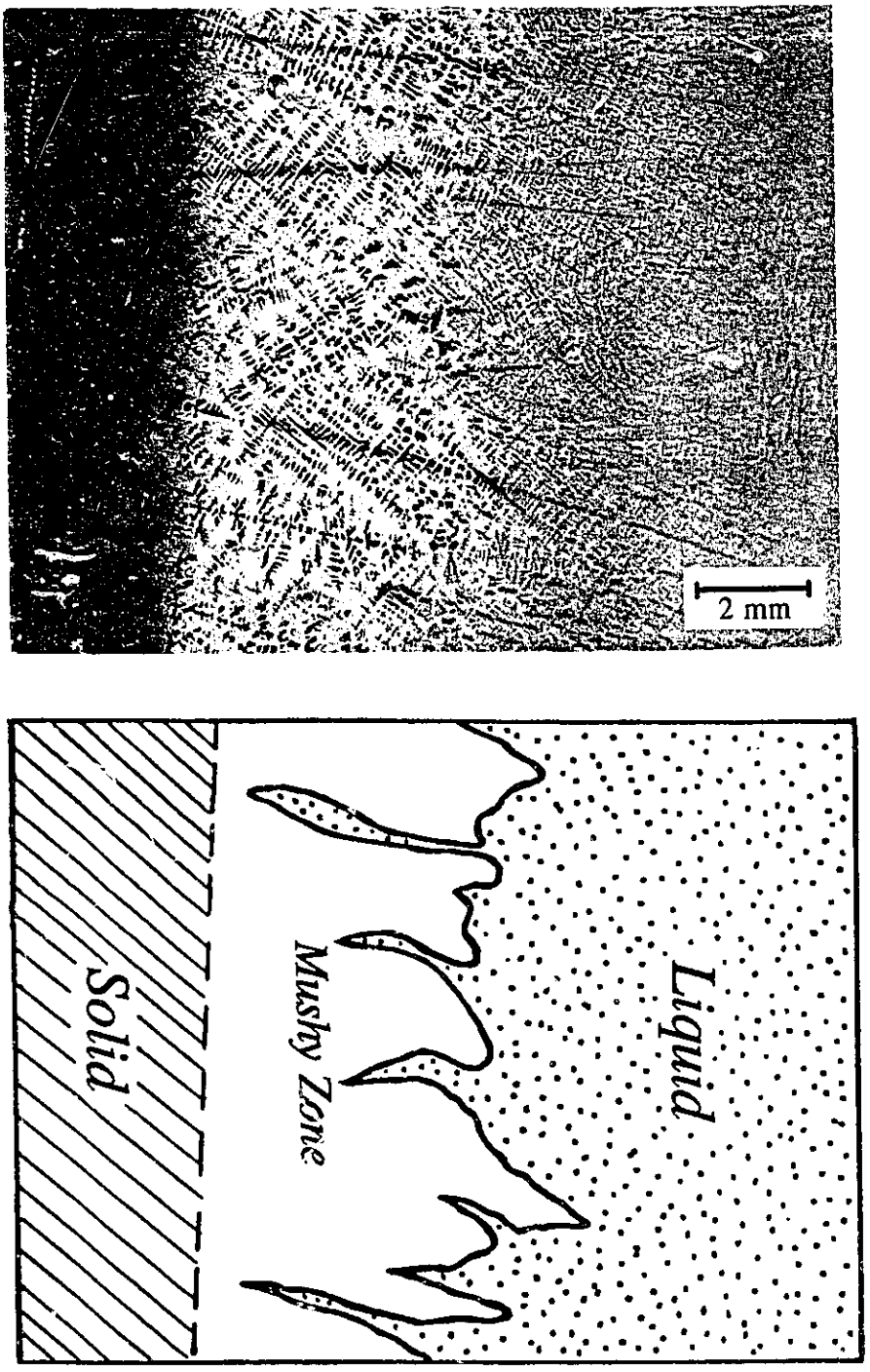

Figure 5.20b : Microstructure of the quenched solid/liquid interfaces of an Sr-modified A356 alloys.

5.7 References

1. M. Bamberger, B.Z. Weiss and M.M. Stupel; "Heat Flow and Dendritic Arm Spacing in Chill-cast Al-Si Alloys", *Mater. Sci. Technol.*, Vol. 3, 1987, pp. 49-56

2. Q.S. Hamed and R. Elliott; "The Dependence of Secondary Dendrite Arm Spacing on Solidification Conditions - Part II : Al-7Si-0.5Mg Alloys Treated With Sr and Sb", *Cast Metals*, Vol. 6, No. 1, 1993, pp. 42-46

3. R.I.L. Guthrie and T. Iida; *The Physical Properties of Liquid Metals*, Oxford University Press, New York, 1988, pp. 147-98

4. A.M. Korolkov, "Casting Properties of Metals and Alloys", Consultants Bureau Enterprises inc., New York, 1963, pp. 55-67

5. W.R.D. Jones and W.L. Bartlett, "The Viscosity of Aluminium and Binary Aluminium Alloys", *J. Inst. Metals*, Vol.81, 1952-53, pp 145-52

6. F. Ajersch and M. Mada; "Viscosity Measurements of Liquid A356 Aluminum Alloy and of A356 With Additions of Solid SiC Particles", Private Report, Metallurgical Engineering Department, Ecole Polytechnique, Montreal, Canada, Feb. 1989

7. T.P. Yao and V. Kondic; "The Viscosity of Molten Tin, Lead, Zinc, Aluminum and Some of Their Alloys", *J. Inst. Met.*, Vol. 81, 1952-1953, pp. 17-24

8. S. Ganesan, R. Speiser and D.R. Poirier; "Viscosities of Aluminum-Rich Al-Cu Liquid Alloys", *Metall. Trans. B*, Vol. 18B, June 1987, pp. 421-24

9. Q.S. Hamed, R. Elliott and P.S. Cooper; "Solidification Characteristics of Sodium and Strontium Modified Al-Si Casting Alloys", *Light Metals*, 1992, pp. 1391-97

10. D. Argo and J.E. Gruzleski; "Porosity in Modified Aluminum Alloy Castings", *AFS Trans.*, Vol. 96, pp. 65-74

11. H. Iwahori, K. Yonekura, Y. Yamamoto and M. Nakamura; "Occurring Behaviour of Porosity and Feeding Capabilities of Sodium and Strontium Modified Al-Si Alloys", *AFS Trans.*, Vol. 98, 1990, pp. 167-73

12. J. Whittenberger and F.N. Rhines; "Origin of Porosity in Castings of Magnesium-Aluminum and Other Alloys", *Trans. TMS-AIME*, Vol. 194, 1952, pp. 409-20

13. R.L. Coble and M.C. Flemings; "On the Removal of Pores from Castings by Sintering", *Metall. Trans.*, Vol. 2, Feb. 1971, pp. 409-15

14. M. Garat, G. Laslaz, S. Jacob, P. Meyer, P. Guerin and R. Adam; "State-of-the-Art Use of Sb-, Na- and Sr-modified Al-Si Casting Alloys", *AFS Trans.*, Vol. 100, 1992, pp. 821-32

15. R. Fuoco, H. Goldenstein and J.E. Gruzleski; "Evaluation of the Effect of Modification-Induced Eutectic Undercooling on the Microprosity Formation in 356 Aluminum Alloy", *AFS Trans.*, Vol. 102, 1994

16. X.G. Chen and S. Engler; "Hydrogen and Porosity in Aluminum-Silicon and Aluminum-Magnesium Alloys", *Metall.*, 45 (10), Oct. 1991, pp. 1-17

17. N. Tenekedjiev and J.E. Gruzleski; "Thermal Analysis of Strontium Treated Hypoeutectic and Eutectic Aluminum-Silicon Casting Alloys", *AFS Trans.*, Vol. 99, 1991, pp. 1-6

18. T.j. Hurley and R.G. Atkinson; "Effects of Modification Practice on Aluminum A356 Alloys", *AFS Trans.*, Vol. 93, 1985, pp. 291-96

19. R.C. Plumb and J.E. Lewis; "The Modification of Aluminum-Silicon Alloys by Sodium", *J. Inst. Met.*, Vol. 86, 1957-58, pp. 393-400

20. M.D. Hanna, S. Lu and A. Hellawell; "Modification in the Aluminum Silicon System", *Met. Trans. A*, Vol. 15A, March 1984, pp.459-69

21. S.C. Flood and J.D. Hunt; "Modification of Al-Si Eutectic Alloys with Na", *Metal Science*, Vol. 15, July 1981, pp. 287-93

22. C.B. Kim and R.W. Heine; "Fundamentals of Modification in the Aluminum-Silicon System", *J. Inst. Met.*, Vol. 92, 1963-64, pp. 367-76

23. G. Chai and L. Backerud; "Factors Affecting Modification of Al-Si Alloys by Adding Sr-Containing Master Alloys", *AFS Trans.*, Vol. 100, 1992, pp. 847-54

24. W. Meyer; "Relation Between Cooling Rate and Cast Structure in Na- and Sr-modified Al-Si Alloys", *Aluminium*, Vol. 54, No.11, Jan. 1978, pp. 700-703

25. K. Eugen Honer and Z. Youling; "Influence of Calcium and Strontium on the Hydrogen Pick-up in Aluminum Alloy Melts by the Example of G-AlSi12", *Giesserei-Forschung*, Vol. 39, Jan. 1987, pp. 34-48

26. S.M.D. Glenister and R. Elliott; "Strontium Modification of Al-12 wt%Si Alloys", *Metal Science*, April 1981, pp. 181-84

27. S. Engler; "Zur Erstarrungsmorphologie von Aluminium-Gubwerkstoffen - Teil III: AlSi-Legierungen", *Aluminium*, Vol. 46, Jan. 1970, No. 1, pp. 121-26

28. S. Engler and K. Gockmann; "Erstarrnngs- und Lunkerverhalten eutektischer Aluminium-Silizium-Legierungen", *Aluminium*, Vol. 50, No. 11, Jan. 1974, pp. 712-18

29. J.R. Denton and J.A. Spittle; "Solidification and Susceptibility to Hydrogen Absorption of Al-Si Alloys Containing Strontium", *Mater. Sci. Technol.*, Vol. 1, April 1985 , pp. 305-11

Chapter 6

The Effect of Sr-Modification on the Melt Inclusion Content

6.1 Introduction

As mentioned earlier in section 1.2.2.1.4, inclusions in the melt offer heterogeneous sites for the nucleation of pores and thus facilitate pore formation. This effect can be so significant that even in the presence of small quantities of inclusions, the critical hydrogen concentration for pore formation can be lowered significantly[1,2]. Some authors have suggested that sodium and strontium modification can facilitate the nucleation of pores by forming inclusions acting as nuclei[3,4,5].

The only investigation on the effect of Sr-modification on the melt inclusion content is the work done by Iwahori *et al* [6]. They showed that Sr addition increases the number of inclusions in the melt. They also studied the rate of vacuum degassing of Na and Sr-modified melts and found that the hydrogen content of an unmodified or Na-modified melt is readily decreased by degassing, while that in a Sr-modified melt decreases only slightly. This was considered to be because the hydrogen, absorbed into the oxide in the melt, is more strongly fixed in the oxides by the addition of strontium to the melt. In addition, when an inclusion removal treatment was carried out on Sr-modified melts, less porosity was found in castings produced from these melts.

The aim of this chapter is to determine if there is an increase in melt inclusion content due to Sr-modification and to examine whether these inclusions can act as heterogeneous sites for the nucleation of pores.

6.2 Melt Inclusion Content

The statistically small numbers of inclusions present in a metal sample makes the detection of these inclusions extremely difficult. Generally, the following techniques are available to define quantitatively and/or qualitatively the melt inclusions.

A commonly used method of inclusion identification and partial quantification is the general class called Liquid Aluminum Filtration[7]. PODFA (Porous Disc Filtration Apparatus) developed by Alcan, and LAIS (Liquid Aluminum Inclusion Sampler) developed by Union Carbide's Linde Division are two commercial variants. In the basic procedure, a known quantity of liquid aluminum is pulled through a ceramic filter. This filter traps and concentrates any inclusions present in the melt. After cooling, the filter is sectioned and examined microscopically. The types of inclusions can be determined along with an estimation of the quantities of each type.

Another inclusion measurement method is the Liquid Metal Cleanliness Analyzer (LIMCA) [8]. The basic principle of this device is that molten aluminum is drawn through a capillary opening which is also conducting a DC current. The presence of non conducting particles in the capillary will increase the voltage drop through the capillary proportional to the particle size. Both the number and size of inclusions can be determined in real time[9].

A third analytical method for inclusion analysis is the electrochemical dissolution of aluminum samples[10]. A metal sample is collected much like a Ransley pin. The pin

is machined and then chemically dissolved in the correct aqueous media. The selection of the solution must be chosen to dissolve the metallic aluminum, but not the inclusion materials. The solution is then filtered to capture the particles and the particle types and sizes are measured with a SEM equipped with feature analysis facilities.

In the present work, a version of the filtration technique (PODFA) was applied to semi-quantitatively measure the inclusion levels in unmodified and Sr-modified A356 melts.

6.2.1 Experimental Procedures

A356 alloy, whose chemical composition is given in Table 2.1, was used in this investigation. In each experiment, an 8-kg melt was prepared in a silicon carbide crucible using an electric resistance furnace. Another silicon carbide crucible with a capacity of about 4 kg was used for the filtration of the melt. A hole with a diameter of 14 mm was made at the bottom of this crucible and a 22 mm diameter porous disk filter was cemented to the bottom of the crucible using a ceramic glue. The crucible was coated with an iron oxide wash for ease of removing the remaining metal after solidification. In each experiment, two crucibles were required (for modified and unmodified melts). These crucibles were preheated up to 800 °C in an electric resistance furnace. The preheated crucibles were then wrapped with an insulating wool and placed in the setup shown in Figure 6.1.

A 3.5 kg metal sample was taken directly from the melt and poured into the crucible. Then the upper cap was closed and air pressure was applied into the chamber until 2 kg of the melt was passed through the filter. A balance located below the filtrate crucible enabled precise determination of the exact amount of the metal (Figure 6.1).

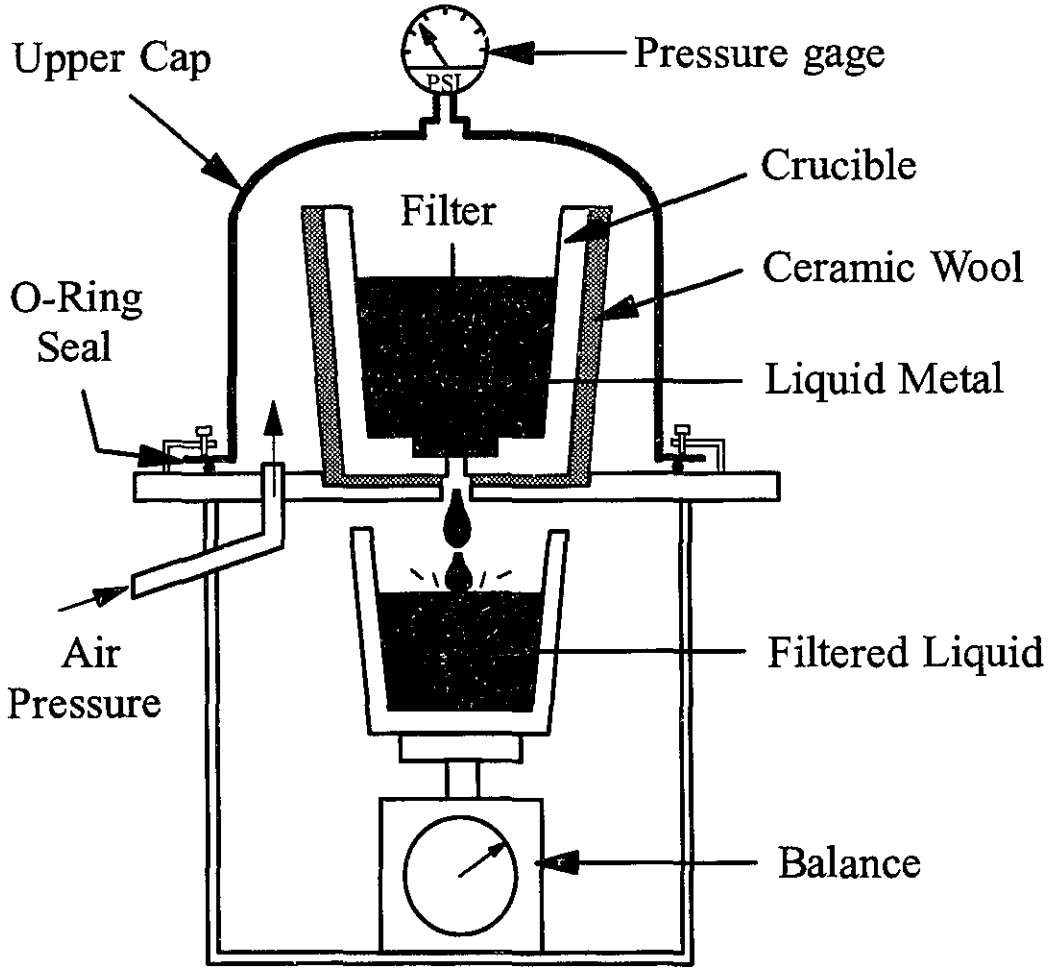

Figure 6.1 : Schematic of the experimental setup used for filtration of the melts

After filtration of the unmodified melt, 0.02 wt%Sr was added to the remaining melt in the form of commercial Al-10 wt%Sr master alloy. The melt was held for about 45 minutes to allow the dissolution of strontium. The same procedure as used with the unmodified melt was followed to filter and sample the Sr-modified melt. Three experiments were carried out on both unmodified and Sr-modified melts. Then, the filters

with the residue were sectioned vertically along the central plane and prepared for metallographic examination. A JEOL-JSM 840 scanning electron microscope was used for metallographic examination, and X-Ray mapping was performed using an Energy Dispersive Spectroscopy (EDS) analyzer attached to the SEM.

6.2.2 Results and Discussion

Typical micrographs of the inclusions over the filter are shown in Figures 6.2 and 6.3 for unmodified and Sr-modified melts, respectively. It can be seen from Figures 6.2 and 6.3 that Sr-modified melts contain larger amounts of inclusions than unmodified melts. Although melt inclusion content was not quantified, the observed difference in melt inclusion content between unmodified and Sr-modified melts in the present work seems to be larger than that reported by Iwahori *et al*[6]. According to their work, Sr modification increased the inclusion level from 38 inclusions/500mm^2 to 43 inclusions/500 mm^2. Nevertheless, it can be concluded both from their work and the present study that Sr-modification increases the inclusion content of an A356 melt.

In the case of Sr-modified alloys, X-Ray mapping was performed for oxygen and strontium. The results showed that the inclusions above the filter are mainly oxides, and strontium was detected only in some of the inclusions. It is important to note that most of the inclusions above the filter had been removed during the sample preparation (i.e., during the grinding and polishing), and X-Ray mapping was carried out only on the retained inclusions in the sample. Since the alumina particles used for polishing may be entrapped in the sample cavities, the samples were cleaned carefully and careful attention was applied in selecting the proper area for X-Ray mapping.

The following hypotheses can be made to account for the observed increase in inclusion content of Sr-modified melts:

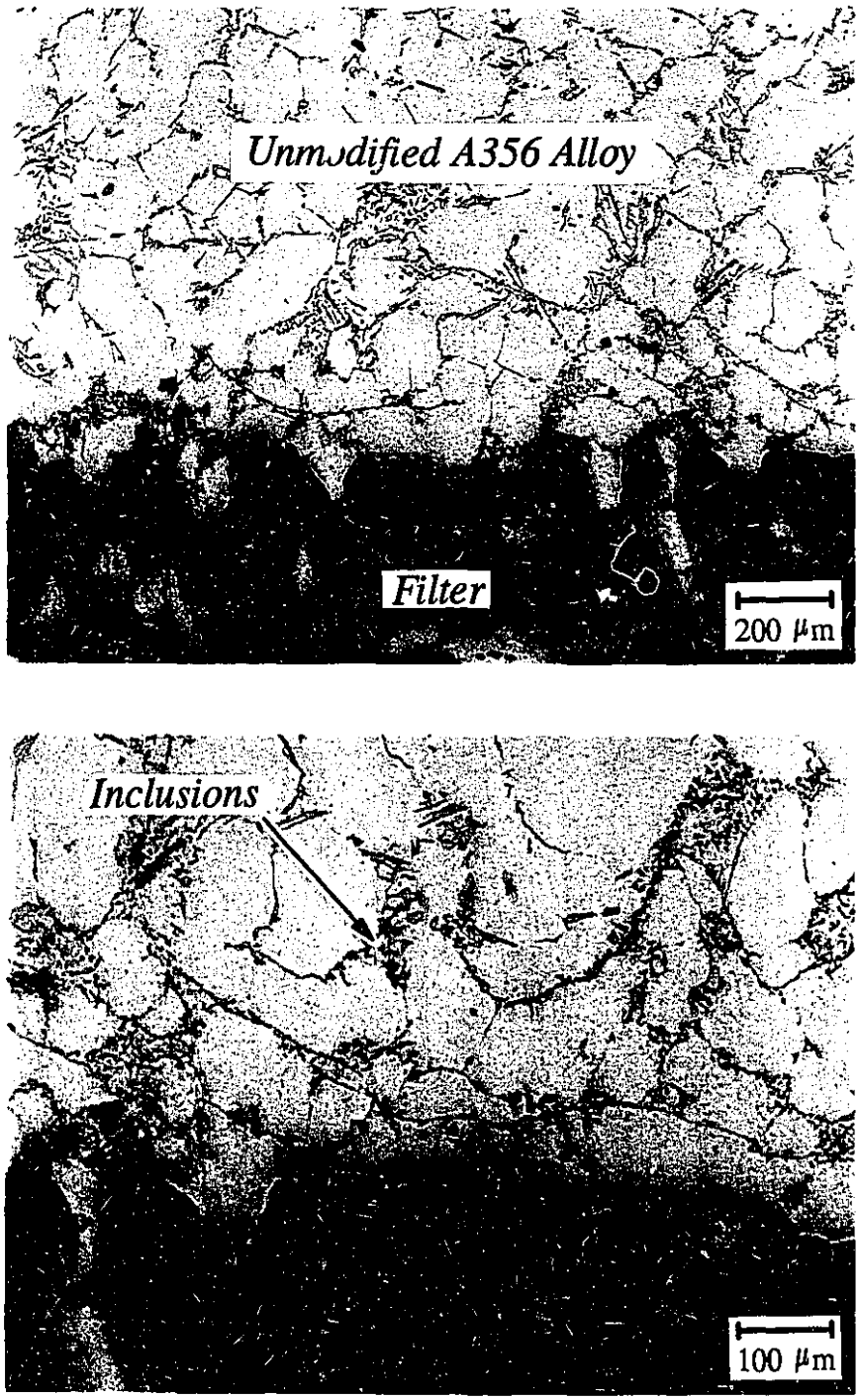

Figure 6.2 : Micrographs showing the inclusions on the filter section of the pressure filtration test for an unmodified A356 alloy.

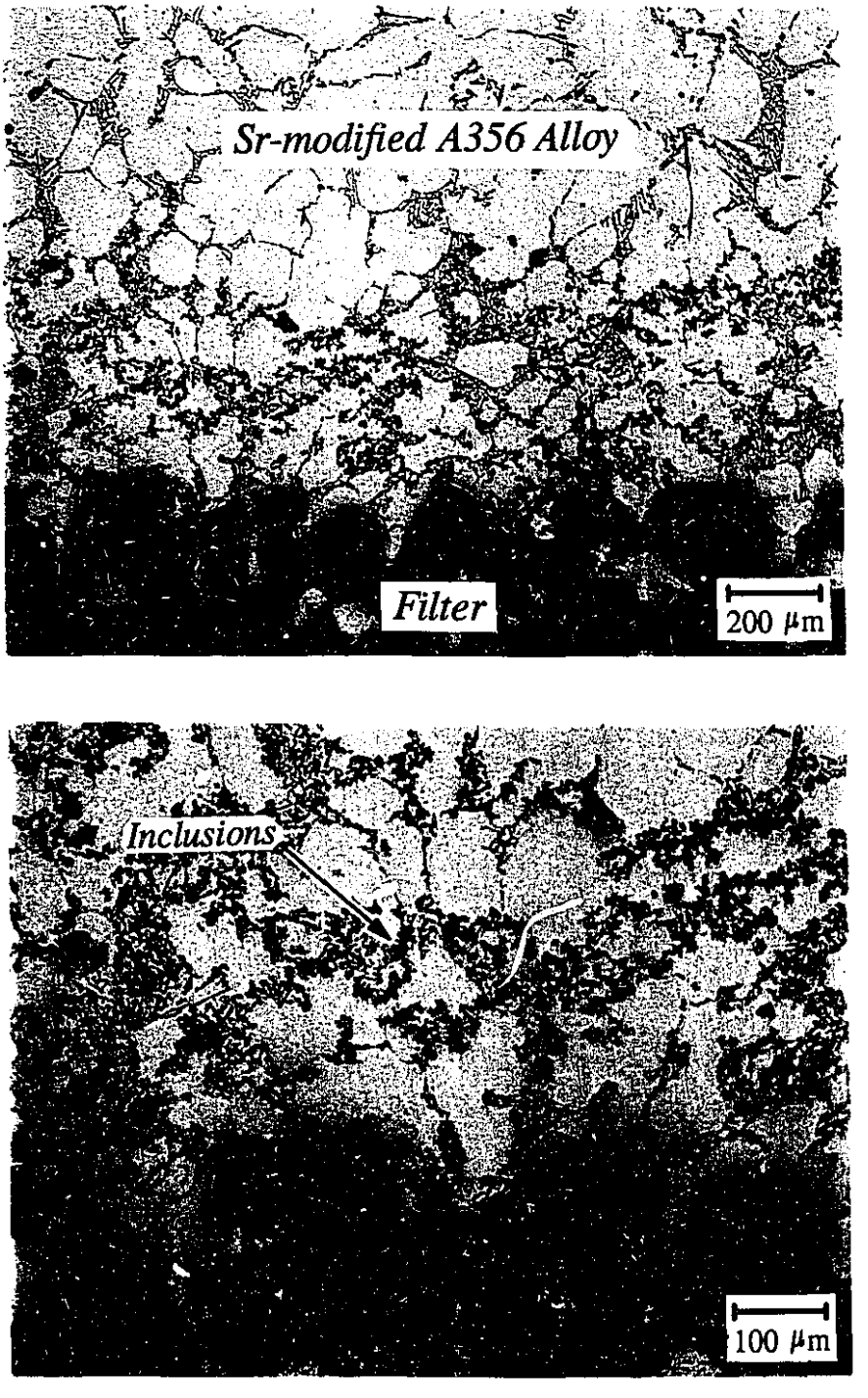

Figure 6.3 : Micrographs showing the inclusions on the filter section of the pressure filtration test for a Sr-modified A356 alloy.

a) more inclusions may be formed in the melt as a result of an increase in the melt oxidation rate in the presence of strontium, or b) the inclusions may be imported to the melt through the strontium master alloy. With respect to the first interpretation, it is therefore, worth studying the oxidation of Al-Si melts to examine whether Sr-modification changes the melt oxidation rate.

6.3 Melt Oxidation Rate

Most of the studies on the oxidation rate of aluminum have been in the solid state [11,12,13,14], and only a few data are available on the oxidation rate of aluminum melts[12,15]. However, to the authors's knowledge, no data are available on the effect of strontium on the oxidation rate of aluminum or its alloys either in the solid or in the liquid states. In this section, therefore, the effect of strontium on the oxidation rate of Al-Si melts is investigated.

6.3.1 Oxidation Theory

Aluminum oxidation is unavoidable due to very low oxygen partial pressure required for oxidation. Aluminum oxide is dense, coherent and is characterized by an oxidation rate that decreases with time. Basically, the oxidation rate is influenced by the coherency of the oxide layer on the surface of the melt. During oxidation, two diffusion fluxes through the oxide layer are involved, i.e., the transport of oxygen anions and the metal cations. If the oxide layer is dense and free of physical discontinuities, metal cation transport is progressively impeded. As a result, the rate of oxide growth diminishes with time. Fick's first law of diffusion can be used to develop an analytical expression to describe the process as [12,15] :

$$(\Delta m)^2 = k_p . t \qquad (6.1)$$

where Δm is the weight gain, t is the oxidation time and k_p is a constant based on a diffusion coefficient. Since diffusion processes are thermally activated, the oxidation constant, k_p , is an exponential function of temperature (i.e., follows an Arrhenius relationship). The general form of the above equation (Eq. 6.1) is graphically depicted in Figure 6.4. Since the resulting curve is a parabola, this type of kinetically self-limiting oxidation is referred to as *parabolic law oxidation*. An important commercial consequence of parabolic law oxidation is that the rate of oxidation decreases with time. A dense, non-porous, and protective oxide is typical of this type of oxidation. The oxidation of molten aluminum produces such an oxide[15].

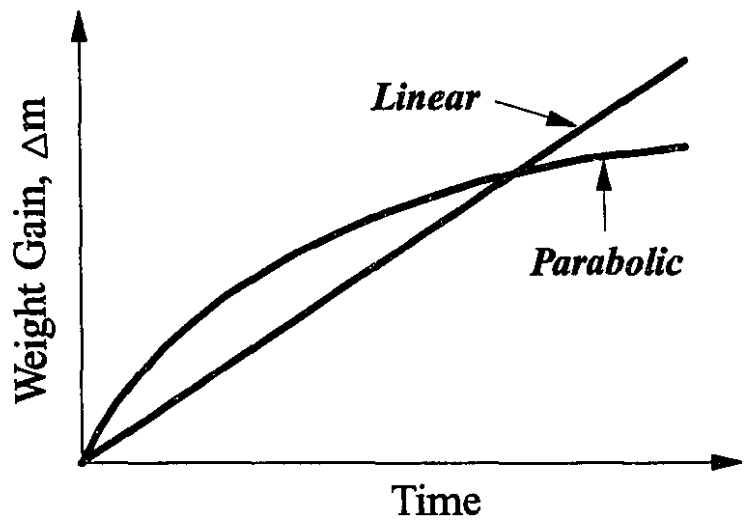

Figure 6.4 : Graphical depiction of linear and parabolic law oxidations

Conversely, if the resulting oxide is porous, the protective value of the developing layer is lost. In this situation, the rate of oxidation is time invariant because little

resistance to cationic transport is present. This mechanism is referred to as *linear oxidation*, and continues until the quantity of metal is consumed (Figure 6.4). The resulting oxide is said to be unprotective. A third class of oxidation mechanism, known as *logarithmic oxidation*, is an intermediate case between the limiting cases of parabolic and linear oxidation. During oxidation, a combination of two or more of these relationships are also quite common. A metal or alloy may, for instance, start to oxidize parabolically and then continue linearly.

In a classic paper, Pilling and Bedworth[11] proposed a practical rationalization of protective and unprotective oxides. Their original work related to oxidation on solid metal surfaces, however, the analysis can be applied to quiescent liquid metals when the metal/oxide couple is confined[15]. The Pilling and Bedworth model recognizes that if the density of an oxide forming on a metal surface is lower than that of the parent metal, the oxide is protective. If the oxide is more dense than the parent metal, the layer is unprotective. The so-called Pilling-Bedworth Ratio (PBR) is defined as:

$$PBR = \frac{volume\ oxide}{volume\ metal} = \frac{M_0\,\rho_m}{M_m N_A\,\rho_0} \qquad (6.2)$$

where M_0 is the molecular wt. of oxide, M_m is the molecular wt. of metal, ρ_m is the metal density, ρ_0 is the oxide density and N_A is the ratio metal atoms/molecules oxide. Tabulated values of PBR for selected oxides are given in Table 6.1.

Table 6.1 : PBR values for different oxides[11].

Metal	Al	Cu	Mg	Mn	Si	Na	Sr
PBR	1.28	1.7	0.84	2.07	2.04	0.32	0.69

The practical significance of this information is that if PBR > 1, the oxide layer is dense, protective, and follows the parabolic law. If PBR < 1, a porous and unprotective oxide is produced, and either linear or logarithmic oxidation prevails. According to Table 6.1, aluminum oxide with PBR > 1 is protective, and if an aluminum melt remains undisturbed, the quantity of oxide formed will therefore be limited. In the case of strontium, the PBR value is less than unity and therefore, strontium oxide is not protective and oxidation continues with an high rate.

It is also worth mentioning that there is no direct connection between the oxidation rate of a metal and the magnitude of the negative free energy of formation (ΔG) [16]. For example, the oxidation rate of aluminum at 600°C is several orders of magnitude less than that of copper, although the free energy of formation at 600 °C for aluminum oxide (ΔG_{Al2O3} = - 220 kcal/mole of oxygen) is considerably larger than for Cu_2O (ΔG_{Cu2O} = -55 kcal/mole of oxygen)[16]. The reason for the variant behaviour of the oxidation rates is the difference in the nature of the defects in the two oxide lattices. Copper oxide shows a considerable concentration of copper ion vacancies and holes which allow for a rapid diffusion of copper ions and electrons. On the other hand, the Al_2O_3 lattice exhibits only a small lattice defect concentration at high temperatures and low oxygen pressures, so that considerably fewer paths for diffusion are available. Moreover, the energy barriers (or potential barriers) which must also be considered in a quantitative approach to diffusion, are evidently high in Al_2O_3.

Since strontium oxide is somewhat more stable than that of either aluminum or silicon[5], the melt oxidation rate should be different in the presence of strontium. Strontium modification may affect the oxidation rate by changing the nature of the oxide forming on the surface of the melt. In this section, the effect of strontium on the oxidation behaviour of liquid Al-Si alloys is investigated using thermogravimetric analysis (TGA).

6.3.2 Experimental Procedure

6.3.2.1 Materials

Materials investigated in the present study were prepared by adding Al-10 wt% Sr master alloy to A356 alloy and binary Al-7 %wt Si alloy. Binary Al-7%Si alloy was prepared by adding pure silicon to commercial pure aluminum. Binary Al-7wt%Si alloy was used in this investigation due to a problem discovered with the oxidation of A356 alloy. This will be discussed later (section 6.3.3). In order to obtain a homogeneous material, the alloys were cast in a cylindrical graphite mould with inner diameter of 35 mm. The castings were then cut and machined to the shape of discs with a diameter of 33 mm and height of 5 mm. Since the quality of the surface is important in oxidation studies, the surfaces of the specimens were ground using 240 and 600 grit grinding papers.

Experiments were done on the following four series of specimens and at least five experiments were carried out on each sample:

1) A356, as received
2) Sr-modified A356 (0.025 wt% Sr)
3) Al-7 wt% Si
4) Sr-modified Al-7 wt% Si (0.025 wt% Sr)

6.3.2.2 Apparatus

In order to monitor the weight change due to oxidation, a thermogravimetric balance (TGB) furnace system was used which allowed the continuous monitoring of sample weight during oxidation in an air atmosphere. The TGB consisted of a

microbalance head attached by a sample lifting mechanism (which allowed the sample to be raised or lowered inside the furnace) to a vertical resistance furnace with a hot zone length of about 150 mm and an inside diameter of about 64 mm. The schematic of the apparatus is shown in Figure 6.5.

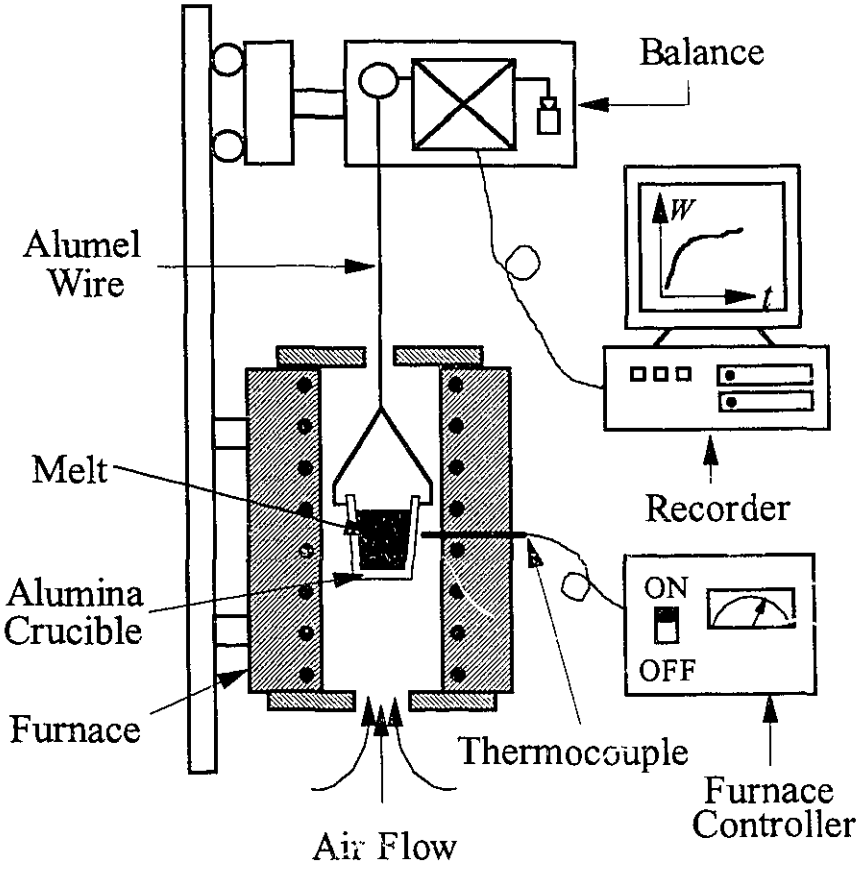

Figure 6.5 : Schematic of the apparatus used in studying the oxidation rate of the melts.

A D-100 series CAHN recording balance was used which is capable of measuring weight changes up to 100 grams with a resolution of about 1 microgram. The

electromagnetic balance was located above the furnace, and the sample was suspended from the sample side of the balance into the furnace. The balance control unit processes the electrical signals from the weighing unit and converts them into a digital form which can be recognized by a computer. The weight change can then be recorded as a function of time.

An alumina crucible, which is inert with respect to the liquid aluminum alloys, with the same dimensions as the sample was used to suspend the sample while it was liquid. The alumina crucible was suspended from the microbalance system inside the furnace by a thin alumel wire. This wire had already been oxidized to some extent by heating at 900 °C for 48 hours to eliminate the error due to the oxidation of the wire during the weight change measurement of the sample.

Before each experiment, the surfaces of the specimen were ground using 600 grit grinding paper to remove the initial oxide layer at the surface, and washed with methyl alcohol to remove any dirt which could cause a weight decrease by burning at high temperature. After the temperature (in the center of the furnace hot zone) was stabilized at 740 °C, the sample was lowered into the furnace and weight gain as a function of time was recorded by the microbalance. In these experiments, a 20 second time interval was chosen for the weight change recording.

To distinguish the sources of error in measuring the weight change of the samples in this setup, for example the oxidation of alumel wire, some experiments were carried out without an aluminum sample. The results showed negligible weight change in the system over a period of 40 hours. To reduce the fluctuations in readings due to the turbulence in the air flow, from the bottom to the top of the process tube, the diameter of the furnace was reduced at the bottom and at the top from 64 mm to 20 mm using an insulating board (Figure 6.5).

After a holding time of about 45 hours, the furnace was turned off and the crucible was moved out of the hot zone and the melt was solidified with an intermediate cooling rate. The sample was then sectioned and the oxide at the surface of the sample was examined using a scanning electron microscope (SEM). Moreover, the oxide layer on the surface was analyzed using X-Ray diffraction and Energy Dispersive Spectroscopy (EDS).

6.3.3 Results and Discussion

For A356 melts, the results showed a weight decrease during the oxidation. This weight loss may be due to the evaporation of the alloying elements which have a high vapour pressure such as, Zn and Mg (A356 alloy has 0.02 wt%Zn and 0.3 wt%Mg). As a result, the weight increase due to oxidation was offset by the weight loss due to evaporation of these elements. As a result, no further experiments were carried out on A356 alloy and only binary Al-7wt%Si alloy was used in the rest of the study.

The weight gain of an unmodified Al-7wt%Si melt at 740 °C in air is plotted versus oxidation time in Figure 6.6. It can be seen that the oxidation curve of the unmodified melt exhibits a region of slow oxidation during the initial stage of oxidation followed by a significant increase in the rate at later stages of exposure. In addition, there seems to be a transition from a linear law oxidation to another linear one with a higher oxidation rate, i.e., from region A to region B in Figure 6.6(a). A similar oxidation behaviour is seen in the work done by Eckert *et al* [15] in Al-3.5%Mg melt. According to them, the oxidation rate is slow at the early stages and then increases significantly. Pilling *et al* [11] have also reported a linear law oxidation for pure aluminum at 600 °C in the solid state. However, Aylmore *et al* [14] has found a parabolic rate law for the oxidation of solid aluminum in dry oxygen in the temperature range of 500-650 °C.

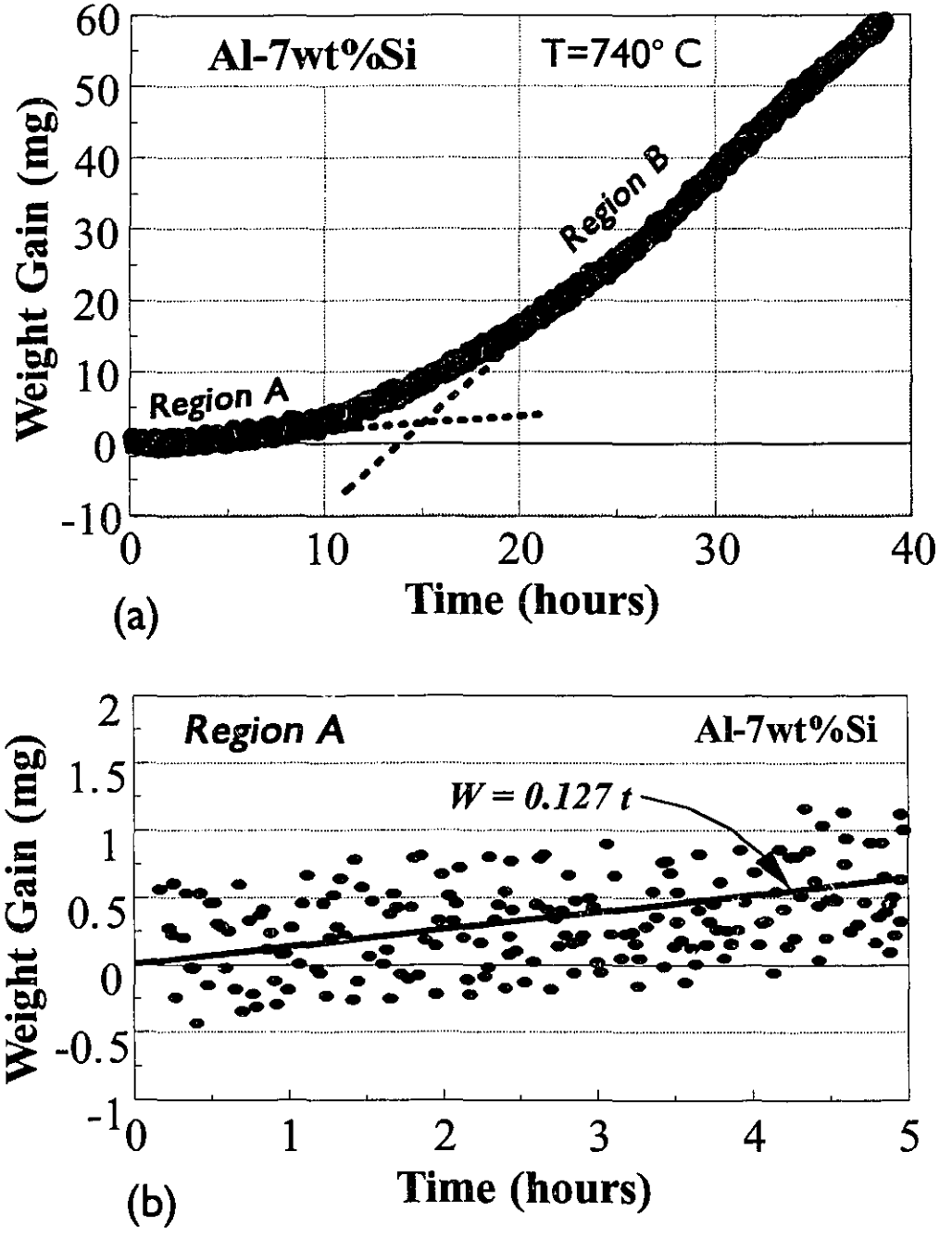

Figure 6.6 : Oxidation of unmodified Al-7wt%Si melt at 740 °C in air as a function of exposure time (a) over 40 hours (b) during the first 5 hours.

The observed increase in oxidation rate after about 10 hours (as shown in Figure 6.6) is probably due to a change in the nature of the oxide on the surface of the liquid to a less protective oxide layer. The micrograph of the oxide layer on the surface of an unmodified melt is shown in Figure 6.7. As can be seen in this Figure, the oxide layer after 40 hours of exposure is not uniform and the oxides are agglomerated. Using Energy Dispersive Spectroscopy (EDS), aluminum and oxygen were detected in the agglomerated particles in Figure 6.7(a) indicating that these particles are indeed aluminum oxide. In addition, it is seen in Figure 6.7(b) that the oxide layer is porous.

The oxidation mechanism of unmodified melts may be explained as follows. During the initial stage of oxidation, aluminum oxide forms on the surface of the melt following a linear law oxidation with a low rate. A porous oxide forms and the oxide tends to agglomerate as round particles. Thus, the oxide layer loses its coherency resulting in an increase in oxidation rate. The oxidation continues as a linear law oxidation, and at longer exposure times than those used here, the oxidation curve is expected to become parabolic due to a very thick oxide layer.

The weight gain of Sr-modified Al-7wt%Si melt at 740 °C in air is plotted versus the oxidation time in Figure 6.8. It is observed that the oxidation curve of Sr-modified melts follows a parabolic law oxidation. Therefore, a protective oxide layer forms on the liquid resulting in a decrease in oxidation rate with time.

The SEM observation of the oxide layer after 40 hours oxidation of Sr-modified melt is shown in Figure 6.9. It can be seen in this Figure that a coherent and non-porous oxide layer forms in the presence of strontium resulting in a parabolic law oxidation. In addition, X-Ray diffraction was performed on the Sr-modified samples at the surface using Cu-Kα radiation on a RIGAKU RU-200B diffractometer (Figure 6.10). The angular range (2θ) between 10 and 110 was investigated with an angular velocity of 1°/min, accelerating voltage of 50 KV, and current of 150 mA.

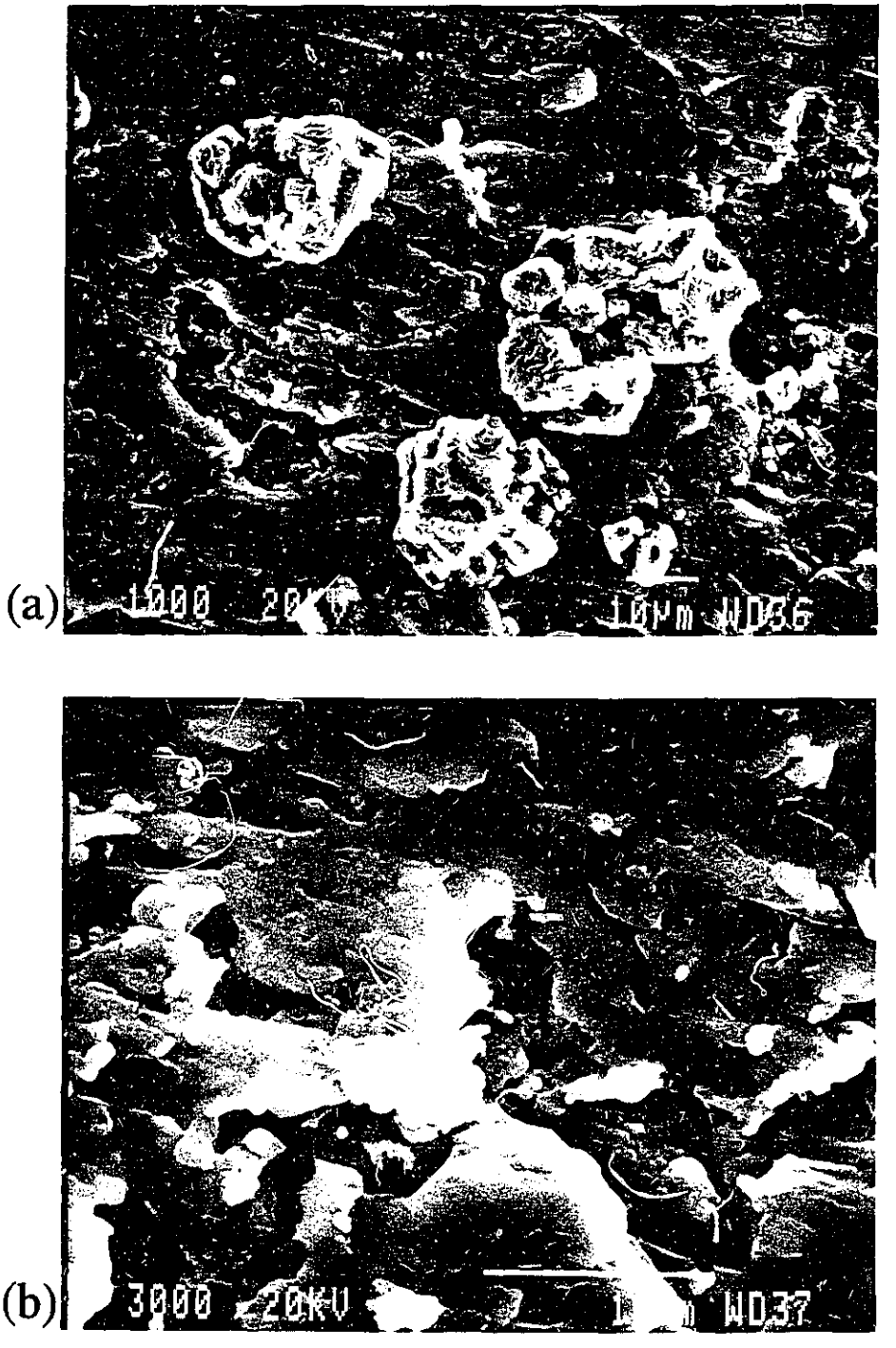

Figure 6.7 : SEM observation of oxide film formed on the surface of unmodified Al-7 wt %Si melt at 740 °C after exposure time of 40 hours in air.

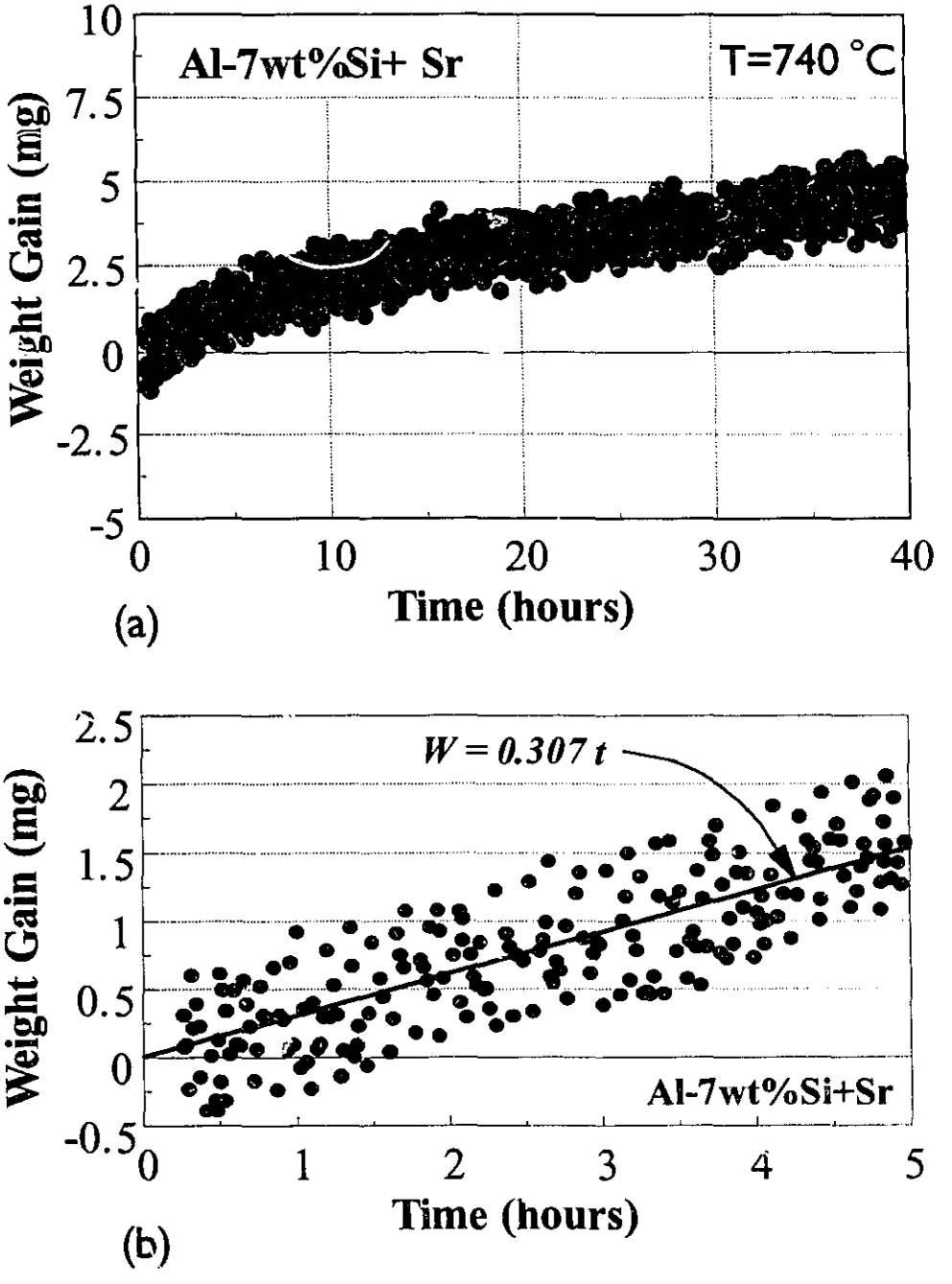

Figure 6.8 : Oxidation of Sr-modified Al-7wt%Si melt at 740 °C in air as a function of exposure time (a) over 40 hours (b) during the first 5 hours.

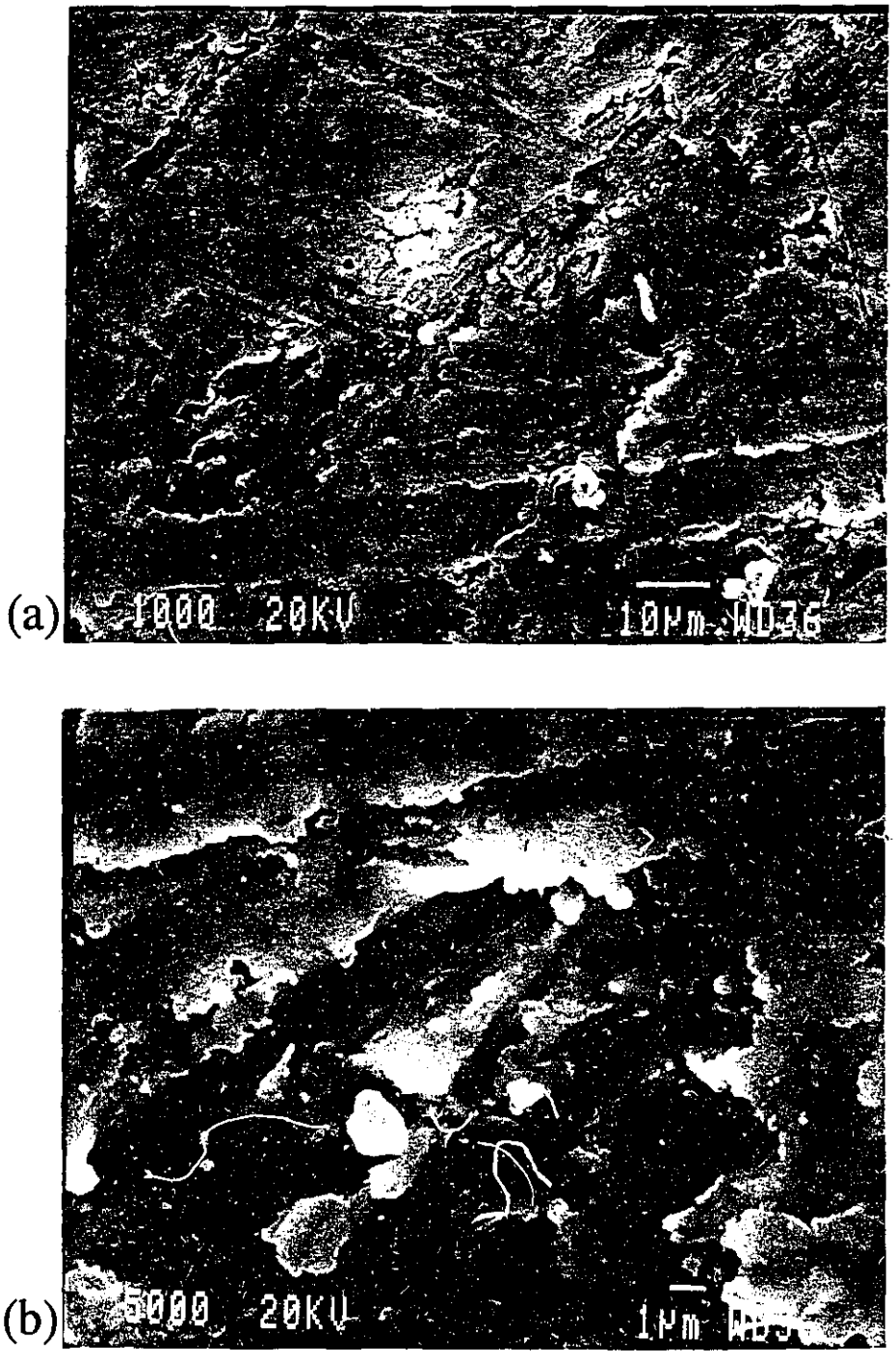

Figure 6.9 : SEM observation of oxide film formed on the surface of Sr-modified Al-7 wt %Si melt at 740 °C after exposure time of 40 hours in air.

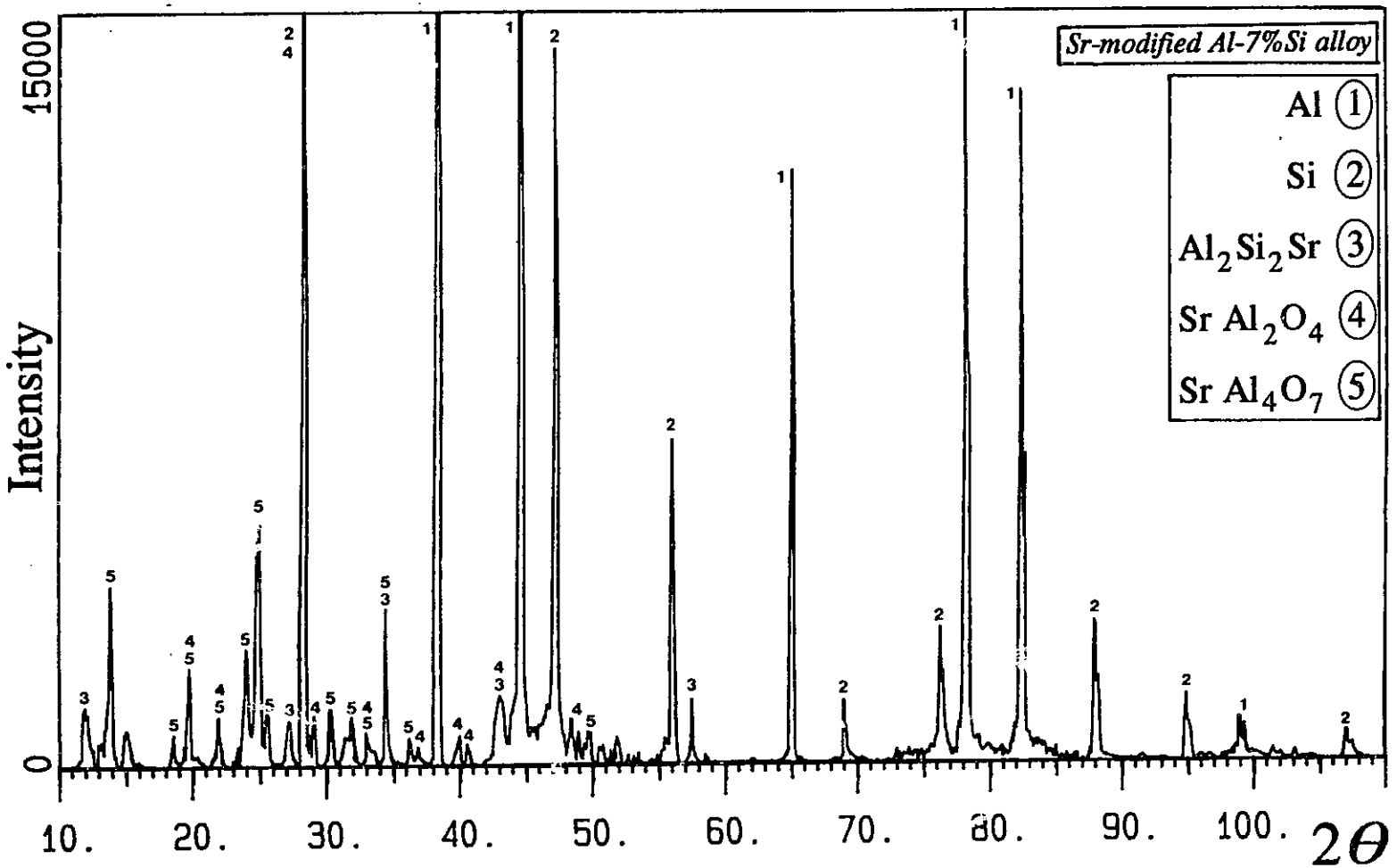

Figure 6.10 : The X-Ray diffraction pattern of Sr-modified samples at the surface.

Using the X-Ray diffraction pattern of Sr-modified samples (as shown in Figure 6.10), the compounds formed in the presence of strontium were determined. In this analysis, strontium was detected in the form of $SrAl_4O_7$, $SrAl_2O_4$ and Al_2Si_2Sr. In these diffraction patterns, we were unable to detect any known phases of aluminum oxide in the sample. In addition, the peaks for SrO in the X-Ray diffraction pattern were overlapped by the peaks of silicon, and therefore, it was difficult to determine whether the sample contained SrO. Garat *et al* [17] have also studied the surface oxide of Sr-modified A356 melt and found that the oxide layer consists mainly of SrO. However, Mohanty[18] has reported that SrO and $Sr(OH)_2$ are unstable in aluminum melts. According to his work, these oxides reduce to elemental Sr which subsequently reacts to form a complex compound of Sr(~15%)-Al(~40%)-Si(~45%).

It is important to note that the aim of this investigation was not to determine the oxidation mechanism of unmodified or modified melts or the analysis of the oxide layer on the melt, but only to compare the oxidation rate of modified and unmodified melts. Using the experimental data of the first 20 hours of the oxidation, the following relationship was found for the weight gain of unmodified and Sr-modified Al-7%Si melts (W) as a function of exposure time (t) :

$$\textit{Unmodified Al-7wt\%Si melt}: \quad W = 0.013\,(t)^{2.39}$$
$$\textit{Sr-modified Al-7wt\%Si melt}: \quad W = 0.537\,(t)^{0.58} \qquad \textbf{(6.3)}$$

These relationships are plotted in Figure 6.11. The oxidation rate at the early stage (the first few hours) after Sr addition is the area of concern. It is observed from Figures 6.6(b), 6.8(b) and 6.11 that the oxidation rate of Sr-modified melts up to about 7 hours after the Sr addition is somewhat higher than in an unmodified melt. Therefore, it can be concluded from this work that Sr increases the melt oxidation rate, and this may be the reason for the observed increase in the melt inclusion content due to Sr-modification.

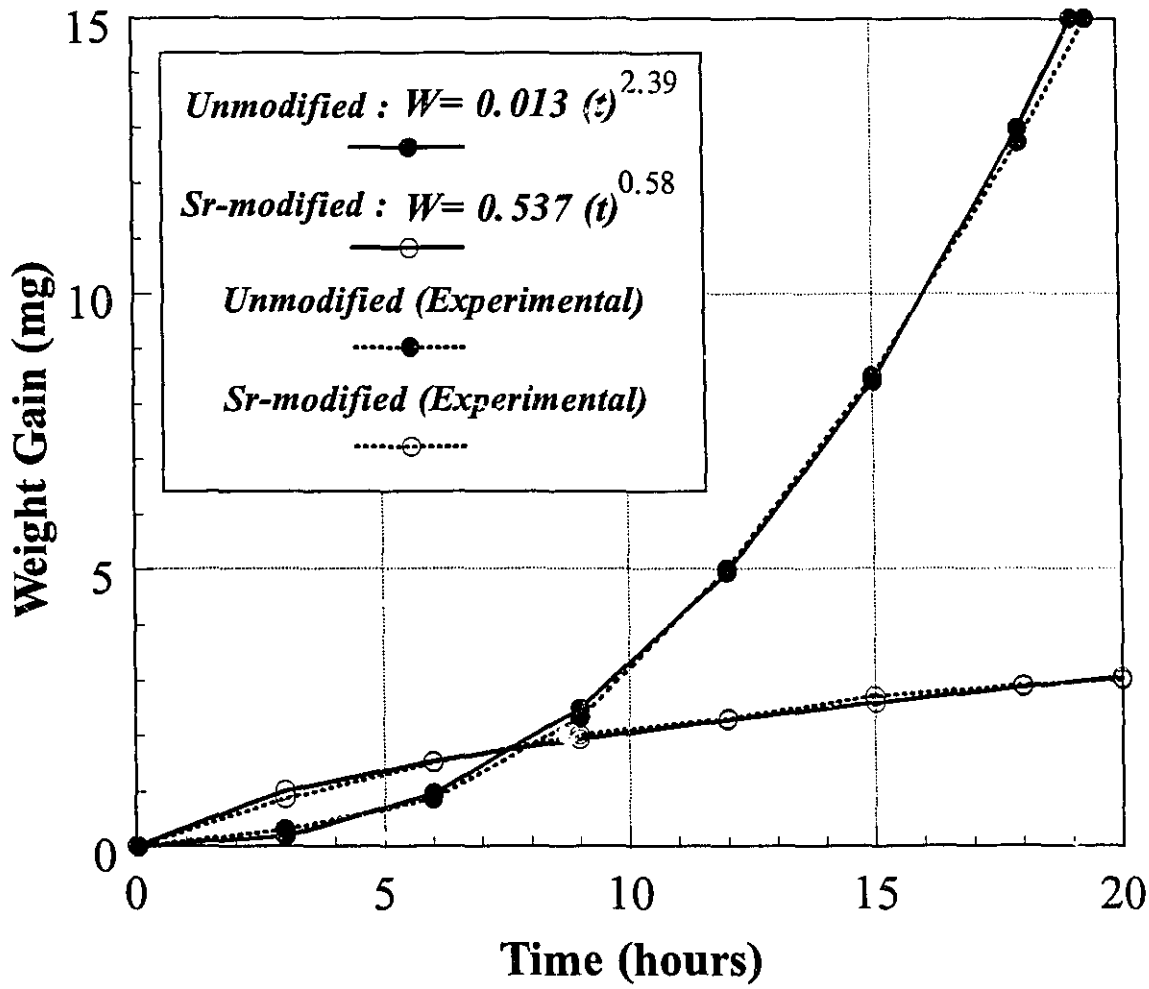

Figure 6.11 : Theoretical and experimental Oxidation curves of unmodified and Sr-modified Al-7wt%Si melt at 740 °C as a function of time.

Now, it is important to examine whether this higher level of inclusions in Sr-modified melts can facilitate the pore nucleation and cause the observed increase in porosity in Sr-modified castings. The role of inclusions in Sr-modified melts on pore formation was investigated as described in the next section using a vacuum solidification technique.

6.4 The Role of Inclusions in Pore Nucleation

The mechanism by which inclusion particles operate in pore formation during solidification is not well understood. If the melt inclusions play a role in the heterogeneous nucleation of bubbles, the number and distribution of pores will depend on the distribution and number of inclusion particles. Several test methods are available to evaluate the effectiveness of inclusions in pore nucleation, with the most common one being the reduced pressure test (RPT). This test, also known as the vacuum gas test or the Straube Pfeiffer test, involves allowing a sample of the melt to solidify at a set reduced pressure, normally 50-100 mm Hg. Since hydrogen solubility is related directly to the square root of pressure, decreased pressure reduces hydrogen solubility resulting in an increase in the tendency for bubble formation in the sample. This tendency is more significant at higher vacuum.

If inclusions can act as nuclei for hydrogen precipitation, gas evolution takes place on the inclusions and at an earlier stage of solidification resulting in a rounder, larger pore size and a higher pore number density. In the presence of larger amounts of inclusions, a larger number of pores should form in the solidified samples. If Sr-modification increases the porosity due to an increase in inclusion content, a larger numbers of pores should be observed in Sr-modified samples solidified under vacuum.

6.4.1 Experimental Procedures

A356 alloy, whose chemical composition is given in Table 2.1, was used in this investigation. The alloy was melted in an electric resistance furnace and the temperature was held constant at 730 °C for both modified and unmodified melts. The melt was held

for more than 3 hours to reach equilibrium with atmosphere. Hydrogen measurements were performed in unmodified and Sr-modified melts using both the Telegas instrument and the LECO sub-fusion method. The experimental procedure for hydrogen measurements was the same as that described in Chapter 2.

After hydrogen measurements, the melt was poured into a thin wall metallic cup located in the reduced pressure setup shown in Figure 6.12. The upper cap was then closed and the vacuum pump was turned on after 45 seconds. A time delay of 45 seconds was chosen in order to allow the liquid to solidify to some extent to prevent gas removal from the liquid into the atmosphere while vacuum was applied. Different vacuum pressures were applied using the control valve on the upper cap (Figure 6.12). The absolute pressures used in this work were 252, 188.5 and 61.5 mm Hg. Due to the good sealing in the system, the desired vacuum pressure was obtained in less than 10 seconds.

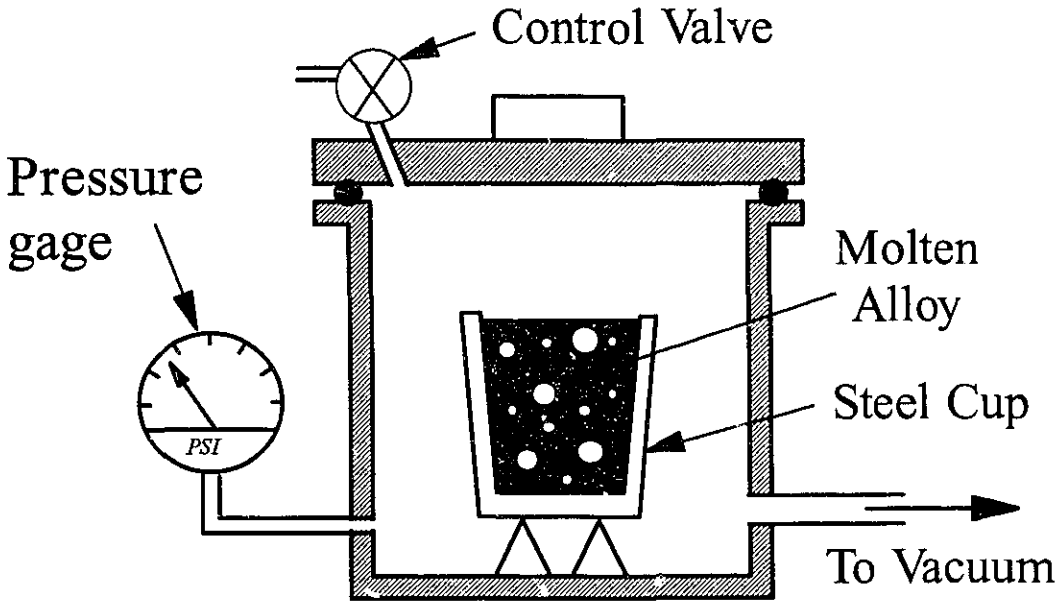

Figure 6.12 : Schematic of the reduced pressure test (RPT) setup

The melt was modified by adding 0.02 wt%Sr in the form of commercial Al-10 wt%Sr master alloy. The same procedure as used in the unmodified melt was carried out on the Sr-modified melt. A minimum of two experiments was done for both modified and unmodified alloys. After solidification, the samples were cut and the pore number density was measured using a LECO 2005 image analysis system. Photographs were also taken of the cross section of the samples.

6.4.2 Results and Discussion

The cross sections of the unmodified and Sr-modified samples are shown in Figure 6.13. As can be seen in this figure, the pore number density in unmodified and Sr-modified alloys are of the same order of magnitude. The same conclusion was derived from pore number density measurements using image analysis. Moreover, it can be seen in Figure 6.13 that the change in the absolute pressure has a significant effect on pore size while it has only a minor effect on the pore number density.

The following hypotheses can be made to interpret these results. First, Sr-modification increases the melt inclusion content, but these inclusions do not act as heterogeneous sites for pore nucleation. A second interpretation could be the presence of a large enough number of inclusions required for gas precipitation and nucleation of pores even in the absence of Sr. As a result, the increase in melt inclusion content due to Sr-modification has no extra effect on pore formation.

Therefore, it can be concluded that Sr-modification increases the melt inclusion content, but these inclusions do not have a significant effect on pore formation.

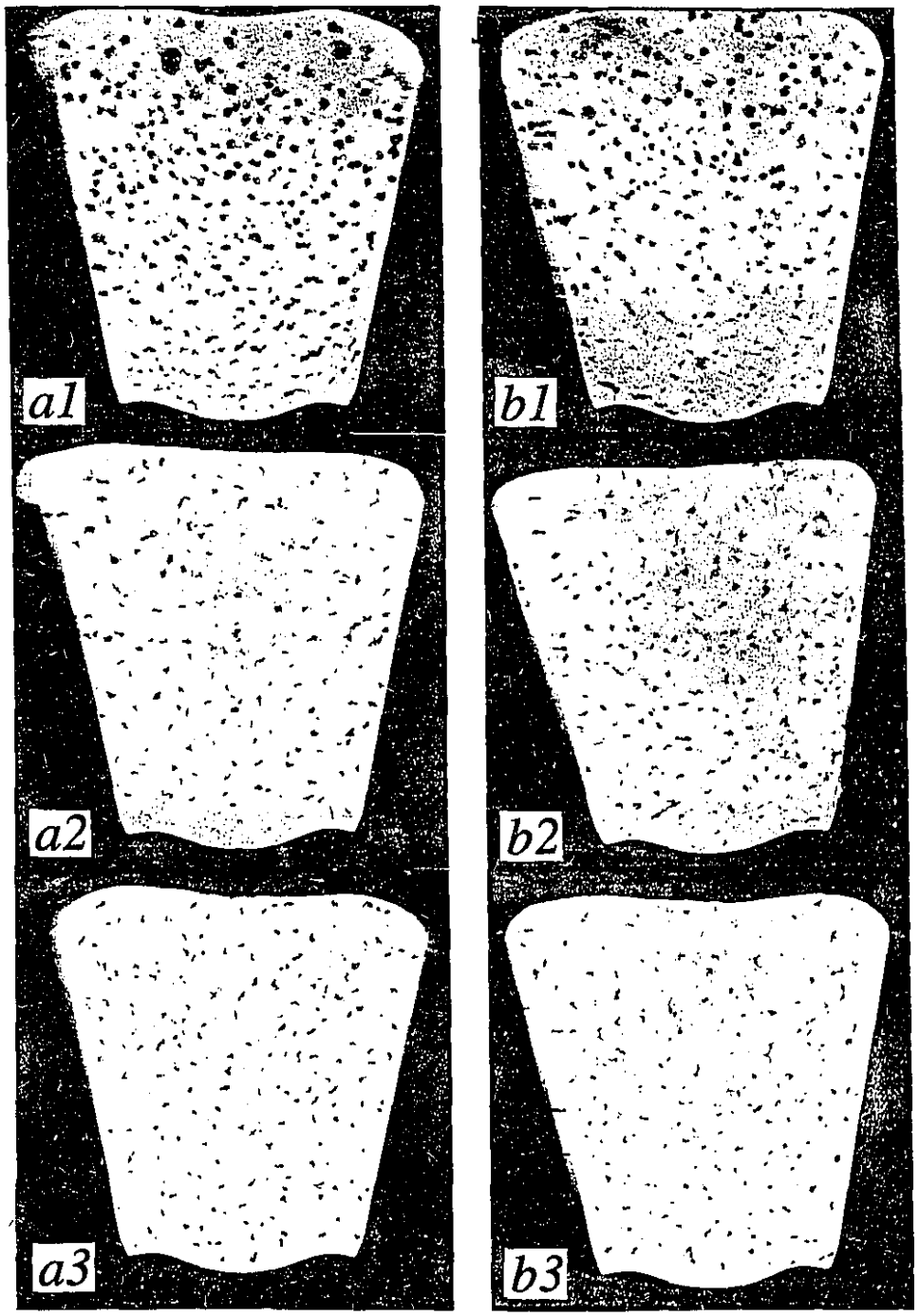

Figure 6.13 : The cross section of (a) unmodified and (b) Sr-modified A356 samples solidified under the vacuum. The absolute pressures are (a1,b1) 61.5 mm Hg (a2,b2) 188.5 mm Hg (a3,b3) 252 mm Hg.

6.5 References

1. S. Shivkumar, L. Wang and D. Apelian; "Molten Metal Processing of Advanced Cast Aluminum Alloys", *J. of Metals*, Jan. 1991, pp. 26-32

2. C.E. Eckert; "Inclusions in Aluminum Foundry Alloys", *Modern Casting*, April 1991, pp. 28-30

3. H. Shahani; "Effect of Hydrogen on the Shrinkage Porosity of Aluminum Copper and Aluminum Silicon Alloys", *Scand. J. Metall.*, No. 14, 1985, pp. 306-12

4. Q.T. Fang and D.A. Granger; "Porosity Formation in Modified and Unmodified A356 Alloy Castings", *AFS Trans.*, Vol. 97, 1989, pp. 989-1000

5. J.E. Gruzleski and B.M. Closset; *The Treatment of Liquid Aluminum-Silicon Alloys*, American Foundrymen's Society, Des Olaines, IL, 1990, pp. 57-157

6. H. Iwahori, K. Yonekura, Y. Yamamoto and M. Nakamura; "Occurring Behaviour of Porosity and Feeding Capabilities of Sodium and Strontium Modified Al-Si Alloys", *AFS Trans.*, Vol. 98, 1990, pp. 167-73

7. D.A. Bates and L.C. Hutter; "An Evaluation of Aluminum Filtering System", *Light Metals*, 1981, pp. 707-21

8. D.A. Doutre; *The Development and Application of a Rapid Method of Evaluating Molten Metal Cleanliness*, Ph. D. Thesis, McGill University, Montreal, Canada, 1984

9. J.P. Martin, R. Hachey and F. Painchaud; "On-line Metal Cleanliness Determination in Molten Aluminum Alloys Using LIMCA II Analyzer", *Light Metals*, 1994, pp. 915-20

10. P. Gimenez, H. D'Hondt and P. Pignault; "Inclusion Separation by Electrochemical Dissolution of 3004 Alloy: A Reference Method", *Production, Refining, Fabrication and Recycling of Light Metals*, Edited by M. Bouchard and P. Tremblay, Pergamon Press, New York, NY, 1990, pp. 213-24

11. N.B. Pilling and R.E. Bedworth; "The Oxidation of Metals at High Temperatures", *J. Inst. of Metals*, Vol. 29, 1923, pp. 529-91

12. O. Kubaschewski and B.E. Hopkins; *Oxidation of Metals and Alloys*, Butterworths & Co. Ltd., London, England, 1962, pp. 1-40

13. K. Thomas and M.W. Roberts; "Direct Observation in Electron Microscope of Oxide Layers on Aluminum", *J. Appl. Phys.*, No.1, Vol. 32, Jan. 1961, pp. 70-75

14. D.W. Aylmore, S.J. Gregg and W.B. Jepson; "The Oxidation of Aluminum in Dry Oxygen in the Temperature Range 400-650 °C", *J. Inst. of Metals*, Vol. 88, 1959-60, pp. 205-8

15. C.E. Eckert; "The Origin and Identification of Inclusions in Foundry Alloys", *AFS Proceedings of 3rd International Conference on Molten Aluminum Processing*, Orlando, Florida, Nov. 9-10, 1992, pp. 17-51

16. K. Hauffe; *Oxidation of Metals*, Plenum Press, New York, NY, 1965, pp. 5-15

17. M. Garat, G. Laslaz, S. Jacob, P. Meyer, P.H. Guerin and A. Adam; "State-of-the -Art Use of Sb-, Na- and Sr-modified Al-Si casting Alloys", *AFS Trans.*, Vol. 100, 1992, pp. 821-32

18. P.S. Mohanty; *Studies on the Mechanisms of Heterogeneous Nucleation of Grains and Pores in Aluminum Casting*, Ph.D. Thesis, McGill University, Montreal, Canada, Feb. 1994, pp. 130-40

Chapter 7

The Effect of Sr-Modification on the Rate of Melt Hydrogen Absorption and the Hydrogen Solubility in the Solid and Liquid States

7.1 Introduction

It has been suggested that strontium and sodium increase the porosity by increasing the susceptibility of Al-Si melts to hydrogen absorption[1,2]. One study, however, has contended that the addition of strontium and sodium to the melt prior to casting reduced the gas content, but increased the porosity of the castings[3]. Manzano-Ramirez *et al* [4] have also reported that a reduction in the hydrogen content and porosity takes place after strontium addition. However, in their work, the density of the samples was taken as an indication of the melt hydrogen content, and the macroshrinkage was measured as porosity without taking into account the microporosity within the casting. Denton and Spittle[1] and Honer and Youling[5] have claimed that strontium-treated melts are more susceptible to gassing than sodium-treated ones. They have suggested that oxidation of Sr during melting causes the structure of the oxide layer on the surface to change and

become more pervious to hydrogen. In the case of Na, unlike Sr, a thick oxide is established on the melt surface acting as a barrier to hydrogen solution. On the other hand, Traenkner[6] has contended that as a modifier, sodium generates more gas than strontium.

Contrary to these propositions, Gruzleski et al[7,8,9] have indicated that Sr-modification does not affect the rate of hydrogen pick-up or regassing from humid atmospheres by molten A356 alloys. They have also reported that the presence of strontium in the melt does not change the rate of degassing. On the other hand, Iwahori *et al* [10] have observed a decrease in the rate of hydrogen degassing (using vacuum degassing) in Sr-modified melts. This was considered to be due to hydrogen absorbtion onto the oxides present in the melt. They have also suggested that somehow the hydrogen is more strongly fixed in the oxides by addition of Sr to the melt.

It is also possible that sodium and strontium affect the porosity in Al-Si castings by changing the hydrogen solubility in the liquid or solid. It has been reported by Samuel[11] that a Bulgarian group have recently claimed that Sb-modification of Al-Si alloys allowed the retention of hydrogen in the solid phase and suppressed its tendency to separate as a gas in the form of pores during solidification. Thus, despite the increased hydrogen content in the alloys, the casting density (or porosity) remains constant. On the other hand, modification with Sb not only refines the Si phase in Al-Si alloys, but also increases the hydrogen solubility in the Al solid solution. Therefore, the observed decrease in porosity by Sb-modification as demonstrated by Fuoco et al [12] may be due to the increase in the hydrogen solubility in the solid state, which can be an indication of the importance of the effect of the solid state hydrogen solubility on porosity.

If the hydrogen solubility in the solid or liquid is reduced, more hydrogen is rejected into the liquid by the growing solid, and consequently the hydrogen in the liquid reaches the solubility limit at an earlier stage of solidification. This facilitates pore

formation and results in more porosity. Because of these apparent contradictions on the effect of modification on the rate of melt hydrogen pick-up and the lack of the data on the effect of modification on hydrogen solubility, this chapter focusses on the effect of Sr-modification on the melt hydrogen content and the hydrogen solubilities in the solid and liquid states.

7.2 Melt Hydrogen Content

7.2.1 Experimental Procedure

The effect of Sr-modification on melt hydrogen pick-up was studied by measuring the hydrogen content of the melt before and after strontium addition. Five Al-Si alloys with different silicon levels of 4.8 wt%, 5.7 wt%, 7 wt% (A356 alloy), 8.1wt% and 12 wt% were used in this investigation. These alloys were prepared by adding pure silicon and commercial purity aluminum to an A356 alloy. The alloys were modified by adding 0.02 wt%Sr in the form of commercial Al-10 wt%Sr master alloy. Due to the difficulties in making hydrogen measurements in Sr-modified melts using the Telegas instrument (as described in Chapter 2), the hydrogen measurements were performed by taking the Ransley samples from the melt before and after Sr addition and analyzing them by the nitrogen carrier fusion technique (LECO™ sub-fusion method) as described in Chapter 2 (section 2.2).

Various hydrogen levels were achieved using different controlled moist atmospheres. In Sr-modified melts, the Ransley samples were taken about 30 minutes after Sr addition to allow for strontium dissolution. In the case of A356 alloy, several hydrogen measurements were carried out within 90 minutes after Sr addition (at two hydrogen levels) in order to determine whether Sr introduced hydrogen into the melt.

7.2.2 Results and Discussion

The results of melt hydrogen measurements before and after strontium addition are given in Figure 7.1 for Al-Si alloys with different silicon contents. It is seen that the melt hydrogen contents before and after strontium addition are essentially the same for all ranges of Si content. Therefore, Sr treatment does not introduce hydrogen into the melt.

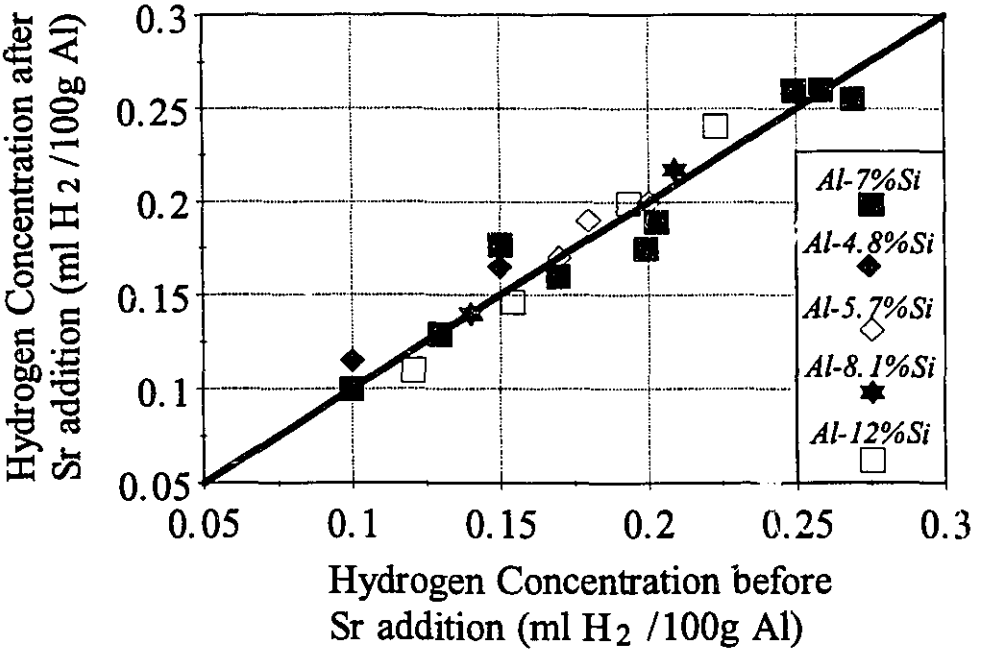

Figure 7.1 : Hydrogen content before and after strontium addition in Al-Si alloys with different silicon contents.

Typical plots of hydrogen content before and after strontium addition versus time are given in Figure 7.2 for hydrogen levels of 0.13 and 0.26 ml/100g in A356 alloy. It is seen that strontium addition does not increase the hydrogen level of the melt as reported previously [7,8,9]. Thus, Sr-modification does not affect the rate of hydrogen pick-up by molten Al-Si alloys.

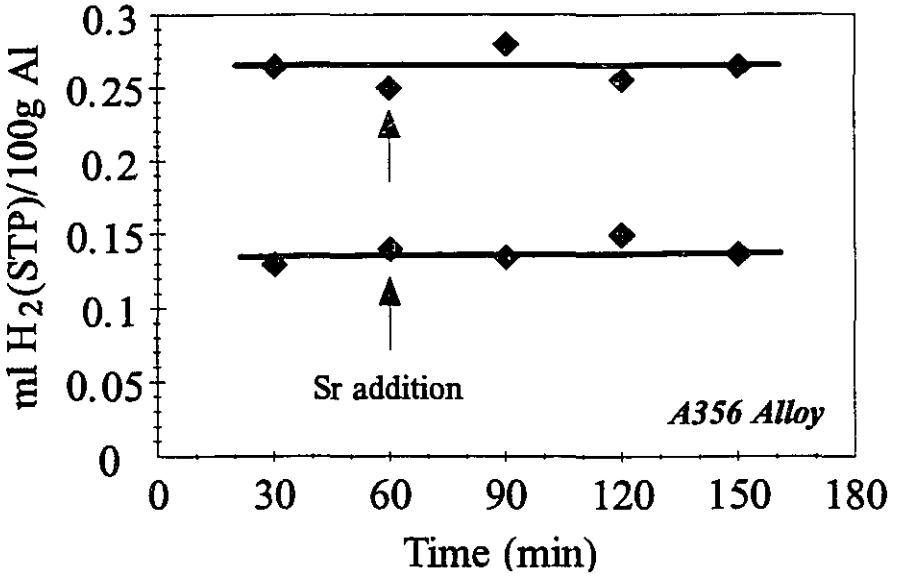

Figure 7.2 : Hydrogen content before and after Sr addition versus time in A356 alloy.

7.3 Hydrogen Solubilities in the Solid and Liquid States

As mentioned earlier, Na or Sr-modification may increase the porosity in castings by decreasing the hydrogen solubilities in solid or liquid aluminum. In this section, the effect of Sr-modification on hydrogen solubilities in the solid and liquid states is investigated.

7.3.1 Hydrogen Solubility in the Solid

The susceptibility of aluminum and its alloys to porosity formation is due primarily to the low solubility of hydrogen in the solid metal and the associated low partition coefficient for hydrogen between the solid and liquid as the metal solidifies[13,14]. If the

hydrogen solubility in the solid is decreased, more hydrogen is rejected into the liquid during solidification, resulting in more porosity. Using a saturation and quenching technique, Ransley *et al*[13] have measured the hydrogen solubility in solid commercial purity aluminum at 1 atm hydrogen pressure in a temperature range of 465-620 °C. The relationship is given as:

$$\log_{10} S_s = -\frac{2080}{T} - 0.778 \qquad (7.1)$$

where S_s is the solubility in solid aluminum, and T is the absolute temperature. The hydrogen solubility is strongly dependent on temperature, melt chemical composition and the partial pressure of hydrogen in the surrounding atmosphere. To the author's knowledge, there are no data available on the effect of alloying elements on the hydrogen solubility in solid Al-Si alloys and specifically on the effect of strontium or sodium. Therefore, a short investigation on the effect of Sr-modification on the hydrogen solubility in solid A356 alloy was carried out.

7.3.1.1 Experimental Procedure

A356 alloy was melted in a silicon carbide crucible using an electric resistance furnace. Using the Telegas instrument, the melt hydrogen content was measured after 3 hours of holding at 730 °C in order to reach equilibrium with the atmosphere. The melt was then transferred into three smaller crucibles, and 0.025 wt%Sr and 2 wt%Li were added to the second and third melts, respectively. Lithium was added into the third melt due to its well known effect on the hydrogen solubility in the solid in order to evaluate the reliability of the method. These three melts were cast at 730 °C into one end closed graphite tubes, 120 mm in height and 12 mm in diameter. The samples were remelted and directionally solidified in an alumina crucible using the apparatus shown in Figure 7.3.

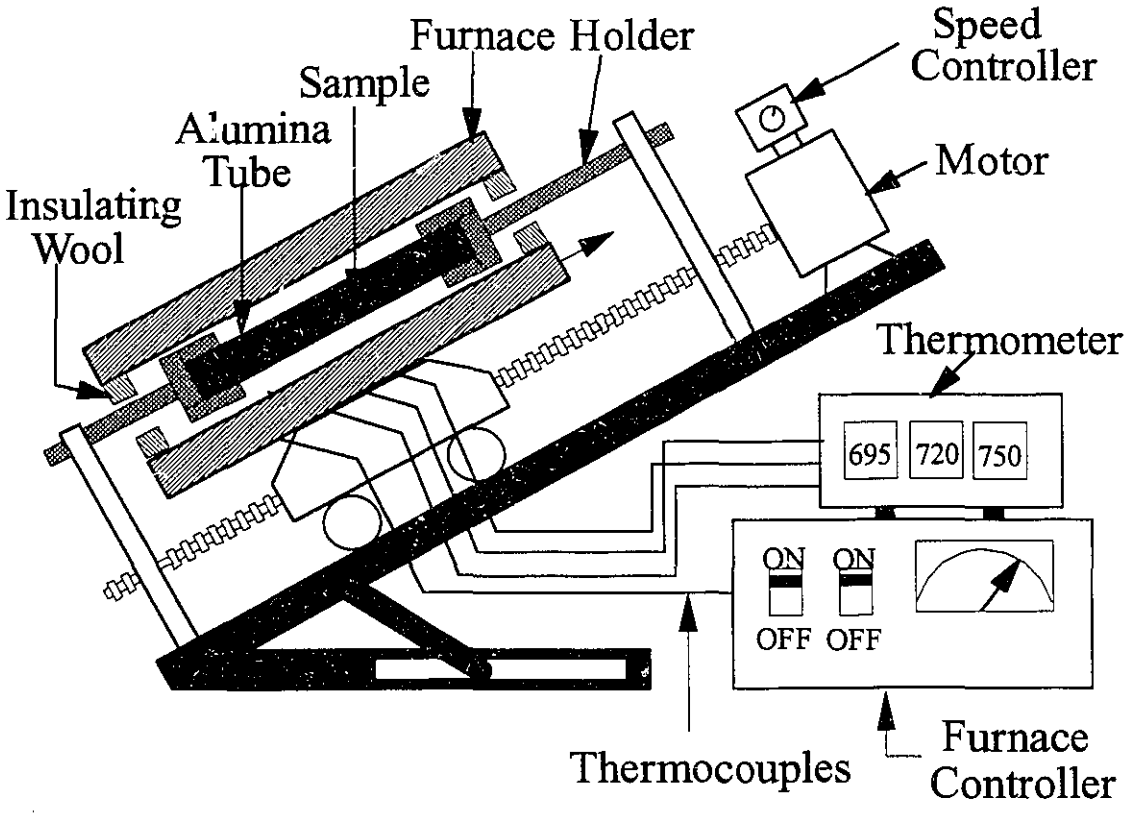

Figure 7.3 : Schematic of the apparatus used for directional solidification of the samples.

The alumina tubes were placed between two holders and the furnace was moved upwards very slowly at a rate of 4 μm per second to provide directional solidification of the samples. The slow solidification rate allowed sufficient time for the diffusion of hydrogen into the liquid at the solid/liquid interface as well as the complete diffusion of hydrogen within the liquid phase.

After solidification, the samples were cut and machined into two pieces and the hydrogen contents were analyzed using the Hot Vacuum Subfusion Extraction Method.

The details of this method can be found elsewhere[15,16]. The retained strontium and lithium in the samples were also analyzed using atomic absorption.

7.3.1.2 Results and Discussion

The hydrogen content of the base A356 melt, measured by the Telegas instrument, was 0.18 ml/100g Al. The chemical analyses of the samples showed that the retained lithium level was 0.75 wt%, while strontium was 0.014 wt%. These concentrations are lower than the target values due to the fading of Sr and Li. Fading was severe as the samples were liquid for a long time.

The results of hydrogen measurements in the solid samples are given in Table 7.1. It can be seen that Sr-modification does not change the equilibrium hydrogen content in solid A356 alloy. As expected, the hydrogen content of solid A356 alloy is significantly increased by lithium addition. This result is in a good agreement with those reported by Talbot *et al*[17] for binary Al-Li alloys. They have reported that 1 %Li increases the solid state hydrogen solubility of aluminum (at 600 °C and 1 atm hydrogen partial pressure) from 0.03 to 0.84 cm^3/100g Al.

It should be noticed that the very slow solidification rates provided sufficient time not only for hydrogen in the solid to reach equilibrium with the liquid at the solid/liquid interface, but also for hydrogen in the liquid to reach equilibrium with the atmosphere. Therefore, the values of the hydrogen content in Table 7.1 correspond to the hydrogen solubility in the solid at a specified hydrogen partial pressure and temperature. Since, the samples were all prepared using the same procedure, and as we are only concerned with a comparison of the results for unmodified and Sr-modified alloys, the hydrogen partial pressure and temperature for the values of hydrogen solubility in Table 7.1 were not determined.

Table 7.1 : The measured hydrogen contents in solid samples by Hot Vacuum Subfusion Extraction Method.

Alloy	Hydrogen content ml/100 g Al
A356	0.091 ±0.028
A356 + Sr	0.095 ±0.012
A356 + Li	0.498 ±0.195

Therefore, it can be concluded from the present study that Sr-modification has virtually no effect on the hydrogen solubility in the solid.

7.3.2 Hydrogen Solubility in the Liquid

Hydrogen is the only gas having a significant solubility in aluminum. The main source of hydrogen comes through the reaction of aluminum with moisture in the melting environment. During solidification, hydrogen is rejected into the liquid from the growing solid and hydrogen bubbles form when the hydrogen in the liquid reaches the solubility limit.

Strontium may increase the porosity by reducing the hydrogen solubility in the liquid. While there have been a number of studies to determine the hydrogen solubility in pure liquid aluminum, very little data is available on the solubility of hydrogen in liquid aluminum alloys[13,18,19,20,21,22]. The effect of the main alloying elements on hydrogen solubility in liquid Al-Si alloys is given by[18]:

$$Hydrogen\ Solubility\ \left(\frac{ml}{100\,g}\right) = [\,1.23 - 0.0733\,(\%\,Cu) - 0.033\,(\%\,Si) + 0.0489\,(\%\,Mg)\,]\,(t - 585)\,(0.00606) \quad (7.2)$$

where t is the temperature in degrees centigrade. The only data available on the effect of Sr on hydrogen solubility in liquid aluminum alloys is unpublished work done by Liu and Bouchard[23] on pure aluminum. Their experimental procedure is based on Sivert's principles and can be found elsewhere[22]. The results of their work on the hydrogen solubility in pure liquid aluminum with and without a strontium addition at 1 atm hydrogen partial pressure are given in Table 7.2.

Table 7.2 : Hydrogen solubilities in liquid aluminum[23]

Alloy	Temperature, C	Hydrogen Solubility (ml/100 g Al)
Al (pure)	700	1.026 ± *
	750	1.430 ± *
Al + 0.02 wt%Sr	700	0.851 ±0.055
	750	1.247 ±0.104

* The standard deviation has not been reported.

There is evidence in Table 7.2 that strontium decreases the hydrogen solubility in liquid aluminum by about 17% at 700 °C and by 14% at 750 °C. This may imply a larger effect at lower temperatures. Since no data is available on the effect of strontium on the hydrogen solubility in liquid Al-Si alloys, it is assumed that strontium reduces the hydrogen solubility in liquid A356 alloy by the same amount as it does in pure aluminum.

At lower hydrogen solubilities, the hydrogen in the liquid reaches the solubility limit at an earlier stage of solidification. As a result, pores can nucleate earlier and grow over a longer period of time resulting in more porosity.

It is important to note that a pore can form at temperatures below the liquidus (i.e., <615 °C for A356 alloy). Moreover, at temperatures < 700 °C, the effect of strontium on hydrogen solubility in liquid A356 alloy may actually be more than 17%. The significance of this 17% decrease in hydrogen solubility on porosity formation will be demonstrated in Chapter 9.

It is worth mentioning that the melt hydrogen content is expected to be decreased after Sr addition due to a decrease in the hydrogen solubility in the liquid. However, it was observed in section 7.2 that the melt hydrogen content did not change by Sr addition (as demonstrated in Figs. 7.1 and 7.2). This may be attributed to the following factors:

a) Hydrogen diffusion from the melt into the atmosphere is a very slow process. As a result, the change in melt hydrogen content over 1.5 hours of hydrogen measurements may not be large enough to be detected using normal measurement methods.
b) As shown in Chapter 6, a thick and non-porous oxide layer forms at the surface of the Sr-modified melts. This oxide layer may inhibit hydrogen diffusion from the liquid into the atmosphere, and in a period of 1.5 hours no significant change may take place.

7.4 References

1. J.R. Denton and J.A. Spittle; "Solidification and Susceptibility to Hydrogen Absorption of Al-Si Alloys Containing Strontium", *Mater. Sci. Technol.*, Vol. 1, April 1985 , pp. 305-11

2. J. Charbonnier, J.J. Perrier and R. Portalier; "Recent Developments in Aluminum-Silicon Alloys Having Guaranteed Structures or Properties", *AFS International Cast Metal Journal*, Vol.3, 1978, pp. 17-26

3. H. Shahani; "Effect of Hydrogen on the Shrinkage Porosity of Al-Cu and Al-Si Alloys", *Scand. J. Metallurgy*, Vol. 14, 1985, pp. 306-312

4. A. Manzano-Ramirez, E. Nava-Vazquez, E. Carrasco-Pimentel and J. Mendez-Nonell; "Some Observations on the Effect of Strontium as Modifier on Gas Content and Solidification Process of the AS7U3 Aluminum Alloy", *Light Metals*, 1993, pp. 839-42

5. K.E. Honer and Z. Youling; "Influence of Ca and Sr on the hydrogen pick-up in Aluminum Alloy Metals, by Example of G-AlSi12", *Giesserei-Forschung*, Vol. 39, Jan. 1987, pp. 34-48

6. F.O Traenkner; "Practical Techniques for Casting Aluminum", *Modern Casting*, Dec. 1981, pp. 44-48

7. J.E. Gruzleski, N. Handiak, H. Campbell and B. Closset; "Hydrogen Measurement by Telegas in Strontium Treated A356 Metals", *AFS Trans.*, Vol. 94, 1986, pp. 147-54

8. F.C. Dimayuga, N.Handiak and J.E. Gruzleski; "The Degassing and Regassing Behaviour of Strontium-Modified A356 Melts", *AFS Trans.*, Vol. 96, 1988, pp. 83-88

9. M.H. Mulazimogla, N. Handiak and J.E. Gruzleski; "Some Observations on the Reduced Pressure Test and Hydrogen Concentration of Modified A356 Alloy", *AFS Trans.*, Vol. 97, 1989, pp. 225-33

10. H. Iwahori, K. Yonekura, Y. Yamamoto and M. Nakamura; "Occurring Behaviour of Porosity and Feeding Capabilities of Sodium and Strontium Modified Al-Si Alloys", *AFS Trans.*, Vol. 98, 1990, pp. 167-73

11. A.M. Samuel and F.H. Samuel; "Various Aspects Involved in the Production of Low-hydrogen Aluminum Castings", *J. Mater. Sci.*, Vol. 27, 1992, pp. 6533-63

12. R. Fuoco, H. Goldenstein and J.E. Gruzleski; "Evaluation of the Effect of Modification-Induced Eutectic Undercooling on the Microporosity Formation in 356 Aluminum Alloy", *AFS Trans.*, Vol. 102, 1994

13. C.E. Ransley and H. Neufeld; "The Solubility of Hydrogen in Liquid and Solid Aluminum", *J. Inst. of Metals*, Vol. 74, 1948, pp. 599-620

14. D.E.J. Talbot; "Effects of Hydrogen in Aluminum, Magnesium, Copper and Their Alloys", *Int. Met. Rev.*, Vol. 20, 1975, pp. 166-84

15. C.E. Ransley and D.E.J. Talbot; "The Routine Determination of the Hydrogen Content of Aluminum and Aluminum Alloys by the Hot-extraction Method", *J. Inst. of Metals*, Vol. 84, 1955-56, pp. 445-52

16. P.N. Anyalebechi; "Techniques for Determination of the Hydrogen Content in Aluminum and Its Alloys", *Light Metals*, A.I.M.E., 1991, pp. 1025-46

17. P.N. Anyalebechi, D.E.J. Talbot and D.A. Granger; "The Solubility of Hydrogen in Solid Binary Aluminum-Lithium Alloys", *Metall. Trans. B*, Vol. 20B, August 1989, pp. 523-33

18. P.D. Hess; "An Empirical Equation For Calculating Solubility of Hydrogen in Molten Aluminum Alloys", *Light Metals*, 1974, pp. 591-97

19. P.N. Anyalebechi, D.E.J. Talbot and D.A. Granger; "The Solubility of Hydrogen in Liquid Binary Al-Li Alloys", *Metall. Trans. B*, Vol. 19B, 1988, pp. 227-32

20. W.R. Opie and N.J. Grant; "Hydrogen Solubility in Aluminum and Some Aluminum Alloys", *Trans. AIME*, Vol. 188, J. Metals, 1950, pp. 1237-41

21. D.E.J. Talbot and P.N. Anyalebechi; "Solubility of Hydrogen in Liquid Aluminum", *Mater. Sci. Technol.*, Vol. 4, Jan. 1988, pp. 1-4

22. H. Liu, L. Zhang and M. Bouchard; "Determination of Hydrogen Solubility in Molten Aluminum and Aluminum-Copper Alloys", *33rd C.I.M. Conference*, Light Metals, Toronto, Ontario, August 1994, pp. 257-68

23. H. Liu and M. Bouchard; Private Report, Département des sciences appliquées, Université du Québec à Chicoutimi, 555, Boulevard de l'Université, Chicoutimi, Québec, Canada G7H 2B1

Chapter 8

Modelling of Porosity Formation

In this chapter, a model is proposed for simulation of actual solidification and porosity formation of the casting described in Chapter 2. This model gives us the opportunity to study the effect of casting and melt variables on porosity and to evaluate the importance of the changes in these variables, due to modification, on pore formation.

8.1 Directional Solidification Model

This model considers the unidirectional solidification of a vertical Al-Si alloy cast in an insulating refractory mould with a riser at the top and a chill (water jet) at the bottom as described in detail in chapter 2. The schematic of the solid-liquid mushy region of the solidifying ingot, and the temperature distribution along the y-axis of the ingot a few minutes after pouring the melt is shown in Figure 8.1. Dendrite tips are approximately at the liquidus isotherm.

As solidification proceeds, the thickness of solidified layer increases, and it acts as a barrier for heat transfer. Therefore, the cooling rate decreases along the casting in the x-direction (Figure 8.2). This causes an increase in the length of the mushy zone with time as shown schematically in Figure 8.2.

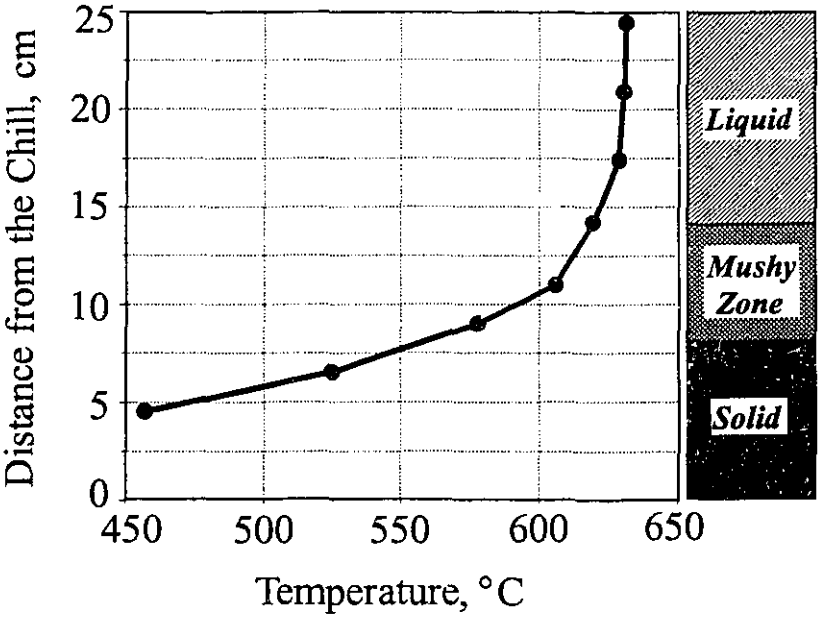

Figure 8.1 : The temperature distribution along the y-axis of the ingot.

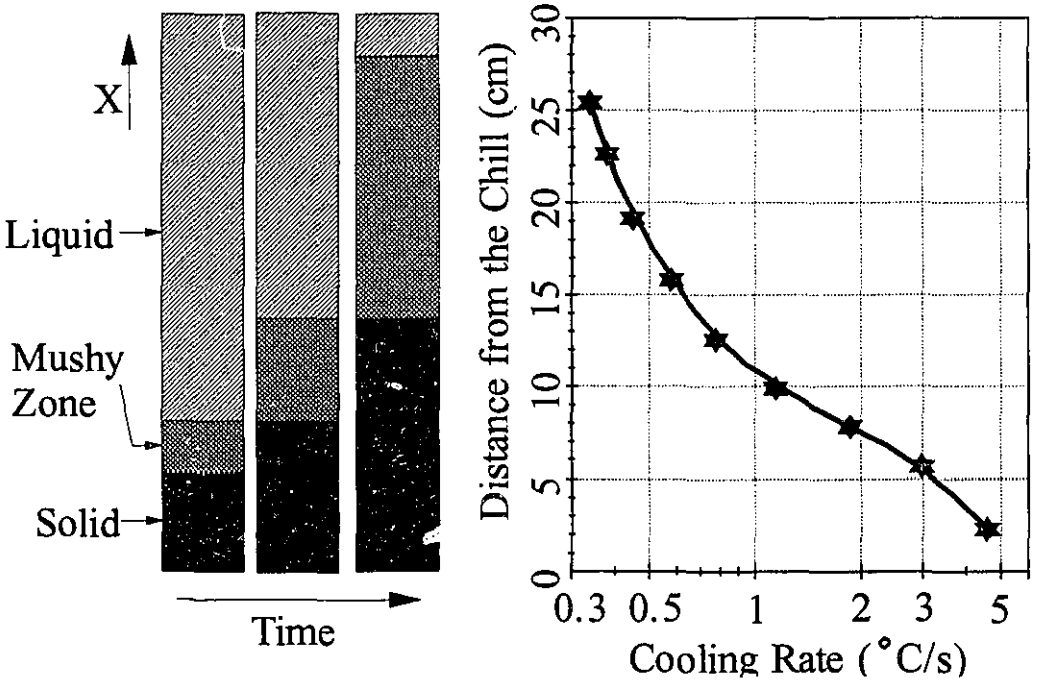

Figure 8.2 : The cooling rate vs. the distance from the chill (from Chapter 2).

The cooling rate as a function of distance from the chill, L, can be estimated from the experimental data (in Chapter 2) shown in Figure 8.2 as:

$$\frac{dT}{dt}\,(°C/s) = 0.2 + 6.79\,\exp\left(\frac{-L}{0.056}\right) \qquad (8.1)$$

where L is in meters, and cooling rate, dT/dt, is in $°C/s$.

As shown schematically in Figure 8.2, the liquidus isotherm moves faster than the solidus isotherm, resulting in an increase in the length of the mushy zone with time. The velocity of these advancing solid and liquid interfaces can be obtained by plotting the distance from the chill of the isotherms for 577 °C and 615 °C (i.e., the solidus and liquidus temperatures in A356 alloy) as a function of time, as shown in Figure 8.3.

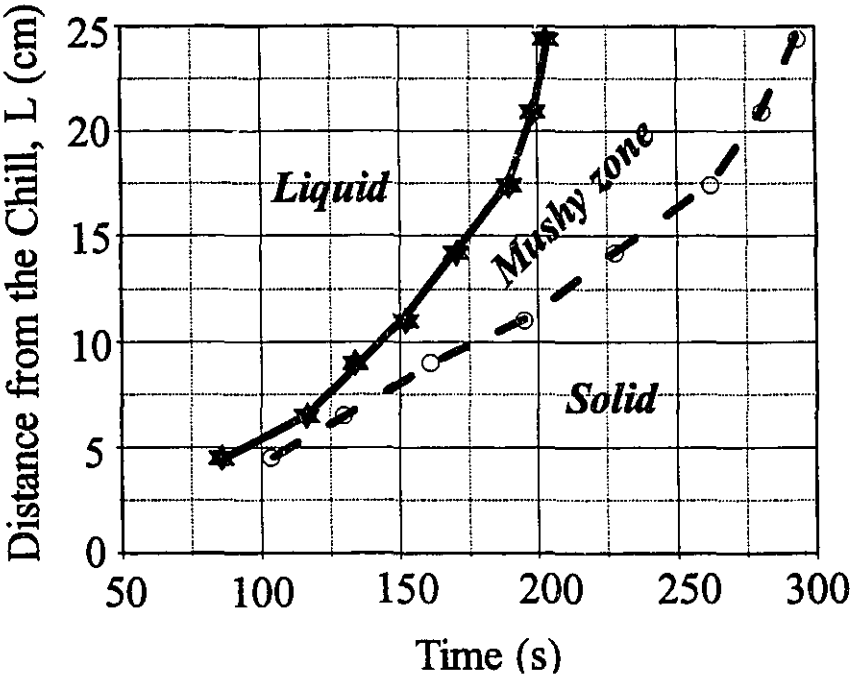

Figure 8.3 : The distance from the chill of the isotherms for 577 °C and 615 °C (i.e., the solidus and liquidus temperatures in A356 alloy) as a function of time.

It is seen in Figure 8.3 that the curve for the advancing solid interface (solidus isotherm) is approximately linear, i.e. the interface is moving with a nearly constant velocity, while the velocity (slope of the curve) of the liquidus isotherm is nonlinear and is changing with the time.

8.2 Formulation of the Model

Porosity formation in aluminum castings during solidification is attributable to a combination of the following two factors:
a. Evolution of hydrogen during solidification from the growing solid into the adjacent liquid due to the difference in hydrogen solubility between the solid and liquid phases.
b. Solidification shrinkage and inadequate liquid mobility (feeding) due to dendrite arm formation during solidification.

As solidification progresses, the volume change resulting from the liquid-solid contraction causes a pressure drop in the remaining liquid, which results in fluid flow between dendrites. If the feeding ability is poor, the dendritic liquid becomes isolated from the bulk liquid and the pressure drop results in evolution of dissolved hydrogen in the melt and dispersed porosity. In addition, the lower hydrogen solubility in the solid phase compared to the liquid also causes evolution of hydrogen into the liquid during solidification. Therefore, the hydrogen content in the liquid increases and eventually exceeds the solubility limit. However, the creation of a new pore requires the establishment of a new surface. Because of this surface barrier, the hydrogen concentration in the liquid will continue to increase above the solubility limit until it reaches a value at which pores can nucleate.

This nucleation may occur predominantly at the root of dendrites or at other heterogeneous sites such as inclusions. Once the pore is nucleated, there is rapid growth

during the initial stages and the hydrogen concentration in the liquid decreases. When the radius of the porosity becomes large enough to decrease the contribution of interfacial energies, the pore may detach from the dendrite arm and move into the intergranular regions (if solidification is mushy) where the space available for growth is larger than in the inter-dendritic regions. Growth in this period occurs at a relatively slow rate. The extent of growth will be determined by the rate of diffusion of hydrogen. Furthermore, at a later stage, the neighbouring dendrites collide, so that interdendritic feeding becomes difficult. At that point, the porosity is assumed to grow to compensate for solidification shrinkage.

As described in Chapter 1, the condition under which a pore can nucleate and be stable is given by the following equation:

$$P_H + P_S \geq P_{atm} + P_M + P_F \tag{8.2}$$

where P_H is the equilibrium pressure of dissolved gas (hydrogen) in the melt, P_S is the pressure drop due to the shrinkage, P_{atm} is the pressure of atmosphere over the system (usually 1 atm), P_M is the pressure due to the metallostatic head, and P_F is the fracture pressure due to surface tension at the pore/liquid interface. The schematic of the pressures acting on a pore is shown in Figure 8.[illegible].

8.3 Shrinkage Pressure (P_S)

During solidification, the volume contraction occurs simultaneously at the solid/liquid interface where hydrogen is rejected. This shrinkage establishes pressure gradients within the casting. Substantial metal flow occurs under this pressure gradient. During this process, liquid metal is forced to pass through a semi-rigid dendritic network to compensate for the shrinkage. In this case, the dendritic network imposes resistance

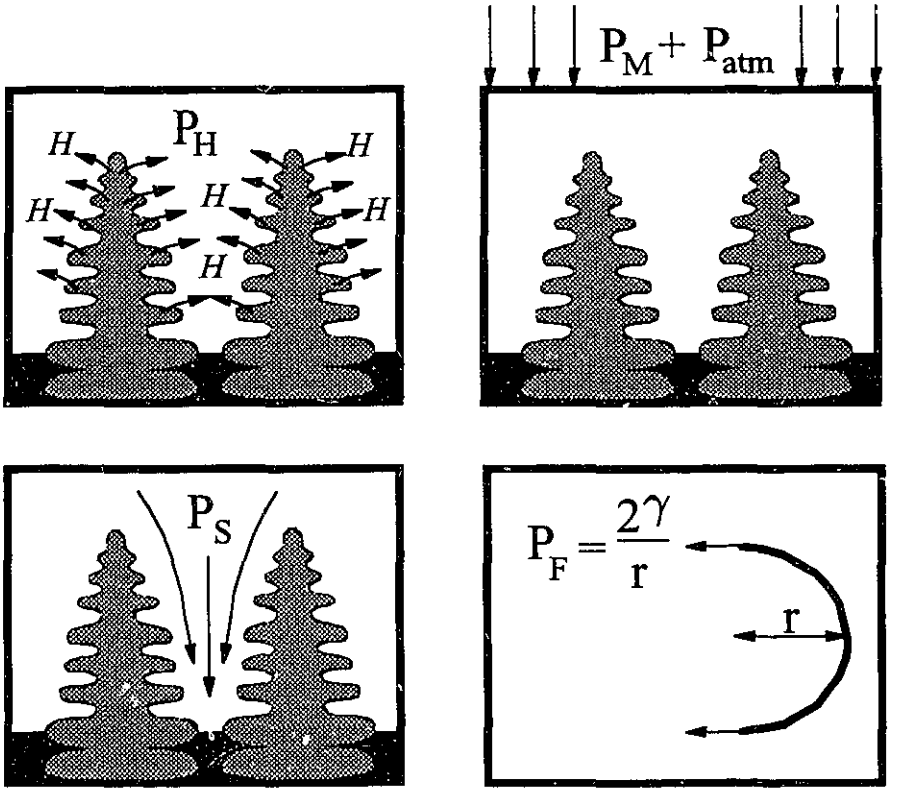

Figure 8.4 : The schematic of the pressures acting in pore formation.

to liquid flow. The flow of interdendritic fluid obeys approximately the same laws as flow through other finely porous media[1]. Thus, the mean interdendritic flow velocity, v_l, is linearly related to the pressure gradient as given by Darcy's law[2] :

$$v_l = -\frac{K}{\mu f_l}(\nabla P + \rho_l g_r) \tag{8.3}$$

where P is the pressure, g_r is acceleration due to gravity, μ is viscosity, and the permeability, K, is a measure of the resistance to the fluid conductivity of a porous material and is a function of pore size and geometry. The term $\rho_l g_r$ will be neglected

in Eq. (8.3), and will be taken into account in the form of the metallostatic pressure, P_M. Therefore, v_l (the linear flow velocity of liquid at any distance, x) in Eq. (8.3) can be written in the form of:

$$v_l = \frac{-K}{\mu f_l} \frac{\partial P}{\partial x} \tag{8.4}$$

Using the Hagen-Poiseulle equation, permeability can be written as[3,4,5] :

$$K = \epsilon . f_l^{\,2} \tag{8.5}$$

where ε is a parameter which depends upon the geometry of the flow channels (i.e. dendrite structure and arm spacing), and is defined as[3,5] :

$$\epsilon = \frac{1}{24 \pi n \tau^3} \tag{8.6}$$

where τ is a tortuosity factor to account for the fact that the liquid flow channels are not straight and smooth, and n is the number of liquid channels per unit area along the face perpendicular to the x direction and is inversely proportional to the square of the secondary dendrite arm spacing (DAS). This equation is valid when the liquid fraction, f_l , is less than about 0.7 [4,6], which is the region of interest in the present work. The restriction to flow will be the greatest at the end of solidification, and is not considerable at liquid fractions less than 0.7. Kubo and Pehlke[6] recommended that f_l should be fixed at a constant value of 0.7 when this parameter exceeds 0.7.

Substituting Eq. (8.6) in Eq. (8.5), permeability, K, can be defined as:

$$K = \frac{(DAS . f_l)^2}{24 \pi \tau^3} \tag{8.7}$$

where f_l is fixed at 0.7 for liquid fractions greater than 0.7.

During solidification, from the conservation of mass in the volume element, and from the fact that the solid is unable to move in the region of coherency, and when no gas porosity is formed, we have[2,7] :

$$\nabla(\rho_l f_l v_l) + \frac{\partial \rho}{\partial t} = 0 \tag{8.8}$$

where t is time, and ρ is the local average density (of liquid and solid). ρ can be defined as a function of liquid volumetric shrinkage, $\beta = (\rho_s - \rho_l)/\rho_s$, as follows:

$$\rho = \rho_l f_l + \rho_s f_s = \rho_l (f_l + \frac{1}{1 - \beta} f_s) \tag{8.9}$$

since,

$$f_l + f_s = 1 \rightarrow \frac{\partial f_l}{\partial t} = - \frac{\partial f_s}{\partial t} \tag{8.10}$$

Therefore,

$$\frac{\partial \rho}{\partial t} = \rho_l (\frac{\partial f_l}{\partial t} + \frac{1}{1 - \beta} \frac{\partial f_s}{\partial t}) = (\frac{- \beta}{1 - \beta}) \rho_l \frac{\partial f_l}{\partial t} \tag{8.11}$$

From Eqs. (8.11) and (8.8), we obtain:

$$\nabla(f_l v_l) = \frac{\beta}{(1 - \beta)} \frac{\partial f_l}{\partial t} = \frac{\beta}{(1 - \beta)} (\frac{\partial f_l}{\partial x} \frac{\partial x}{\partial t}) \tag{8.12}$$

The product $f_l v_l$ is numerically equal to the volumetric flow rate of liquid passing through a planar section of unit area normal to the x-axis. Equation (8.12) therefore describes the rate of change of the liquid volume flow, caused by solidification shrinkage,

as we move through the mushy zone. To solve Eq. (8.12), the relationship between liquid fraction and distance, x, in the mushy zone as well as dx/dt are required.

In Al-Si alloys , the diffusivity of silicon in the solid is slow enough that Scheil Equation can be applied[1,2] :

$$f_l = \left(\frac{m_l C_0}{T - T_M} \right)^{\frac{1}{(1 - K_0)}} \tag{8.13}$$

where C_0 is the initial silicon concentration in the alloy, in wt. pct., m_l is the liquidus slope, T is the temperature, T_M is the melting point of pure aluminum, and K_0 is the equilibrium distribution coefficient of silicon between solid and liquid. In this model K_0 is taken to be a constant and the solidus and liquidus lines in the phase diagram are considered to be linear. From linear regression of the available data on the liquidus temperature (for hypoeutectic Al-Si alloys)[8,9], m_l is calculated to be -6.85 °C/wt. pct., and the liquidus temperature, T, can be written as a function of silicon concentration, C_L, as:

$$T = 660 - 6.85\ C_L \tag{8.14}$$

To solve Eq. (8.12), f_l should be written as a function of distance, x, in the mushy zone. Assuming the origin of the coordinate system (e.g., x = 0) to be at L = 8.65 cm in Figure 8.1, the temperature as a function of x in the region of the mushy zone (i.e., in the range between solidus and liquidus temperatures) can be calculated as:

$$T = \frac{569 + 26409\ x}{1 + 41\ x} \tag{8.15}$$

where temperature is in °C, and x is in meters. Substituting Eq. (8.15) in Eq. (8.13), and using the values in Table 8.1, the fraction of liquid, f_l , can be calculated as a function of x (in meters) within the mushy zone as follows:

$$f_l^x = \left(\frac{6.85\ (\ 1\ +\ 41\ x\ )\ C_0}{651\ x\ +\ 91} \right)^{1.15} \qquad (8.16)$$

It is important that Eq. (8.16) is valid in the mushy region for $T \geq T_E$, where T_E is the eutectic temperature. It is also necessary to determine the derivative of x with time (i.e., dx/dt) in the mushy zone. The average of this value in the mushy region may be calculated as the slope of a line approximately halfway between the curves for solidus and liquidus in Figure 8.3 with a negative sign. This average value of dx/dt is calculated to be about -0.001 m/s.

Table 8.1 : Constants used in calculations (for Al-Si alloys).

Constant	Value used in the calculations	Note:
K_0	0.13	Refs. [9],[10]
m_l	- 6.85	Calculated from Refs. [8],[9]
T_M	660 ^{0} C	
T_E (unmodified alloy)	575 ^{0}C	Measured in section 5.4.1

It can be calculated from Eq.(8.16) that the fraction of liquid for an Al-7%Si alloy above T_E (i.e. at $T_E + \varepsilon$) is about 52%, while at a temperature below T_E (i.e. at $T_E - \varepsilon$),

it will be zero. Therefore, due to this drastic change in liquid fraction with a small variation of temperature, Eq. (8.12) cannot be represented as a continuous function. For this purpose, eutectic liquid is assumed to solidify with an undercooling, which is represented in terms of distance as X_0 - X_1 in Figure 8.5.

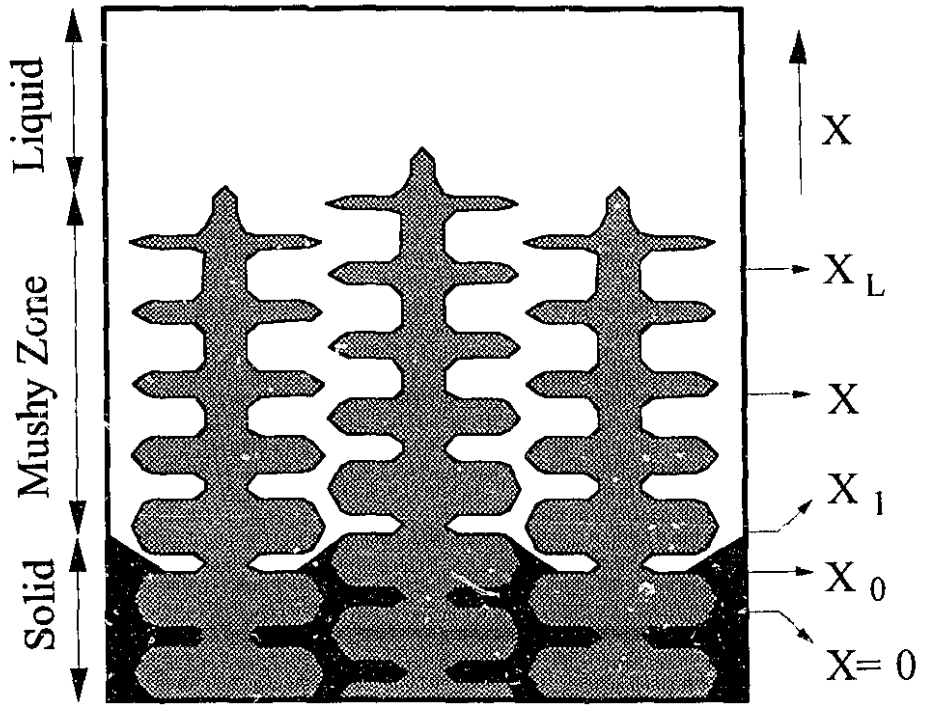

Figure 8.5 : Detail of solid-liquid region in Fig. 8.1.

Therefore, solid α-phase forms within the region of $X > X_1$, and the interdendritic eutectic liquid solidifies within the range of X_0-X_1. The fraction of liquid within the range of $X > X_1$ is calculated from Eq.(8.16), and within the narrow range of $X_0 < X < X_1$, the volume fraction of liquid is assumed to be linear.

Now integrating Eq. (8.12) from X_0 to X, the velocity of the liquid at any distance x within the mushy zone can be calculated as follows:

$$f_l v_l|_x - f_l v_l|_{x_0} = -1\times10^{-3}\left(\left[\frac{\beta_E}{(1-\beta_E)}f_l\right]_{x_0}^{x_1} + \left[\frac{\beta_\alpha}{(1-\beta_\alpha)}f_l\right]_{x_1}^{x}\right) \quad (8.17)$$

where β_α is the volumetric shrinkage due to the formation of solid α-phase, β_E is the volumetric shrinkage of the interdendritic eutectic liquid (see chapter 4), and x_0 , x_1 and x are as shown in Figure 8.5. Since the fraction of liquid, f_l , is zero at x = x_0 , from Eq. (8.17) , we obtain:

$$v_l^x = -1\times10^{-3}\left(\left[\frac{\beta_E}{1-\beta_E} - \frac{\beta_\alpha}{1-\beta_\alpha}\right]\frac{f_l^{x_1}}{f_l^x} + \frac{\beta_\alpha}{1-\beta_\alpha}\right) \quad (8.18)$$

where v_l^x is the flow velocity at distance, x ; and x_1 (in meters) is the point where the liquid is at the eutectic temperature. f_l^{x1} and f_l^x are fraction of liquid at x_1 and x , and are calculated from Eq. (8.16). The negative value of v_l^x is due to the liquid flow in opposite direction of the interface movement. The value of x_1 is a function of eutectic temperature and can be calculated for modified and unmodified Al-Si alloys from Eq. (8.15), and using the values in Table 8.1. The β_E and β_α can be calculated from the available data on the solid and liquid densities of Al-Si alloys reported by Poirier *et al*[10]. These data are given in Table 8.2.

Table 8.2 : Volumetric shrinkage of eutectic and α alloys calculated from the data in Ref[10].

$\rho_{s(E)}$* (g/cm^3)	$\rho_{l(E)}$* (g/cm^3)	$\rho_{s(\alpha)}$** (g/cm^3)	$\rho_{l(\alpha)}$*** (g/cm^3)	⟶	β_E	β_α
2.548	2.454	2.567	2.382	⟶	3.69%	7.24%

* Calculated at eutectic temperature (577 °C)

** Average value for α-solid with silicon concentration between 0 to 1.5 wt. pct. Si

*** Average value for liquid with 1.5 wt% Si at temperature range of 577-615 °C

Now, integrating Eq. (8.4) , we find that:

$$\Delta P = P_{x_L} - P_x = \int_x^{x_L} \left(-\frac{\mu}{K} f_l^x v_l^x\right) dx \qquad (8.19)$$

where ΔP is the pressure drop within the distance between the point where mass feeding stops, x_L , and a point somewhere deep inside the two-phase mushy zone, x (Figure 8.5). Within the distance between x_1 and x_L , the liquid must filter through a coherent network of solid dendrites and feeding is expected to be difficult. The experimental evidence available suggests that solid coherency begins to occur at a fraction solidified equal to about 0.2 or 0.3 in large-grained aluminum alloys[7,11]. In the present model, x_L is assumed to occur at the point where the fraction of liquid is 0.8.

Consequently, the pressure drop with distance can be calculated by substituting Eqs. (8.7) and (8.18) in Eq.(8.19), resulting in the following equation:

$$\Delta P = P_{x_L} - P_x$$

$$= \int_x^{x_L} \frac{24\times10^{-3}\,\mu\,\pi\,\tau^3}{DAS^2\, f_l^{x\,2}} \left(\left[\frac{\beta_E}{1-\beta_E} - \frac{\beta_\alpha}{1-\beta_\alpha}\right] f_l^{x_1} + \left[\frac{\beta_\alpha}{1-\beta_\alpha}\right] f_l^x \right) dx \qquad (8.20)$$

where viscosity is in kg/m.s, secondary dendrite spacing, DAS, is in meters, and $f_l{}^x$ is as defined in Eq. (8.16).

Secondary dendrite arm spacing along the casting can be estimated from the cooling rate according to[12] :

$$\log \frac{dT}{dt} = \frac{1.659 - \log(DAS\times10^6)}{0.4} \qquad (^\circ C/s) \qquad (8.21)$$

where secondary dendrite arm spacing , *DAS*, is in meters. Substituting Eq. (8.1) in Eq. (8.21), the dendrite arm spacing, *DAS*, can be calculated as a function of distance, x , within the mushy zone. *DAS* changes within the distance x_1 to x_L in the mushy zone between 38 to 42 μm (calculated from cooling rate data). Since the variation of DAS within the mushy zone is not significant and for simplicity in integrating Eq. (8.20), an average value of *DAS* , *i.e.* $DAS_{avg} = 40 \times 10^{-6}$ m, is used. Equation (8.20) then becomes:

$$P_S = P_{x_L} - P_x = \int_x^{x_L} \frac{0.0754\,\mu\,\tau^3}{DAS_{avg}^2\; f_l^{x\,2}} \left(\left[\frac{\beta_E}{1-\beta_E} - \frac{\beta_\alpha}{1-\beta_\alpha} \right] f_l^{x_1} + \left[\frac{\beta_\alpha}{1-\beta_\alpha} \right] f_l^{x} \right) dx \qquad (8.22)$$

where P_S is the shrinkage pressure at point x within the mushy zone.

8.4 Internal Gas Pressure (P_H)

During solidification, hydrogen is rejected at the solid-liquid interface into the interdendritic liquid due to the large difference in hydrogen solubility between liquid and solid aluminum and the rapid diffusion of monoatomic hydrogen in liquid aluminum. To obtain the hydrogen concentration in the liquid during solidification, it is necessary to determine how fast is the diffusivity of hydrogen in liquid and solid aluminum.

Several workers have reported on the diffusivity of hydrogen in pure aluminum[13,14,15,16]. The hydrogen diffusivity in pure liquid aluminum in the temperature range 780-1000 °C, has been determined to vary with the absolute temperature according to[15] :

$$D_l = 3.8\times10^{-2} \exp\left(-\frac{2315}{T}\right) \quad cm^2/s \qquad (8.23)$$

where T is absolute temperature in K. The activation energy of diffusion in the solid state is higher by a factor of 2 than for the liquid metal. The diffusivity in solid aluminum between 360-600 °C is estimated to be[16] :

$$D_s = 1.1\times10^{-1} \exp\left(-\frac{4922}{T} \right) \quad cm^2/s \tag{8.24}$$

where T is absolute temperature in K.

During solidification, there is a hydrogen concentration gradient in the liquid and solid due to the evolution of hydrogen into the liquid. This concentration gradient causes a diffusion flux of hydrogen through the liquid and solid. The diffusion distance, x, as a function of time, t, is commonly defined as [17] :

$$x = \sqrt{D \cdot t} \tag{8.25}$$

It is assumed in Eq. (8.25) that hydrogen concentration at $x = 0$ (i.e., at maximum concentration) is constant, and there is no diffusion due to convection nor any restriction on the diffusion path. In Figure 8.6, the hydrogen diffusion distance is plotted as a function of time for different temperatures in both solid and liquid aluminum using Eqs. (8.23) to (8.25).

As shown in Figure 8.6, the temperature dependence in the solidification range of 575-615 °C (i.e. in the range between solidus and liquidus temperatures of A356 alloy) is not significant and can be neglected. The diffusion of hydrogen in both liquid and solid aluminum is rapid, and in the temperature range of interest, hydrogen can diffuse about 500 μm in the liquid and 200 μm in the solid in one second.

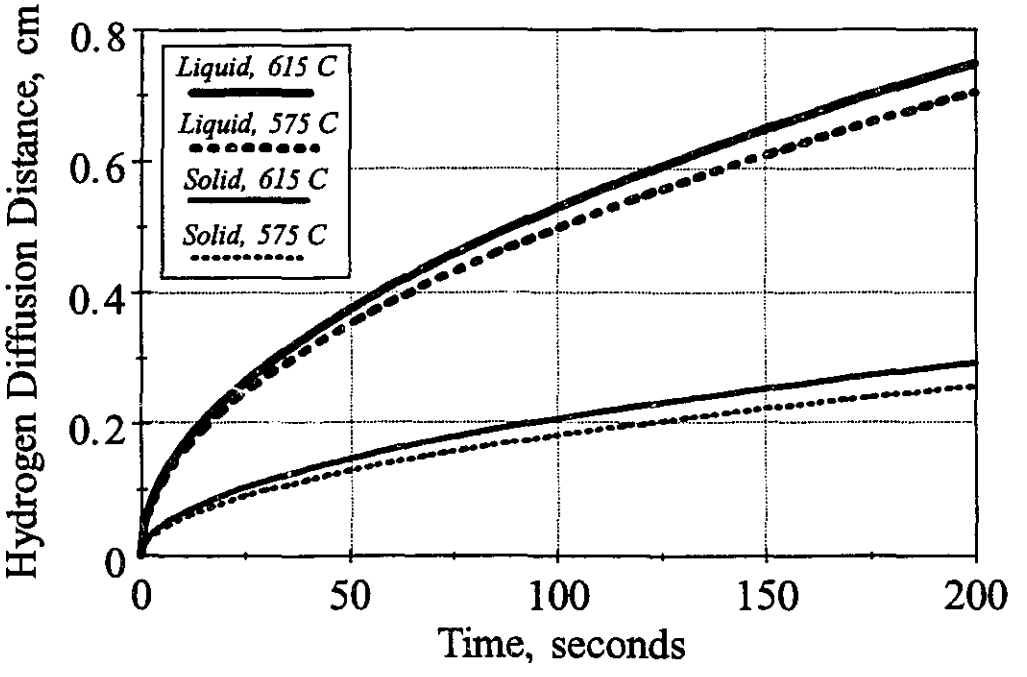

Figure 8.6 : The hydrogen diffusion distance as a function of time for solid and liquid aluminum at 615 °C and 575 °C.

In this case, assuming complete diffusion of hydrogen in the solid and liquid perpendicular to the x-direction (in Figure 8.5), the liquid composition during solidification is given by the equation[2]:

$$CH_L = \frac{CH_0}{K_H + (1 - K_H)\, g_l} \tag{8.26}$$

Where CH_L is the hydrogen concentration in the liquid (cm^3/100 g Al); CH_0 is the

concentration of hydrogen in the bulk liquid prior to solidification (cm^3/100 g Al); g_l is the fraction of liquid, by weight, in the mushy region; and K_H is the distribution coefficient of hydrogen between solid and liquid.

It is more convenient in Eq. (8.26) to use volume fraction of liquid (f_l) instead of weight fraction of liquid (g_l). Weight fraction liquid, g_l, can be expressed in terms of volume fraction liquid, f_l, as:

$$g_l = \frac{\rho_l f_l}{\rho_s f_s + \rho_l f_l} = \frac{(1-\beta) f_l}{1 - \beta f_l} \qquad (8.27)$$

where ρ_l and ρ_s are densities of liquid and solid, respectively, and β is volumetric shrinkage defined as $\beta = (\rho_s - \rho_l) / \rho_s$. Generally, shrinkage in aluminum alloys is about 5-6% (β=0.055). The liquid weight fractions of interest are between $g_l = 0.5$ and $g_l = 0.95$. The volume fraction of liquid, f_l, calculated from Eq. (8.27) for these two values are 0.514 and 0.952, respectively. Therefore, it is a good assumption that weight and volume fractions are equivalent, and thus interchangeable (i.e. $g_l = f_l$).

We need also to know the partial pressure of hydrogen gas which is in equilibrium with liquid metal having a dissolved hydrogen content, CH_l. This can be calculated by inserting Eq. (8.26) into Sieverts' law as follows:

$$P_H = C_F \left(\frac{CH_l}{S_l} \right)^2 = C_F \left(\frac{CH_0}{S_l} \right)^2 \left(\frac{1}{f_l + K_H (1 - f_l)} \right)^2 \qquad (8.28)$$

where P_H is in $N.m^{-2}$, C_F is a conversion factor (= 101325 $N.m^{-2}$ /atm), S_l is the hydrogen solubility in the liquid, and f_l is the volume fraction of liquid which was calculated in Eq. (8.16) in the region of the mushy zone.

Since there are no data for hydrogen dissolved in solid Al-Si alloys, the equilibrium partition ratio for dissolved hydrogen (K_H) in Al-Si alloys is assumed to be the same as in pure aluminum. Then according to Talbot[13]:

$$\log K_H = \log\left(\frac{C_{H(S)}}{C_{H(l)}}\right) = \frac{181}{T} - 1.369 \qquad (8.29)$$

where $C_{H(S)}$ and $C_{H(l)}$ are the hydrogen concentrations in the solid and liquid phases, respectively, K_H is the extrapolated value of the equilibrium partition ratio for hydrogen in aluminum for temperatures less than its melting point, and T is absolute temperature. According to Eq. (8.29), K_H varies only slightly in the solidification range of Al-Si alloys; at 615 °C, K_H= 0.068 and, at the eutectic temperature 575 °C, K_H= 0.07. In the following analysis, an average value of 0.069 is used for K_H.

The hydrogen solubility in aluminum and its alloys in the liquid, S_l, and in the solid, S_s, has been studied by several workers[18,19,20,21,22]. The results from their work show that the hydrogen solubility is strongly dependent on the temperature, and alloying elements affect the hydrogen solubility in liquid and solid states. For Al-Si alloys, silicon is the main alloying element, and the lower silicon concentration in the α-phase dendritic solid compared to the liquid causes evolution of silicon into the liquid during solidification. The increase in silicon concentration of the liquid and the decrease in temperature from the liquid towards the solid within the mushy zone results in a change in liquid hydrogen solubility, S_l, as a function of distance, x. Therefore, it is necessary to determine the liquid hydrogen solubility, S_l, in Eq. (8.28) as a function of temperature and silicon content through the solid-liquid region of Figure 8.5.

Opie and Grant[18] determined the solubility of hydrogen in Al-Si melts for $0 < Si < 16$ wt. pct. and $973 < T < 1273$ K. They presented their results in the form of the

Van't Hoff equation:

$$\log S_l = -\frac{A}{T} + B \qquad (8.30)$$

where S_l is the solubility in the liquid state, in cm^3 of H_2 per 100 g of alloy in equilibrium with 1 atm pressure of H_2 , A and B are parameters that depend on the silicon concentration, and T is temperature in K. Using regression analysis, the values of A and B can be expressed in terms of Si concentration as[10]:

$$A = a_0 + a_1 C_i^{0.5} + a_2 C_i + a_3 C_i^{1.5} \qquad (8.31)$$

and

$$B = b_0 + b_1 C_i^{0.5} + b_2 C_i + b_3 C_i^{1.5} \qquad (8.32)$$

where C_i is the wt. pct. of silicon in the melt. The values of these coefficients are given in Table 8.3.

Table 8.3 : Coefficients for Eqs. (8.31) and (8.32)

a_0	a_1	a_2	a_3	b_0	b_1	b_2	b_3
2550.0	-14.65	203.0	-47.86	2.620	-0.09268	0.2271	-0.05411

The hydrogen solubility in the solid is much lower than in the liquid. For commercial purity aluminum at 1 atm hydrogen pressure and between 465-620 °C, hydrogen solubility in the solid is reported to be in the form of Eq. (8.30), where A and B are 2580 and 1.399, respectively [13].

Therefore, the internal hydrogen partial pressure, P_H , can be calculated as a function of distance, x , within the mushy zone by inserting Eq. (8.15) in Eq. (8.30), and substituting Eqs. (8.30) and (8.16) in Eq. (8.28), resulting in the following equation:

$$P_H = \left(\frac{\sqrt{101325}}{f_l^x + 0.069\,(1 - f_l^x)} \right)^2 \times 10^{\left(\frac{2A(1+41x)}{569+26409x} - 2B \right)} \times CH_0^2 = K_{PH}\, CH_0^2 \quad (8.33)$$

where the values A and B are calculated from Eqs. (8.31) and (8.32) and using the coefficients in Table 8.3. The melt silicon content, C_L, in Eqs. (8.31) and (8.32) is a function of x , and can be calculated by inserting Eq. (8.15) into Eq. (8.14).

In this model, hydrogen diffusion in the x direction within the mushy zone is assumed to be negligible. The diffusion of hydrogen in liquid aluminum is rapid, and hydrogen can diffuse about 500 μm in the liquid in one second (Figure 8.6). In this work, however, the solid-liquid interface (at 9 cm from the chill) moves with a velocity of about 800 μm per second which is faster than the diffusion rate of hydrogen in liquid aluminum (i.e. 500 μm/s). Therefore, the diffusion of hydrogen over the length of the mushy zone (in the x direction) can be ignored, and the interdendritic eutectic liquid should solidify with the hydrogen content calculated from the evolution of hydrogen by growing α-phase dendrites.

8.5 Fracture Pressure (P_F)

Considering mechanical equilibrium of a macroscopic gas pore in the melt, the pressure difference, ΔP, across the interface, i.e. between the inside of the pore and the liquid within the mushy zone is a function of surface tension of the melt, and can be

expressed as [23] :

$$\Delta P = P_F = \gamma \left(\frac{1}{r_1} + \frac{1}{r_2} \right) \qquad (8.34)$$

where ΔP is the fracture pressure of the liquid, P_F in $N.m^{-2}$, γ is the surface tension of the liquid (N/m), and r_1, r_2 are the principle radii of curvature (m). For a spherical bubble, the radius of the pore is assumed to be proportional to the secondary dendrite arm spacing, and $r_1 = r_2 = DAS/4$ [24]. Poirier *et al* [23] considered the conical groove existing between primary dendrites and showed that the width of this groove at any point in the mushy region depends on the volume fraction of liquid, f_l . For a cylindrical pore, they calculated the radii of curvature to be $r_1 = f_l d_1 / 4$ and $r_2 = \infty$, where d_1 is the primary dendrite spacing. Therefore, Eq. (8.34) can be written as:

$$P_F = \frac{4\gamma}{f_l d_1} \qquad (8.35)$$

and for a spherical bubble, Eq. (8.34) can be written as:

$$P_F = \frac{8\gamma}{f_l d_1} \qquad (8.36)$$

Since usually the combined sum of the gas pressure (P_H) and the shrinkage pressure (P_S) is insufficient to cause pore nucleation, homogeneous nucleation is not a feasible mechanism for initiation of pores, and some foreign particle is necessary to assist in heterogeneous nucleation of the pore. Particles such as inclusions and solid nuclei may nucleate pores [25].

In the case of the heterogeneous nucleation of a bubble in the presence of a foreign substrate in the melt, Campbell[26] showed that the activation energy for nucleation decreases by $f(\theta)$, and Eq. (8.36) is modified to :

$$P_F = 1.12\ f(\theta)^{0.5}\ (\frac{8\,\gamma}{f_l \cdot d_1}) \qquad (8.37)$$

where $f(\theta) = (2 + 3\cos\theta - \cos^3\theta) / 4$ and is equal to 1 for homogeneous nucleation. θ is the normal angle of contact measured, for instance, by a sessile-drop technique (see Figure 3.1).

In this model, the primary dendrite arm spacing , d_1 , is assumed to be the same as in Al-Cu alloys, and to be 2.5 times the secondary arm spacing (DAS)[7]. As mentioned for Eq. (8.22), an average value of DAS, i.e. $DAS_{avg} = 40\text{x}10^{-6}$ m, is used within the mushy region. The fraction of liquid, f_l , in Eq. (8.37) as a function of distance x has already been defined in Eq. (8.16). Therefore, the fracture pressure can be calculated at any distance x within the mushy region.

During solidification, the surface tension of the liquid, γ, within the mushy region changes due to both the temperature gradient and the variation of silicon concentration in the interdendritic liquid along the mushy zone. The effect of temperature and silicon concentration on the surface tension of liquid aluminum have been studied separately by different authors. Taking into account the effect of temperature and silicon concentration, the surface tension in considered for the liquid which lies along the liquidus of the Al-Si phase diagram. Poirier *et al.*[10] defined the surface tension of hypoeutectic Al-Si alloys along the liquidus as:

$$\gamma = 0.864 - \frac{24.781\,C_L + 2.7856\,C_L^2 - 0.11532\,C_L^3}{1000} \quad (N/m) \qquad (8.38)$$

where surface tension, γ, is in N/m, and liquid composition, C_L , is in wt%Si. Therefore,

the surface tension of interdendritic liquid, γ, can be obtained as a function of distance, x, within the mushy region by substituting Eqs. (8.15) and (8.14) in Eq. (8.38).

The fracture pressure (Eq. (8.37)) represents the additional pressure to nucleate a pore, caused by surface tension forces, from the beginning of solidification. As the rate of solidification increases, the primary and secondary dendrite arm spacing decreases. Consequently, any porosity that forms must squeeze into a smaller space, and the pressure caused by surface tension increases. Rapid solidification therefore makes it more difficult for porosity to form.

8.6 Condition For Pore Formation

The condition for pore formation was expressed in Eq. (8.2). This equation is similar to Eq. (8.22) for shrinkage pressure. In fact, the term P_X in Eq. (8.22) represents the chemical (or gas) pressure, P_H ; and the term P_{XL} is the combination of fracture pressure, P_F , and the mechanical pressure at x_L which is equal to the sum of atmospheric pressure, P_{atm} , and metallostatic pressure, P_M . The metallostatic pressure, P_M , can be calculated as:

$$P_M = \rho\, g_r\, h \tag{8.39}$$

where ρ is density of liquid, g_r is acceleration due to gravity, and h is the height of liquid above the x position in the casting.

Therefore, substituting Eqs. (8.33), (8.22), (8.37) and (8.39) in Eq. (8.2) and using constants in Tables 8.1, 8.2 and 8.3, the initial melt hydrogen content required for pore formation, CH_0^{cr} ,can be obtained as a function of distance x within the mushy as follows:

$$CH_0^{cr} = \sqrt{\frac{P_F + P_{atm} + P_M - P_S}{K_{PH}}} = f(x) \qquad (8.40)$$

where P_{atm} is 101325 N.m^{-2}, and K_{PH}, P_S, P_F and P_M are as defined in Eqs. (8.33), (8.22), (8.37) and (8.39), respectively.

Therefore, the effect of the changes in different variables such as surface tension, volumetric shrinkage, feeding capability (i.e. the length of the mushy zone and viscosity), inclusions and hydrogen solubility on porosity formation can be studied from Eq. (8.40). In the five preceding chapters, the effect of modification on these variables was studied separately. In the following chapter, the changes in these variables are considered to be equivalent to a change in initial hydrogen content required for pore formation, and this will be used as a standard for the comparison of the effectiveness of the changes in these variables, due to modification, on porosity formation.

8.7 References

1. T.S. Piwonka and M.C. Flemings; "Pore Formation in Solidification", *Trans. TMS-AIME*, Vol.236, 1966, pp. 1157-65

2. M.C. Flemings; *Solidification Processing*, McGraw Hill, New York, NY, 1974, pp. 30-80, 135-50 and 234-54

3. R. Mehrabian, M. Keane, and M.C. Flemings; "Interdendritic Fluid Flow and Macrosegregation; Influence of Gravity", *Metall. Trans.*, Vol. 1, May 1970, pp. 1209-20

4. D.R. Poirier; "Permeability for Flow of interdendritic Liquid in Columnar-Dendritic Alloys", *Metall. Trans. B*, Vol. 18B, March 1987, pp. 245-55

5. D. Apelian, M.C. Flemings and R. Mehrabian; "Specific Permeability of Partially Solidified Dendritic Networks of Al-Si Alloys", *Metall. Trans.*, Vol. 5, Dec. 1974, pp. 2533-37

6. K. Kubo and R.D. Pehlke; "Mathematical Modelling of Porosity Formation in Solidification", *Metall. Trans. B*, Vol. 16B, June 1985, pp. 359-66

7. G.K. Sigworth and C. Wang; "Mechanisms of Porosity Formation during Solidification: A Theoretical Analysis", *Metall. Trans. B*, Vol. 24B, April 1993, pp. 349-64

8. J.L. Murray and A.J. McAlister; "The Al-Si (Aluminum-Silicon) System", *Bulletin of Alloy Phase Diagrams*, Vol. 5, No.1, 1984, pp. 74-90

9. P. Thevoz, J.L. Desbioiles, and M. Rappaz; "Modelling of Equiaxed Microstructure Formation in Casting", *Metall. Trans. A*, Vol. 20A, Feb. 1989, pp. 331-22

10. K. Yeum and D.R. Poirier; "Predicting Microporosity in Aluminum Alloys", *Light Metals*, 1988, pp. 469-76.

11. M.C. Flemings; "Behaviour of Metal Alloys in the Semisolid State", *Metall. Trans. B*, Vol. 22B, June 1991, pp. 269-93

12. G. Gustafsson, T. Thorvaldsson, and G.L. Dunlop; "Development of microstructure in Al-7Si-0.3Mg-0.2Fe Alloy", *The Metallurgy of Light Alloys*, Institute of Metallurgists, London, March 1983, pp. 288-94

13. D.E.J. Talbot; "Effects of Hydrogen in Aluminum, Magnesium, Copper, and Their Alloys", *Int. Metall. Rev.*, Vol.20, 1975, pp. 166-84.

14. C.J. Smithells; *Metals Reference Book*, 5th Ed., Butterworths, London, 1975

15. W. Eichenauer and J. Markopoulos; "Measurement of the Diffusion Coefficient of Hydrogen in Liquid Aluminum", *Z. Metallkunde*, Vol. 65, 1974, pp. 649-52

16. W. Eichenauer, K. Hattenbach and A. Pebler; "The Solubility of Hydrogen in Solid and Liquid Aluminum", *Z. Metallkunde*, Vol. 52, 1961, pp. 682-84

17. D.R. Gaskell; An Introduction to Transport Phenomena in Materials Engineering, Macmillan Publishing Company, New York, NY, 1992, pp. 476-491

18. W.R. Opie and N.J. Grant; "Hydrogen Solubility in Aluminum and Some Aluminum Alloys", *Trans. AIME*, Vol. 188, J. Metals, 1950, pp. 1237-41

19. D.E.J. Talbot and P.N. Anyalebechi; "Solubility of Hydrogen in Liquid Aluminum", *Mater. Sci. Technol.*, Vol.4, Jan. 1988, pp. 1-4

20. C.E. Ransley and H. Neufeld; "The Solubility of Hydrogen in Liquid and Solid Aluminum", *J. Inst. Met.*, Vol.74, 1948, pp. 599-620

21. P.D. Hess; "An Empirical Equation For Calculating Solubility of Hydrogen in Molten Aluminum Alloys", *Light Metals*, 1974, pp. 591-97

22. P.N. Anyalebechi, D.E.J. Talbot and D.A. Granger; "The Solubility of Hydrogen in Liquid Al-Li Alloys", *Metall. Trans.*, Vol.19B, 1988, pp. 227-32

23. D.R. Poirier, K. Yeum and A.L. Maples; "A Thermodynamic Prediction for Microporosity Formation in Aluminum-Rich Al-Cu Alloys;", *Metall. Trans. A*, Vol. 18A, Nov. 1987, pp. 1979-87

24. S. Shivkumar, D. Apelian and J. Zou; "Modelling of Microstructure Evolution and Microporosity Formation in Cast Aluminum Alloys", *AFS Trans.*, Vol. 98, 1990, pp. 897-904

25. P.S. Mohanty; Ph.D. thesis, McGill University, Montreal, PQ, Canada, 1994

26. J. Campbell; *The Solidification of Metals*, ISI Publication No. 110, The Iron and Steel Institute, London, 1967, pp. 18-26

Chapter 9

General Discussion

As illustrated in Chapter 2, Sr-modification increases the pore volume fraction, the pore size and the pore number density of A356 alloy significantly, and these changes are much higher at lower cooling rates and at higher hydrogen contents. Moreover, it was indicated that the observed increase in porosity in modified alloys is due to a change in both nucleation and growth mechanisms of the pore, and is not due to one single factor.

The increase in porosity in Sr-modified Al-Si alloys may be caused by one or more of the following factors:

a) a reduction in the surface tension of the liquid.

b) an increase in the volumetric shrinkage.

c) a reduction in interdendritic feeding by:

1) a decrease in dendrite arm spacing (DAS).

2) an increase in the viscosity of the liquid.

3) an increase in the length of the mushy zone.

4) a change to a more irregular solid-liquid interface shape.

d) an increase in the total solidification time, i.e. the time available for hydrogen diffusion and growth of porosity.

e) an increase in the inclusion content of the melt (i.e., the inclusions which can act as heterogeneous sites for pore nucleation).

f) an increase in the rate of melt hydrogen absorption and thus the hydrogen content of

the melt.

g) a reduction in the hydrogen solubility in the solid or liquid states.

Throughout this thesis, the effect of Sr-modification on these parameters has been investigated and the following major points drawn in the various chapters.

1) Surface Tension:

- The addition of about 0.01 wt%Sr to A356 alloy decreases the surface tension of the liquid from 0.79 N/m to 0.64 N/m (by about 19%) at 685 °C.
- Strontium addition of about 0.01 wt% increases the contact angle between A356 melt and an alumina substrate from 135° to 142°.

2) Volumetric Shrinkage:

- Sr-modification increases the solid density of Al-Si alloys while the liquid density remains almost constant.
- Sr-modification increases the volumetric shrinkage by about 3.5% (in Archimedean method) to 12% (in sessile-drop method).

3) Dendrite Arm Spacing (DAS):

- The addition of 0.02 wt%Sr to A356 alloy decreases the dendrite arm spacing from 60 $\pm$8.2 μm to 54.5 $\pm$6.6 μm (by about 9%) at a cooling rate of about 0.4 °C/s. This decrease in DAS is within the range of the standard deviation.

4) Viscosity:

- Assuming that strontium has the same effect as sodium on viscosity, Sr-modification may increase the viscosity of A356 melt by about 31%.

5) Length of the Mushy Zone:

- Sr-modification suppresses the eutectic temperature by about 7 °C, and therefore, increases the freezing range or the length of the mushy zone.
- Sr-modification has the same effect as a 1% decrease in silicon content on the freezing range. This increase in freezing range obtained by decreasing the melt silicon content was observed to have a small effect on porosity.

6) Solidification Time:

- Sr-modification does not change the total solidification time and has no effect on the time available for the diffusion of hydrogen and the growth of the pores.

7) Solid/Liquid Interface Morphology:

- The solid-liquid interface of an unmodified alloy seems to be more irregular compared to the modified alloy. For this reason, an unmodified alloy may have more of a tendency to liquid entrapment and to microporosity formation.

8) Melt Inclusion Content:

- Sr-modification increases the melt oxidation rate and the inclusion content of Al-Si melts. However, these inclusions do not have a significant effect on pore nucleation. The following two hypotheses were made to explain this behaviour:

a) These inclusions in Sr-modified A356 alloy do not act as heterogeneous sites for pore nucleation.

b) A sufficient number of inclusions is always present for gas precipitation and nucleation of pores, even in the absence of strontium. As a result, the increase in melt inclusion content due to Sr-modification has no additional effect on pore formation.

9) Rate of Melt Hydrogen Absorption:

- Sr-treatment does not affect the rate of hydrogen pick-up by molten Al-Si alloys and does not introduce hydrogen into the melt.

10) Hydrogen Solubility in the Solid and Liquid States:

- Sr-modification has virtually no effect on the hydrogen solubility in solid A356 alloy.
- The addition of 0.02 wt%Sr decreases the hydrogen solubility in liquid aluminum by about 17% at 700 °C and by about 14% at 750 °C.

Among all of these parameters, therefore, only the changes in the following factors may influence pore formation and cause the observed increase in porosity in modified alloys: surface tension, volumetric shrinkage, DAS, viscosity, length of the mushy zone and liquid state hydrogen solubility. Having established the effect of strontium on these, it is necessary to determine whether the changes in these factors can account for the significant observed increase in porosity associated with modification.

The importance of the changes in these parameters on porosity can be evaluated using the mathematical model presented in Chapter 8. The effects of the changes in surface tension, volumetric shrinkage, DAS, viscosity, length of the mushy zone and liquid state hydrogen solubility will be expressed in terms of the initial hydrogen content required for pore formation which was calculated in Eq. (8.40) as:

$$CH_0^{cr} = \sqrt{\frac{P_F + P_{atm} + P_M - P_S}{K_{PH}}} = f(x) \qquad (9.1)$$

where P_{atm} is atmospheric pressure, K_{PH} is a function of liquid state hydrogen solubility

as calculated in Eq. (8.33), P_S is a function of volumetric shrinkage, viscosity and DAS as calculated in Eq. (8.22), P_F is a function of surface tension and DAS as calculated in Eq. (8.37), P_M is as calculated in Eq. (8.39) and x is the distance within the mushy zone. The origin of the coordinate system (e.g., x=0) is assumed to be in the solid and at a distance of 8.65 cm from the chill end (in Figure 8.1).

For an Al-7%Si alloy directionally solidified as described in Chapter 2, the initial melt hydrogen content required for pore formation, CH_0^{cr}, is plotted as a function of distance, x, within the mushy zone in Figure 9.1 by solving Eq. (9.1) and using the values in Tables 8.1, 8.2, 8.3 and 9.1. The Fortran program used for solving this equation is given in the Appendix.

Table 9.1 : Constants used in calculations (for an Al-7%Si alloy).

Constant	Value used in the calculations	Note:
C_0	7 wt%Si	As A356 alloy
DAS_{avg}	40×10^{-6} m	Calculated in section 8.3
Viscosity, μ	2.8×10^{-3} N.S/m^2	From Figure 5.3
Tortuosity factor, τ	2	Ref. [1] in Chapter 8
P_{atm}	101325 N/m^2	
Contact Angle, θ	135 ° 142 °	unmodified alloys Sr-modified alloys
K_H	0.069	Calculated in Eq. (8.29)

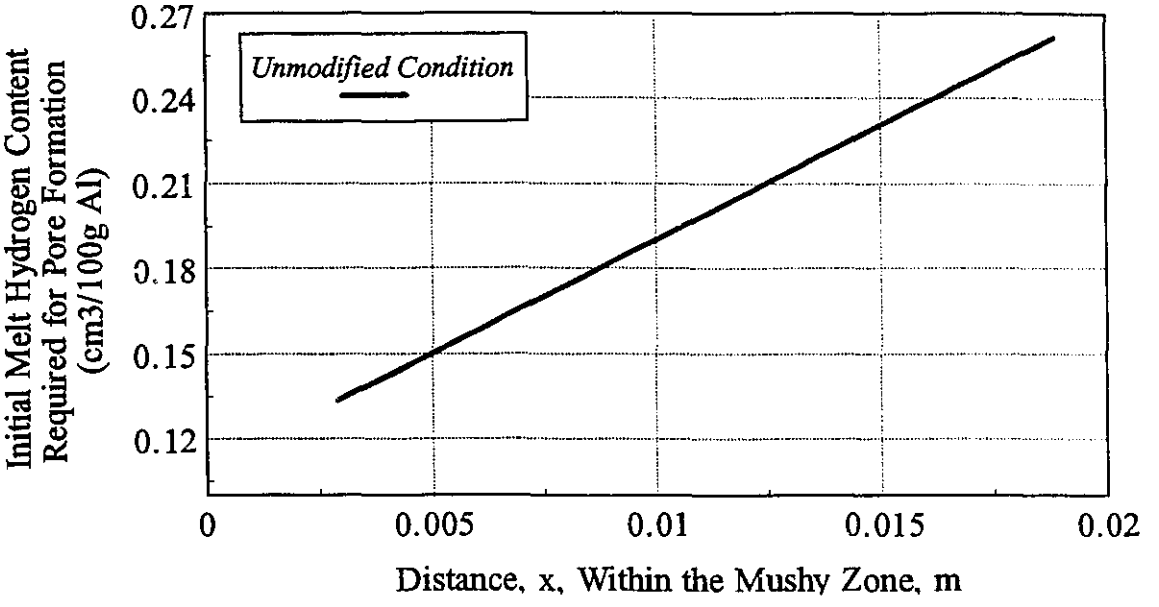

Figure 9.1: The initial melt hydrogen content required for pore formation as a function of distance, x, within the mushy zone for an unmodified Al-7%Si alloy (where x=0 is at a distance of 8.65 cm from the chill end).

It can be seen in this figure that the deeper within the mushy zone, the lower the initial melt hydrogen content required for pore nucleation, and consequently, the easier the porosity formation. This is due to the feeding problem within the dendritic network and the rejection of hydrogen into the liquid during solidification. It is also observed that a minimum melt hydrogen content of about 0.14 $cm^3/100g$ Al is required for a pore to nucleate and to grow.

Equation 9.1 was solved for the time that the solid interface is at a distance of 8.65 cm from the chill end. At this position in the casting, the average cooling rate is

about 1.5 °C (in Figure 8.2), and the porosity at a hydrogen content of 0.13 $cm^3/100g$ Al is almost zero (in Figure 2.10). Therefore, the hydrogen limit of 0.14 $cm^3/100g$ Al calculated from Eq. 9.1 is in good agreement with the experimental results.

Increasing the volumetric shrinkage by a maximum of 12% (due to modification) leads to the melt hydrogen content required for pore formation shown in Figure 9.2. As can be seen, the two curves are superimposed and are not distinguishable one from the other. A 12% increase in volumetric shrinkage does not have a significant effect on pore formation, and therefore, is not the reason for the observed increase in porosity in modified alloys. The solubility of Sr in solid aluminum is almost zero which results in the rejection of Sr into the interdendritic liquid during solidification, and enrichment in eutectic liquid. The 12% increase in volumetric shrinkage is likely related to a change in the eutectic contraction (β_E).

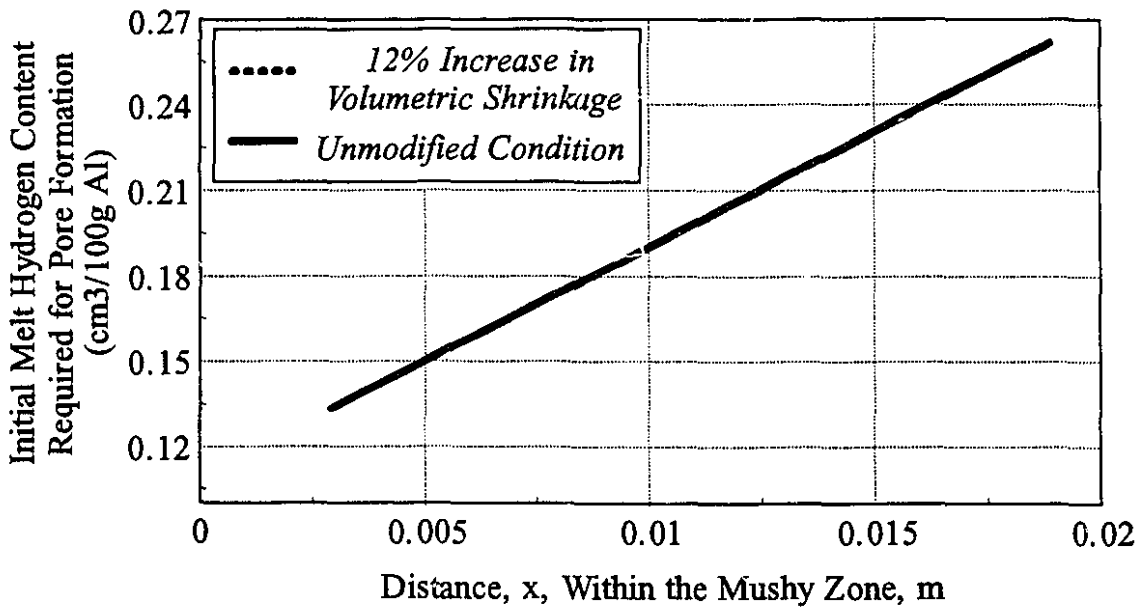

Figure 9.2 : The effect of the 12% increase in volumetric shrinkage on the melt hydrogen content required for pore formation within the mushy zone.

The effects of the 31% increase in viscosity and the 9% decrease in DAS (due to modification) on the initial melt hydrogen content required for pore formation (in Figure 9.1) are shown in Figures 9.3 and 9.4, respectively. These figures show that the changes in viscosity and DAS do not have a significant effect on pore formation. The reason for this is that Eq. (9.1) was derived for a directionally solidified Al-7%Si casting (as described in Chapter 2), and therefore, the feeding problem within the mushy zone is not significant enough to play an important role in pore formation. However, this behaviour could be different in industrial castings which do not freeze in a directional manner.

The effects of the 19% decrease in surface tension and the 17% decrease in the hydrogen solubility in the liquid on the initial melt hydrogen content required for pore formation are plotted as a function of distance, x, within the mushy zone in Figures 9.5 and 9.6, respectively.

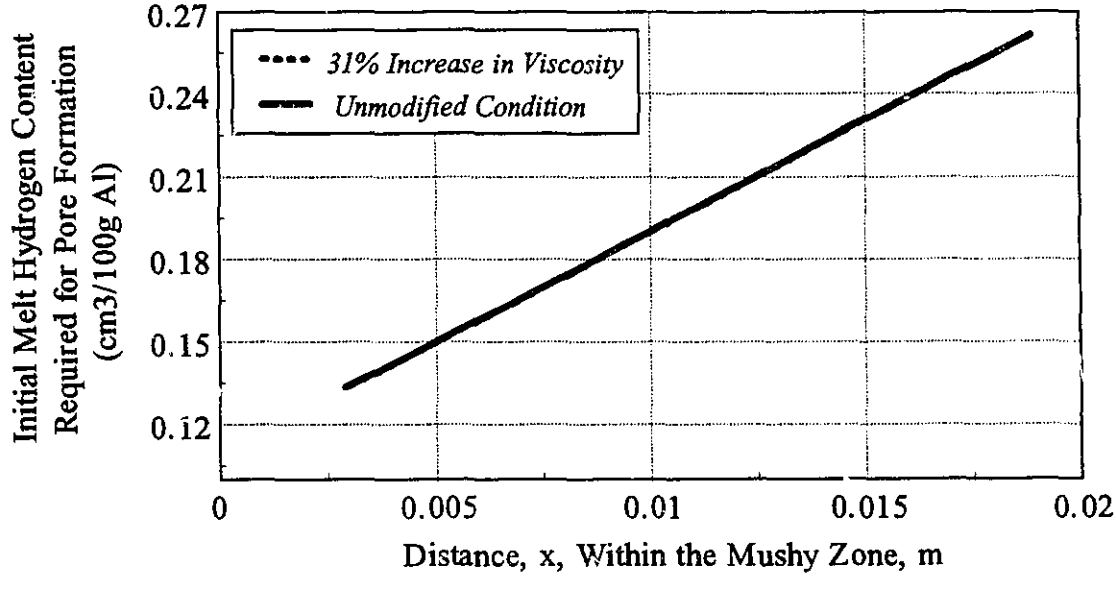

Figure 9.3 : The effect of the 31% increase in viscosity on the melt hydrogen content required for pore formation vs. distance, x, within the mushy zone.

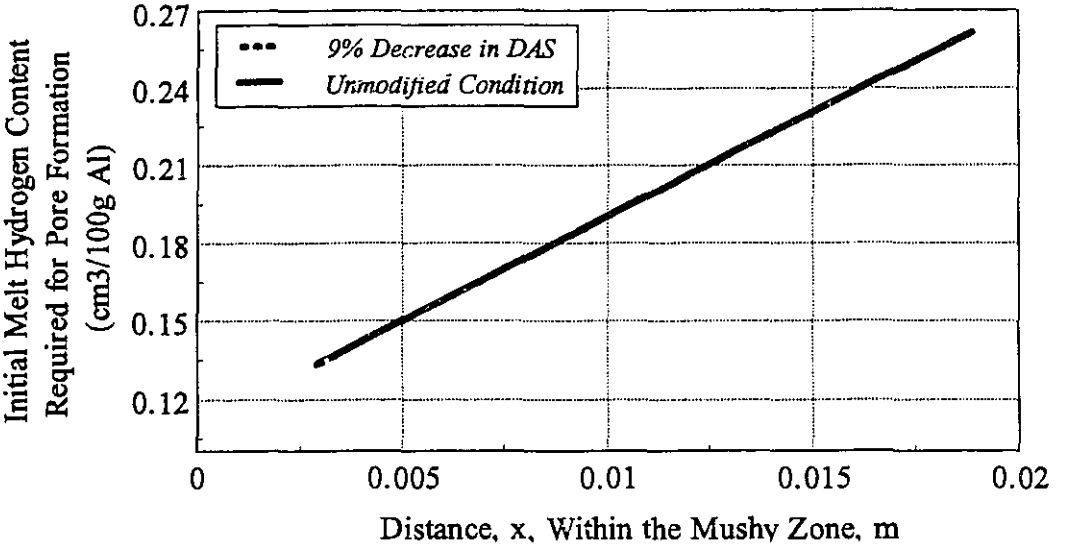

Figure 9.4 : The effect of the 9% decrease in DAS on the melt hydrogen content required for pore formation vs. distance, x, within the mushy zone.

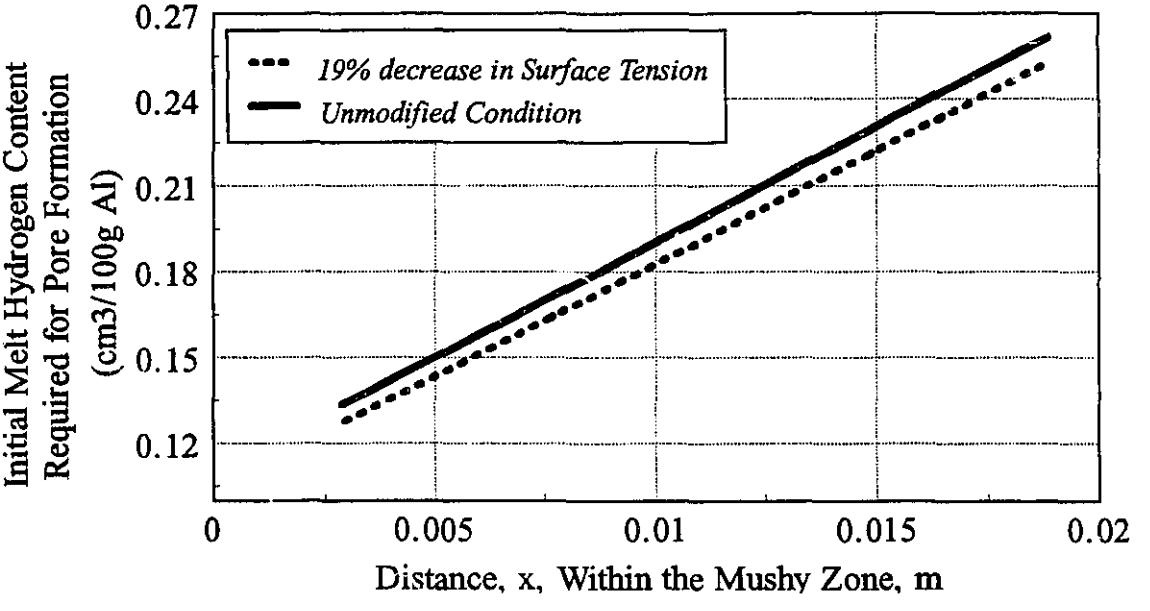

Figure 9.5 : The effect of the 19% decrease in surface tension on the initial melt hydrogen content required for pore formation within the mushy zone.

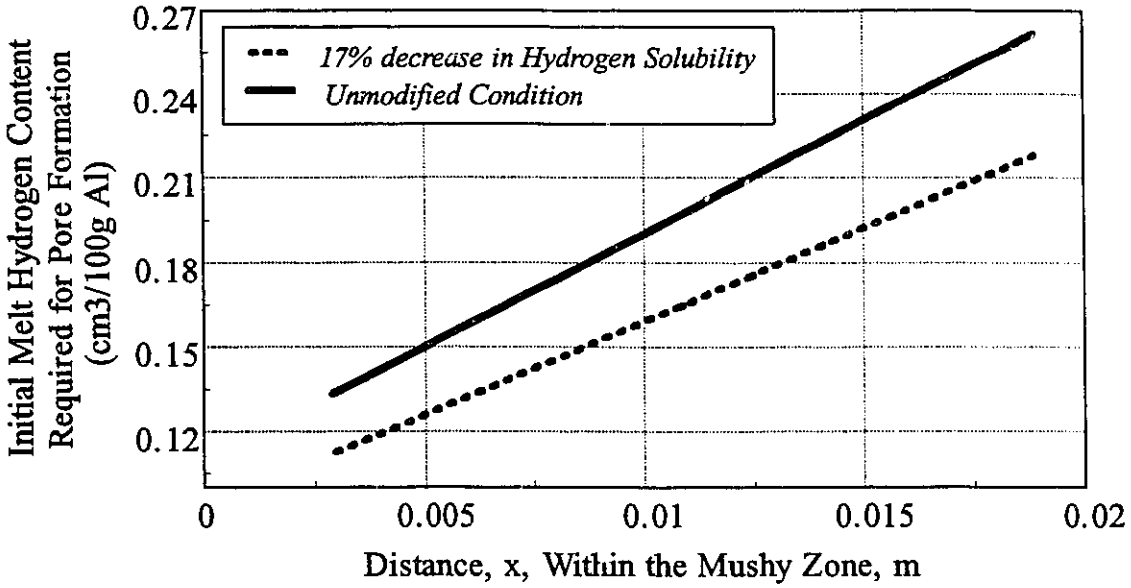

Figure 9.6 : The effect of the 17% decrease in liquid state hydrogen solubility on the melt hydrogen content required for pore formation within the mushy zone.

The decrease in the surface tension and hydrogen solubility in the liquid due to modification reduce the initial melt hydrogen content required for pore formation. As a result, pores can form in the earlier stages of solidification for the same hydrogen level as occurs in an unmodified alloy and grow over a longer period of time prior to complete solidification. The effect of the 17% decrease in the hydrogen solubility on porosity formation is larger than the 19% decrease in the surface tension. It is also worth mentioning that a change in hydrogen solubility in the liquid also affects the porosity formation by changing the equilibrium partition ratio for dissolved hydrogen, i.e. K_H in Eq. (8.28). However, this change in K_H has a negligible effect on pore formation.

The final parameter to be discussed is the effect of the increase in the length of the mushy zone. Sr-modification and a 1% decrease in silicon content have a similar

effect on the length of the mushy zone. The experimental results in section 5.4.2 showed that a 1% change in the melt silicon content exerted only a small effect on porosity. The effect of a decrease in eutectic temperature by a maximum of 7 °C (due to modification) on the initial melt hydrogen content required for pore formation is plotted as a function of distance, x, within the mushy zone in Figure 9.7.

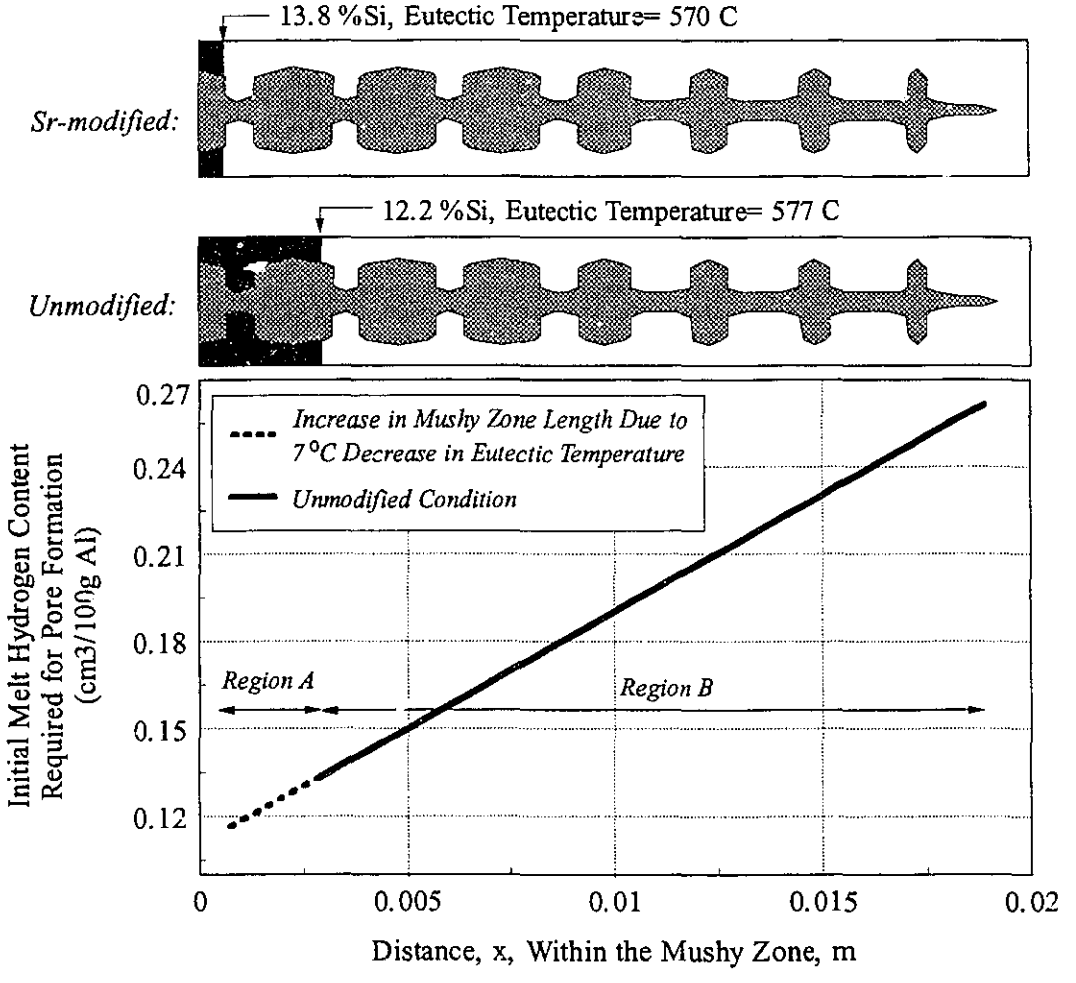

Figure 9.7 : The effect of the increase in the length of the mushy zone (due to a 7°C decrease in eutectic temperature) on the initial melt hydrogen content required for pore formation vs. distance, x, within the mushy zone.

Two distinct regions, i.e regions A and B, are clearly distinguished in this figure. In region B, the curves are corresponding and the decrease in eutectic temperature has no effect on the initial melt hydrogen content required for pore formation. In region A, the solid fraction of primary α(Al)-phase is increased in the modified alloy resulting in an increase in the hydrogen concentration in the interdendritic liquid at the bottom of the dendrites (due to the rejection of hydrogen into the interdendritic liquid by growing solid). Moreover, the silicon concentration in this interdendritic liquid is increased from 12.2% to 13.8% which results in a decrease in the surface tension and the liquid state hydrogen solubility of the liquid.

The overall effect of these changes in region A (i.e., deep within the mushy zone and at the bottom of the dendrites) is a lower initial melt hydrogen content required for pore formation. If the condition for pore formation is easily satisfied, a pore can form at early stage of solidification ,i.e. within region B, and the decrease in the eutectic temperature does not have a significant effect on pore formation. When a pore forms at later stage of solidification, i.e. within region A at the bottom of the mushy zone, the effect of the decrease in eutectic temperature on pore formation becomes significant.

In addition, it is understood from this discussion that the reduction of eutectic temperature in modified alloys may facilitate porosity formation not only due to an increase in the shrinkage pressure (because of the increase in the length of the mushy zone and the interdendritic feeding problem), but also due to an increase in the hydrogen concentration in the liquid and a decrease in the surface tension and the liquid state hydrogen solubility (due to the increase in the silicon concentration).

The initial melt hydrogen contents required for pore formation in Figures 9.5 to 9.7 are replotted in Figure 9.8. The effect of the decrease in hydrogen solubility in the liquid on porosity formation is more significant than the effect of either the decrease in the surface tension or the increase in the length of the mushy zone.

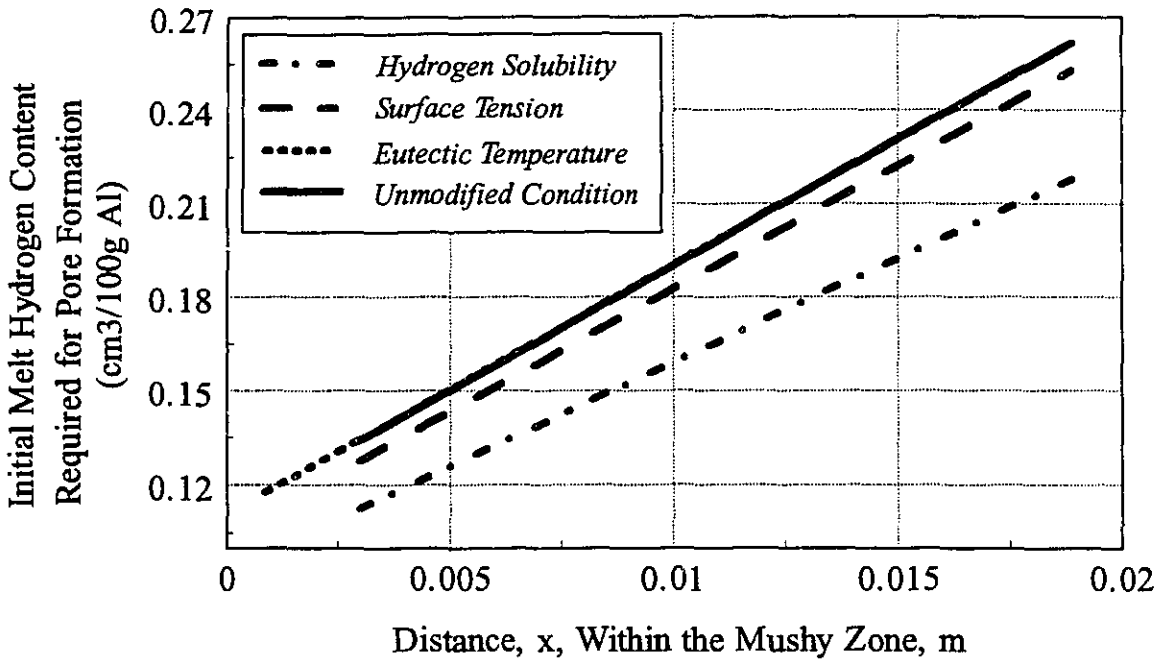

Figure 9.8 : The comparison of the effects of the decrease in surface tension, in hydrogen solubility, and in eutectic temperature on the melt hydrogen content required for pore formation vs. distance, x, within the mushy zone (replotted from Figures 9.5 to 9.7).

A close examination of the curves corresponding to the changes in these parameters and the curve for the unmodified condition in Figure 9.8 shows that the decrease in the surface tension (by 19%), the hydrogen solubility (by 17%) and the eutectic temperature (by 7 °C) associated with modification are equivalent to a decrease in the hydrogen content required for pore formation by about 0.01 cm^3/100g Al, 0.03 cm^3/100g Al and 0.015 cm^3/100g Al, respectively. In total, the changes in these three factors due to modification can be taken as equivalent to an effective increase in hydrogen

content of about 0.055 cm^3/100g Al.

Using the experimental results in Figure 5.8, it is seen that the measured effect of Sr-modification on porosity is equivalent to an increase in the melt hydrogen content of about 0.06 cm^3/100g Al. This is almost the same as that obtained from the present model due to the changes in the surface tension, the hydrogen solubility and the eutectic temperature (i.e., 0.055 cm^3/100g Al).

Therefore, the decrease in the hydrogen solubility in the liquid, the decrease in the surface tension and the decrease in the eutectic temperature (or the increase in the length of the mushy zone) appear to be responsible for the observed increase in porosity in modified alloys. Among these parameters, the decrease in the hydrogen solubility in the liquid plays the main role in porosity formation.

Chapter 10

Conclusions and Future Work

10.1 Conclusions

Based on the experimental results and the theoretical analysis in the previous chapters, the following major conclusions can be drawn:

1. Sr-modification increases the pore volume fraction, the pore size and the pore number density of A356 alloy significantly, and these changes are much higher at lower cooling rates and at higher hydrogen contents.

2. The addition of Sr to Al-Si alloys:
   a) reduces the surface tension of the liquid,
   b) increases the volumetric shrinkage due to an increase in solid density,
   c) decreases the dendrite arm spacing (DAS),
   d) increases the viscosity of the liquid,
   e) increases the length of the mushy zone,
   f) changes the solid-liquid interface to a more regular shape,
   g) does not change the total solidification time,
   h) increases the melt inclusion content, but these inclusions do not have a significant effect on pore nucleation,

i) has no effect on the rate of melt hydrogen pick-up and does not introduce hydrogen into the melt,

j) reduces the hydrogen solubility in the liquid state but has virtually no effect on the solid state solubility.

3. Using a mathematical model for pore formation, it is concluded that the decrease in the hydrogen solubility in the liquid, the decrease in eutectic temperature and the decrease in the surface tension appear to be the reasons for the observed increase in porosity in modified alloys. Among these parameters, the decrease in the hydrogen solubility in the liquid plays the main role in porosity formation.

10.2 Suggestions For Future Study

There are a few aspects which are suggested for further study in order to give a better view of some of the propositions made in this thesis and to extend the results to industrial applications. These are outlined below:

1. The effect of Sr-modification on different parameters was investigated at one level of strontium only (i.e., 0.02 wt% Sr). It would be useful to perform the experiments at different Sr levels.

2. It would be interesting to study the reason for the increase in the density of the solid Al-Si alloys on the addition of Sr.

3. Although the change in silicon content seems to be the only practical method to change the freezing range and to study the effect of the length of the mushy zone on porosity, this approach does not indicate the real effect of the length of the

mushy zone. Thus, further investigations should be carried out on this matter.

4. The effect of Sr-modification on the liquid state hydrogen solubility has been studied in pure aluminum. It should also be studied in commercial Al-Si alloys.

5. Since no increase in porosity has been reported in Sb-modified Al-Si castings, it would be useful to study the effect of Sb on the parameters investigated in this thesis. Such a study would help to substantiate the conclusions of this work.

6. Since the increase in porosity due to modification is caused by changes in the surface tension, the liquid state hydrogen solubility and the mushy zone length, new alloying systems could be developed to offset the effect of these parameters and to prevent porosity formation. For example, Mg and Li increase the liquid state hydrogen solubility, and therefore, Al-Si alloys with higher Mg concentration could be used or alloys could be modified using Li.

Statement of Originality

The author sincerely believes that all aspects addressed in this thesis constitute distinct contributions to knowledge and claims the originality of the items listed below:

- The effect of Sr-modification on porosity (i.e., pore volume fraction and pore size) has been studied quantitatively in directionally solidified Al-Si alloys as a function of cooling rate, the melt hydrogen content and the silicon concentration.

- A fundamental study has been carried out to quantitatively determine the effect of Sr-modification on the following variables:
  - Surface tension
  - Volumetric shrinkage and the theoretical solid and liquid densities
  - Dendrite arm spacing
  - Total solidification time
  - Shape of the solid/liquid interface
  - Length of the mushy zone
  - Oxidation behaviour and the quality of the oxide film on the liquid surface
  - Inclusion levels and the role of inclusions on pore nucleation.
  - Rate of melt hydrogen absorption
  - Hydrogen solubility in the solid state.

- A simple mathematical model for pore formation has been developed to study the effect of casting and melt variables on porosity and to evaluate the importance of the changes in these variables (due to modification) on porosity formation.

Appendix

```
C*************************************************************************
C        MODELLING OF POROSITY FORMATION IN AL-SI ALLOYS
C*************************************************************************
C  UNITS: t=second, X=meter, T= C, CH=cm3/100 g Al,
C  C0  = Melt Silicon Concentration (wt%Si)
C  VIS = Liquid Viscosity
C  TE  = Eutectic Temperature (C)
C  TT  = Tortuosity Factor
C  BA  = Average Volumetric Shrinkage for Alpha Phase
C  BE  = Average Volumetric Shrinkage for Eutectic phase
C  CH0 = Initial Melt Hydrogen Content
C  The temperature(C) versus X(m) at time 2.706 min:
C  T=(569+26409 X)/(1+41 X) OR --->
C  X=(T-569)/(26409-41*T)
C
C  FL=[(6.85*C0*(1+41 X))/(651*X+91)]**1.15  OR  --->
C  X=(6.85*C0-(91*(FL^0.87)))/((651*(FL**0.87))-(6.85*41*C0))

      CHARACTER*20 DATA
      REAL K1,K2,K3,KA,KB,KH,KPH,LL,LM,LCX,L,N,I,J
      C0=7.0
      VIS=2.8E-3
      TE=577.0
      TT=2.0
      BA=0.0724
      BE=0.0369
      WRITE(*,*)'ENTER FILE NAME'
      READ(*,500)DATA
      OPEN (3,FILE=DATA,FORM='FORMATTED')
```

```
C  Alloy Selection:
C  SUR=0 For Unmodified Alloy /and/ SUR=1 For Modified Alloy
      SUR=0.0
C  Liquidus Temperature:
      TL=660-6.85*C0

      X1=(TE-569)/(26409-41*TE)
      FLX1=((6.85*C0*(1+41*X1))/(651*X1+91))**1.15
      FXL=0.8
      XL=((6.85*C0)-(91*(FXL**0.87)))/((651*(FXL**0.87))-(6.85*41*C0))
C  LM = Length of the Mushy Zone
      LM=((TL-569)/(26409-41*TL))-X1

      IF (XL.LE.X1) WRITE (*,*) 'MUSHY ZONE IS TOO SMALL'
      IF (XL.LE.X1) STOP

      DO 5 X=X1,XL,(XL-X1)/20.0
      T=(569+26409*X)/(1+41*X)
      CL=(660-T)/6.85
C  FL = Liquid Fraction at position X
      FL=((6.85*C0*(1+41*X))/(651*X+91))**1.15

C  Calculation of Fracture Pressure (PF) - (Due to Surface Tension):
C  SURX = Surface Tension of Interdendritic Liquid at X Position
C  Cooling Rate : COLR(X) = 0.2+(6.79*EXP(-(0.0865+X)/0.056))
C  DAS(X)=(10**(1.659-(0.4*ALOG10(COLR))))*1.0E-6
C  DAS=Average Dendrite Arm Spacings:
      DAS=40E-6

C  Surface Tension as a function of Melt Silicon Content:
      SURX=(864-24.781*CL+2.7856*(CL**2)-0.11532*(CL**3))/1000

      IF(SUR.EQ.0) SURX=SURX
```

```
      IF(SUR.EQ.1) SURX=SURX*0.64/0.79
      IF(SUR.EQ.0) TETA=135
      IF(SUR.EQ.1) TETA=142
      FTETA=(2+(3*COS(TETA*3.1416/180))-((COS(TETA*3.1416/180))**3))/4
C  For a Spherical Bubble:
      PF=1.12*(FTETA**0.5)*(8*SURX/(2.5*DAS*FL))

C  Calculation of External Pressures:
C  PM  = Metallostatic Pressure
C  PA=Atmospheric Pressure
C  Den = Density of the liquid above the mushy zone
C  LCX = Distance of the Position X from the Chill End
C  LL  = Total Length of the Casting(m)

      LCX=0.0865+X
      LL=0.33
      DEN=2454
      PM=DEN*9.81*(LL-LCX)
      PA=101325.0
C  Calculation of Shrinkage Pressure (PS):
      K1=((BE/(1-BE))-(BA/(1-BA)))*FLX1
      K2=(BA/(1-BA))
      K3=(24E-3*VIS*3.14*(TT**3))/(DAS**2)

      Y=2.3
      CALL QSIMP(X,XL,Y,C0,S1)
      Y=1.15
      CALL QSIMP(X,XL,Y,C0,S2)
      PS=K3*((K1*S1)+(K2*S2))

C  Calculation of Gas Pressure (PH2):
      KH=0.069
      CF=101325.0
```

```
C  SL = Hydrogen Solubility at Position X
      A=2550-14.65*(CL**0.5)+203*CL-47.86*(CL**1.5)
      B=2.62-0.09268*(CL**0.5)+0.2271*CL-0.05411*(CL**1.5)
      SL=(10.0**((-A/(T+273))+B))

C  IF(X.EQ.X1) FL=0

      KPH=CF/(SL**2)*((1/(FL+(KH*(1-FL))))**2)

C  CHL = Melt Hydrogen Concentration at X Position
C  CHL = CH0/(FL+(KH*(1-FL)))
C  The Condition for Pore Formation: PH-PF=PA+PM-PS

C  CH0 = Initial Hydrogen Required for Pore Formation:
      CH0=((PF+PA+PM-PS)/KPH)**0.5
C  PH=KPH*(CH0**2)

      WRITE (3,*) X,CH0
C  WRITE (*,*) PH,PF,PS
    5 CONTINUE
  500 FORMAT(A)
      STOP
      END
C*************************************************************************
      FUNCTION FUNC(X,YM,C0)
C  REAL*8 M
      FUNC=((651*X+91)/(6.85*C0*(1+41*X)))**YM
      RETURN
      END
C*************************************************************************
      SUBROUTINE QSIMP(A,B,YM,C0,S)
      PARAMETER (EPS=1.E-6, JMAX=20)
      OST=-1.E30
```

```
      OS= -1.E30
      DO 11 J=1,JMAX
      CALL TRAPZD(A,B,YM,C0,ST,J)
      S=(4.*ST-OST)/3.
      IF (ABS(S-OS).LT.EPS*ABS(OS)) RETURN
      OS=S
      OST=ST
   11 CONTINUE
C     PAUSE 'Too many steps.'
      WRITE (*,*) 'Too many steps.'
      END
C*********************************************************************
      SUBROUTINE TRAPZD(A,B,YM,C0,S,N)
      IF (N.EQ.1) THEN
      S=0.5*(B-A)*(FUNC(A,YM,C0)+FUNC(B,YM,C0))
      IT=1
      ELSE
      TNM=IT
      DEL=(B-A)/TNM
      X=A+0.5*DEL
      SUM=0.
      DO 11 J=1,IT
      SUM=SUM+FUNC(X,YM,C0)
      X=X+DEL
   11 CONTINUE
      S=0.5*(S+(B-A)*SUM/TNM)
      IT=2*IT
      ENDIF
      RETURN
      END
C*********************************************************************
```